Environmental Performance Measures in Optimizing Traffic Signals for Fuel and Emissions Efficiency

by

Suhaib Alshayeb

Bachelor of Science in Civil Engineering, Jordan University of Science and Technology, 2016

Master of Science in Civil Engineering, Florida Atlantic University, 2019

Submitted to the Graduate Faculty of the

Swanson School of Engineering in partial fulfillment

of the requirements for the degree of

Doctor of Philosophy

University of Pittsburgh

2022

UNIVERSITY OF PITTSBURGH

SWANSON SCHOOL OF ENGINEERING

This dissertation was presented

by

Suhaib Alshayeb

It was defended on

February 17, 2022

and approved by

Melissa Bilec, PhD, Professor, Department of Civil and Environmental Engineering

Vikas Khanna, PhD, Associate Professor, Department of Civil and Environmental Engineering

B. Brian Park, PhD, Professor, Engineering Systems and Environment Department

Mark Magalotti, PhD, Lecturer, Department of Civil and Environmental Engineering

Dissertation Director: Aleksandar Stevanovic, PhD, Associate Professor, Department of Civil and Environmental Engineering

Environmental Performance Measures in Optimizing Traffic Signals for Fuel and Emissions Efficiency

Suhaib Alshayeb, Ph.D.

University of Pittsburgh, 2022

Designing traffic signal timings is a cost-effective method of improving traffic flows along urban arterials. Proper signal timings can significantly enhance primary mobility metrics (delay and stops), and significantly improve traffic safety and sustainability measures (Fuel Consumption 'FC' and Vehicular Emissions 'VEs'). The last decade has seen a growing concern to minimize traffic sustainability measures through various transportation applications. The overarching theme of this research is to develop a framework for signal timing optimization to improve traffic sustainability measures. The research first developed an Environmental Performance Index (Env-PI) as a linear relationship between delay and stops with a variable "*K*" (aka stop penalty) that assigns an FC weight to each stop. In addition, the research investigated individual impacts of multiple operating conditions (e.g., vehicle type, speed) on stop-induced FC and *K*, in simulation environment. The results showed that various operating conditions affect the *K* differently. Consequently, the research then explores the compound influence of those conditions on the *K* value, but this time from both FC and VEs perspectives. The outcomes of such experiments indicated that the *K* varies significantly for various combinations of conditions and sustainability metrics, suggesting that minimizing FC does not necessarily minimize all VEs. The research subsequently developed predictive models for the FC-based *K*s utilizing FCs collected from a large vehicular fleet from the field. The models' estimates are shown to be very accurate; hence, they are used to validate the simulated *K* values obtained in the earlier research stages. The findings

revealed that the simulated *K*s strongly correlate with the field *K*s; thus, simulated *K*s are credible to be implemented in signal optimization practice. In the next step, the FC-PI was deployed as an objective function to optimize signals on a corridor with 13-signalized intersections. The results show that FC-PI could achieve significant FC and VEs savings. Finally, this research proposed a methodology to integrate the effect of all deceleration-acceleration events (both full and partial stops) in the Env-PI to increase its accuracy. Collectively, this research is a significant step to facilitate a novel practical approach to optimize signal timings to reduce FC and VEs.

Table of Contents

List of Tables

List of Figures

Nomenclature

AFCM	Analytical Fuel Consumption Model
AIMSUN	Advanced Interactive Microscopic Simulator for Urban and Non-Urban Networks
ATSPM	Automated Traffic Signal Performance Measures
AVENUE	Advanced & Visual Evaluator for road Networks in Urban arEas
CAVs	Connected and Autonomous Vehicles
CMEM	Comprehensive Modal Emission Model
CO	Carbon monoxide
CO_2	Carbon dioxide
CORSIM	Core Simulation and modeling traffic software
CSSP	Cruising Speed Stop Profile
CTM	Cell Transmission Model
DB	Driving Behavior
DTW	Dynamic Time Warping
DynaTAIWAN	Dynamic simulation-assignment model
Env-PI	Environmental Performance Index
FC	Fuel Consumption
FR	Fuel Rate
FZP	Fritzing Part file (vehicle record file from Vissim)
GA	Genetic Algorithm

HC	Hydrocarbons
HCM	Highway Capacity Manual
HDDV	Heavy-Duty Diesel Vehicle
HGV	Heavy Goods Vehicle
HW	Head Wind
ICE	Internal Combustion Engine
IDM	Intelligent Driver Model
LC DOT	Lake County, Division of Transportation
LDT	Light-Duty Truck
LDV	Light-Duty Vehicle
LWR	Lighthill-Whitham-Richards models
MAF	Mass Air Flow
Matlab	MATrix LABoratory (a proprietary multi-paradigm programming language and numeric computing environment developed by MathWorks.)
MGGP	Multigene Genetic Programming
MOVES	Motor Vehicle Emission Simulator
NOx	Nitrogen oxides
OVM	Optimal Velocity Model
PATH	Partners for Advanced Transportation Technology (microscopic traffic flow model)
PCU	Passenger Car Unit
PI	Performance Index
PMs	Particulate Matters

Python	Interpreted high-level general-purpose programming language
RBC(D)	Ring Barrier Controller (Diagram)
SATURN	Simulation and Assignment of Traffic to Urban Road Networks
SUMO	Software Update Monitor
Synchro	Traffic Engineering Software Package
TRANSIMS	TRansportation ANalysis SIMulation System
TRANSYT-7F	Traffic Network Study Tool, version 7F
TW	Tail Wind
Vissim	Verkehr In Städten – SIMulationsmodell (a microscopic multi-modal traffic flow simulation software)
Vistro	Vision Traffix and Optimization
VOC	Volatile Organic Compound
VT-CPFM	Virginia Tech Comprehensive Power-based Fuel Consumption Model
VT-Micro	The Virginia Tech Microscopic emission model
WCSS	Within-Cluster Sum of Squares

1.0 Introduction

Every year, the world typically adds 51 billion tons of greenhouse gas emissions (e.g., CO_2) (Gates, 2021). Those emissions contribute to global warming and cause deadly effects (e.g., heatwaves, severe rainstorms, droughts, etc.). According to the Environmental Protection Agency (EPA), transportation constitutes about 30% of total U.S. greenhouse emissions in 2019, where 18% came from light-duty vehicles (EPA, 2019a). That is significantly caused by the increasing growth of traffic demand combined with the capacity limitations of existing transportation network infrastructures, which increased the consumption of fossil fuels over the last few decades. In addition to the negative impact on the environment, an increase in fuel consumption affects both human health (by increasing harmful pollutants) and the economy (increases transportation expenditures). Thus, there has been a long-standing interest in reducing fuel consumption and vehicular emissions in the transportation sector.

Road intersections are primary fuel consumption and emission hotspots because they entail long idling times and many deceleration-acceleration events. One of the most practical and cost-beneficial ways to enhance traffic progression and make urban streets safer is to coordinate traffic by performing signal timings optimization (Webster, 1958; Robertson, 1969). Efficient traffic movements on urban arterials are achieved through minimal delay and stop-and-go events. Additionally, proper signal retiming saves time for emergency vehicles, reduces the number of incidents, better utilizes transportation facilities' current capacity, reduces fuel consumption and vehicular emissions (Sunkari, 2004). This research is concerned explicitly with reducing fuel consumption and vehicular emissions caused by traffic signals.

1.1 Problem Statement

One of the first serious efforts to optimize signal timings was made by Webster, 1958 who developed a method to optimize signal timings by minimizing vehicular delay (as the primary objective function), which became the basis for almost all of the similar subsequent studies. The problem with such an objective function is that it can significantly increase the number of stops. That is because minimizing delay at signalized intersections requires a short cycle length where all movements are served with green time as quickly as possible. Such a short cycle length will likely force most vehicles to stop before passing the intersection. More stops means higher fuel consumption due to frequent changes in deceleration-acceleration levels (Rakha and Ding, 2003). To solve this issue, Robertson, 1969 developed the performance index (PI) – a composite measure representing a linear function of delay and number of stops - to judge the quality of a set of signal timings. The PI is calculated as: PI = Delay + *K* (number of stops), where *K* represents a weighing factor equals zero if the PI is equal to the total delay, whereas positive values of *K* add a penalty for each stop due to signal operations.

The oil crisis of the early '70s raised concerns about the amount of fuel consumed in traffic. This concern had spread to all traffic operations segments, and it eventually raised the question of how signalized intersections can be accommodated to minimize fuel consumption. Consequently, a few studies assessed the impact of traffic signals on fuel consumption rates (Claffey 1971; Bauer 1975; Courage and Parapar 1975; Lieberman and Cohen 1976; Cohen and Euler 1978; Hurley Jr and Ball, 1979). In a significant study conducted by Robertson et al., 1980, the PI was an effective objective function to balance delay and fuel consumption in signal timing optimization. One year later, Akcelik, 1981 derived the *K*-factor for three fleet distributions (light vehicles, heavy vehicles, and composite fleet with 10% of heavy vehicles) and a cruising speed of 60 km/h. Although the results show that the *K*-factor varies for different fleet distributions, no efforts were made to investigate the factors impacting its value.

Based on the *K* values tested and derived by Robertson et al., 1980 and Akcelik., 1981, one can observe that the *K*-factor seems to range anywhere from 2 to 104 seconds. Hence, it can be concluded that higher values of the *K*-factor were attributed to various vehicular and driving characteristics that would increase the fuel consumption of the vehicles stopped at the intersections. Although those two studies (Robertson et al., 1980; Akcelik., 1981) recognized that *K* value (calibrated to lead to minimal fuel consumption) varies significantly based on several factors, such factors were never adequately investigated, nor was a variable *K* incorporated in the signal retiming practice. Furthermore, the consensus of the current practice in signal optimization is problematic as it uses a low and constant *K*-factor for all PI calculations. For example, Synchro (Husch and Albeck, 2008) is one of the major signal optimization tools that have been used in the US practice in the past few decades. Synchro uses the PI as the major objective function for network signal optimization, and it uses a constant value of 10 for the *K*-factor. Such value does not reduce fuel consumption as shown in previous studies (Robertson et al., 1980; Akcelik., 1981).

1.2 Research Goal and Objectives

This research addresses a gap in the crucial piece of knowledge on the importance of the *K*-factor; that is, to confirm that the *K* is a function of multiple operational factors and explain how such factors impact the *K*-factor. Thus, the primary hypothesis of this research is that by considering various operating conditions (driving and road) when estimating *K*-factor for signalized intersections, various *K* values will be obtained, and there will be different trade-off points for delays and stops for various operational conditions. This hypothesis can then be branched out to develop multiple Environmental Performance Indices (Env-PIs) to reduce fuel consumption and vehicular emissions for different operating conditions. **This research aims to develop a family of environmental performance measures to be used in signal timing optimization to minimize fuel consumption and vehicular emissions**. This goal is achieved through a few research objectives, which are:

1. Develop an analytical model to compute a correct value of the stop penalty and investigate, through simulation experiments, the individual impact of various operating conditions on stop-related fuel consumption and stop penalty's value.
2. Derive a series of simulated emission-based stop penalties.
3. Validate simulation results using fuel consumption measurements from the field and develop a multi-dimensional relationship between various operational conditions and the stop penalty.
4. Optimize traffic signal plans to reduce fuel consumption and emissions using the developed environmental performance measure.
5. Integrate the impact of deceleration-acceleration events and multiple stops in the Env-PI.

1.3 Organization of the Dissertation

This dissertation is divided into seven chapters. Chapter 1 – Introduction provides preliminary broad background information on the importance of traffic signal control, especially in the ongoing interest in creating a more sustainable environment. The problem statement is then defined. Finally, the goal and objectives of the research are identified. Chapter 2 investigates the impacts of various operational Conditions on fuel consumption and stop penalty at signalized intersections. Considering that Chapter 2 dealt mainly with fuel consumption estimates, Chapter 3 focused on health-related emission types by studying the effects of different operating conditions on simulated emissions-based stop penalty at signalized intersections. Chapter 4 develops field-based prediction models for stop penalty in traffic signal timing optimization. Chapter 5 optimizes traffic signal timings based on FC-PI - as a surrogate measure for fuel consumption. Chapter 6 covers the impact of deceleration-acceleration events on the Env-PI. Finally, Chapter 7 provides the conclusions, findings, and recommendations of this research.

2.0 Investigating Impacts of Various Operational Conditions on Fuel Consumption and Stop Penalty at Signalized Intersections

This chapter has been published as:

Alshayeb, S., Stevanovic, A., & Effinger, J. R. (2021). Investigating Impacts of Various Operational Conditions on Fuel Consumption and Stop Penalty at Signalized Intersections. *International Journal of Transportation Science and Technology*.

When optimizing signals relevant traffic agencies adopt policies to either improve mobility performance measures (e.g., delay and stops), environmental aspects, or safety of signalized intersections. One of such policies, mainly implemented through so-called Performance Index (PI), advocates that reduction of excess fuel consumption should be achieved by minimizing the PI - a linear combination of delays and stops. The key factor of such a PI is the stop penalty "*K*", which represents a weighting factor, or a stop equivalency measured in seconds of delay. In the contemporary signal optimization practice, this *K* is given a constant value (e.g., 10 seconds) and it is not recognized as a parameter that is dependent on various operational conditions. This Chapter challenges that common view and presents a methodology to derive the *K*-factor and investigate impacts of various operational conditions (e.g., cruising speed) on the *K* value. The Chapter uses traffic simulation model coupled with a modal fuel consumption and emission model to investigate second-by-second fuel consumption during stopping events at a signalized intersection. The experiments are performed on a hypothetical, yet realistic, intersection under several operational scenarios. The findings show that the *K* varies significantly with all the investigated operational conditions. More importantly, results indicate that the *K*-factor should be much larger than used by current signal timing practices. The implications of these findings may lead to significant changes in current polices for signal timing optimization. Chapter 4 validates these findings with second-by-second vehicle trajectory and fuel consumption data from the field.

2.1 Introduction

Fuel consumption from the transportation sector accounts for about 30% of total US greenhouse emissions (EPA, 2019a). Intersections along urban arterials contribute significantly to those 30% because they entail queuing conditions and many stop-and-go events, making intersections one of the primary spots where excess fuel is consumed. The increase in fuel consumption also brings harmful impacts to the environment, contributing to climate change by increasing outputs of carbon dioxide (CO_2) in the Earth's atmosphere and to human health by increasing levels of particulate matters (PMs) and other harmful pollutants (McMichael et al., 1996).

Multiple studies have confirmed that traffic signal optimization is one of the effective ways to increase the capacity of existing urban networks (Webster, 1958, Robertson, 1969, Sunkari, 2004). The prevailing method to optimize traffic signals (to achieve efficient traffic movements on urban arterials) is by minimizing delay and the number of stops. Prior research studies substantiate a belief that minimizing number of stops reduces fuel consumption, considering that most of the excess fuel is consumed during deceleration-acceleration phases of a stopping event (Rakha & Ding, 2003, El-Shawarby et al., 2005). However, while minimizing delay does not necessarily minimize number of stops, it does reduce fuel consumption of vehicles when their engines idle during the waiting time in a queue.

The oil crisis of the early '70s attracted a few researchers to address how signalized intersections can be accommodated to minimize fuel consumption. Consequently, a few studies assessed the impact of cycle length on fuel consumption. Bauer, (1975), Courage and Parapar, (1975), and Hurley Jr and Ball, (1979) showed that the cycle length required to minimize fuel consumption is longer than the one needed to minimize delay. Hence a balance between delay and number of stops should be made not only to balance between mobility metrics (delay and stop), but also to reduce fuel consumption. In contrast, Cohen and Euler, (1978) concluded that delay, fuel consumption, and emissions are all minimized at the same cycle length value. Nevertheless, these research efforts were based on field measurements without identifying factors (e.g., speed, grade, driving behavior), which impact extra fuel consumption from stopping at signalized intersections (Claffey, 1971, Claffey, 1977).

Several studies (Kwak et al., 2012, Liao 2013, Zhao et al., 2018) proposed optimization models to find a right balance between delay and number of stops when optimizing traffic signal settings. However, the Performance Index [PI = Delay + *K* (number of stops)] developed by Robertson, 1969 is still one of the most popular objective functions, and heavily used in the contemporary traffic signal optimization practice (Husch and Albeck, 2008). One of the reasons for such a wide use of the PI is that it can be adjusted to achieve an optimal outcome for one of the three primary performance measures used in most of the traffic signal retiming policies: delay, number of stops, and fuel consumption. The PI enables policy makers to define how much weight (known as a *K*-factor or stop penalty) to give to each of these measures, to achieve the optimal traffic signal operations. A value of zero *K* is used when only delay is supposed to be minimized. In contrast, positive values of *K* add a penalty (measured as an equivalent delay) for each stop due to signal operations. For example, Robertson, 1969 used a *K* factor of 8 seconds in his original study. However, he concluded that the *K* value could be chosen to achieve any desired balance between delay and number of stops.

The utilization of the stop penalty (*K*) to reduce fuel consumption was proposed by a few studies (Courage and Parapar, 1975, Robertson et al., 1980, Akcelik, 1981). In that case, the *K* value represents a weighting factor of a number of seconds of delay equivalent to a stop from a fuel-consumption perspective. Courage and Parapar, (1975) and Akcelik, (1981) defined *K*-factor in a way that it depends on the fuel consumed during the deceleration, idling, and acceleration phases of a stop-and-go event (discussed in Section 2.2). Hence, one could conclude that factors impacting fuel consumption during the driving phases of a stop-and-go event (e.g., vehicle type, fleet distribution, and road gradient) also impact the *K* value.

To the best of the author's knowledge, there have not been research efforts to address individual impact of various operational conditions (road and driving) on the *K* value. Moreover, both studies (Courage and Parapar, 1975, Akcelik, 1981) that computed *K*-factor did not provide an exact analytical expression on how to calculate the *K* value. Therefore, this Chapter addresses these shortcomings by presenting a comprehensive methodology to derive the *K*-factor and by investigating the impact of various operational conditions factors on *K* value. To test the proposed methodology, traffic simulation Vissim (PTV Vissim, 2020) was used to generate vehicles' trajectories from a set of scenarios with various operational conditions, which were then used to estimate fuel consumption from the Comprehensive Modal Emission Model (CMEM) (An et al., 1997). Although other models could have been used to model traffic (e.g., Aimsun) and fuel consumption (VT-Micro), Vissim and CMEM were selected because of their flexibility and compatibility with each other. More information about Vissim and CMEM are given in Sections 2.4.2 and 2.4.3. The results of this chapter constitute a basis for the following chapters, which aim to develop a new methodology to properly integrate various K values into signal timing optimization practice to address environmentally driven signal retiming policies.

The rest of the chapter is organized as follows: Section 2 describes the relevant literature. Section 3 presents the major operational conditions which impact vehicular fuel consumption and the K value. Section 4 presents the methodology. Section 5 discusses the experimental results, whereas Section 6 summarizes the Chapter and provides conclusions.

2.2 Literature Review

This section summarizes the most relevant studies addressing the computation and evaluation of the K-factor and gives an overview of a few other studies that proposed similar performance indices to the one developed by Robertson, 1969. It should be noted that none of the studies reviewed below have explicitly provided a mathematical expression to compute the K-factor. Therefore, all equations provided here are interpretations of how they calculated the K-factor, based on the descriptions provided by those studies.

Courage and Parapar, (1975) used TRANSYT model and its PI objective function (Robertson, 1969) to investigate the impact of cycle length on two groups of PIs – those that reduce delay and those that reduce fuel consumption. The authors calculated the K value by dividing the fuel consumed per one-stop (including fuel consumption during deceleration, idling, and acceleration phases) by the fuel consumed during one hour of idling converted to one second as shown in Equation 2.1.

$$K = 3600 \cdot \left(\frac{FC_S}{FC_I}\right) \tag{2.1}$$

Where:

K – stop penalty [seconds].

FC_S – fuel consumption per vehicle stop [gallon].

FC_I – fuel consumption per vehicle-hour idling [gallon/veh-hour].

3600 – a conversion factor to obtain K value equivalent to a number of seconds (instead of hours) of delay from fuel consumption perspective.

Courage and Parapar, (1975) computed the stop penalty using fuel measurements collected in field by Claffey, (1971) for 30-mph cruising speed and level terrain. As a result, a constant K value of 60 seconds was derived and used to compute the PI. The same authors recognized the impact of various speeds on the K-factor, but they assumed that such impacts can be neglected. Their conclusion could be attributed to the fact that they did not possess high-resolution trajectory and fuel consumption data. In summary, their research showed an apparent trade-off between travel delay and fuel consumption in the signal optimization problem, which can be achieved by adjusting the K value.

Robertson et al., (1980) investigated the impact of various K values (0, 2, 5, 10, 20, 50, and 100 seconds) on the delay and fuel consumption on several coordinated signals in Glasgow. The authors found that fuel consumption can be reduced by 6-8% when signals are optimized to reduce delay, exclusively (K=0). They also recommended fuel consumption-driven K of 20 seconds to make a proper trade-off between delay and stops and achieve an additional 3% reduction in fuel consumption with no tangible increase in delay. This influential work set the stage for PI to become a standard performance measure not only when fuel consumption minimization is sought but in general when signal timings are optimized (Husch and Albeck, 2008; PTV Vistro, 2014). The main drawback of this research's conclusion is that it did not consider or mention the impact of other operational and driving factors on the *K*.

Akcelik, (1981) rederived the *K* by dividing the fuel consumption during deceleration and acceleration phases by the idling fuel rate during the stopped delay time at the signal as shown in Equation 2.2. It should be noted that Akcelik subtracted excess fuel consumed due to delay contribution of the deceleration and acceleration phases of the stopping event. This approach seems slightly more accurate from the other efforts (e.g., by Courage and Parapar, 1975) because it made a better distinction between stops and delay through their equivalent fuel consumption(s). This distinction was not 100% accurate because Akcelik combined fuel consumption associated with delay caused by the deceleration and acceleration and fuel consumption during idling (stopped delay). Deriving the *K*-factor in this way was mainly driven by the need to combine fuel consumptions from all delays to suit the elemental fuel consumption model proposed in the same study. The *K* value was derived for three fleet distributions (light vehicles, heavy vehicles, and composite fleet with 10% of heavy vehicles) and a cruising speed of 60 km/h, which resulted in *K* values of 54, 104, and 60 seconds, for the three respective fleet distributions.

$$K = 3600 \cdot \left(\frac{FC_S - (FC_I \cdot d_s) - (FC_I \cdot d_h)}{FC_I} \right) \tag{2.2}$$

Where:

K – stop penalty [seconds].

FC_S – fuel consumption per vehicle stop [liter].

FC_I – fuel consumption per vehicle-hour idling [liter/veh-hour].

d_s – stopped delay [hour].

d_h – deceleration-acceleration delay [hour].

3600 – a conversion factor to obtain K factor in seconds.

Akcelik used Equation 2.2 to calculate *K*-factor based on various field measurements of fuel consumption from different studies (Claffey, 1971, Claffey, 1977, Courage and Parapar, 1975, Dart and Mann, 1978, Robertson, 1980). He found that *K* value varies from 26 to 228 seconds. Such a wide range can be explained by the fact that various elements that impact fuel consumption at a signalized intersection were included in various data sets but not recognized as such. For example, while the value of *K* strongly depends on the vehicle type and vehicle engine, it is also a function of other factors (e.g., driving behavior/aggressiveness, road gradient, cruising speed).

In the past few decades, various performance indices (like the one developed by Robertson, (1969)) have been proposed. Reljic et al. (1992) proposed a PROMETHEE-based optimization procedure to optimize signal plans for various objective functions, including a fuel-consumption function as a linear combination of delays and stops, with a *K* value equal to 20 seconds, as recommended by (Robertson et al., 1980). Oda et al. (2004) optimized signals to reduce CO_2 using the same PI from Robertson (1969), but with weights applied both for delay and number of stops, instead of just one weight for the number of stops. Li et al. (2004) developed an optimization model to minimize a newly proposed performance index as a weighted sum of three objectives: delay, fuel consumption, and emissions. Although those last two studies (Oda et al., 2004, Li et al., 2004) extended the concept of weighting stops against delay, they did not derive or mention how much weight should be given to each stop in terms of fuel consumption or emissions.

To summarize, several studies considered this topic before but none of them made any comprehensive efforts to investigate what factors could have impact on the stop penalty and fuel consumption at signalized intersections. Moreover, various signal timing policies claim that reducing fuel consumption is one of the primary goals of traffic signal optimization (Gordon, 2010; Urbanik et al, 2015). However, using a low and constant value of the *K*-factor, makes such policies unsubstantiated. To address these shortcomings in the body of existing knowledge, this chapter addresses that matter by exploring the individual influences of various operational conditions (vehicle type, fleet distribution, driving behavior, road gradient, cruising speed, and wind effect) on the stop-related fuel consumption and *K*-factor.

2.3 Major Factors Impacting Stop-Related Fuel Consumption

Vehicular fuel consumption depends on numerous factors (Claffey, 1971, Redsell et al., 1993) which can be broadly classified in six categories: vehicle-related, traffic-related, travel-related, driver-related, roadway related, and weather-related factors (Ahn et al., 2002). In the recent years, few studies (Mock, 2012, Zhou et al. 2016) attempted to define further subcategories, summarized in Figure 2.1, and their impact on fuel consumption.

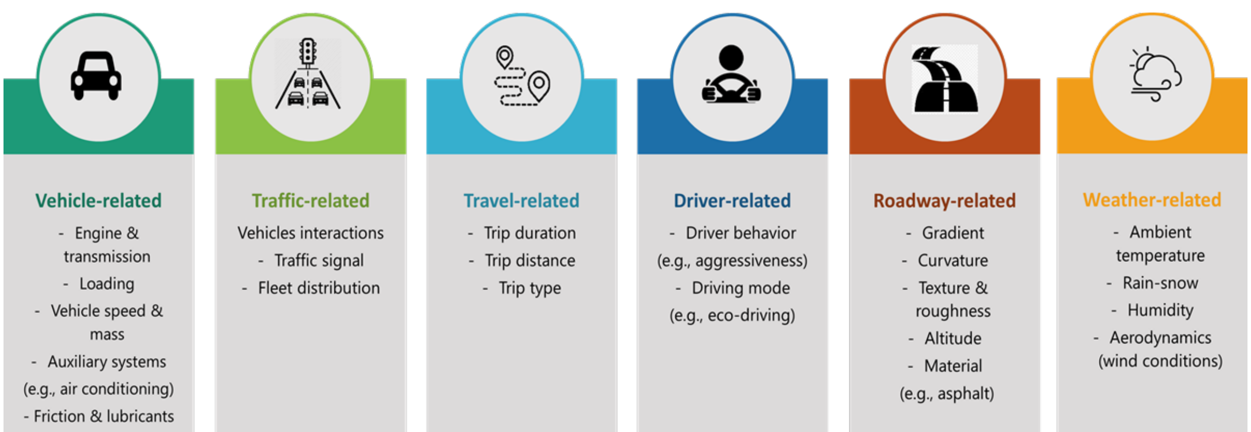

Figure 2.1 Variable effects of influencing factors on fuel consumption.

According to those impacts, the major factors affecting fuel consumption during a stop at a signalized intersection considered in this Chapter are summarized below. It should be noted that the list of factors selected is not inclusive and it presents factors with major impact on fuel consumption caused by stopping at signalized intersection.

1. Distribution of vehicular types and engines: vehicle mass, engine power, fuel used per engine's displacement, and the engine efficiency (to transfer the power to the wheels) are important factors affecting fuel consumption during acceleration (National Research Council, 2011). With all other factors being equal, higher vehicle masses and ability to achieve faster acceleration increase fuel consumption, which increases the value of *K*. It should be noted that vehicles with start-stop technology (vehicles that shut engine off while idling) are out of the scope of this research. Still, those vehicles can be integrated in the methodology presented in Section 2.4. That can be done be giving a constant value of K (e.g., 10 seconds) for those vehicles until future research proposes a methodology to compute the stop penalty based on the energy used while idling (e.g., fuel used to turn engine on).
2. The proportion of heavy vehicles in fleet distribution (Kaisar et al., 2019): as the amount of fuel consumed depends on the vehicle type and engine, it is logical to expect that vehicular fleets composed of various proportions of light-duty vehicles (LDVs) and heavy-duty diesel vehicles (HDDVs) will result in different fuel consumptions, hence yielding to a variety of *K* values.
3. Driver's behavior: the amount of fuel consumed depends significantly on the individual driver's driving habits. Injection of an extra (fuel/gasoline) into the engine occurs when one applies a sudden momentary thrust with the acceleration pedal (Claffey, 1977). Such behavior will, therefore, cause higher fuel consumption during the acceleration phase, resulting in a higher *K*.

4. Road gradient: fuel generally increases when vehicles travel uphill and have to combat gravity. On the other hand, potential energy is added to the engine's kinematic energy when traveling downhill; thus, less fuel is required for downhill-travelling vehicles to achieve the cruising speed (Claffey, 1971), resulting in a lower *K*.
5. Cruising speed: additional fuel needed to accelerate to the original speed of travel depends principally on the original cruising speed, which is a factor of the speed limit. For a stopping event, a deceleration from a higher speed to zero, followed by acceleration again to the original cruising speed, yields to a higher excess fuel consumption (Rakha and Ding, 2003) (resulting in a higher *K*) than when the original speed is lower.
6. Wind effect: wind also impacts effective speed of a moving vehicle, based on its direction (components of headwind and tailwind) and intensity. A vehicle accelerating upwind/downwind will consume more/less fuel than a vehicle accelerating without wind. This effect is most profound for trucks, whose fuel consumptions can vary remarkably in conditions with either headwind or tailwind (Heide and Mohazzabi, 2013). This research considers the wind effect on fuel consumption of heavy vehicles because it was feasible to model such effect in CMEM. In addition, the wind effect is most important for trucks because of their large frontal and rear areas and heavy mass.

2.4 Methodology

When a vehicle stops at a signalized intersection, it must go through three driving phases. Firstly, the vehicle decelerates from its original cruising speed to zero (deceleration phase). Secondly, the vehicle waits for the signal to turn green, during which time the vehicle's engine idles (idling phase). Thirdly, once the signal turns green, the vehicle accelerates from zero to its cruising speed (acceleration phase). Those three phases form the concept of the "Cruising Speed Stop Profile" (CSSP), where cruising speed after acceleration is assumed to be the same as before the deceleration phase. Figure 2.2c) shows three of such profiles for cruising speeds of 30, 40, and 45 mph. It can be stated that for a CSSP, the total amount of fuel consumed is:

$$FC_{CSSP} = FC_D + FC_I + FC_A \tag{2.3}$$

Where:

FC_{CSSP} – total fuel consumed during a CSSP [gallons, liters, or grams].

FC_D – fuel consumed during the deceleration phase; [same unit as FC_{CSSP}].

FC_I – fuel consumed during the idling phase; [same unit as FC_{CSSP}].

FC_A - fuel consumed during the acceleration phase; [same unit as FC_{CSSP}].

Figure 2.2 shows other relevant profiles of a vehicle making a stop at a signalized intersection. Figure 2.2a) shows a vehicular trajectory in a time-distance domain. Figure 2.2c) and Figure 2.2e) show how speed and acceleration vary over time during a CSSP, respectively. Finally, Figure 2.2g) depicts the most interesting relationship – how instantaneous fuel consumption changes over time during a CSSP. This part of Figure 2.2 will be in the focus to explain how such a CSSP can be used to accurately compute the relevant *K*-factor. It should be noted that although Figure 2.2a), Figure 2.2c), Figure 2.2e), and Figure 2.2g) represent trajectory and relevant data for a simulated vehicle, such data series are very similar to the actual field data as shown in Figure 2.2b), Figure 2.2d), Figure 2.2f), and Figure 2.2h).

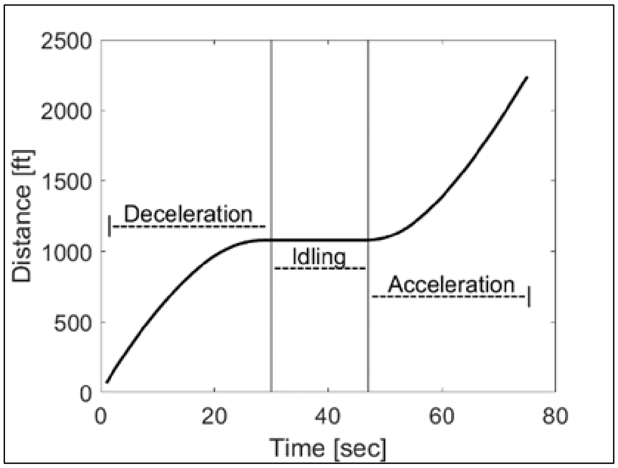

a) Simulated stop profile

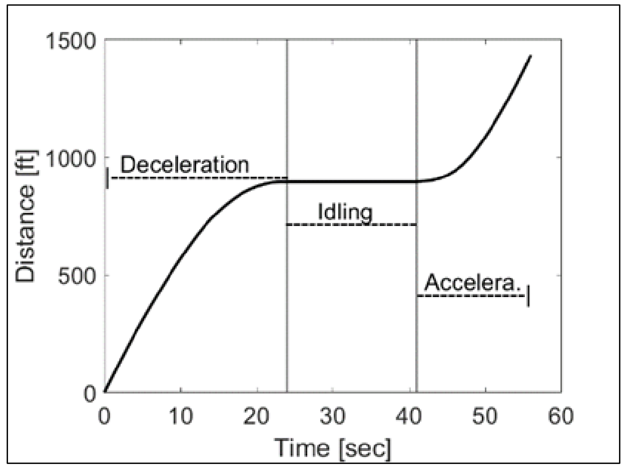

b) Field stop profile

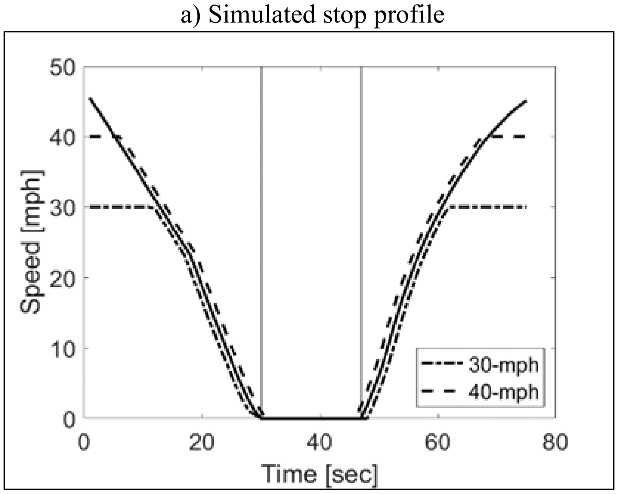

c) Simulated speed profile

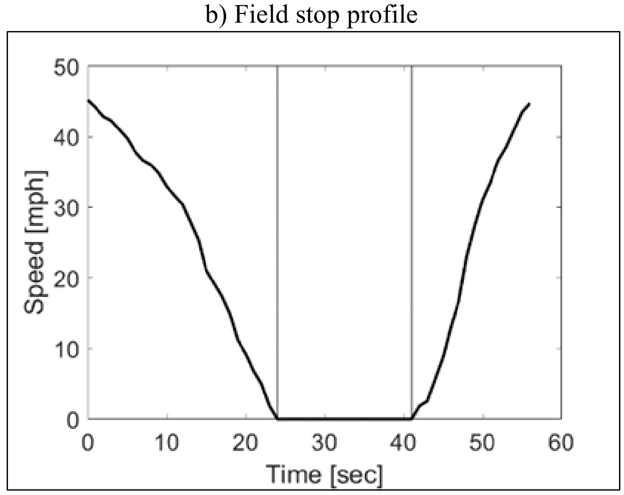

d) Field speed profile

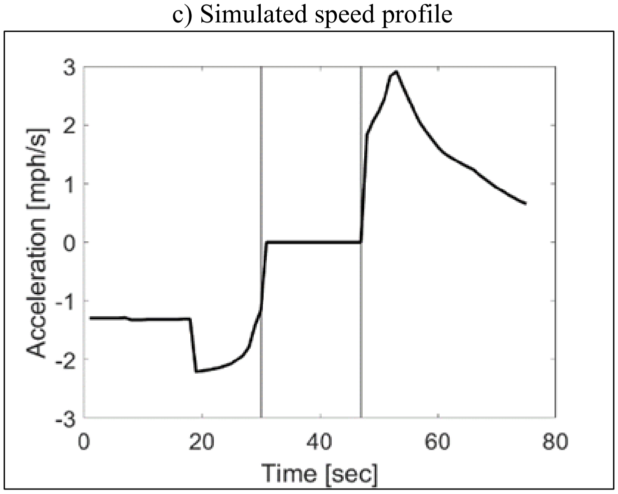

e) Simulated acceleration profile

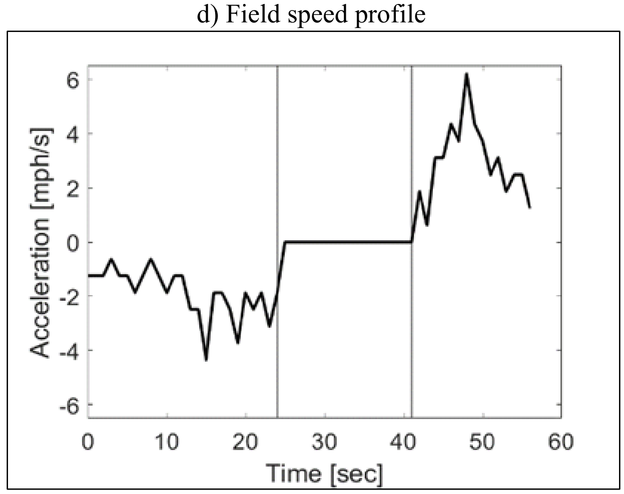

f) Field acceleration profile

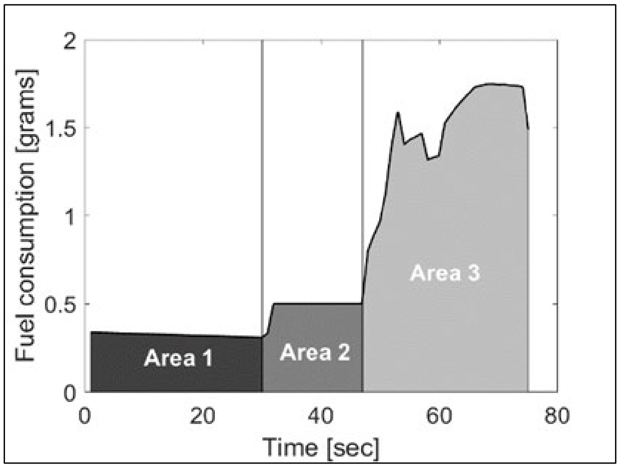

g) Simulated fuel consumption profile

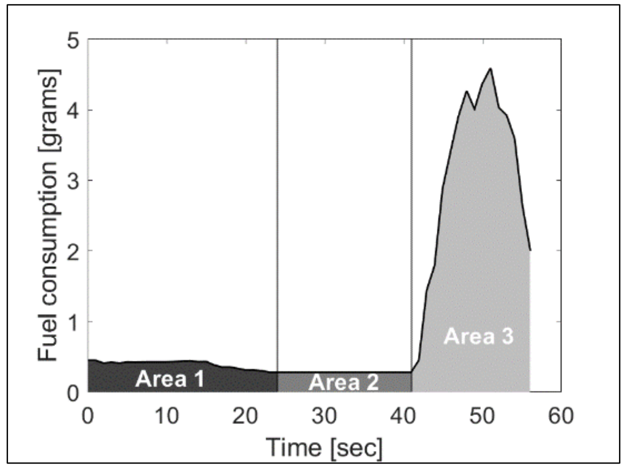

h) Field fuel consumption profile

Figure 2.2 Dynamics and kinematics of vehicular stops at a 45-mph cruising speed.

Figure 2.2g) and Figure 2.2h) show that stopping at an intersection will also induce fuel consumption during the idling phase, but this part of the fuel consumption should be attributed to the concept of stopped delay, as it is important to separate 'delays' from 'stops', the two commonly used traffic performance measures for signalized intersections. Such a separation is needed because the delay during idling (or waiting time) in queue at traffic signal (referred to as stopped delay hereafter) can be extended over a long time depending on the red interval, and it is related to specific signal timing parameters (cycle length and split), which are different from those which are more impactful on the actual stops (consisting of only acceleration and deceleration, and associated delays). On the other hand, deceleration and acceleration are associated with the action of stopping (referred to as a stop hereafter), which is related to those signal timing parameters that mainly impact traffic progression (e.g., offset and phase sequence). Therefore, while developing a methodology to understand fuel consumption during the entire process of a CSSP, this study separates extra fuel consumption attributed to the stop from that attributed to stopped delay. For this reason, it is vital to observe fuel consumption experienced under each CSSP regime, as shown by various areas under the fuel consumption rate curves shown in Figure 2.2g) and Figure 2.2h). Based on Figure 2.2g) and Figure 2.2h), one can conclude that a stop is equivalent to stopped delay, from fuel consumption perspective, only if:

$$FC_D + FC_A = K_e \cdot FC_I \tag{2.4}$$

Where: K_e is fuel-consumption equivalency factor between stops and delays. Then we get:

$$K_e = \frac{FC_D + \ FC_A}{FC_I} \tag{2.5}$$

The K_e from Equation 2.5 is a unitless number representing ratios of fuel consumptions (those associated with the stop and others associated with the stopped delay). The idling phase duration depends significantly on the red interval's length. Therefore, in order to assign a weight value that represents a number of seconds of stopped delay equivalent to a stop, from a fuel-consumption perspective, FC_I is divided by the total idling time (seconds) (T_I) to obtain a stop-penalty K [sec]:

$$K = \frac{FC_D + \ FC_A}{\frac{FC_I}{T_I}} \tag{2.6}$$

To consider the fact that most of vehicular fleets consist of both LDVs and HDDVs, the stop penalty of a fleet (K_{fleet}) can be expressed as shown in Equation 2.7 below, where p is the percentage of HDDVs (%) in the fleet:

$$K_{fleet} = \frac{(1-p)(FC_D + \ FC_A)_{LDVs} + p(FC_D + \ FC_A)_{HDDVs}}{(1-p)\left(\frac{FC_I}{T_I}\right)_{LDVs} + p\left(\frac{FC_I}{T_I}\right)_{HDDVs}} \tag{2.7}$$

Although K_{fleet} value, as calculated by Equation 2.7, may include a minor error due to impact of accelerations and decelerations of mixed-fleet vehicles, such error is neglected at this point for two reasons: 1. The potential error is applied systematically across all intersection movements, thus making the relative importance of each movement's *K* similar to their true values, 2. The magnitude of impact of such an errors on the *K* is estimated to be much smaller than the error which is being addressed (e.g. in current practice, the adopted *K* values are several times lower than the true value).

Figure 2.2g) and Figure 2.2h) show instantaneous (second-by-second) fuel consumed during each of the three driving phases of a CSSP. The area under the fuel consumption rate curve, shown in Figure 2.2g) and Figure 2.2h), represent the total fuel consumed during a CSSP for a particular vehicle under specific operational conditions (e.g., cruising speed, road gradient). Thus, Area 1, Area 2, and Area 3, shown in Figure 2.2g) and Figure 2.2h), represent the fuel consumptions during the deceleration, idling, and acceleration phases, respectively. Areas 1-3 can be computed as the integration of the fuel consumption rate curve between any two time points t_1 and t_2:

$$FC = \int_{t1}^{t2} FR(t) \cdot dt \tag{2.8}$$

This chapter focuses on modeling second-by-second fuel consumption measurements from CMEM, in which case the area under the curve can be approximated by using an appropriate discretization:

$$FC = \sum_{i=1}^{n} FR(i) \cdot \Delta_i \tag{2.9}$$

Where:

FC – total fuel consumed within n elementary intervals of Δi.

FR(i) – fuel consumption rate (vary with *i*).

Δi – elementary time interval.

The *FR* modeling in CMEM (An et al., 1997) reads as:

$$FR(t) = \emptyset(t).(K(t).N(t).V + \frac{P(t)}{\mu}).\frac{1}{44} \quad (2.10)$$

Where:

FR(*t*) – fuel rate [grams/second].

$\emptyset(t)$ – stoichiometric fuel/air equivalence ratio.

K(*t*) – the engine friction factor.

N(*t*) – engine speed [revolutions/seconds].

V – engine displacement [liter].

P(*t*) – engine power output [kW].

μ – a measure of indicated efficiency [default value is 0.4].

44 – the lower heating value of typical gasoline [kJ/gram].

For any given CSSP, *K* value depends significantly on the fuel consumption during the acceleration and deceleration phases. One can observe from Figure 2.2e), Figure 2.2f), Figure 2.2g) and Figure 2.2h) that fuel consumption is the lowest during deceleration, followed by idling, whereas much higher fuel consumption is observed during acceleration. In summary, it can be stated that the main operational conditions that increase the extra fuel consumption due to a stop caused by a traffic signal are the ones that cause higher fuel consumption during the acceleration phase, and/or longer time required to make a complete stop. That is because the extra fuel consumption during the deceleration phase mainly depends on the duration of the stopping process, which depends on several factors, including the driver's behavior and the traffic dynamics in front of the stopping vehicle. Thus, regardless of how small the fuel consumption (per unit of time) during deceleration is, longer deceleration times consume more fuel. Therefore, the methodology, developed in this Chapter, to estimate the impact of various factors on *K* value incorporates modelling scenarios, in Vissim and CMEM, which include various factors to determine different values of excess fuel consumption for various operational conditions.

2.4.1 Various Variables of Operational Conditions Impacting Fuel Consumption

When investigating the individual impact of a particular factor (e.g., vehicle type) on fuel consumption, all other factors (e.g., cruising speed, road gradient, fleet distribution, driver behavior, and wind speed) were kept constant, at their default values (discussed in Section 2.4.4.3). A total of 74 experiments were designed to cover a wide range of variables for each of the investigated operational condition factors. Table 2.1 shows a summary of the variables that were tested individually for each investigated factor.

Table 2.1 Variables for various operational conditions impacting fuel consumption.

Vehicle type		**Fleet distribution**	**Driver behavior**	**Road gradient**	**Cruising speed**	**Wind effect**
CMEM	This Chapter	LDV: HDDV	Acceleration functions	(%)	(mph)	(mph-direction)
Category-4	LDV1	100:0	Func1	-7	20	50 tailwinds
Category-5	LDV2	99:1	Func2	-6	25	40 tailwinds
Category-6	LDV3	98:2	Func3	-5	30	30 tailwinds
Category-7	LDV4	97:3	Func4	-4	35	20 tailwinds
Category-8	LDV5	96:4	Func5	-3	40	10 tailwinds
Category-9	LDV6	95:5	Func6	-2	45	No wind
Category-10	LDV7	94:6	Func7	-1	50	10 headwinds
Category-11	LDV8	93:7	Func8	0	55	20 headwinds
Category-24	LDV9	92:8	Func9	1	60	30 headwinds
Category-25	LDV10	91:9	Func10	2	65	40 headwinds
Category-26	LDV11	90:10	Func11	3		50 headwinds
Category-27	LDV12		Func12	4		
Category-5 HDD	HDDV1			5	Not applicable	
Category-6 HDD	HDDV2	Not applicable	Not applicable	6		Not applicable
Category-7 HDD	HDDV3			7		

The levels of each of the factors in Table 2.1 were selected according to the following points:

1. While CMEM contains 28 LDV categories and 3 HDDV categories, only 12 LDVs and all three HDDV categories were included in the experiments. The rest of the LDVs were excluded due to their irrelevancy (age: 1983-1986 and predominantly driven outside of the US). The first two columns in Table 2.1 list how considered vehicles are categorized in CMEM as opposed to this Chapter.
2. Eleven proportions of heavy vehicles in the fleet were considered to investigate the impact of various fleet distributions on fuel consumption and *K*, as shown in Table 2.1.
3. The impact of driver's behavior on fuel consumption is investigated by analyzing various acceleration-deceleration functions, where each function represents a single unique driving behavior. Previous studies (Stevanovic and Gundogan, 2012; Crash Avoidance Metrics Partners, 2019) have shown that Vissim's default acceleration-deceleration functions do not replicate actual driver's behavior in the field. For that reason, stochastic acceleration-deceleration functions, which were calibrated and validated in a previous study (Stevanovic and Gundogan, 2012), were used as seed default functions in Vissim to generate 12 driving behaviors (discussed in Section 2.4.4.3) that were applied deterministically in all subsequent experiments.
4. A maximum grade for federally funded highways in the US is specified in design tables based on terrain and design speeds. Such grades go up to 6% in mountainous and hilly urban areas with exceptions of up to 7% grades on mountainous roads with speed limits below 60 mph (Hancock and Wright, 2013). Hence, to follow

these general recommendations, this Chapter adopted, as shown in Table 2.1, a road gradient range between -7% and +7% to investigate the impact of the road slope on fuel consumption and the value of *K*.

5. Speed limits of signalized corridors in the United States vary depending on number of geometrical and traffic conditions. They usually range from 20 mph on local residential streets (speeds can go as low as 10-15 mph within school zones) to 65 mph on some low-density multilane highways. This Chapter defined ten different cruising speeds, as shown in Table 2.1, to cover most of the possible speed limits that could impact fuel consumptions and *K* factor.
6. A set of experiments representing various wind speeds and directions (headwind (HW) and tailwind (TW)) were performed to investigate the wind impact on fuel consumed by HDDVs during one-stop. The range of wind speed was limited to 50-mph because investigating the impact of higher (not normal) wind speeds is outside the scope of this Chapter.

2.4.2 Traffic Simulation Program

PTV Vissim is a microscopic, time-step and behavior-based model developed to simulate urban traffic and public transport operations. Besides the fact that Vissim is a popular tool in the traffic community, it was selected in this Chapter for the following reasons:

1. Its ability to accurately model traffic signals and other operations (e.g., speed and acceleration) at a resolution of 0.1 seconds.
2. It provides several vehicle classes (e.g., cars and heavy vehicles) and allows users to identify the proportion of each class in the fleet.

3. Vissim outputs vehicle trajectory files (FZP) are well fitted to be used in CMEM to obtain second-by-second fuel consumption estimates.

2.4.3 Model for Estimation of Fuel Consumption

CMEM is a microscopic fuel consumption and emission model that estimates second-by-second fuel consumption and emissions based on different modal operations from in-use vehicle fleet. The required inputs for CMEM include vehicle activity (second-by-second speed trace, at a minimum) and fleet composition of traffic being modeled, where those inputs can be obtained from Vissim. In addition to that, CMEM was selected for this Chapter for two reasons:

1. It can estimate fuel consumption for various vehicle types.
2. It allows users to incorporate the impact of road gradient (for all vehicles) and wind effect (for heavy vehicles only) on fuel consumption estimates.

Fuel consumption estimates in this Chapter were not validated against field data, for two reasons:

1. CMEM has already been calibrated and validated by using data from the National Cooperative Highway Research Program (An et al., 1997).
2. Many studies have already validated estimates from CMEM, and they concluded that CMEM is generally accepted as a model that can generate verifiable fuel consumption estimates (Rakha et al. 2003, Barth at al. 2001).

It is worth mentioning that the CMEM model allows users to change the calibration parameters of the modeled vehicles. Such flexibility is helpful when modeling new generations of vehicles with more fuel-efficient engines.

2.4.4 Experimental Setup

This section first describes the modelling of the test-bed intersection and then it explains how various operational conditions were modeled in Vissim and CMEM. Third, default values for the evaluated factors were identified to ensure consistent comparisons. Finally, procedures to estimate fuel consumption from CMEM, and compute *K*, are provided.

2.4.4.1 Modeling of A Hypothetical Intersection

To support development of the proposed methodology, a total of 74 experiments were simulated on a hypothetical 4-leg intersection with two through-traffic lanes at each approach. The Vissim traffic simulation software was used with each traffic simulation, which run 1,100 seconds including 200 seconds of warmup time. Each of the simulation runs was long enough to gather relevant results for approximately 167 vehicles (performing stops at the intersection), which represents a good statistical sample size. The right and left turning vehicles were not included in the analysis for two reasons: 1. to reduce unnecessary noise in the results (e.g., those vehicles behave differently), and 2. signals are mainly coordinated to reduce stops and fuel consumption for through movements while it is more acceptable that, if must, left- and right-turning vehicles may stop. Traffic volumes from a typical 4-leg intersection in Lake County, Chicago, IL were used to model realistic traffic flows. Figure 2.3 shows directional volumes for this intersection. A two-phase fixed-time signal timing plan was operated on the simulated intersection. A desired cycle length of 180 seconds was applied as a result of a common method to calculate cycle length based on a volume to capacity ratio of 0.95, saturation flow headways of 2 sec, a lost time of 4 seconds per phase, and relevant critical volumes. The green splits for the two phases resulted in 137 seconds for the major road and 35 seconds for the minor street.

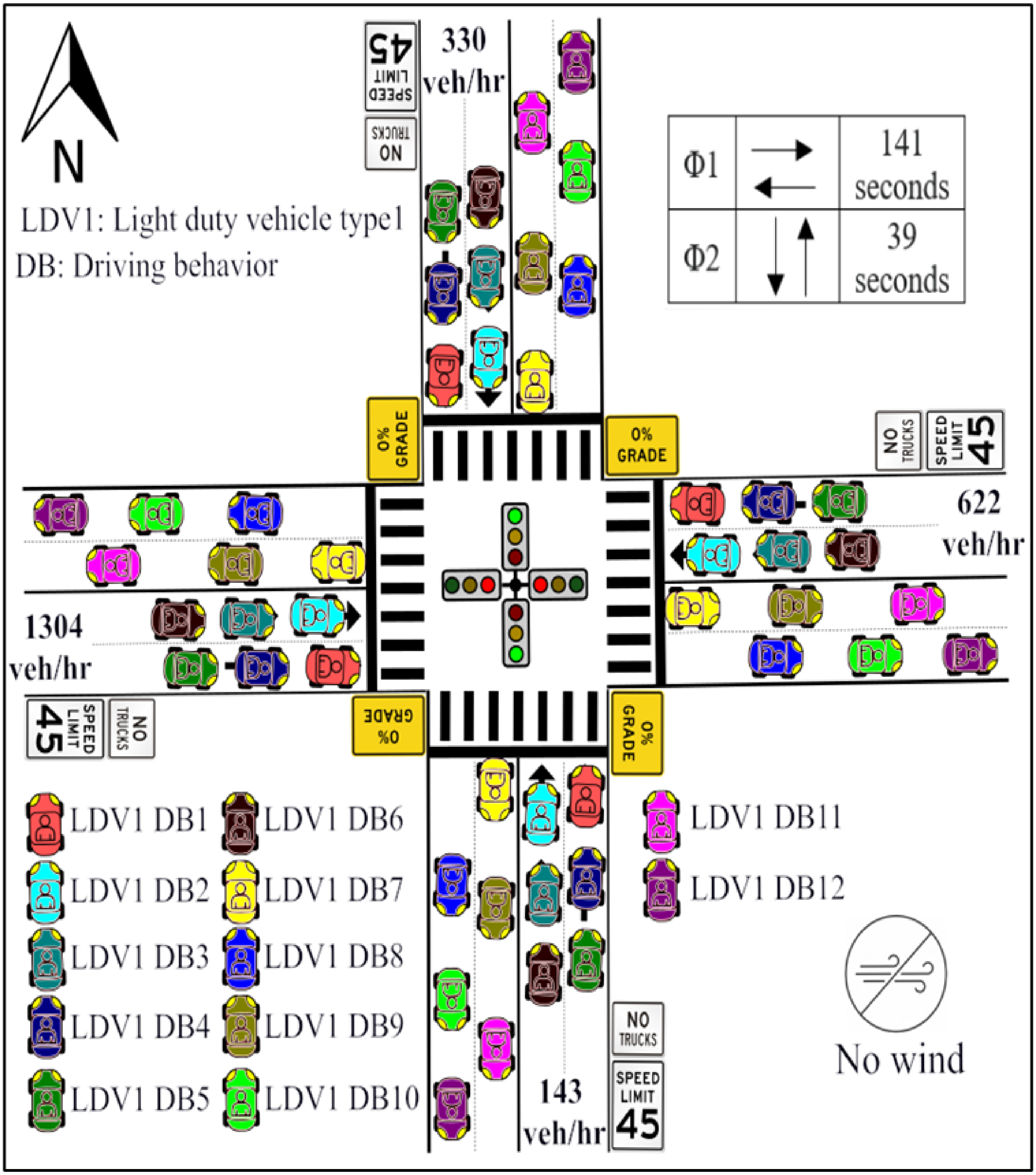

Figure 2.3 Layout, volumes, and splits of the hypothetical intersection.

2.4.4.2 Modeling of Various Operational Conditions

Various operational conditions were modeled in Vissim and CMEM to investigate their individual impacts on fuel consumption, and *K*. Two vehicle classes (light-duty vehicle 'LDV' and heavy-duty diesel vehicle 'HDDV') were modeled in Vissim, whereas 15 vehicle types (12 LDVs and 3 HDDVs) were modeled in CMEM. Various proportions of heavy vehicles in the fleet distribution were modeled in Vissim by changing the relative flow percentage of each vehicle class in the vehicle compositions for each intersection approach. Also, multiple driver's behaviors were modeled in Vissim by adjusting the desired and maximum deceleration-accelerations functions. Road gradients were first modeled in Vissim by defining grades for each link starting from the stop line to the point where vehicles reach their original cruising speeds. Similarly, the same road gradients were specified in CMEM during the process of postprocessing Vissim trajectory data. In this way both Vissim and CMEM were able to consider impact of the road gradients on the fuel consumption – Vissim from kinematic perspective whereas CMEM from the perspective of increased engine loads.

Cruising speed, for each experiment, was modeled in Vissim by setting proper value in the desired speed distribution function. As mentioned previously, the Cruising Speed Stop Profile (CSSP) starts as a deceleration event from a particular cruising speed and ends when the vehicle reaches the same speed after the acceleration phase. For all of the experiments, the desired speed distribution was defined in Vissim to ensure that the vehicles satisfy these cruising speed conditions. This was done in a way to ensure that a complete CSSP was achieved for every cruising speed defined.

The effect of wind was included by adding information (in CMEM) on wind speed and direction for HDDVs only. The reason that LDVs were not included is because the CMEM does not support this functionality for small passenger cars. Figure 2.4 shows the process of modeling traffic at the test-bed intersection, performing various experiments, post-processing data trajectories from Vissim, estimating fuel consumption (based on trajectories) in the CMEM, and post-processing fuel consumption estimates in Matlab to compute the value of *K*.

A controlled comparison of various experiments requires that fuel consumption estimations are based on an approximately equal number of stopped vehicles in each experiment. That is not easy to achieve when cruising speeds vary (in various experiments) because vehicles need different times to travel to the modeled intersection's stop line. Such conditions may result in a situation where the same vehicle (same ID) stops at the intersection on a red signal in one scenario but goes through the green signal in another. This challenge was overcome by adjusting the start time of the relevant green interval to ensure a comparable number of stops under each experiment. As a result, 167 vehicles were consistently identified to have stopped at the signal in each experiment.

Additionally, the same vehicles (with the same IDs, from each simulation) were used to derive fuel consumptions and compare results. This approach was adopted to ensure that the results do not include 'noise' introduced by the stochastic nature of simulation-generated driving behavior (and other simulation parameters) for various individual vehicles in the traffic stream. That was especially important to ensure that the times needed to travel from the beginning of the links (at the four approaches) to the relevant stop lines are consistent.

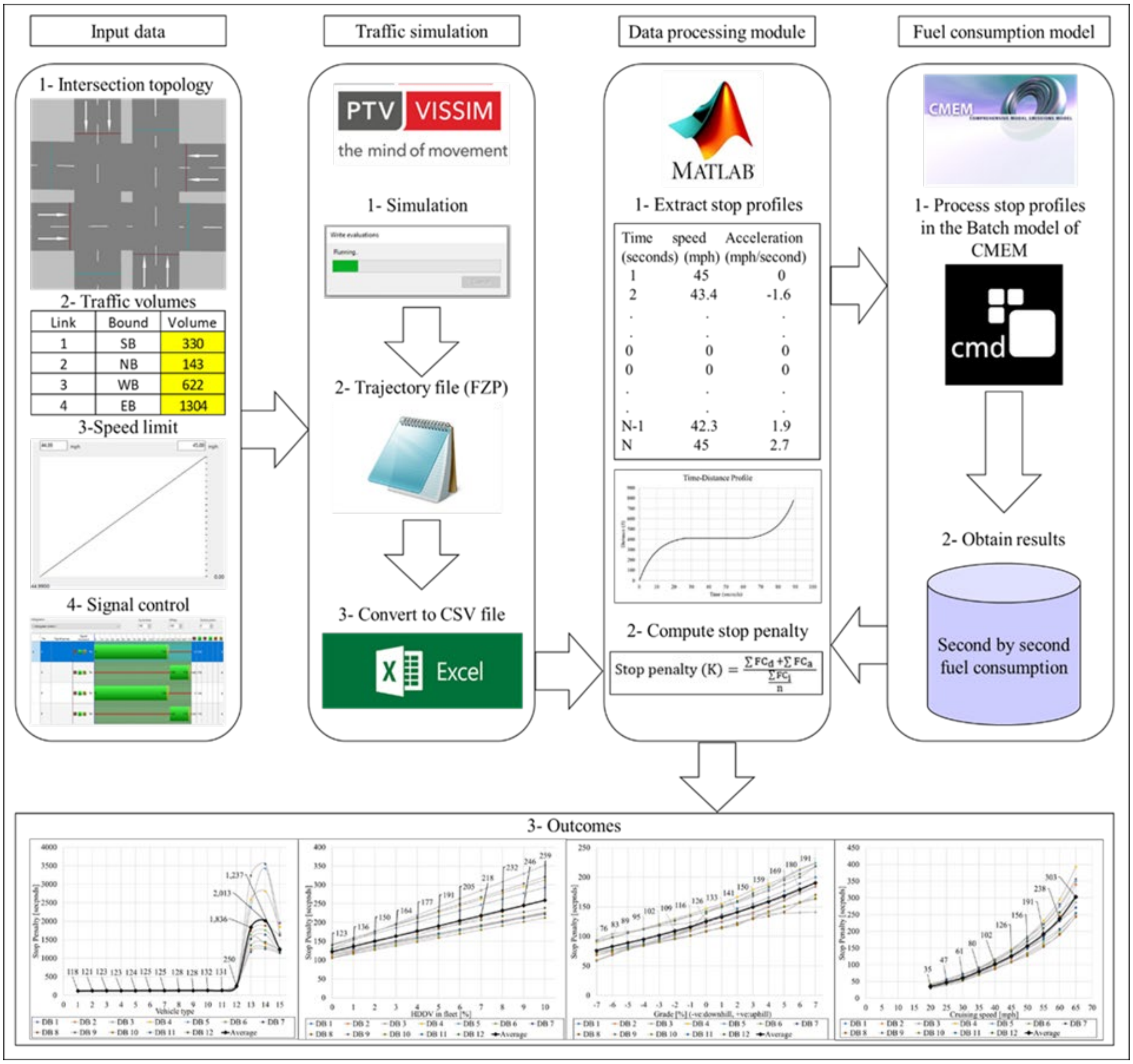

Figure 2.4 Vissim-Matlab-CMEM connection.

2.4.4.3 Default Variables for Various Operational Conditions

A default value for each of the evaluated factors was identified, as a reference value used when comparing fuel consumption results, to ensure consistent comparisons. LDV1, HDDV3, no-heavy vehicles, 12 deterministic acceleration-deceleration functions, level terrain, 45-mph, and no wind were selected as default values for LD vehicle type, HDD vehicle type, driving behavior, road gradient, cruising speed, and wind speed, respectively. Figure 2.3 shows all those default values.

Acceleration and deceleration functions adopted from a previous study (Stevanovic and Gundogan, 2012) are stochastic, meaning that each stopped vehicle in the simulation can have a unique deceleration-acceleration function. The use of such stochastic functions results in uncontrollable experiments because the impacts of various deceleration-acceleration functions (driving behaviors) on the *K* cannot be captured. To solve this issue, the Dynamic Time Warping (DTW) (Sakoe and Chiba, 1978) and k-means clustering (Hartigan and Wong, 1979) algorithms were used to classify the stochastic driving behaviors of all of the 167 stopped vehicles into 12 deterministic categories. Such deterministic categories are fully controllable during the experiments, which guarantees accurate quantifying of the impact of various driving behaviors during experimental scenarios as well as the impact of other factors (e.g., cruising speed) on the *K* factor.

To apply the DTW and k-means algorithms, results from a simulation run (with all of the previously mentioned default values (Figure 2.3), except cruising speed which was set at 65-mph, were used to partition the 167 deceleration-acceleration functions into 12 distinctive clusters. The 65-mph speed was used because it covers a wider range of deceleration-acceleration rates compared to the rates of any of the lower speeds. It should be mentioned that in Vissim, driving behavior of a specific vehicle is not a function of cruising speed; thus, various levels of driver's aggressiveness (either on deceleration or acceleration side) can be observed through an entire set of cruising speeds. The clustering process was done in two stages. Firstly, the DTW algorithm was applied on all 167 behavior functions to find dissimilarity factors between the groups of deceleration-acceleration functions. Secondly, the resulting dissimilarity factors were entered into a k-means clustering algorithm (Hartigan and Wong, 1979) to cluster behavior functions into 12 distinctive groups.

The DTW is an algorithm used to measure the similarity between two sequences, which may vary in length (time) (Sakoe and Chiba, 1978). DTW algorithm was applied because it represents a way to apply a non-linear (elastic) alignment for distances between points in two data series. This elastic alignment (illustrated in the bottom part of Figure 2.5a)) produces a more intuitive way (e.g., more than one based on Euclidean distances) to align the *i-th* point from one time series with the *i-th* point from the other time series (as shown in the upper part of Figure 2.5a)) (Tsiporkova, 2020). This approach allows two similar shapes to be matched even if their time intervals (or whichever variable is on the x axis) are not of the same length, which is the case when dealing with deceleration-acceleration functions resulting from various vehicles and drivers.

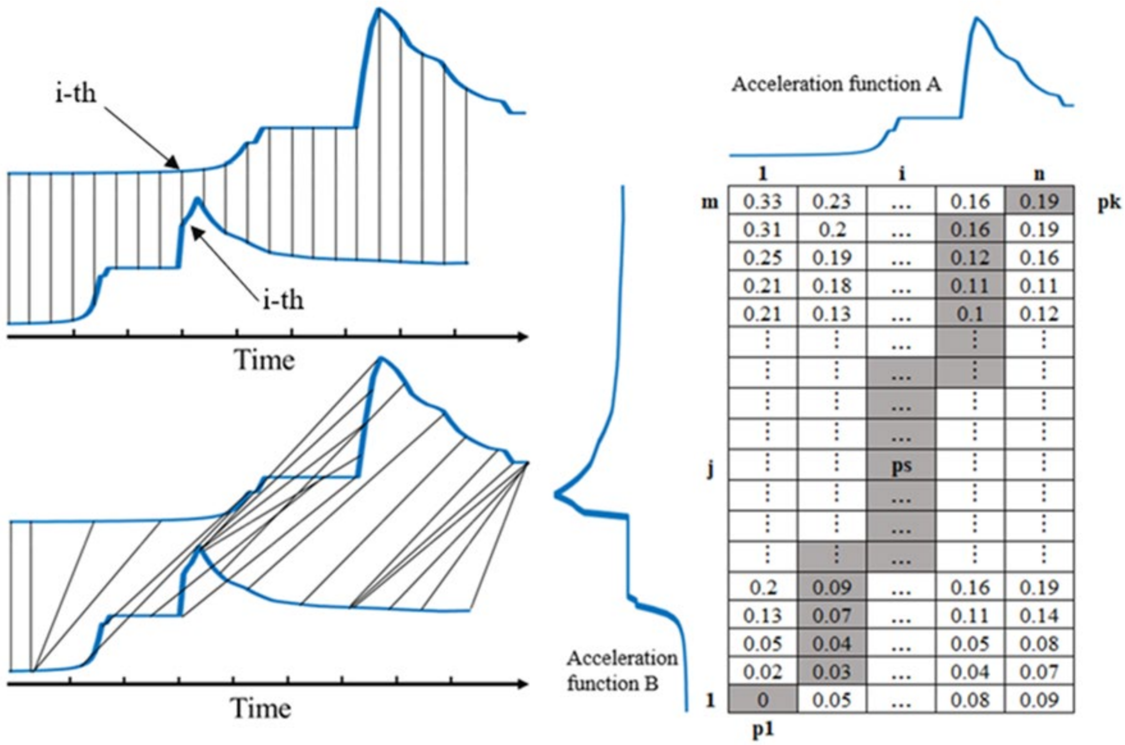

a) Difference between linear (top) and non-linear (bottom) alignments when measuring similarity between two time series.

b) Dissimilarity matrix of two time series (*A* and *B*) after applying the DTW algorithm

Figure 2.5 Using Dynamic Time Warping algorithm with behavior functions.

To find the best alignment between two arbitrary time series *A* and *B* (shown in Figure 2.5b)), one needs to find the path through the grid $p = p1, ..., ps, ..., pk$. $ps = (i_s, j_s)$, which minimizes the total distance between them. Then the time-normalized distance between series *A* and *B* is computed as:

$$D\ (A, B) = \frac{\sum_{S=1}^{K} D(P_S).W_S}{\sum_{S=1}^{K} W_S} \tag{2.11}$$

$D(Ps)$ is the distance between i_s and j_s, and $Ws > 0$: weighting coefficient. Finally, the best alignment path between A and B is found as the minimum distance between A and B:

$$P_0 = arg_p\ min(D(A, B)) \tag{2.12}$$

The best alignments between all of the deceleration-acceleration functions from the 167 stopped vehicles were computed using a built-in Matlab function replicating Equations 2.11 and 2.12 (Sakoe and Chiba, 1978). Such alignments express how dissimilar deceleration-acceleration functions are to each other; thus, they can be called dissimilarity factors. Figure 2.6a) shows a sample of dissimilarity factors from the resulted dissimilarity matrix of 167 x 167, where each cell of the matrix represents the dissimilarity between two deceleration-acceleration functions of two vehicles. A lower value indicates that the two deceleration-acceleration functions (representing trajectories of two vehicles) are more similar.

Subsequently, the factors from the dissimilarity matrix were fed into an unsupervised clustering k-means algorithm that aims to partition a given set of n observations (data points) into k clusters by minimizing the total Within-Cluster Sum of Squares (WCSS) (Hartigan and Wong, 1979):

$$WCSS = arg_S\ min \sum_{i=1}^{m} \sum_{x=1}^{n} ||x - \mu_i||^2 \tag{2.13}$$

Acceleration & deceleration functions	1	2	3	4	5	…	167
1	0	80	43	193	110	113	93
2	80	0	154	539	174	267	89
3	43	154	0	104	22	29	40
4	193	539	104	0	90	32	151
5	110	174	22	90	0	13	23
⋮	113	267	29	32	13	0	31
167	93	89	40	151	23	31	0

(a) Dissimilarity factor between behavior functions.

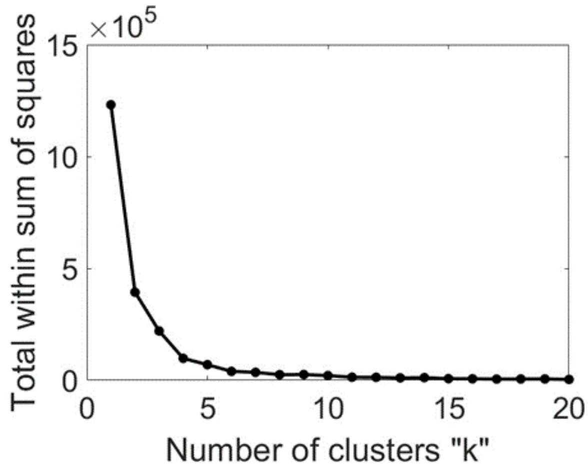

(b) Selection of optimal "k" clusters.

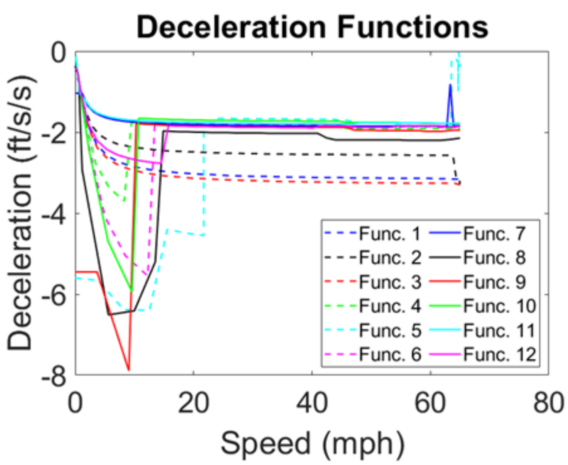

(c) 12-deceleration functions.

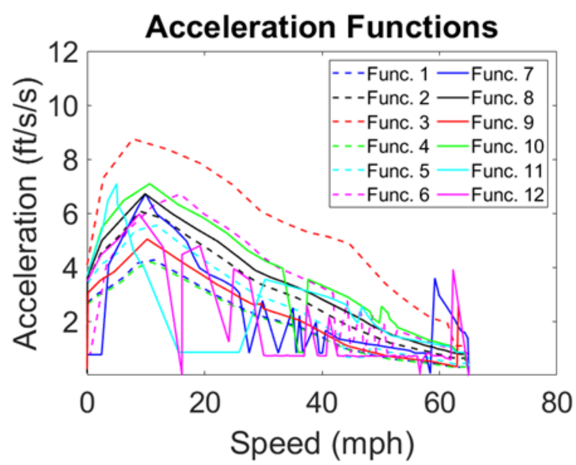

(d) 12-acceleration functions.

Figure 2.6 Partitioning behavior functions of stopped vehicles into mutual clusters.

Where μi is the mean point of the centroid of cluster i ($i = 1, 2, ..., m$), and n is the number of observations in each cluster i. The number of clusters is determined by using the 'elbow method', which is based on the rate of 'diminishing returns' (Hartigan and Wong, 1979). The elbow method (shown in Figure 2.6b)) uses a chart of the quality of clustering performance (as a function of the number of clusters) to select a point at the elbow of the curve to indicate how many clusters to use. One can observe from the result of the Elbow method (shown in Figure 2.6b)) that 4-6 clusters are suggested. However, the authors decided to be more conservative and proceed with 12 distinctive deceleration-acceleration functions to cover a wider variety of potential driving behaviors. Figure 2.6c) and Figure 2.6d) show the 12 deceleration and the 12 acceleration functions, respectively, that came out of the clustering process. These 12 deceleration-acceleration combinations were then used as default and deterministic functions in Vissim. This meant that a vehicle deceleration-acceleration behavior in Vissim would not be a result of a stochastic process, but each vehicle would fall within one of the 12 deceleration-acceleration combinations, where each combination would cover approximately the same portion of vehicular fleet. In this way, it was ensured that by utilizing such deterministic functions, the authors could completely control the experiments and exactly determine causes of the possible variations in estimated fuel consumption.

Although vehicles of each of the 12 distinctive deceleration-acceleration clusters behave similarly (from acceleration and deceleration perspective), the fuel consumptions are still computed for all of the 167 stopped vehicles in each experiment. This was done to account for the unique deceleration distance of each vehicle, considering that such distance is a function of cruising speed etc., and may not be the same for each approaching vehicle. The following steps explain how fuel consumption and K are computed for each experiment:

1. Vissim outputs (FZP files), which include second-by-second speeds and accelerations (decelerations), is processed in Matlab to extract individual trajectories of all fully stopped vehicles.
2. Trajectories from step 1 are processed in Matlab to obtain CSSPs of fully stopped vehicles (e.g., decelerating from a cruising speed of 45-mph, reaching a zero-speed, and then accelerating to the original cruising speed of 45-mph).
3. CSSPs from step 2 are processed in CMEM to estimate fuel consumption by each stopped vehicle.
4. Given the second-by-second speeds and fuel consumption, Equation 2.6 is used to calculate the K value of each CSSP.
5. Steps 1-3 were applied to all 167 stopped vehicles, for each experiment, with 12 different deterministic deceleration-acceleration functions. The average fuel consumption and K for all 167 stopped vehicles were calculated for each of the 12 Vissim simulations, representing various deceleration-acceleration functions. Then, the average fuel consumption and K from 12 Vissim simulations were computed for each experiment. A software code was developed to interface Vissim, Matlab, and CMEM to speed up the computation process and produce outputs from all experiments in a consistent manner.

2.5 Results and Discussion

The amount of consumed fuel (in grams) for a CSSP representing each of the various experiments, from Table 2.1, are presented in Table 2.2. Figure 2.7 illustrates the fuel consumption results for three representative cases for each of the investigated variables: the default value and two extreme cases (e.g., lowest and highest). For each of the results from Table 2.2, values of *K* are illustrated (for each variable individually) as a function of a specific fuel consumption factor in Figure 2.8. Each of the charts in Figure 2.8 (except 8c)) includes 13 data series out of which 12 represent each of the 12 deterministic deceleration-acceleration functions investigated in the Chapter, and the bolded line represents an average of those 12 data series. Figure 2.8c) is an exception because it already shows the impact of various driving behaviors on *K* value. It is worth noting here that Figure 2.8a) was developed for all vehicle types tested in the Chapter, Figure 2.8b), Figure 2.8c), Figure 2.8d), and Figure 2.8e) were produced for the default Light-duty vehicle type (LDV1), and Figure 2.8f) was generated for default Heavy-duty diesel vehicle type (HDDV3).

Table 2.2 Impact of various operational conditions on fuel consumption (FC).

Vehicle type		Fleet distribution		Driver behavior		Road gradient		Cruising speed		Wind effect	
Variable	FC (g)	Variable	FC (g)	Variable	FC (g)	Variable	FC (g)	Variable	FC (g)	Variable	FC (g)
LDV1	56.6	100:0	56.6	Func1	45.7	-7	34.8	20	16.1	50 tailwinds	473.8*
LDV2	57.2	99:1	62.5	Func2	47.2	-6	37.6	25	21.8	40 tailwinds	505.6
LDV3	55.5	98:2	68.7	Func3	49.5	-5	40.8	30	27.2	30 tailwinds	510.8
LDV4	52.5	97:3	74.4	Func4	51.9	-4	43.5	35	36.7	20 tailwinds	513.3
LDV5	57.8	96:4	80.1	Func5	53.2	-3	46.3	40	46.4	10 tailwinds	525.6
LDV6	54.6	95:5	86.5	Func6	55.4	-2	49.6	45	56.6	No wind	549.0
LDV7	55.5	94:6	92.3	Func7	56.3	-1	52.7	50	70.3	10 headwinds	587.2
LDV8	59	93:7	98.4	Func8	58.4	0	56.6	55	85.5	20 headwinds	628.5
LDV9	58.7	92:8	104.1	Func9	60.5	1	59.2	60	106.6	30 headwinds	690.8
LDV10	111.2	91:9	110.9	Func10	62.2	2	63.7	65	135.3	40 headwinds	835.4
LDV11	56.8	90:10	117.6	Func11	63.7	3	67.1			50 headwinds	979.5
LDV12	55.9			Func12	65.4	4	71.1				
HDDV1	816.5					5	75.0	Not applicable		*Values are for HDDVs	
HDDV2	894.4	Not applicable		Not applicable		6	80.2				
HDDV3	549.0					7	85.6				

Results of the experiments with various vehicle types (columns 1 and 2 in Table 2.2) show that each vehicle type consumes a different amount of fuel, which will result in various *K* values, as shown in Figure 2.8a). For light-duty vehicles, the results indicate that, if vehicles use the same fuel type, the fuel consumption is more sensitive to the vehicle's mass than the vehicle type (e.g., fuel consumption of LDV10 (Gross Vehicle Weight (GVW)>8500 lbs) is much higher than that of LDV6 type (a normal sedan-like car)).

However, when compared to the default category (LDV1), fuel consumptions from all of the LDVs (except LDV 10) fall within a range of 0.35 – 4.24% difference. The situation is much different for the HDDVs, where the absolute fuel consumptions are much higher than those of the LDVs; but also, the differences between older trucks (HDD1 and HDD2, representing HDDVs from '90s) and the default truck HDD3 are much higher 48.7-63%. Such difference could be a result of recent improvements of the truck fuel economies, who seems to be higher than those of the LDVs. Based on these results, it would be fair to expect that even newer vehicles (e.g., those manufactured after 2010) would result in even lower fuel consumptions (and emissions footprints) at signalized intersections, which will reduce the value of *K*.

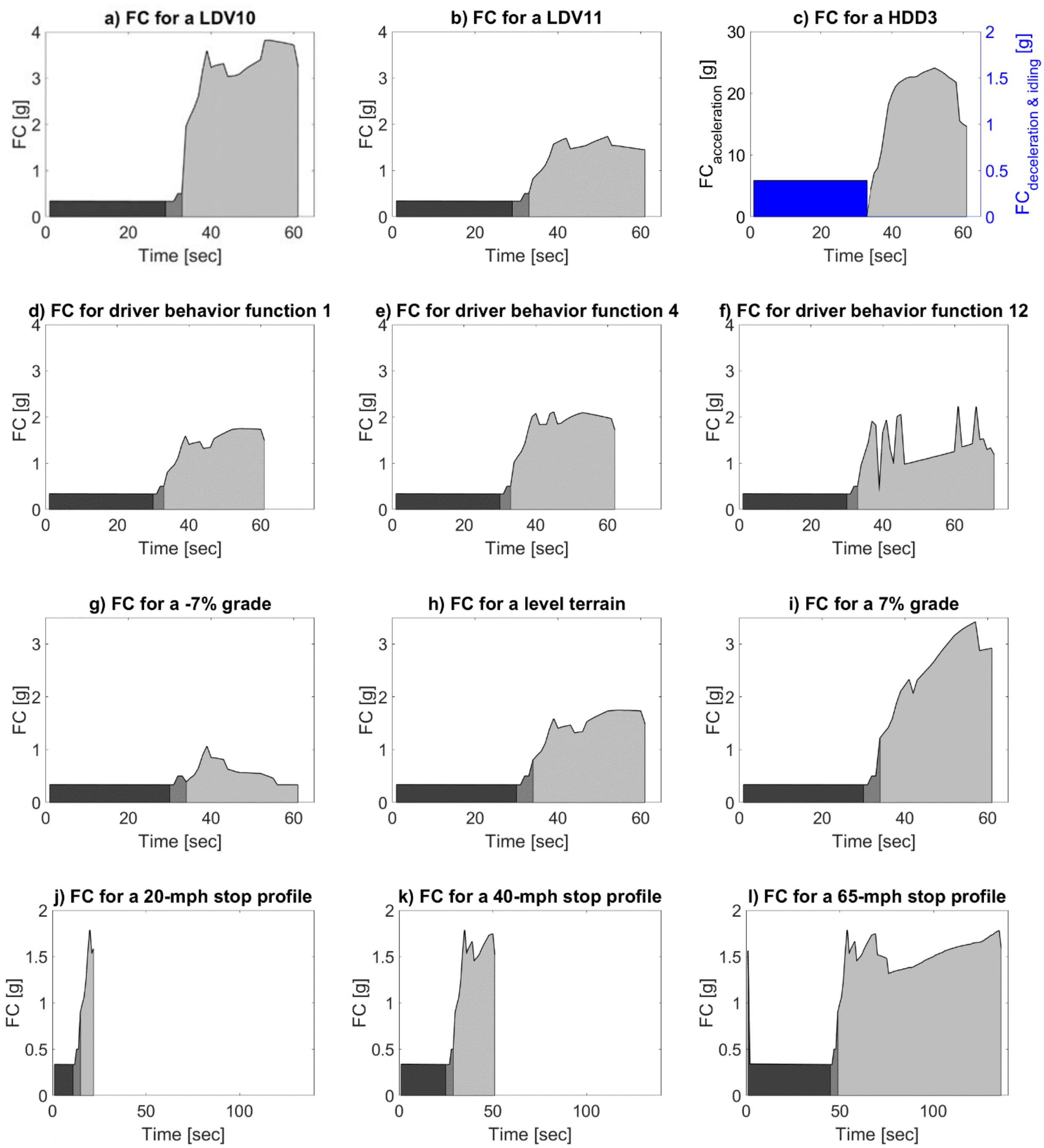
a) FC for a LDV10
b) FC for a LDV11
c) FC for a HDD3
d) FC for driver behavior function 1
e) FC for driver behavior function 4
f) FC for driver behavior function 12
g) FC for a -7% grade
h) FC for a level terrain
i) FC for a 7% grade
j) FC for a 20-mph stop profile
k) FC for a 40-mph stop profile
l) FC for a 65-mph stop profile
FC [g]
$FC_{acceleration}$ [g]
$FC_{deceleration \& idling}$ [g]
Time [sec]

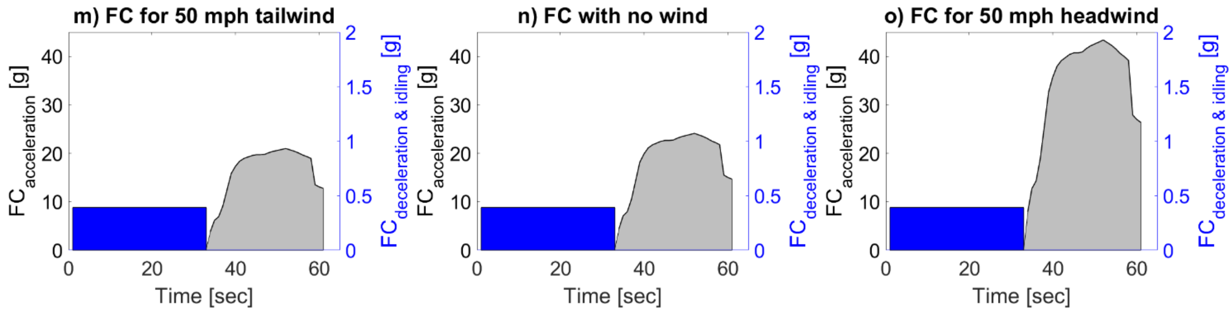

Figure 2.7 Impact of various operational conditions on excess fuel consumption (FC) caused by a single stop.

Going back to Figure 2.7 parts a)-c), one can observe how fuel consumption changes for three selected vehicle types: LDV10, LDV11, and HDDV3. These results indicate that the fuel consumption of HDDV3 during acceleration mode is ~5-10 times higher than the relevant fuel consumption of LDV10 and LDV11. Similarly, Figure 2.7c) shows that the fuel rate of a truck (e.g., HDDV3) is significantly higher during the deceleration phase than the fuel rates of the other vehicles (e.g., LDV10 and LDV11). Such a characteristic of HDDVs is expected to result in a significant impact on the *K* value, when a fleet contains a high HDDV percentage, as discussed next.

Table 2.2 (columns 3 and 4) also reveals that fuel consumption shows an approximately linear relationship with an increase in the percentage of HDDVs. For an HDDV proportion in the fleet of 0-10%, each one percent of extra HDDVs adds, on average, 6 grams of consumed fuel at each intersection stop. Naturally, if more fuel is consumed a penalty of each stop of such a HDDV-significant fleet will increase, as shown in Figure 2.8b). The highest value for *K* is reached with the highest percentage of HDDVs in the fleet. Based on Figure 2.8b), it can be concluded that every increase of 1% of HDDVs in the fleet costs around 11 seconds of extra waiting-idling time (based on the equivalent fuel consumption) for every additional stop at a traffic signal. In fact, the final K value for an intersection approach would be based on two factors: 1. Vehicle types constituting arriving (average) fleet (e.g., LDVs and HDDVs), and 2. Percentage of each of those vehicle types in the fleet.

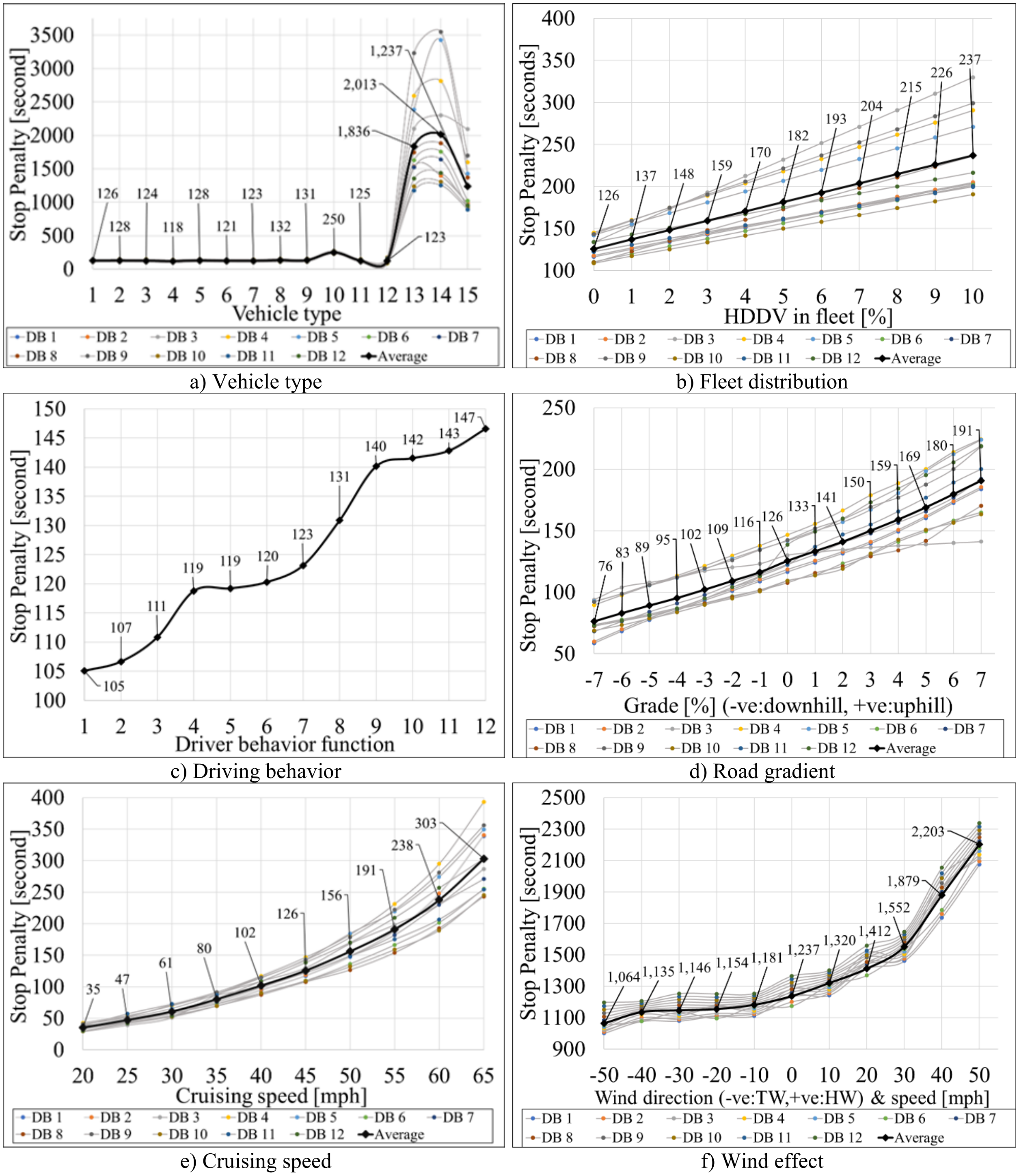

Figure 2.8 Impact of various operational conditions on Stop penalty (*K*), where DB: Driver behavior.

Columns 5 and 6 in Table 2.2 show how fuel consumptions vary for the 12 deceleration-acceleration functions. There is no clearly recognizable pattern to correlate such fuel consumption variations with some intuitive expectations related to different driving behaviors, as such behaviors are usually based on unique mental and physical characteristics of the drivers. Nevertheless, fuel consumption variations can reach up to 40% in difference (e.g., when function #1 is compared to function #12). Figure 2.7 parts d)-f) show how fuel consumptions range for selected deceleration-acceleration functions. Although the differences in fuel consumptions from Figure 2.7 parts d)-f) cannot be easily quantified by a naked eye, Figure 2.8c) shows that the impact of those differences is significant on the *K* value (ranging from 105 to 147 seconds for various deceleration-acceleration functions). Considering that those 12 functions were all generated from a single stochastic deceleration-acceleration combination, it is expected that the *K* could diversify even more with a higher degree of stochasticity in driving behavior.

Similar to the percentage of HDDVs in the fleet, it is observable from Table 2.2 (eighth column) that the fuel consumption increases linearly with an increase of the road gradient. Figure 2.7 parts g)-i) show that the road gradient's impact is very significant, especially during the acceleration mode. For instance, a vehicle traveling on 7% uphill terrain will consume as much as ~2.5 times more fuel than a vehicle traveling downhill on the same segment (with a gradient of -7%). Furthermore, an interesting finding is that the extra fuel consumed on an uphill stop (e.g., 5.4 extra grams per CSSP for +7% compared to a CSSP with +6%) cannot be compensated by the savings gained by stopping on a downhill direction of the same road segment (e.g., 2.8 fewer grams per CSSP for -7% when compared to a CSSP -6%). These findings make the road gradient one of the most important factors to consider when defining *K* for an intersection approach.

The results of experiments with various cruising speeds are presented in Table 2.2 (tenth column). They show that the cruising speed (often correlated to the prevailing speed limit) substantially impacts the fuel consumption of a CSSP. In relation to the cruising speed, the *K*-factor growth seems to have an exponential shape, as shown in Figure 2.8e). This is especially observable for cruising speeds higher than 45 mph. Figure 2.7 parts j)-l) illustrate how the area under the fuel consumption curves increases significantly when the cruising speed increases. This finding can be interpreted as if stopping a vehicle at a higher cruising speed introduces a much more significant interruption than stopping a vehicle traveling at a lower speed. However, it should be noted that the fuel costs of stopping do not come from the stopping (decelerating) activity per se as much as they are a result of the acceleration process for the vehicle to regain its previous cruising speed. For example, as observable from Table 2.2, a stopped vehicle previously traveling at 45 mph will use twice as much of the excess fuel (to accelerate to the same speed) as a stopped vehicle traveling at 30 mph; thus, resulting in an approximately double value of *K*, as shown in Figure 2.8e).

Results of the wind speed and direction have shown, as expected, that headwinds cause the HDDV to generate more energy (which requires more fuel) to overcome the energy of the wind blowing in the opposite direction. Similar to the impact of the road gradient, although tailwinds save fuel consumption, as shown in Table 2.2 and Figure 2.7 parts m)-o), the amount of fuel savings gained from a tailwind of certain speed cannot recover the fuel increase caused by a headwind of the same speed magnitude. Those results are reflected on the *K* value as depicted in Figure 2.8f); thus, they confirm the importance of including wind effect in *K* calculations, especially for fleets with a high percentage of HDDVs.

In summary, results suggest that *K*-factor should be significantly larger than the one used in the existing traffic signal optimization practice. Results also show that the *K* value required to minimize fuel consumption varies with different operational conditions, hence *K*-factor cannot be a single value as it is widely used. Specifically, findings showed that vehicle type, driving behavior, and cruising speed had the major impact on the stop-induced fuel consumption. Although the percentage of heavy vehicles in the fleet and road gradient also have a significant impact, such impact is not in the magnitude of the major factors (e.g., vehicle type). Although most of the government agencies focus on the quantity of traffic arriving at a signalized intersection (when optimizing traffic signals), the results of this chapter indicate that dynamics of traffic should be also considered, if the objective is to minimize fuel consumption. For instance, some traffic streams may encompass a higher percentage of heavy vehicles than the other; or an approach could be situated on a slope thus causing certain traffic movements to create much larger negative environmental footprints than what the current practice would account for. However, these factors are not considered in the current signal retiming practices and that is why our signal retiming policies should be modified. The following subsection provides a step-by-step procedure that can be used to compute the *K* values under various operational conditions based on the results obtained in this chapter.

2.5.1 Computation of Stop Penalty

The stop penalty should be specified on the turning-movement level. However, it is not likely that many of the factors will have different values for various turning movements. Still, such flexibility should exist to ensure that a realistic stop penalty can be calculated for every turning movement at an intersection under special circumstances. This approach is important so that traffic signal engineers can have flexibility to decide which movements to include in the analysis. This section provides an approximation step-by-step procedure to compute the stop penalty based on the results presented in Figure 2.8. Furthermore, a detailed example is given to show how the procedure should be applied.

The following procedure describes a logic that an engineer can follow when deciding which *K* factors (stop penalties) to apply for various intersection's movements. Once such *K* factors are defined, it is possible (with the use of relevant signal optimization software) to properly balance signal timings to optimally trade-off between delays for stops at various intersections, to reduce excessive fuel consumption. The procedure starts by determining the stop penalty based on vehicle type and driving behavior while all other factors assume their default values. Those default values are level-terrain (0% grade), 45-mph cruising speed, and no winds. Subsequently, the determined stop penalties are adjusted to consider the impact of potential deviations in grade, cruising speed, and wind. The proposed procedure should be applied for each vehicle type, separately.

1. Use Table 2.3 to determine the stop penalty for each vehicle type and its driving behavior at the movement (or approach) of interest.
    1.1. Your *K* is YYY
2. Apply specific Road gradient – R_{gra}
    2.1. Is your R_{gra} for this movement equal to default value (0%)?
        2.1.1. Yes, K = YYY; move to the next factor, Step 3
        2.1.2. No, compute a correction factor (C_{fg}) for *K* for your R_{gra}, and apply necessary % changes for the road gradient.

$$C_{fg} = \frac{K_{actual\ grade}}{K_{0\%}} \tag{2.14}$$

Where: $K_{0\%}$ is the stop penalty when road grade is 0%, $K_{actual\ grade}$ is the stop penalty for the actual grade on the movement of interest. $K_{0\%}$ and $K_{actual\ grade}$ are found from Figure 2.8d) and Figure 2.9a) for LDVs and HDDVs, respectively.

Table 2.3 Variables for various operational conditions impacting fuel consumption.

Vehicle	Driving behavior											
type	1	2	3	4	5	6	7	8	9	10	11	12
LDV1	105.1	106.6	110.8	118.8	119.2	120.3	123.2	130.9	140.2	141.6	142.9	146.6
LDV2	110.7	111.0	111.4	119.1	120.7	124.8	129.6	137.8	139.3	142.2	144.3	147.1
LDV3	108.0	108.7	110.9	113.5	115.0	119.1	120.1	120.1	135.6	141.9	143.0	147.5
LDV4	100.7	101.7	102.2	108.3	109.8	114.4	114.6	125.6	126.0	134.2	135.4	137.2
LDV5	113.0	113.4	114.1	119.2	120.7	123.1	125.3	126.1	142.1	145.8	147.0	150.6
LDV6	106.2	106.8	108.4	110.6	112.1	113.1	115.6	123.0	129.2	141.7	142.1	145.0
LDV7	104.8	106.4	106.4	113.6	115.1	119.5	119.7	127.3	135.8	139.0	139.4	143.7
LDV8	113.4	114.6	115.3	120.0	121.6	127.9	130.9	138.8	142.5	148.9	149.6	155.4
LDV9	114.1	115.8	117.2	123.0	124.5	128.9	130.2	130.4	140.9	147.9	148.1	152.5
LDV10	229.8	231.2	232.2	240.1	241.6	246.4	247.6	260.9	263.7	266.2	266.4	271.4
LDV11	107.2	107.2	109.1	116.8	118.3	122.0	123.1	131.6	136.4	142.2	142.9	148.0
LDV12	87.5	89.0	90.8	100.6	102.1	107.9	112.3	120.5	150.1	163.8	168.7	177.7
HDDV1	1172.6	1239.6	1351.9	1521.7	1531.7	1533.2	1630.5	1747.3	2099.7	2387.3	2589.6	3232.8
HDDV2	1252.9	1305.4	1394.2	1395.8	1437.0	1638.7	1756.1	1883.4	2301.6	2813.9	3425.2	3550.1
HDDV3	891.6	896.0	923.8	955.1	984.6	986.1	1023.6	1370.2	1426.9	1596.3	1697.4	2092.4

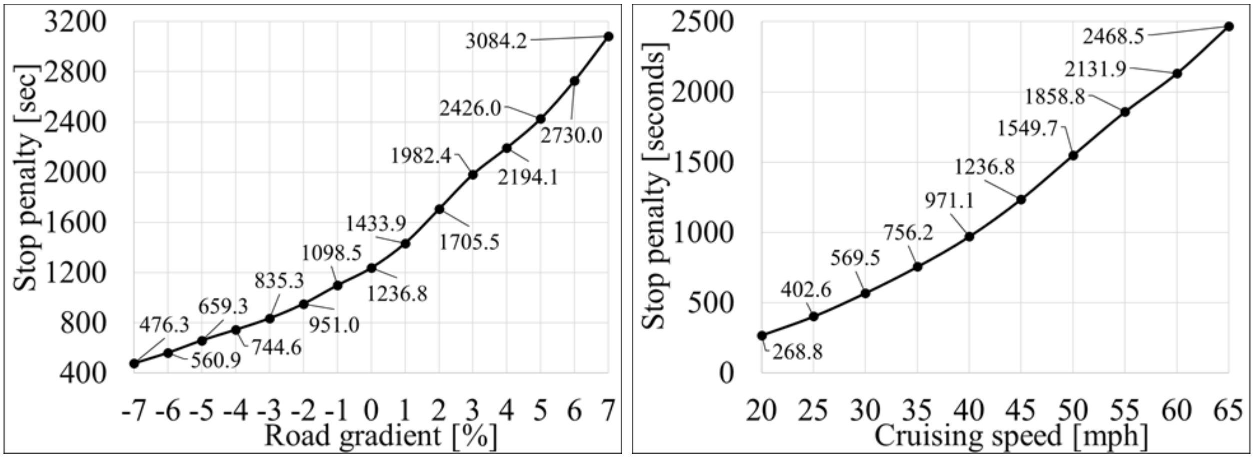

a) Road gradient b) Cruising speed

Figure 2.9 Impact of road gradient and cruising speed on Stop penalty (*K*) of a representative HDDV.

Note: when taking road gradient use always the exit side of the intersection for that specific movement as the road gradient has very significant impact when a vehicle accelerates, which always happens on the exit side of the intersection movement.

2.1.3. Multiply this correction factor with the current value of *K*

$$K = YYY \times C_{fg} \tag{2.15}$$

3. Apply specific Cruising Speed – C_{spe}

3.1. Is your C_{spe} for this movement equal to the default value (45-mph)?

3.1.1. Yes, *K* is equal to the value from step 2.1.1 or 2.1.3; move to the next factor, Step 4

3.1.2. No, compute a correction factor (C_{fs}) for *K* for your C_{spe}, and apply necessary changes for the cruising speed.

$$C_{fs} = \frac{K_{actual\ speed}}{K_{45}} \tag{2.16}$$

Where: K_{45} is the stop penalty when cruising speed is 45-mph, $K_{actual\ speed}$ is the stop penalty for the actual cruising speed on the movement of interest. K_{45} and $K_{actual\ speed}$ are found from Figure 2.8e) and Figure 2.9b) for LDVs and HDDVs, respectively.

3.1.3. Multiply this correction factor with the *K* value from step 2.1.1 or 2.1.3

$$K = YYY \times C_{fs} \tag{2.17}$$

4. Is your vehicle type heavy-duty diesel?
    4.1. Yes, move to the next factor, Step 5.
    4.2. No, your final *K* is the outcome from steps 3.1.1 or 3.1.3.
5. Apply specific Wind effect – W_{eff}
    5.1. Is your W_{eff} for this movement equal to the default value (no wind)?
        5.1.1. Yes, your final *K* is equal to the value from step 3.1.1 or 3.1.3.
        5.1.2. No, compute a correction factor (C_{fw}) for *K* for your W_{eff}, and apply necessary changes in wind effect.

$$C_{fw} = \frac{K_{actual\ wind}}{K_{no\ wind}} \tag{2.18}$$

Where: $K_{no\ wind}$ is a stop penalty when there is no wind, $K_{actual\ wind}$ is a stop penalty for the actual wind speed and direction on the movement of interest. $K_{no\ wind}$ and $K_{actual\ wind}$ are found from Figure 2.8f), for HDDVs only.

5.1.3. Multiply outcomes from steps 3.1.1 or 3.1.3 with this correction factor.

$$K = YYY \times C_{fw} \tag{2.19}$$

6. Use the following equation to compute the final stop penalty for the entire fleet (on that movement).

$$K_m = \sum_{i=1}^{n} p_i \cdot K \tag{2.20}$$

Where: K_m is the stop penalty for the movement of interest, p is the percentage of each vehicle type (i), K is the stop penalty for vehicle type (i) at movement m, and n is the number of all vehicles of types.

7. Go back to step 1 to apply the same procedure for other movements or vehicle types.

Example: What is the stop penalty of an approach at a signalized intersection under the following conditions: vehicle types: 99% is LDV1 and 1% is HDDV1, driving behavior function=1, road gradient =3%, cruising speed =35-mph, Head wind (speed =30-mph)?

1. Using Table 2.3, it can be found that $K_{LDV1} = 105.1\, seconds$ and $K_{HDDV1} = 1172.6\, seconds$.
2. The next step is to adjust each of the above determined stop penalties for road gradient of 3%.

$$C_{fgLDV1} = \frac{150}{126} = 1.19$$

$$C_{fgHDDV1} = \frac{1982.4}{1236.8} = 1.60$$

$$K_{LDV1} = 1.19 \times 105.1 = 125.07\, seconds$$

$$K_{HDDV1} = 1.60 \times 1172.6 = 1876.16\, seconds$$

3. The next step is to adjust each of the above computed stop penalties for cruising speed of 35-mph.

$$C_{fsLDV1} = \frac{80}{126} = 0.63$$

$$C_{fsHDDV1} = \frac{756.2}{1236.8} = 0.61$$

$$K_{LDV1} = 0.63 \times 125.07 = 78.79\ seconds$$

$$K_{HDDV1} = 0.61 \times 1172.6 = 715.29\ seconds$$

4. The next step is to adjust K_{HDDV1} for effect of a headwind of 30 mph

$$C_{fwHDDV1} = \frac{1552}{1237} = 1.25$$

$$K_{HDDV1} = 1.25 \times 715.29 = 894.11\ seconds$$

5. The next step is to use Equation 2.20 to account for the impact of vehicular distribution in the fleet. Finally, the stop penalty for the entire approach is:

$$K_{approach} = (0.99 \times 78.79) + (0.01 \times 894.11) = 86.94\ seconds$$

2.6 Conclusions and Future Research

This Chapter argued that the stop penalty (*K*-factor), used to balance between fuel consumption (or number of stops) and delay in one of the most popular objective functions in the signal retiming practice, is a function of multiple operational conditions and not a constant value as mistakenly recognized by our current signal retiming practice. This is certainly true when one seeks to reduce the fuel consumption as one of the primary objectives of many traffic signal retiming policies. Obviously, the *K*-factor dependency on several operational conditions suggests that the *K*-factor will most likely be different for various approaches at each signalized intersection. That is because each approach at a signalized intersection has unique operational conditions. Thus, having a better understanding of the factors that cause the major observed variations in the *K* value will lead to better signal optimization practices. The following concluding remarks have been reached:

- Operational conditions during stop-and-go events at traffic signals significantly impact excess fuel consumption caused by such stops. The findings have shown that all of the six investigated factors significantly impact fuel consumption, which results in different *K* values.
- Stop penalty for various LDVs ranges between 118-second to 132-second except for LDV with GVW>8500lbs, which results in a stop penalty twice as high as those of other LDVs. This result may indicate that the fuel consumption is more sensitive to the vehicle's mass than the fuel/engine type. Such a conclusion may also be reached by observing the stop penalties of HDDVs, which resulted in ~9-15 times higher values than the average stop penalty from the LDVs.
- An increase of 1% of HDDVs in the fleet distribution adds extra 11 seconds of equivalent delay from the fuel consumption perspective. Similarly, a 1% uphill gradient adds up to ~11 seconds of fuel consumption-equivalent delay if a vehicle is stopped on uphill terrain.
- When accelerating from a stop-line at a signalized intersection, an aggressive driving behavior can increase the fuel consumption of a stopping vehicle by up to 42-seconds of equivalent waiting-idling time, when compared to a "normal" acceleration behavior.
- The increase of fuel consumption and the *K* with an increase of cruising speed seems to follow an exponential trend. For the most common speed limits on urban

arterials (35-45 mph), a stop-and-go event from-and-to a cruising speed of 45-mph (common for major arterials) costs 46 seconds more (of equivalent fuel consumption during idling) than a stop for a vehicle traveling at a cruising speed of 30-mph (e.g., common for side-streets).

- Wind can significantly increase or decrease the stop penalty of HDDV. The findings show that the stop penalty for trucks facing significant headwinds could be increased by up to 970 seconds compared to a no-wind conditions. Thus, this should be seriously considered for signalized intersections of the roadways with frequent and heavy winds and a high percentage of HDDVs.

Although this Chapter has confirmed the significance of individual impacts of major operational conditions on fuel consumption during a stop, further research is needed (possibly with field data) to validate the experimental findings (covered in Chapter 4). Also, more research is needed to investigate the compound effects of various operational conditions (covered in Chapter 3). Most importantly, further research should focus on applying the fuel consumption-driven stop penalties on coordinated signal corridors to test how such stop penalties impact various corridor signal performance measures (covered in Chapter 5). Considering that this chapter focused on computing the stop penalty by using fuel consumption estimates, the focus of the following chapter will be on developing an emission-based stop penalty calculated by using health-related emission types.

3.0 Impact of Various Operating Conditions on Simulated Emissions-Based Stop Penalty at Signalized Intersections

This chapter has been published as:

Alshayeb, S., Stevanovic, A., & Dobrota, N. (2021). Impact of Various Operating Conditions on Simulated Emissions-Based Stop Penalty at Signalized Intersections. *Sustainability*, *13*(18), 10037.

Sustainability has become one of the most important goals when optimizing traffic signals. This goal is achieved through utilizing various objective functions to reduce sustainability metrics (e.g., fuel consumption and emissions). However, most available objective functions do not distinguish between the reduction mechanism of various types of emissions. Further, such functions do not consider the compound impact of multiple operational conditions (e.g., road gradient) influencing emissions on the optimized signal plans. This Chapter derives a new Environmental Performance Index representing a surrogate measure for emission estimates that can be used as an objective function in signal timings optimization to reduce emissions under various operational conditions. The Environmental Performance Index is a linear combination of delays and stops. The key factor of the Environmental Performance Index is the emissions-based stop penalty, which represents an emission stop equivalency measured in seconds of delay. This Chapter also uses traffic simulation and emission models to investigate the compound impact of several operational conditions on the stop penalty. Results show that the stop penalty varies significantly with all the investigated conditions and that the stop penalty is unique for different types of emissions. These findings may have significant implications on the current practice of sustainable signal timing optimization.

3.1 Introduction

Various emission types are determinantal to public health and the environment of the Earth as a whole. On the one hand, some pollutants (e.g., carbon monoxide) cause various health issues (e.g., severe respiratory and cardiovascular problems) (EPA, 2019b, EPA, 2019c), whereas on the other hand, other gases (e.g., carbon dioxide) cause damage to the environment (e.g., climate change) (EPA, 2019d). The industrial and population growth, coupled with rapid urbanization, has led to a drastic increase in automobiles and roadways. Consequently, fuel consumption from the transportation sector contributes to almost 55% of the total health-harmful emissions inventory in the U.S. and 28% of total U.S. greenhouse gas emissions (EPA, 2019e, EPA, 2019f).

Alleviating emissions burden through traffic signal control has been of interest because of its cost-effectiveness and non-reliance on encouraging motorists to adjust their driving habits (e.g., driving at lower speeds) (Stevanovic et al., 2009; Park et al., 2009). Former studies (Stevanovic et al., 2009; Rakha and Ding, 2003) stated that extra emissions and fuel consumption at signalized intersections are intimately associated with unnecessary stop-events and extra seconds of delay while idling. However, the general practice of optimizing signals to minimize delay does not necessarily minimize extra stops; hence emissions could increase (Stevanovic et al., 2009; Park et al., 2009; Rakha and Ding, 2003). Thereby, several studies (Li et al., 2004; Zhao et al., 2018; Kwak et al., 2012) have been conducted to find a Pareto-optimal signal timings solution to balance delay and stops. Over time, in some studies, the balancing between delay and stops has shifted gradually to a tradeoff process between delay and sustainable metrics (e.g., fuel consumption and emissions) (Courage and Parapar, 1975; Li et al., 2004; Stevanovic et al., 2009; Park et al., 2009; Kwak et al., 2012; Liao, 2013; Zhao et al., 2018).

However, most current literature does not differentiate between reducing fuel consumption and emissions. Thus, a question that needs to be raised is whether minimizing fuel consumption truly minimizes a few, some, or all emission types? Results from earlier studies indicate that one or more emission types do not linearly correlate with fuel consumption (Ma and Nakamura, 2010; Akcelik, 1981). Hence, one can infer that signal plans, which minimize fuel consumption, might reduce emissions but do not necessarily minimize various emission types.

The emergence of modern technologies to retrieve high-resolution (e.g., 10 Hz) signal performance measures (mobility and environmental) led to several objective functions being used to characterize vehicular emissions in the signal optimization process (Dobrota et al., 2021a, 2021b, 2022). Although introduced several decades ago, the Performance Index (PI), developed by Robertson, 1969, is undoubtedly still one of the most widely used objective functions in the current signal timing optimization practice (Husch and Albeck, 2006). The PI, shown in Equation 3.1, is a linear combination of delays and stops with a *K*-factor that assigns a weight for each stop in seconds of delay.

$$PI = D + K \times S \tag{3.1}$$

Where:

PI – performance index [second].

D – link delay [second].

K – stop penalty [second].

S – number of stops on the link [second].

A few earlier studies on signal optimization (Courage and Parapar, 1975; Akcelik, 1981; Robertson et al., 1980) used the PI to find a balance between delay and fuel consumption because of their (somewhat) contradicting nature. Robertson et al. 1980 confirmed that assigning more weight to each stop by increasing the *K* value reduces fuel consumption. Subsequent studies on the topic, summarized in (Akcelik, 1981), showed that the *K* value ranges from 26 to 228 seconds. Recent studies (Stevanovic et al., 2021, Alshayeb et al., 2021a) showed that the *K*-factor is a function of various operating conditions that impact the fuel consumption estimates during a stop-event. The same recent studies also indicated that the *K* value derived for fuel consumption is not equal or linearly correlated with the *K* values derived for various vehicular emissions. Thus far, the *K*-factor has not been considered nor investigated from an emission point of view. This Chapter attempts to fill this gap by achieving two primary objectives:

1. Deriving a universal environmental objective function using an emissions-based stop penalty as a tradeoff between vehicular delay and individual emission types.
2. Investigating the impact of various vehicular, topological, operational, and external conditions on the proposed objective function.

According to Banister's sustainable paradigm (Banister, 2008), the first objective of this Chapter requires promoting the public acceptability of reasonable delay at signalized intersections instead of a minimum delay that is usually used as the main objective function to retime traffic signals. Consequently, this Chapter contributes significantly to the research on sustainable signal timing optimization by introducing a family of implementable objective functions to minimize emissions. The derived objective function can be easily integrated into signal timing optimization practice to address environmentally driven signal retiming policies.

The structure of the Chapter takes the form of seven sections, including this introductory section. The second part reviews the most notable studies concerning vehicular emissions and the optimization of traffic signals to minimize emissions and fuel consumption. Section three lays out the theoretical dimensions of the derived objective function. The methods used to investigate the impact of various conditions on the emissions-based stop penalty are provided in section four. The fifth section introduces and examines the findings of the research. Discussion of the findings is given in section six. Finally, the conclusions summarize the Chapter, mention its limitations, and provide insights for future research.

3.2 Literature Review

Emission is a general term used to describe various gases and particles emitted into the air by multiple sources (EPA, 2019g). Such gases and particles can be detrimental solely or combined when two or more pollutants react to a harmful chemical compound. As mentioned previously, the transportation sector contributes significantly to harmful emissions. Hence, many studies have been conducted, on several aspects of transportation, to create a more sustainable transportation atmosphere. Some of these aspects are freight mobility (Touratier-Muller and Jaussaud, 2021; Karam and Hegner Reinau, 2021; Iqbal et al., 2021a; 2021b; Ardalan et al., 2021), bikes (Hull Grasso et al., 2020; Zhao et al., 2021), and intelligent transportation systems (Croce et al., 2021; Pribyl et al., 2021; Gamboa-Rosales et al., 2020; Arafat at al., 2021a; 2021b; Alzoubaidi 2021a; 2021b; Xiao et al, 2021; Kodi et al., 2021). Regarding the traffic signal control aspect, the past fifty years have seen increasingly accelerated progress in improving traffic signal timings to reduce emissions to help save people's lives and the habitability of our planet (Courage and Parapar, 1975; Claffey, 1976; Robertson et al., 1980; Akcelik, 1981; Smith et al., 2001; Li et al., 2004; Stevanovic et al., 2009; Park et al., 2009; Ma and Nakamura, 2010; Kwak et al., 2012; Liao, 2013; Zhao et al., 2018). This section briefly reviews the literature from two critical aspects for this Chapter:

1. Primary vehicular emission types.

2. The most remarkable objective functions to decrease emissions and fuel consumption through signal timing optimization.

3.2.1 Major Vehicular Emissions

Vehicles do not always need to be moving to release emissions (Rubin et al., 2006; Zhang et al., 2018); thus, vehicular emissions can be classified according to the vehicle operating mode in which emissions are emitted into three categories:

1. Evaporative "non-tailpipe" emissions are mainly driven by diurnal fuel evaporation, residual engine heat following vehicle operation inducing hot soak emissions and running evaporative loss emissions that occur while vehicles are running (Rubin et al., 2006).
2. Refueling emission are volatile organic compound (VOC) vapor and entrained droplets displaced from the fuel tank ullage (Zhang et al., 2018).
3. Tailpipe "exhaust" emissions are the most evident because they are emitted while running the vehicle (Frey et al., 2003). The focus of this Chapter was on tailpipe emissions because they are profoundly emitted at road intersections constituting the most significant percentage (~71 ± 9% of the total vehicular emissions) of all types of vehicular emissions (Pierson et al, 1999; Rubin et al., 2006).

Table 3.1 summarizes the primary tailpipe emissions and their impact on public health and the environment.

Table 3.1 Impact of primary vehicular emissions on public health and environment.

Emission Type	Emission Category	Effect
Carbon Monoxide (CO)	Tailpipe	Reduces the amount of oxygen transported in the bloodstream to critical organs such as the heart and brain (EPA, 2019h). It can also cause dizziness, confusion, unconsciousness, and death at high concentrations (EPA, 2019h).
Carbon dioxide (CO_2)	Tailpipe	Increases the Earth's temperature (global warming), causing climate change (EPA, 2019i). It is noted here that CO_2 is not an air pollutant, but it is one of the major greenhouse emissions emitted by vehicles.
Nitrogen oxides (NO and NO_2, together called NOx)	Tailpipe	Contributes to global warming (EPA, 2019d), acid rain (EPA, 2019j), and depletion of the ozone layer (Portmann et al., 2021). It also damages the human respiratory tract and increases a person's vulnerability to respiratory infections and asthma (EPA, 2019k).
Hydrocarbons (HC), also known as volatile organic compounds (VOCs) or non-methane hydrocarbons (NMHC) (Touratier-Muller et al., 2021)	Evaporative, refueling, and tailpipe	Reacts with nitrogen oxides in the presence of sunlight to form ground-level ozone, which can trigger various health problems, including chest pain, coughing, throat irritation, and congestion (EPA, 2019l).
Particulate matter of size < 10 microns (PM_{10}) and < 2.5 microns ($PM_{2.5}$) including black carbon (BC)	Tailpipe	PM caused several health issues, including cardiovascular effects, such as cardiac arrhythmias and heart attacks, and respiratory effects, such as asthma attacks and bronchitis (EPA, 2019c).

Despite the importance of particulate matter (PMs) as harmful pollutants, the PMs were not considered in this Chapter because most commercially available emissions models do not provide PM estimates for vehicles powered by gasoline. Despite the primary source of PMs generation being diesel-powered vehicles (Panis et al., 2006), most available emissions models do not estimate high-resolution (second-by-second) PMs measures for such vehicles. Although a few models (e.g., VT-Micro (Rakha et al., 2004)) can estimate second-by-second PMs measures for HDDVs, the publicly available versions of such models are not suitable to conduct the large number of scenarios performed in this Chapter (discussed in Section 3.4.1).

One way to classify road intersections is based on the type of traffic control devices (Stevanovic et al., 2019; taraneh et al., 2020; Ali et al., 2021; Ali et al., 2022). That involves two types of intersections: 1. Unsignalized intersections, where the right of the way is defined using the traffic control signs (e.g., stop or yield), and 2. Signalized intersections, where traffic lights are used to spatially and temporally allocate conflicting traffic streams (Roess et al., 2004).

The design of both intersection types does not follow an exact rule. Still, it considers the effect of multiple factors (e.g., physical space and signal timings) simultaneously to provide safe and efficient mobility (Roess et al., 2004; Niels at al., 2020; Gavric et al., 2022). This Chapter focuses on the excess tailpipe emissions induced by non-optimal signal timings at signalized intersections. Moreover, the proposed methodology applies to various signalized intersections' designs.

3.2.2 Relevant Objective Functions

A large and expanding body of literature has investigated reducing vehicular emissions through the retiming of traffic signals. This subsection summarizes the objective functions used in the most notable signal optimization studies endeavoring to reduce fuel consumption and emissions. The studies reviewed here have used a common approach in their models by integrating a traffic model, fuel consumption and emissions model, and an optimization method to improve an objective function. Table 3.2 summarizes the reviewed studies according to those integrated elements.

There are two types of traffic models used in the reviewed studies, which are deterministic (also known as analytical or macroscopic) models (e.g., (Lighthill and Whitham, 1955; Richards, 1956)) and stochastic (also known as microscopic) simulation models of more realistic real-world traffic through the application of computer programs (e.g., (PTV Vissim, 2020)). Similarly, analytical (with pre-computed fuel consumption and emissions factors) (e.g., Frey et al., 2002) and microscopic (second-by-second) (e.g., (Scora and Barth, 2006)) fuel consumption and emissions models were utilized to estimate the objective function and measure the improvement in emission savings. Although utilizing macroscopic models is computationally efficient, approaches of this kind carry various well-known limitations, such as the inability to capture the individual characteristics of drivers; hence, they generate less accurate emissions estimates. Therefore, studies that used high-resolution models seem to be more reliable than those that utilized analytical models. The optimization methods used by research presented here can be broadly classified into three techniques: 1. Calculus-based using the first derivative, 2. Guided random search utilizing the Genetic Algorithm (GA) approach, and 3. The enumerative technique as a common way to solve mixed-integer mathematical programs.

Several objective functions were developed and optimized using one of the optimization techniques mentioned above. Those objective functions represent either fuel consumption and emissions directly (e.g., (Stevanovic et al., 2009; Park et al., 2009)), Performance Indexes (PIs) associated directly with fuel consumption emissions (e.g., (Li at el., 2004; Oda et al., 2004)), or a combination of both (e.g., (Osorio and Nanduri, 2015)). A major criticism of using fuel consumption and emissions directly as an objective function is that it fails to recognize the difficulties that arise when attempting to estimate fuel consumption and emissions in a specific site in the field. Another problem with this approach is that it might reduce emissions at the expense of worsening mobility metrics (e.g., delay). The former issue also applies to the objective functions where direct mobility and emissions measures are combined. Moreover, regardless of their objective function, most of the literature lacks accuracy because they do not consider various operational conditions (e.g., vehicle type and road gradient) that impact the emissions estimates at signalized intersections. Therefore, this Chapter derived an environmental objective function that can be tailored to a specific emission type and considers various operational conditions.

Table 3.2 Most notable objective functions used in signal timings optimization to reduce fuel consumption and emissions.

Study	Traffic Model	Emissions Model	Optimization Technique	Optimized Parameter(s)	Objective Function	Nomenclature
Li et al., 2004	Analytical	Analytical	Calculus-based	Delay, fuel consumption, and emissions	$PI = \alpha \frac{D}{\mathrm{Di}} + \beta \frac{F}{\mathrm{Fi}} + \gamma \frac{E}{\mathrm{Ei}}$	*D*: delay, *F*: fuel consumption, *E*: emissions, α, β, and γ: relative significance weights, *D*i, *F*i and *E*i: values of *D*, *F* and *E* for the initial signal-timing scenario.
Oda et al., 2004	AVENUE	Analytical	Calculus-based	Delay, stops, and CO_2	$PI = \sum (\alpha \cdot d + \beta \cdot S)$	*D*: delay, *S*: stops, α and β: weight coefficients.
Stevanovic et al., 2009	VISSIM	CMEM	Genetic algorithm	Fuel consumption and CO_2	$FR(t) = \emptyset \cdot (K \cdot N \cdot V + \frac{P}{\mu}) \cdot \frac{1}{44}$ $CO_2 = a \cdot FR + r$	*FR(t)*: fuel rate, $\emptyset$: stoichiometric fuel/air equivalence ratio, *K*: the engine friction factor, *N*: engine speed, *V*: engine displacement, *P*: engine power output, μ: a measure of indicated efficiency, and 44—the lower heating value of typical gasoline. *a* and *r* are the CO_2 index coefficients.
Park et al., 2009	CORSIM	VT-Micro	Genetic algorithm	Fuel consumption and emissions (as a posteriori)	$\ln(FC) = \left\{ \sum_{i=0}^{3} \sum_{j=0}^{3} L_{i,j}^{e} \cdot s^{i} \cdot a^{j} \right.$	$L_{i,j}^{e}$: represent model regression coefficients for fuel consumption (*FC*) at speed (*s*) exponent *i* and acceleration (*a*) exponent *j*.
Ma and Nakamura, 2010	Analytical	Analytical	Calculus-based	NOx	$NOx = \left(\frac{d_{NOx_i}}{d_t} \cdot \sum_{i=1}^{n} D_s \right) + (NOx_d + NOx_a)$	$\frac{d_{NOx_i}}{d_t}$: emission rate of idle mode for vehicle *i*, D_s: stopped delay, *n*: stops, *d*: deceleration phase, *a*: acceleration phase.
Kwak et al., 2012	TRANSIMS	VT-Micro	Genetic algorithm	Fuel consumption	$\ln(FC) = \left\{ \sum_{i=0}^{3} \sum_{j=0}^{3} L_{i,j}^{e} \cdot s^{i} \cdot a^{j} \right.$	Same as Park et al., 2009
Zhang et al., 2013	Cell Transmissions model (CTM)	Analytical	Genetic algorithm	Emissions as bulk	$E_{j,k_f} = \sum_{i=1}^{I} \left\{ \frac{t_{i,j,k_f}}{T_{j,k_f}} \cdot ER_i \right\}$	E_{j,k_f}: average emission rate on link *j* for speed range *k* on facility *f*, ER_i: *VSP* modal average emission rate for *VSP* Mode *i*, *VSP*: vehicle specific power, *t*: time spent in *VSP* mode, *T*: total travel time on link.
Lv et al., 2013	Analytical	MOVES and Analytical	Genetic algorithm	CO	$CO = \begin{cases} 1791.49 \cdot D^{0.04153}, v = 45 \\ 1331.28 \cdot D^{0.03099}, v = 40 \\ 883.5 \cdot D^{0.02133}, v = 35 \end{cases}$	*D*: delay, *v*: speed
Khalighi and Christofa, 2015	Analytical and AIMUSN	Analytical	Mixed-integer nonlinear program	Emissions as bulk	$E_{j,k_f} = \sum_{i=1}^{I} \left\{ \frac{t_{i,j,k_f}}{T_{j,k_f}} \cdot ER_i \right\}$	Same as Zhang et al., 2013
Osorio and Nanduri, 2015	Analytical and AIMUSN	Analytical	Metamodel simulation-based	Travel time and emissions (as bulk)	$f = f^{t} \frac{w^{t}}{n^{t}} + f^{CO2} \frac{w^{CO2}}{n^{CO2}} + f^{NOx} \frac{w^{NOx}}{n^{NOx}} + f^{VOC} \frac{w^{VOC}}{n^{VOC}} + f^{PM} \frac{w^{PM}}{n^{PM}}$	f^{T}, f^{CO2}, f^{NOx}, f^{VOC}, f^{PM}: expected travel time and various emission types, w^{T}, w^{CO2}, w^{NOx}, w^{VOC}, w^{PM}: economic weighting parameters, n^{T}, n^{CO2}, n^{NOx}, n^{VOC}, n^{PM}: normalization constants for travel time and emission types.
Han et al., 2018	Lighthill-Whitham-Richards (LWR) model	Analytical	Mixed-integer linear program	Throughputs and emissions (as a posteriori)	$f = \max \sum_{k=1}^{m} \frac{1}{k+1} \sum_{I_i \in \tau} q_i^k$	*M*: total number of time intervals, τ: prescribed set of links, q_i: the flow at which vehicles exit link *Ii*

The critical element of the derived objective function is the emissions-based stop penalty. Furthermore, the Chapter investigates the combined impact of various operational conditions: vehicle type, the proportion of heavy vehicles in the fleet, driving behavior, road gradient, cruising speed, and wind effect on the emissions-based stop penalty. The investigation was done using a full-factorial experimental design representing different operational conditions. The traffic simulation Vissim (PTV Vissim, 2020) was employed to perform the dynamics part of the experiments and generate vehicles' trajectories (also known as floating car data) for numerous scenarios. Those trajectories were then used to estimate emissions (HC, CO, NOx, and CO_2) from the Comprehensive Modal Emission Model (CMEM) (Scora and Barth, 2006). Finally, the emissions-based stop penalty was computed for each tested emission type under all investigated scenarios.

3.3 Environmental Objective Function

This section presents the derivation of the proposed objective function. For the reader's convenience, Table 3.3 summarizes the notation used in this section.

Table 3.3 Nomenclature.

Variable	Description
E_i	Total amount of emission type *i* emitted during an entire stop (gallons, liters, or grams)
E_{D_i}	Total amount of emission type *i* emitted during deceleration mode (gallons, liters, or grams)
E_{I_i}	Total amount of emission type *i* emitted during idling mode (gallons, liters, or grams)
E_{A_i}	Total amount of emission type *i* emitted during acceleration mode (gallons, liters, or grams)
i	Emission type
K_{Ee}	Ratio between the amount of emission induced by stop and one caused by stopped delay
E_{DA}	Emissions during deceleration and acceleration modes (gallons, liters, or grams)
K_E	Emissions-based stop penalty (seconds)
T_I	Idling phase duration (seconds)
t_1 and t_2	Any two-time points where: $t_1 < t_2$ (seconds)
E	General term for emission despite of the emission type (gallons, liters, or grams)
E_r	Emission rate (gallons, liters, or grams per unit time)
t	Any point of time (seconds)
Δ_t	Time interval between any two-time points (seconds)
a, b, c, and d	Time points of starts and ends of various driving phases, as characterized in Figure 1 (seconds)
$Env - PI$	Environmental Performance Index (seconds)
j	Link
n	Total number of links
$CO - PI$	Carbon monoxide Performance Index (seconds)
D_j	Stopped delay on link *j* (seconds)
S_j	Total stops on link *j* (seconds)
e_i	Amount of emission type *i* estimated by CMEM (grams)
a_i and r_i	Index coefficients of emission type *i*
FR	Fuel rate (grams/sec)
$\emptyset(t)$	Stoichiometric fuel/air equivalence ratio
$K(t)$	Engine friction factor
$N(t)$	Engine speed (revolutions/seconds)
V	Engine displacement (liters)
$P(t)$	Engine power output (kW)
μ	Indicated efficiency (default value is 0.4)

The original definition of the *K*-factor referred to the number of seconds of delay that is equivalent to a single stopping maneuver (Robertson, 1969). A few studies (Akcelik, 1981; Stevanovic et al., 2021; Alshayeb et al., 2021a) redefined the *K*-factor as the number of seconds of idling delay (referred to as stopped delay hereafter) that consume the same amount of fuel consumed during a stop. This research defines the stop penalty as the number of seconds of stopped delay equivalent to excess emissions caused by the action of stopping (deceleration and acceleration phases, referred to as a stop hereafter), and this is called stop penalty K_E. Consequently, the K_E value required to reduce a specific emission type was derived based on the amount of a specific gas emitted during the three driving modes of a complete stop. These modes are deceleration, idling, and acceleration, and they all form what is known as the vehicular stop profile shown in Figure 3.1. The total amount of a particular gas emitted during a stop is expressed in Equation 3.2, where all units are identical and can be expressed in gallons, liters, or grams:

$$E_i = E_{D_i} + E_{I_i} + E_{A_i} \tag{3.2}$$

To compute how many seconds of delay emit the same amount of a particular emission type caused by a stop, we need to find the ratio (K_{Ee}) between the amount of that emission type induced by the stop and the one caused by the stopped delay (Figure 3.1). Thus, it is essential to separately identify extra emissions caused by the stop, represented as E_{DA} ($E_D + E_A$), from those emitted during the stopped delay, represented as E_I. As all ratios, the K_{Ee} expressed in Equation 3.3 is unitless. Hence, when the E_I is divided by the idling phase duration (T_I), which varies based on the duration of the red interval, the result gives the number of seconds of stopped delay that emit the same excess emissions equivalent to a stopping event. That is what is defined as the emissions-based stop penalty (K_E) (given in Equation 3.4).

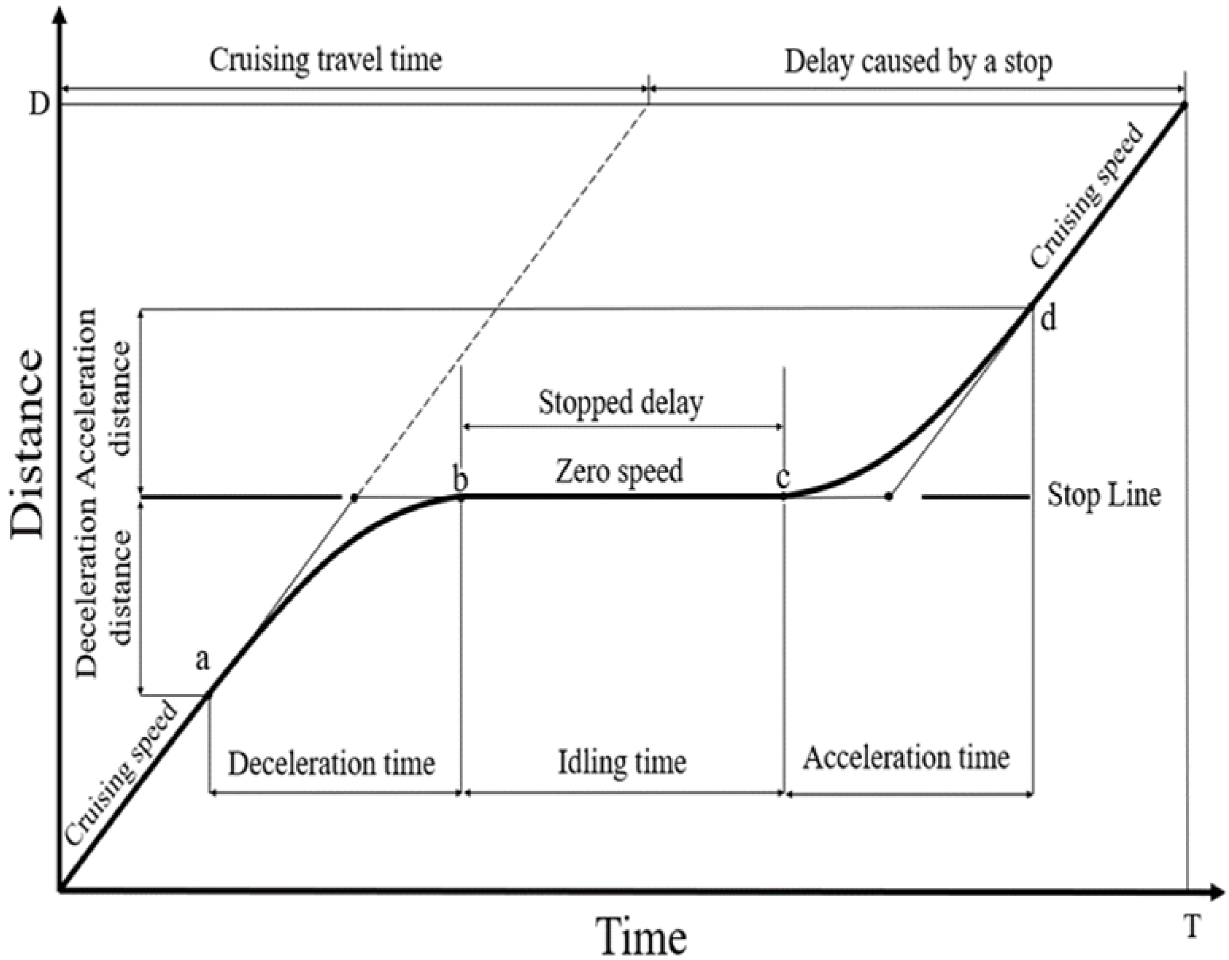

Figure 3.1 Time-distance (stop) profile of a full stop.

$$K_{Ee} = \frac{E_{DA}}{E_I} \tag{3.3}$$

$$K_E = \frac{E_{DA}}{\frac{E_I}{T_I}} = \frac{E_{DA} \cdot T_I}{E_I} \tag{3.4}$$

Figure 3.2 shows instantaneous (second-by-second) emitting rates of four emission criteria (HC, CO, NOx, and CO_2) during a complete simulated stop from 20 mph and back. It is noted here that Figure 3.2 is from a single simulated trajectory in Vissim, where emission estimates were estimated by using the CMEM software for the same simulated trajectory. Area 1, Area 2, and Area 3 represent the emissions during the deceleration, idling, and acceleration phases, respectively. The sum of those three areas under each emission criterion's curve is the total amount of that criterion emitted during a stop for a particular vehicle under specific operational conditions (e.g., cruising speed, road gradient). Areas 1–3 under any curve can be found by doing a definite integral of the time-dependent variable emission rate (E_r) curve between any two-time points t_1 and t_2:

$$E = \int_{t1}^{t2} E_r(t) \cdot dt \tag{3.5}$$

With the availability of second-by-second emission estimates, the amount of emissions caused by a stop (Equation 3.3) can be computed as the sum of the emissions in every time interval (Δ_t) of driving (Equation 3.6), where points *a*, *b*, *c*, and *d* are the starts and ends of various driving phases as characterized in Figure 3.1.

$$E_i = \sum_{t=a}^{b} E_{D_i}(t) \cdot \Delta t + \sum_{t=b}^{c} E_{I_i}(t) \cdot \Delta t + \sum_{t=c}^{d} E_{A_i}(t) \cdot \Delta t \tag{3.6}$$

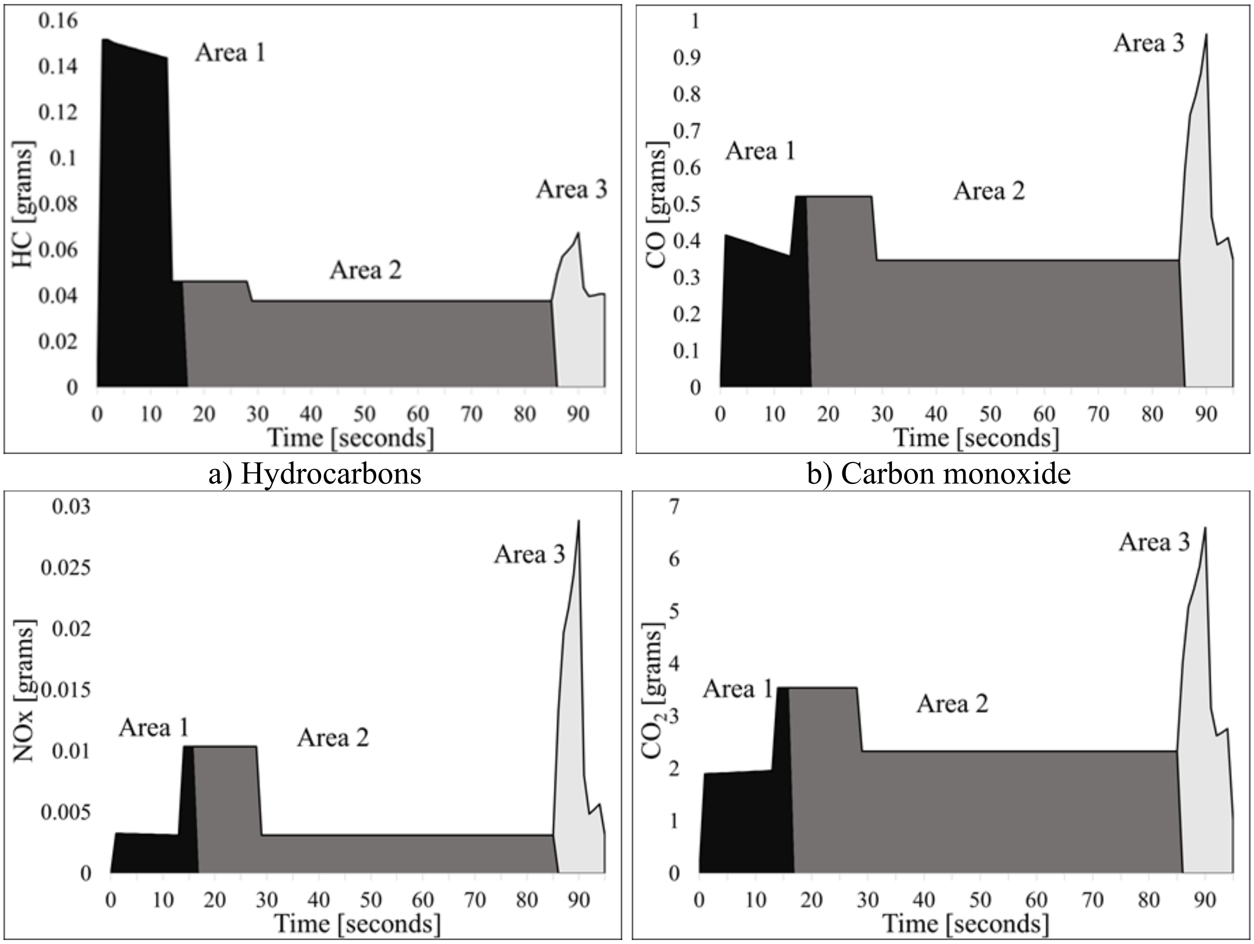

a) Hydrocarbons
b) Carbon monoxide
c) Nitrogen oxides
d) Carbon dioxide

Figure 3.2 Various emission type footprints caused by a single stop (20-mph-zero-20-mph).

The K_E can then be calculated by substituting the values of E_{DA} and E_I with their values from Equation 3.6, as follows:

$$K_E = \frac{\left(\sum_{t=a}^{b} E_{D_i}(t) \cdot \Delta t \ + \ \sum_{t=c}^{d} E_{A_i}(t) \cdot \Delta t\right) \cdot \ \sum_{i=b}^{c} \Delta t}{\sum_{t=b}^{c} E_{I_i}(t) \cdot \Delta t} \tag{3.7}$$

It is apparent from Equation 3.7 that the K_E varies based on the amount of emission during each of the deceleration, idling, and acceleration modes. Furthermore, Figure 3.2 shows that various emission criteria are emitted at different rates during each driving mode. Thus, it is anticipated that K_E would vary for different emission types. For that reason, an Environmental

Performance Index (Env-PI) is defined as a generic objective function that can be derived to reduce a particular emission criterion (E) (e.g., HC, CO, NOx, and CO_2) caused by stopping at traffic signals. The Env-PI for a network can be computed by summing the Env-PIs for all movements in the network as follows:

$$Env - PI = \sum_{j=1}^{n} D_j + \frac{\left(\sum_{t=a}^{b} E_{D_i}(t) \cdot \Delta t \; + \; \sum_{t=c}^{d} E_{A_i}(t) \cdot \Delta t\right)_j}{\left(\frac{\sum_{t=b}^{c} E_{I_i}(t) \cdot \Delta t}{\sum_{t=b}^{c} \Delta t}\right)_j} \cdot S_j \tag{3.8}$$

Consequently, the Env-PI for a particular emission type can be defined as one of a family of similar Env-PIs. For example, HC-PI, CO-PI, NOx-PI, and CO_2-PI are all members of the Env-PI family that are explicitly derived to reduce HC, CO, NOx, and CO_2, respectively. For the sake of giving an example that Env-PI could be derived for any emission criterion, Equation 3.9 shows a CO-PI. That suggests that the CO-PI may result in different signal timings for a particular network than those derived for any other Env-PIs. Therefore, the relevant Env-PI should be used when optimizing signals to reduce a specific emission criterion.

$$CO - PI = \sum_{j=1}^{n} D_j + \frac{\left(\sum_{t=a}^{b} CO_{D_i}(t) \cdot \Delta t \; + \; \sum_{t=c}^{d} CO_{A_i}(t) \cdot \Delta t\right)_j}{\left(\frac{\sum_{t=b}^{c} E_{I_i}(t) \cdot \Delta t}{\sum_{t=b}^{c} \Delta t}\right)_j} \cdot S_j \tag{3.9}$$

This Chapter uses the microscopic power demand emissions model CMEM to estimate second-by-second emissions (Scora and Barth, 2006). CMEM estimates various emissions as a function of the fuel rate, which depends on the air-fuel ratios occurring during internal fuel combustion. Equation 3.10 shows the general form of the equation used to estimate a particulate emission criterion E_i (Scora and Barth, 2006).

$$e_i = a_i \cdot FR + r_i \tag{3.10}$$

$$FR(t) = \emptyset(t).(K(t).N(t).V + \frac{P(t)}{\mu}).\frac{1}{44} \tag{3.11}$$

The following section presents the data and methods used to investigate the impact of six major factors influencing the K_E. Those factors are 1- Vehicular type, 2- Proportion of heavy vehicles in fleet distribution, 3- Driver's behavior, 4- Road gradient, 5- Cruising speed, and 6- Wind effect. It is noted here that the factors investigated in this Chapter are not exclusive. They were primarily selected because they can be feasibly modeled in relevant simulation models (e.g., Vissim and CMEM), as explained in the following section.

3.4 Data and Methods

This Chapter adopts a four-step sequential method that starts with designing a full-factorial experiment to generate all possible scenarios for the combined impact of all studied factors on the K_E. The next step was to model a test-bed intersection in Vissim. Subsequently, a Vissim-Python-CMEM interface was developed to ensure proper representation of both the dynamics and kinematics elements of the designed scenarios. Finally, the K_E was computed for each investigated emission criterion, and all performed scenarios.

3.4.1 Full-Factorial Experiment Design

A full-factorial experiment (Fisher, 1992) was designed to create scenarios for various operating conditions and studied their combined effect on the K_E. The levels of the various investigated factors were chosen in such a way to ensure the diversity of the operating conditions, such as vehicle type, road gradient, speed limit, etc., as detailed in Table 3.4. Regarding vehicle types, this Chapter included 12 Light-duty vehicles (LDVs) and 3 Heavy-duty diesel vehicles (HDDVs) in the experiments. Those 15 vehicle types are out of 31 types available in CMEM and were chosen because they form the largest percentage of the entire vehicle fleet used to develop the CMEM. The first column in Table 3.4 shows the category number of the selected vehicle groups as they have been named in CMEM (and in this Chapter). It is worth mentioning that the CMEM was developed using vehicles made in the years 1990–2000. Using such a relatively older fleet might not precisely represent the current fleet operating in the field. However, CMEM was the most suitable model for this study because of its command prompt interface, which allows users to run thousands of vehicular trajectories efficiently. In addition, the error that might be introduced to the stop penalty value because of using an older fleet would be considered minor compared to using a constant stop penalty value. CMEM developers have chosen the vehicle/technology categories based on a vehicle's emissions contribution. The emissions standards used to categorize the tested vehicles are the "California Vehicle Emissions Standards" (Barth et al., 2000). It is noted here that LDV1-LDV11 are powered by gasoline, whereas LDV12 and HDDV1–HDDV3 are powered by diesel.

Table 3.4 Levels for various operational conditions impacting K_E.

Vehicle Type		Fleet Distribution	Driver Behavior	Road Gradient	Cruising Speed	Wind Effect
CMEM	This Chapter	LDV:HDDV	Acceleration functions	(%)	(mph)	(mph direction)
Car, Category 1	LDV1	100:0	Function 1	−7	20	50 tailwind
Car, Category 2	LDV2	99:1	Function 2	−6	25	40 tailwind
Car, Category 3	LDV3	98:2	Function 3	−5	30	30 tailwind
Car, Category 4	LDV4	97:3	Function 4	−4	35	20 tailwind
Car, Category 5	LDV5	96:4		−3	40	10 tailwind
Car, Category 6	LDV6	95:5		−2	45	No wind
Car, Category 7	LDV7	94:6		−1	50	10 headwind
Car, Category 8	LDV8	93:7		0	55	20 headwind
Car, Category 9	LDV9	92:8		1	60	30 headwind
Car, Category 10	LDV10	91:9		2	65	40 headwind
Car, Category 11	LDV11	90:10		3		50 headwind
Car, Category 12	LDV12			4		
Truck, Category 5	HDDV1			5		
Truck, Category 6	HDDV2			6		
Truck, Category 7	HDDV3			7		

Percentages range between 0% and 10%, with an increment of 1% of heavy vehicles in the fleet, were considered. Following the general recommendations for maximum grades (Hancock and Wright, 2013), This Chapter adopted a road gradient range between -7% and 7%. Cruising speeds (represented by speed limits) usually range from 20 to 65 mph, depending on the geometrical and traffic conditions. Thus, 10 speed limits, with an increment of 5 mph, were chosen to cover all possible speed limits between 20 and 65 mph. The aerodynamic effects were represented by various wind speeds and directions (headwind (HW) and tailwind (TW)). The wind speeds range from zero-wind to a wind of 50 mph, with an increment of 10 mph, for both HWs and TWs. This research only considers the impact of wind on K_E of HDDVs because the wind effect is most profound for trucks, and CMEM does not model the wind effect for LDVs. Finally, the impact of the driver's aggressiveness on K_E is investigated by analyzing four acceleration–deceleration functions, where each function represents a single unique driving behavior. More details about the tested driving-behavior functions are provided in Section 3.4.7.

A total of 27,000 scenarios have been generated representing all possible combinations of the independent factors impacting K_E for the range of values of each factor given in Table 3.4. The exception is the fleet distribution, which was investigated by utilizing Equation 3.12 that computes the K_E for a movement as the sum of the percentage (p) of each vehicle type (i) multiplied by its relevant average stop penalty (K_{Ei}) for all vehicles of type n. It is worth noting that investigating the impact of multiple vehicle types from the same class is out of this Chapter's scope. Thus, LDV1 and HDDV1 are selected to investigate the impact of fleet distribution on the K_E. For LDVs, a total of 7200 experiments were designed (12 (vehicle types) × 4 (driving behaviors) × 15 (grades) × 10 (cruising speeds)). For HDDVs, a total of 19,800 experiments were designed (3 (vehicle types) × 4 (driving behaviors) × 15 (grades) × 10 (cruising speeds) 11 (wind effects)). Lastly, using the results of the 13,200 experiments, Equation 3.12 was applied to investigate the impact of fleet distribution on the K_E. Those 13,200 experiments represent the impact of 11 fleet distributions times (1 (LDV) × 4 (driving behaviors) × 15 (grades) × 10 (cruising speeds) + 1 (HDDV) × 4 (driving behaviors) × 15 (grades) ×10 (cruising speeds)).

$$K_E = \sum_{i=1}^{n} p_i \cdot K_{Ei} \tag{3.12}$$

3.4.2 Traffic and Emissions Models

Certainly, the best way to measure the impact of various operating conditions on the K_E is through field experimentation and data collection. However, collecting real-world emissions data across all ranges of factors is a challenging and very costly task. A massive dataset is needed to include all possible combinations of factors affecting stop-related emissions and their relevant stop penalties. Therefore, this Chapter is primarily based on simulation experiments, aiming to mimic the real-world vehicular stopping mechanisms under all the possible scenarios, as explained in the following sections.

3.4.3 Traffic Simulation Program

PTV Vissim (PTV Vissim, 2020) is a microscopic model developed to simulate urban traffic and public transport operations. Vissim is a popular tool in the traffic community because it is easy to use and can simulate and test almost any traffic-related scenario before being implemented in the field. In addition to the previous advantages, Vissim was selected in this Chapter for the following reasons:

1. Its ability to accurately model traffic signals and other operations (e.g., speed and acceleration) at a resolution of 1 second.
2. It provides the possibilities to model all of the investigated factors in this Chapter (e.g., road gradient per link and driving behavior).
3. Vissim can be easily interfaced with relevant programming languages (e.g., Python), allowing the user to manipulate the investigated factors' attributes and perform many experiments efficiently.
4. Vissim outputs vehicle trajectory (also known as floating car data) files (FZP), which are well fitted for modeling in CMEM to obtain second-by-second emission estimates.

3.4.4 Modal Emission Model

CMEM (Scora and Barth, 2006) is a power-demand emissions model that estimates second-by-second fuel consumption and emissions (HC, CO, NOx, and CO_2) based on vehicular speed and acceleration traces. The developers of CMEM used more than 300 tested vehicles to develop the model. CMEM has one estimation module for LDVs and another for HDDVs; thus, a user needs to separate vehicles in the fleet before processing their trajectories in CMEM into LDVs and HDDVs. A second-by-second speed trace is required at minimum as an input for CMEM to estimate various emissions, where those inputs can be acquired from Vissim. CMEM was selected for this Chapter for three reasons:

1. CMEM can estimate emissions for various vehicle types.
2. It allows users to include the influence of road gradient (for all vehicle classes) and wind effect (for HDDVs only) on emissions estimates.
3. CMEM has already been calibrated and validated using data from the National Cooperative Highway Research Program (An et al., 1997). Moreover, a few studies have already validated estimates from CMEM, and they concluded that CMEM is a generally accepted model that can generate verifiable emissions estimates (Barth et al., 2001; Rakha et al., 2003). Therefore, no calibration or validation efforts were needed to perform the methodology of this Chapter.

3.4.5 Modeling of A Test-Bed Intersection

A four-leg intersection, IL-21 in Washington Street in Lake County, Chicago, IL, was selected to apply the modeling scenarios for the sake of applying the methodology of this Chapter.

The intersection has four traffic lanes (two through and one exclusive for each of the right and left turns) at each approach. The Division of Traffic at Lake County, in the Chicago metro area, provided the directional volumes and turning movement counts for the modeled intersection (Figure 3.3). An eight-phase fixed-time signal timing plan was operated on the simulated intersection. A cycle length of 140 s was modeled, as shown in the Ring-Barrier Diagram in Figure 3.3. The simulation time was 1100 s, including 200 s for warmup time. This simulation time is long enough to gather relevant results for a minimum of 400 stopped vehicles at the intersection in each performed scenario, representing a sufficient statistical sample size.

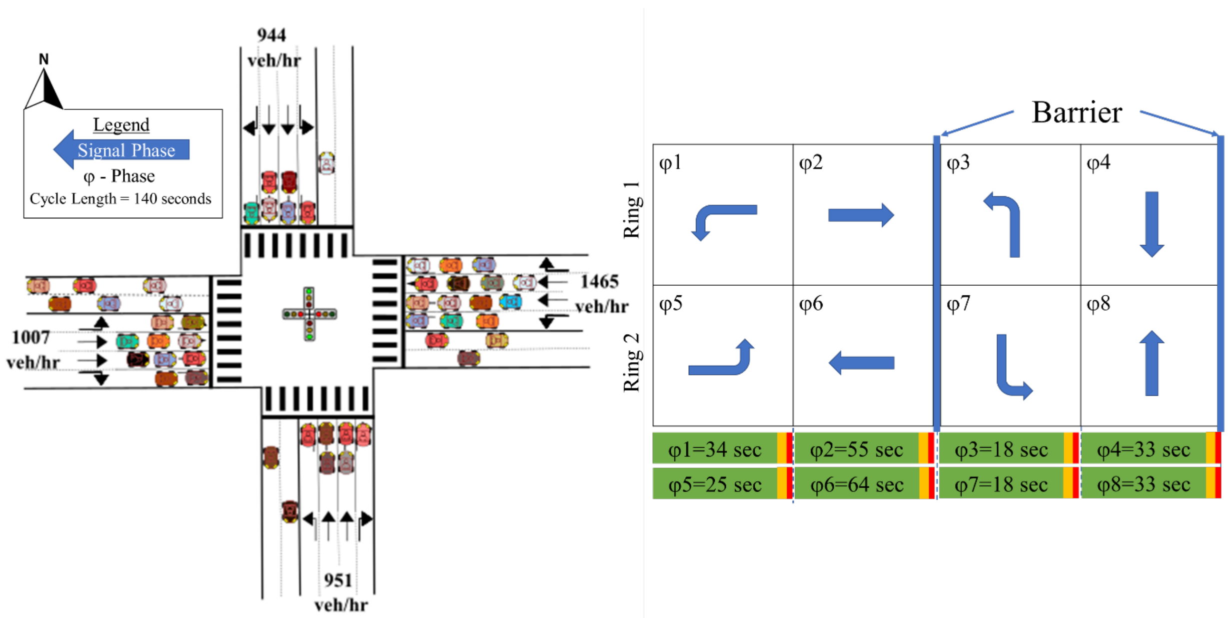

Figure 3.3 Layout, volumes, and splits of the modeled intersection.

3.4.6 Modeling of Various Operating Conditions

All the investigated factors, except the impact of wind, were modeled in Vissim and CMEM, whereas the wind effect was modeled only in CMEM. For the vehicle type, two vehicle classes were modeled in Vissim; cars and heavy goods vehicles (HGVs), which were modeled as LDVs and HDDVs in CMEM. The percentages of cars and HGVs in Vissim were modeled by changing the relative flow value of each vehicle class in the vehicle compositions defined for each intersection approach.

Vissim models cruising speeds by using stochastic desired speed distributions, which assigns the proportion of the vehicles in the fleet that drive higher, lower, and in between the defined minimum and maximum speeds. However, the goal of modeling cruising speeds in this Chapter was to ensure that all stopped vehicles decelerate from a particular speed and then accelerate back to the same original speed. Thus, this Chapter defined ten deterministic speed distributions in Vissim for the speeds from 20 to 65 mph with 5-mph steps. Deterministic speed distributions were modeled by setting relative values to each distribution's minimum and maximum speeds. For example, minimum and maximum speeds of 24.99 mph and 25 mph are set to obtain a 25-mph cruising speed before and after stopping for all stopped vehicles. CMEM then uses second-by-second speeds from trajectories to estimate emissions.

Modeling road gradient was done in Vissim to cover the impact on the acceleration and then in CMEM to consider the influence of increased power demand on the emissions estimates. Investigated grades were defined as percentages (e.g., -2% and 2%) for each link in Vissim, starting from the stop line to the point where vehicles reach their original cruising speeds. Afterward, the road gradients (expressed in degrees and radians, respectively, for LDVs and HDDVs) were added to the trajectories from Vissim before further processing in CMEM.

CMEM supports defining headwind and tailwind directions for various speeds on the trajectories processed in the HDDVs module only. Thus, the obtained HGV stop profiles from Vissim were assigned a wind direction and speed according to the performed scenario. Finally, the driving behaviors investigated in this Chapter were represented by various desired deceleration–accelerations functions, as explained in the following subsection.

3.4.7 Modeling of Driving Behaviors

The desired acceleration or deceleration value assigned to vehicles at each time step in the simulation is one of the most critical and relevant elements to determine driver behavior in Vissim (PTV Vissim, 2020). Vissim defines acceleration and deceleration values (referred to as acceleration–deceleration functions hereafter) as functions of the current speed. Both acceleration–deceleration functions consist of three curves representing the minimum, median, and maximum possible acceleration–deceleration values at different speeds (PTV Vissim, 2020). Although Vissim provides default acceleration–deceleration functions for various vehicle classes, utilizing those functions is problematic from two aspects. First, the default acceleration–deceleration functions in VISSIM are based on an older dataset from Europe. Consequently, a few studies (Stevanovic and Gundogan, 2012; Partners, 2019) indicated that such functions do not apply to current fleets in the US. Second, the acceleration–deceleration functions in Vissim are stochastic because the acceleration or deceleration value, at a certain speed, lies within a specific range between the minimum and maximum values. That means that each stopped vehicle in the simulation can have a unique driving behavior, making it impossible to capture the impact of deceleration–acceleration functions (driving behaviors) on the K_E. Moreover, using stochastic functions adds noise to the results of the impact of the other factors.

Two actions were taken to overcome the issues emerging from using Vissim's default acceleration–deceleration functions. First, this Chapter used a vehicular trajectories dataset of 177 vehicles, including 1850 hours of driving and more than 40,000 traveled miles, to develop a set of acceleration–deceleration functions representative of the US fleet. Second, the Dynamic Time Warping (DTW) (Sakoe and Chiba, 1978) and k-means clustering (Hartigan and Wong, 1979) algorithms were utilized to classify the newly developed stochastic acceleration–deceleration functions into four deterministic functions utilizing a relatively large sample of stopped vehicles. Such deterministic functions enable fully controllable experiments, which guarantee accurate quantifying of the impact of various driving behaviors and other factors (e.g., cruising speed) on the K_E factor.

3.4.7.1 Modeling of Driving Behaviors

The dataset used to develop the acceleration–deceleration functions was collected by the Idaho National Lab (INL, 2021) for the Department of Energy (Department of Energy, 2021). The dataset was retrieved from field driving runs conducted on various urban arterials in Michigan under different operating conditions. This Chapter used the high-resolution (up to 0.1 s) speed data recorded in the dataset to compute second-by-second acceleration–deceleration values at different speeds. The computed acceleration–deceleration values were distributed to a speed range from 0 to 140 mph with an increment of 10 mph, as shown in Figure 3.4. When developing the curves in Figure 3.4, it was noticed that the maximum and minimum acceleration–deceleration values at different speeds are extreme values and rarely occurred on few occasions. Hence, such extreme values cannot be generalized and used for an entire simulated fleet. Thus, the maximum and minimum curves are not the ultimate maximum and minimum; instead, the curves were prepared by computing the averages of the maximum and minimum 20% of the acceleration–deceleration values at various speeds. The next step was to use such stochastic functions retrieved from the field data to generate deterministic driving behavior functions.

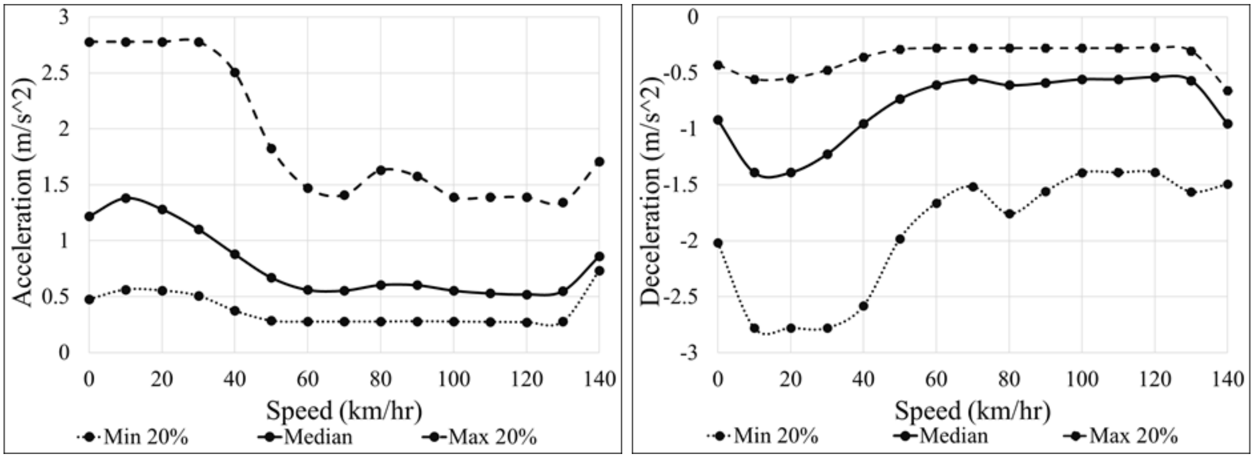

a) Desired acceleration function b) Desired deceleration function

Figure 3.4 Desired acceleration–deceleration functions developed using vehicular field trajectories.

3.4.7.2 Generating Deterministic Driving Behaviors

As mentioned previously, using stochastic acceleration–deceleration functions create many driving behaviors within a single tested scenario, defeating the purpose of the Chapter's investigation. This issue was alleviated by conducting a simulation run on the modeled test-bed intersection to obtain a large sample of deterministic acceleration–deceleration functions for individual stopped vehicles in the simulation. Then, the acceleration– deceleration functions of those stopped vehicles were extracted from Vissim and compared internally by using the DTW algorithm. This algorithm provided a dissimilarity score between every acceleration–deceleration function and all the other functions. Finally, such dissimilarity scores were fed into the k-means clustering algorithm to group all acceleration–deceleration functions into an optimal number of groups. Nominal operating conditions were modeled for this simulation run (e.g., level-terrain and acceleration– deceleration functions in Figure 3.4) except for the speed, which was selected to be

60 mph. The reason for choosing 60 mph is that the time taken by a vehicle to accelerate from 0 to 60 mph is a commonly used performance measure for vehicle acceleration (McConville and Cook, 1996). The simulation run resulted in over 400 stopped vehicles, which were used in the process described in Figure 3.5.

The comparison of two time series (e.g., deterministic acceleration–deceleration functions) is usually made by producing a distance metric between every two points that coincide in the two input time series (Figure 3.6a). As a result, such a distance is not appropriate for comparing deterministic acceleration–deceleration functions because they vary in length. Thus, the DTW algorithm was used because it applies a non-linear (elastic) alignment through time-normalization for distances between points in two data series (Figure 3.6b) (Sakoe and Chiba, 1978). In this way, the pattern match is recognized between two similar time intervals even if they do not have the same length.

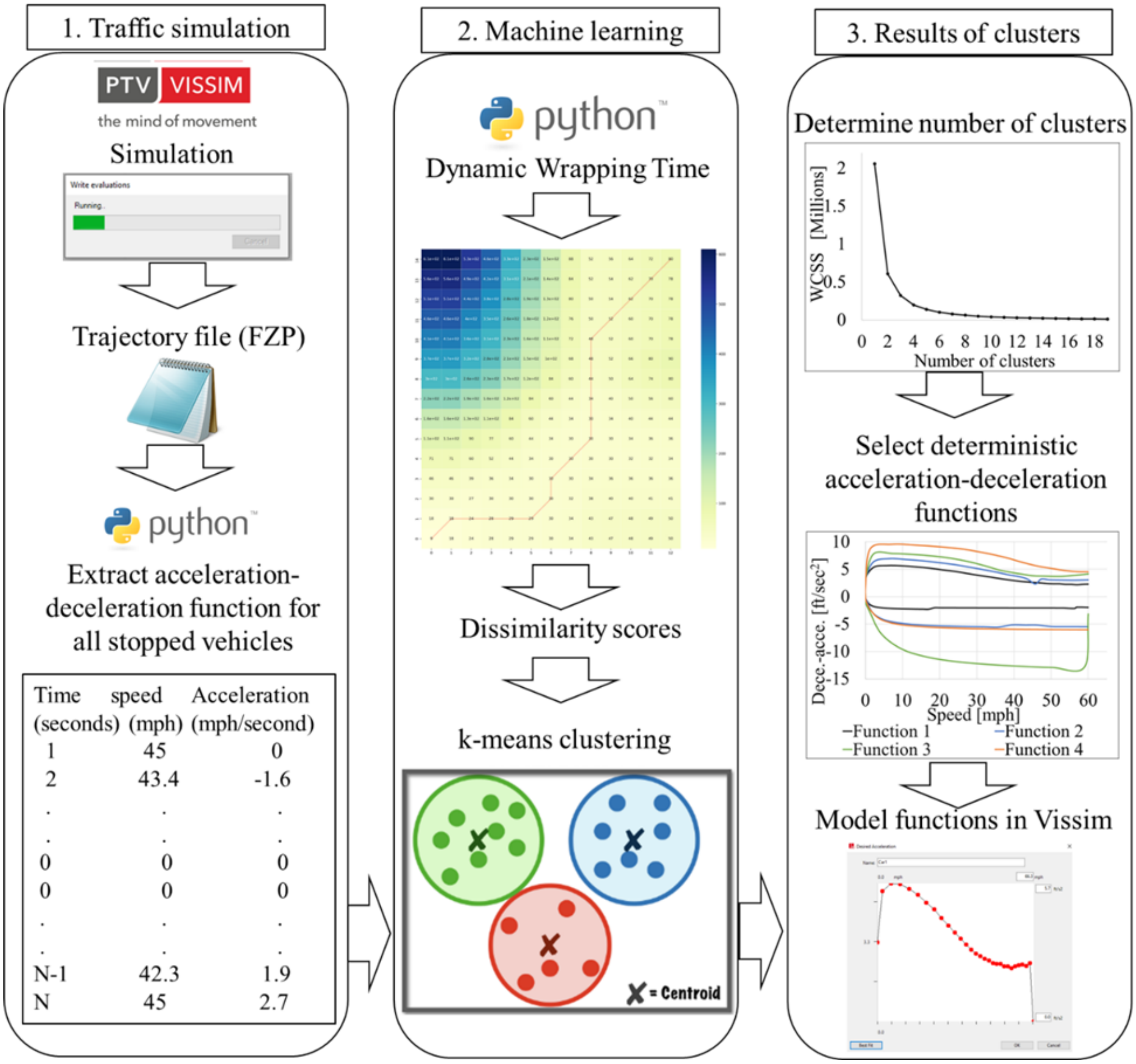

Figure 3.5 Clustering stochastic driving behaviors into deterministic groups.

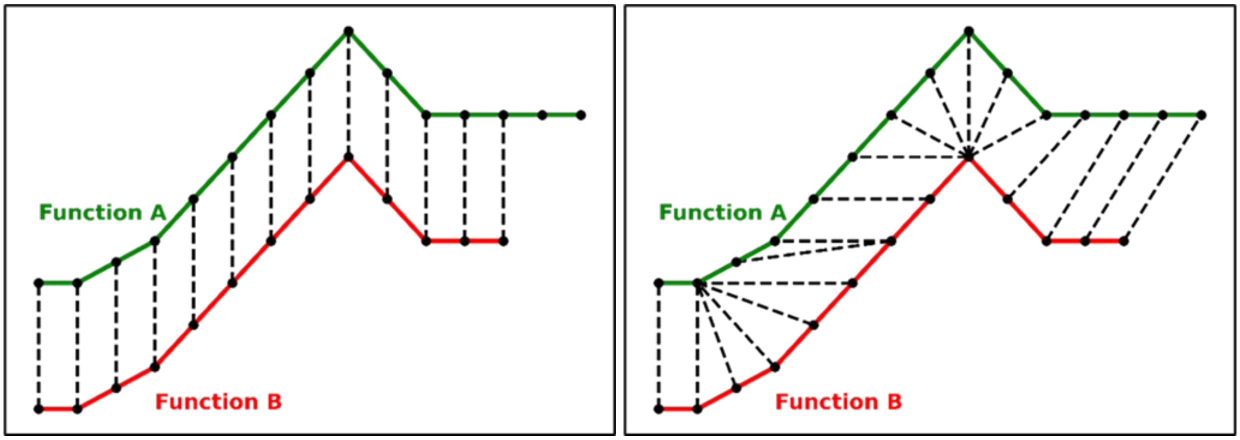

a) Regular comparison b) DTW algorithm comparison

Figure 3.6 Difference between linear and elastic alignments when comparing two time series.

The following is an overview of the DTW and k-means algorithms. Acceleration–deceleration functions in Figure 3.6 can be expressed as a sequence of feature vectors A and B.

$$\begin{aligned} A &= a1, a2, ---, a_x, ---, a_X \\ B &= b1, b2, ---, b_y, ---, b_Y \end{aligned} \tag{3.13}$$

Using the aid of an x-y plane, shown in Figure 3.7, where A and B sequences are developed along the x and y-axes, respectively. The timing differences between A and B can be depicted by a sequence of points $\Delta t = (x, y)$:

$$F = \Delta t(1), \Delta t(2), ---, \Delta t(k), ---, \Delta t(K) \tag{3.14}$$

Sequence F can represent a function that creates a mapping from the time axis of function A to function B, which is called a wrapping function (F). This function coincides with the diagonal function $x = y$ when the difference in time between A and B is zero, whereas it shifts further up or down as the time difference grows. Distance d can be used as a measure of the difference between any two points a_x and b_y as follows:

$$d(\Delta t) = d(x, y) = ||a_x - b_y|| \tag{3.15}$$

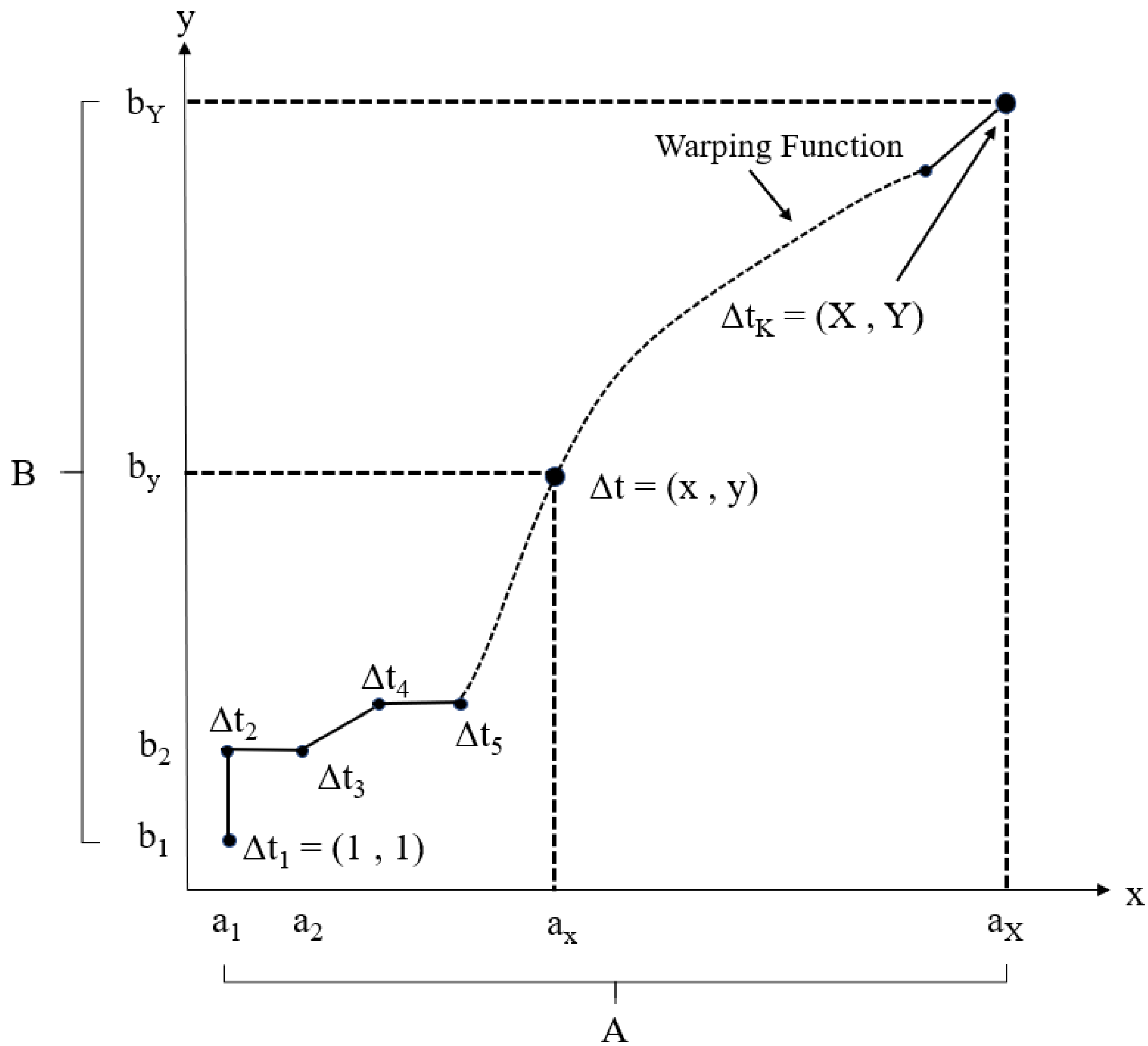

Figure 3.7 Representation of a typical DTW programming algorithm.

Then, the weighted summation of distances on the function *F* is expressed as:

$$E(F) = \sum_{k=1}^{K} d\big(\Delta t(k)\big) \cdot w(k) \tag{3.16}$$

Where: *w(k)* is a non-negative weighting coefficient introduced to allow *E(F)* to measure flexible features on the compared time series and measure the goodness of the function *F* (Sakoe and Chiba, 1978). The dissimilarity score (*D*) is then defined as the distance between functions *A* and *B* after eliminating time differences between them, as shown in Equation 3.17, where *w(k)* in the denominator is utilized to compensate for the effect of the number of points (*K*). In conclusion, a lower dissimilarity score means the series is more similar.

$$D(A,B) = Min_F \left[\frac{\sum_{k=1}^{K} d\big(\Delta t(k)\big) \cdot w(k)}{\sum_{k=1}^{K} w(k)}\right] \tag{3.17}$$

Once the dissimilarity scores between all the deceleration-acceleration functions from the 400 stopped vehicles were computed, the widely used k-means clustering algorithm was then applied to the unique values of the dissimilarity scores aiming to divide them into k similar groups. The clustering was done such that changing the cluster of any dissimilarity score will not minimize the Within-Cluster Sum of Squares (WCSS) (Hartigan and Wong, 1979):

$$WCSS = arg_S\, min \sum_{i=1}^{m} \sum_{x=1}^{n} ||x - \mu_i||^2 \tag{3.18}$$

Where: μi is the averages of dissimilarity scores contained within cluster *i* (*i* = 1, 2, …, *m*), and *n* is the number of dissimilarity scores in cluster *i*.

The next step was to determine the optimum number of clusters by using the heuristic Elbow method, which requires the following steps:

1. Perform k-means clustering for n number of clusters.

2. Compute WCSS for each clustering result.
3. Graph the WCSS (y-axis) and the number of clusters (x-axis) as introduced by Thorndike (Thorndike, 1953).
4. Determine the optimum number of clusters at which a point marks a sudden flattening of the curve.

This point on the curve suggests that using more clusters is no longer worth the decrease in WCSS. According to the Elbow method chart (Figure 3.8a), four clusters were selected to be the optimal number of clusters. Figure 3.8b presents the four selected deterministic acceleration–deceleration functions. The deceleration and acceleration of the selected functions from 60 to 0 mph and from 0 to 60 mph, respectively, are as follows: (−1.92, 3.4), (−4.4, 4.2), (−7.35, 4.9), and (−4.65, 6.3) for function 1, function 2, function 3, and function 4, respectively, all units in ft/sec^2. The final step was to model those functions in Vissim as desired acceleration–deceleration functions.

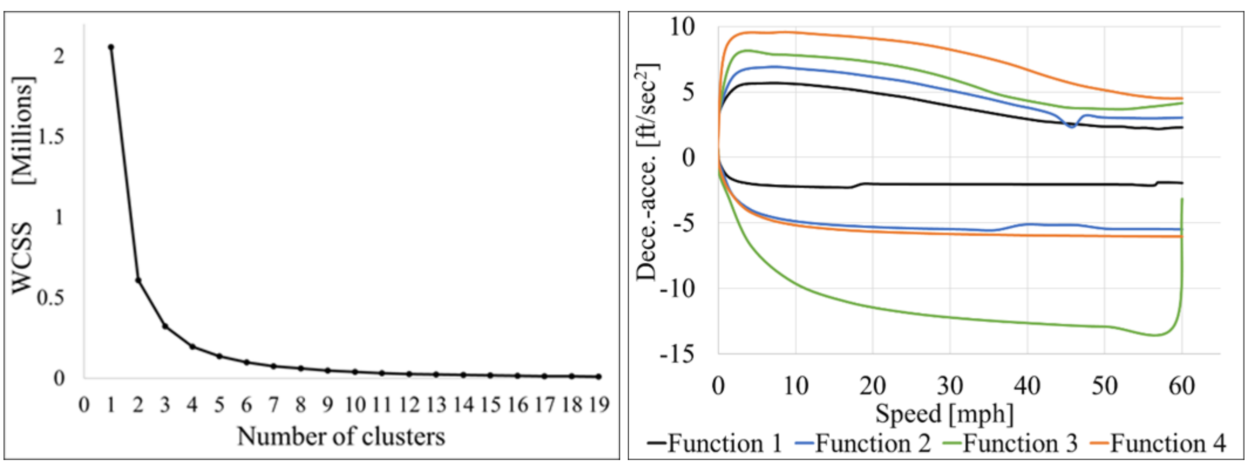

a) The optimal number of clusters b) Acceleration–deceleration functions

Figure 3.8 Results of k-means algorithm.

3.4.8 Vissim–Python–CMEM Interface

This section focuses on the interfaces formed among Vissim, Python, and CMEM. A robust code developed in Python controls Vissim externally and connects Vissim with the LDV and HDDV modules in CMEM (Figure 3.9). The code starts with a for-loop to iterate the investigated operating factors in Vissim based on the scenario to be performed. The code then runs the simulation in Vissim, which provides simulation time, a vehicle identifier, a vehicle type (LDV or HDDV), speed, acceleration or deceleration, and the number of stops on a second-by-second basis. The Python interface code uses Vissim's vehicular trajectories to extract stop profiles for all stopped vehicles. Following this, the code formats stop profiles to be processed in CMEM and assigns a CMEM-based vehicle category to the LDVs and HDDVs. The code then calls the LDV or HDDV module in CMEM for each vehicle through the command prompt. CMEM uses individual vehicle data to estimate instantaneous emissions for each vehicle. Next, the code computes the emissions-based stop penalty for each emission type for each stop profile. Finally, the average stop penalty for each emission type is calculated for each scenario.

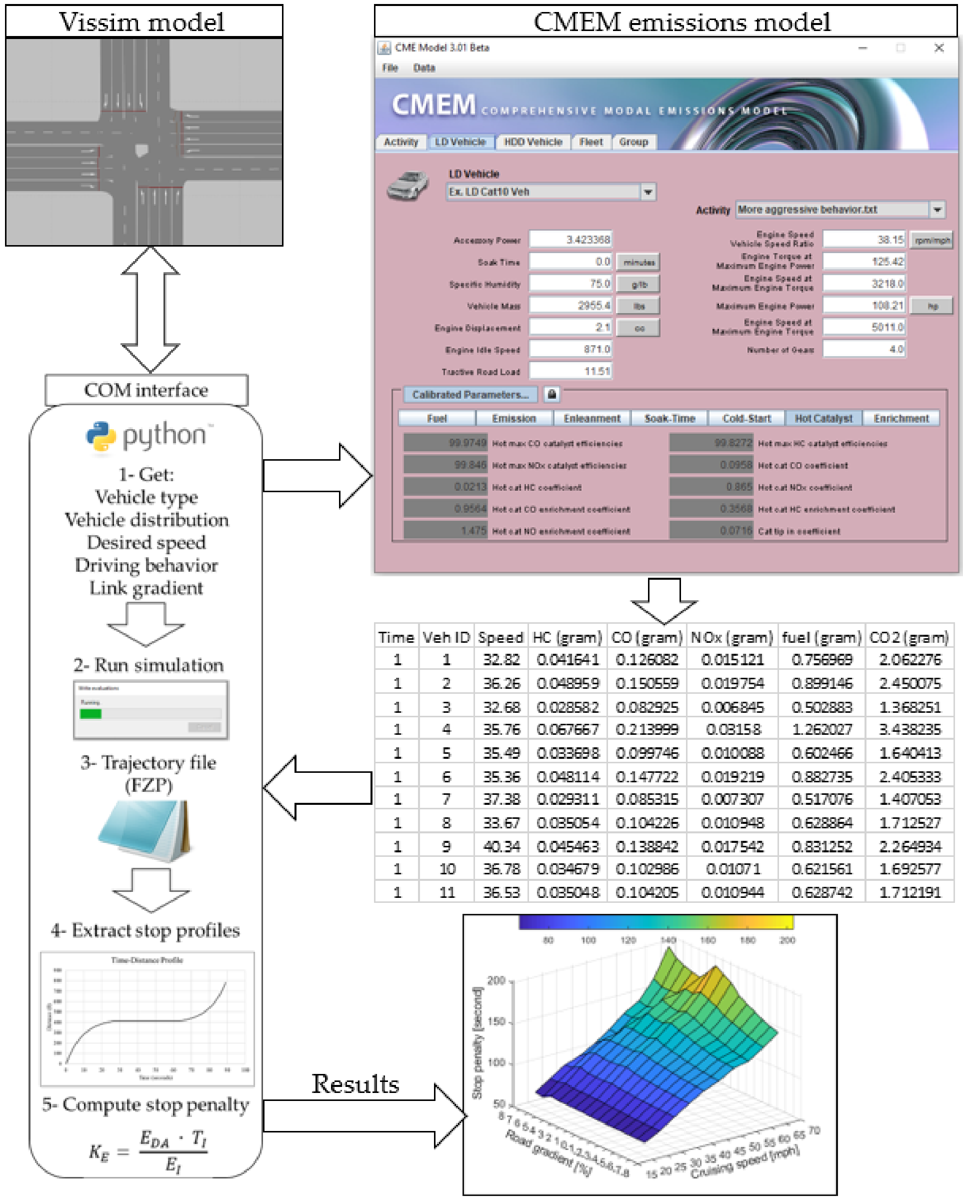

Time	Veh ID	Speed	HC (gram)	CO (gram)	NOx (gram)	fuel (gram)	CO2 (gram)
1	1	32.82	0.041641	0.126082	0.015121	0.756969	2.062276
1	2	36.26	0.048959	0.150559	0.019754	0.899146	2.450075
1	3	32.68	0.028582	0.082925	0.006845	0.502883	1.368251
1	4	35.76	0.067667	0.213999	0.03158	1.262027	3.438235
1	5	35.49	0.033698	0.099746	0.010088	0.602466	1.640413
1	6	35.36	0.048114	0.147722	0.019219	0.882735	2.405333
1	7	37.38	0.029311	0.085315	0.007307	0.517076	1.407053
1	8	33.67	0.035054	0.104226	0.010948	0.628864	1.712527
1	9	40.34	0.045463	0.138842	0.017542	0.831252	2.264934
1	10	36.78	0.034679	0.102986	0.01071	0.621561	1.692577
1	11	36.53	0.035048	0.104205	0.010944	0.628742	1.712191

Figure 3.9 Vissim–Python–CMEM integration.

3.5 Results

Figure 3.10 shows the individual impact of the tested factors on the K_E to assess how each of the tested factors impacts the K_E.

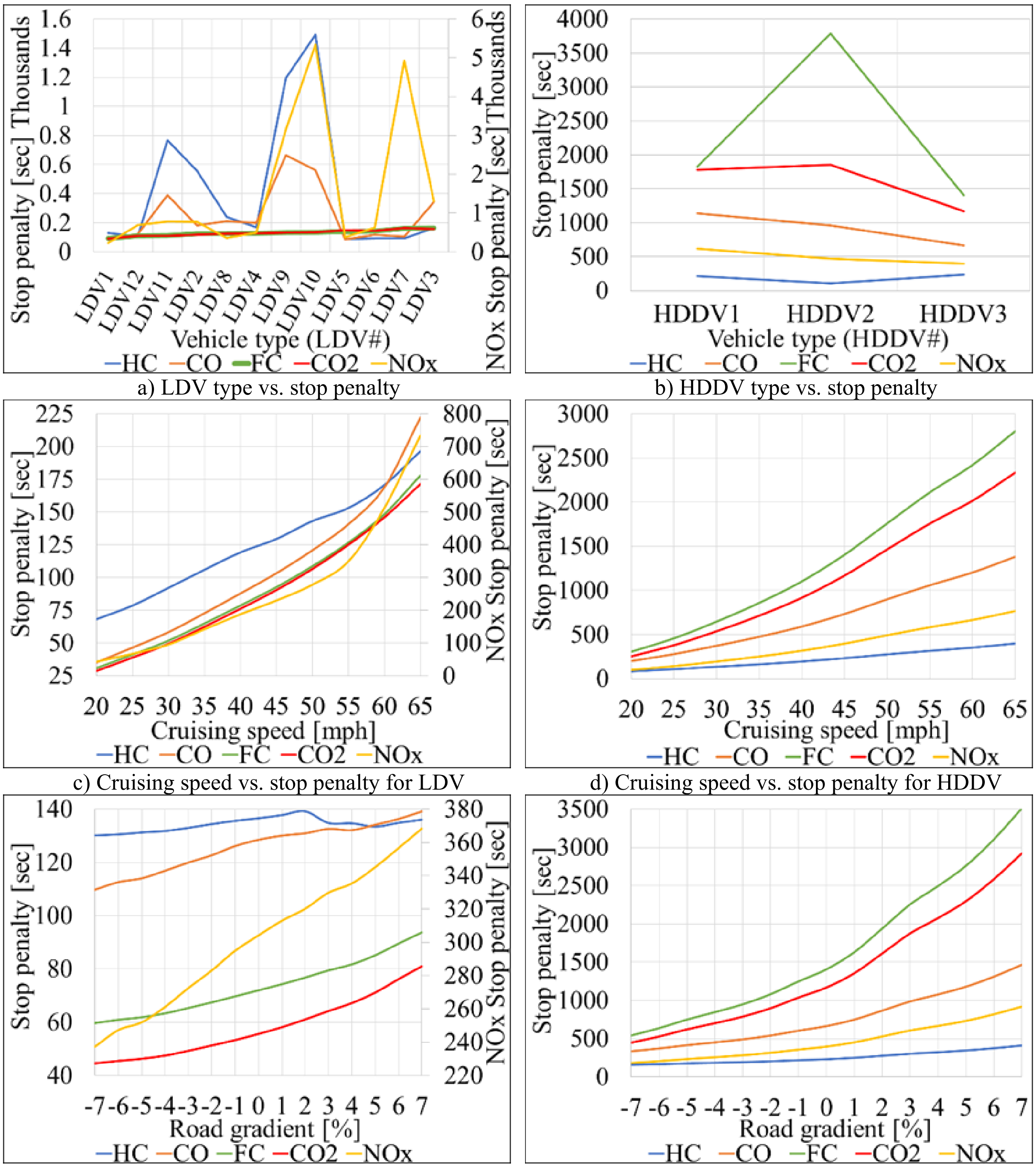

a) LDV type vs. stop penalty

b) HDDV type vs. stop penalty

c) Cruising speed vs. stop penalty for LDV

d) Cruising speed vs. stop penalty for HDDV

e) Road gradient vs. stop penalty for LDV

f) Road gradient vs. stop penalty for HDDV

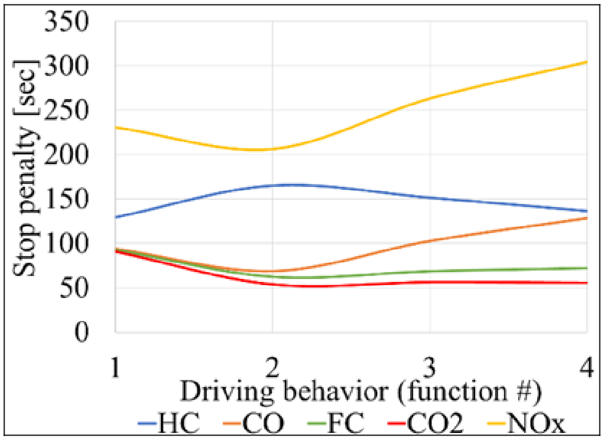

g) Driving behavior vs. stop penalty for LDV

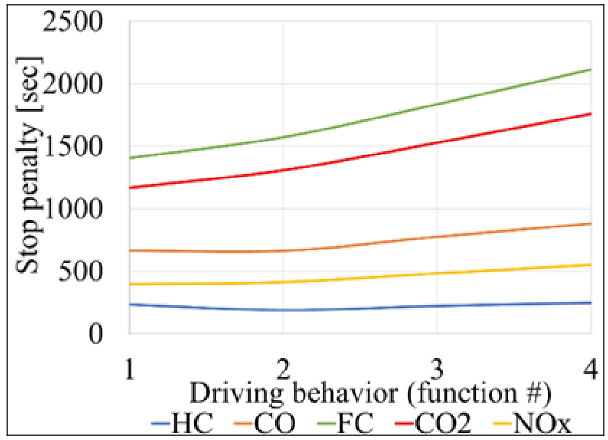

h) Driving behavior vs. stop penalty for HDDV

Figure 3.10 Individual impact of several independent factors on the stop penalty.

The left part of Figure 3.10 (a,c,e,g) presents the individual impact of various LDVs, speeds, grades, and driving behavior on the K_E of different emission types and fuel consumption. Similarly, the right part of Figure 3.10 (b,d,f,h) shows the impact of the aforementioned factors on the K_E for the HDDVs. The individual impact was determined by varying one factor while keeping all other factors constant. It is apparent from Figure 3.10 that the K_E of the HDDVs is ~3–10 times large than that of the LDVs. These experimental results provide apparent evidence that various emission criteria are not necessarily linearly correlated. Thus, minimizing a particular criterion does not necessarily minimize others. This conclusion is expected and suggests that a unique value of the stop penalty is required to minimize each emission criterion. For example, for a movement with a road gradient of 2%, a K_E value of 139, 130, 76, 61, and 320 s is required to minimize HC, CO, FC, CO_2, and NOx, respectively. A careful analysis of these values could help us define signal optimization strategies for various cities based on their sensitivity to a particular emission type.

The individual impact of wind speed and direction and the percentage of heavy vehicles in the fleet are shown in Figure 3.11. It can be seen from Figure 3.11a that wind solely has a significant impact on the K_E, especially at high headwind speeds (> 20 mph). That is because the wind direction and speed directly impact the effective speed of a moving vehicle. Thus, an accelerating vehicle upwind/downwind produces more/less fuel consumption and emissions than an accelerating vehicle with no wind conditions.

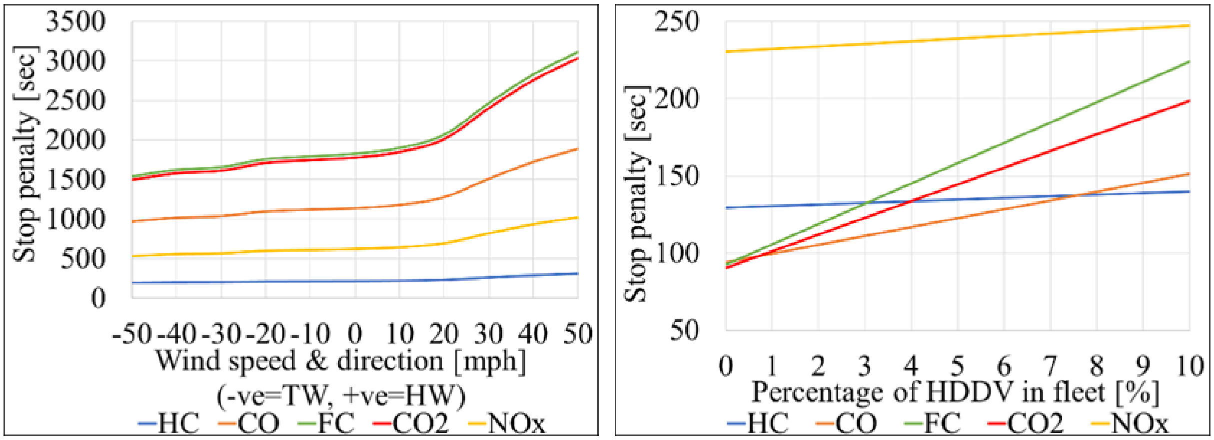

a) Wind vs. stop penalty

b) % HDDVs in fleet vs. stop penalty

Figure 3.11 Individual impact of wind effect and percentage of heavy vehicles on the stop penalty.

The results in Figure 3.10 and Figure 3.11 prove the importance of the combined effect of different operating conditions on the K_E. The combined impact of multiple factors on the K_E is visualized by using the 3D plots in Figure 3.12 to depict several relationships between the independent factors and the K_E. The plots shown in Figure 3.12 are based on the results of LDVs. The same patterns for all the plots can be seen from the results of HDDVs (Appendix B2). Each plot presents the fluctuation in the K_E of a particulate emission criterion (E) at a bivariate level, meaning that only two parameters are varied. At the same time, all other factors were fixed at their nominal values. Those values are LDV1, level-terrain, 45-mph speed, and acceleration–deceleration function 1. For example, Figure 3.12a shows a significant change in the K_{HC} with the increase of cruising speed and road gradient for LDV1 and the driving behavior function 1. Although the other emission criteria (Appendices B1 and B2) follow a similar relationship between speed, grade, and stop penalty as the one shown for the HC, the magnitude of the K_E is unique (higher or lower) for each criterion.

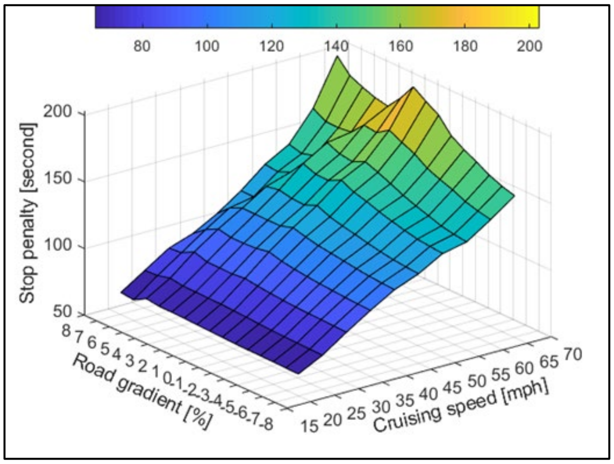

a) Cruising speed and road gradient vs. K_{HC}

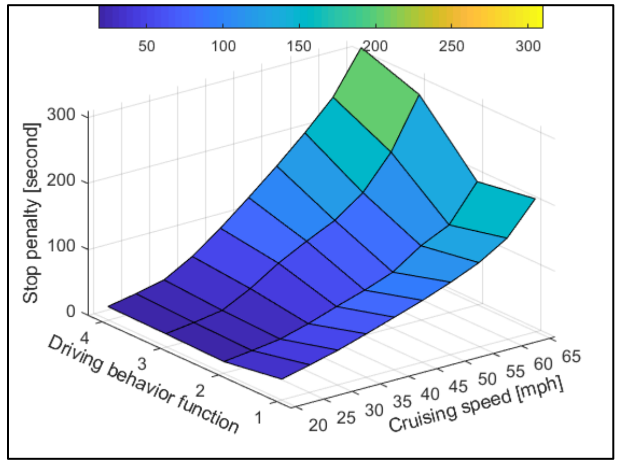

b) Cruising speed and driver behavior vs. K_{CO}

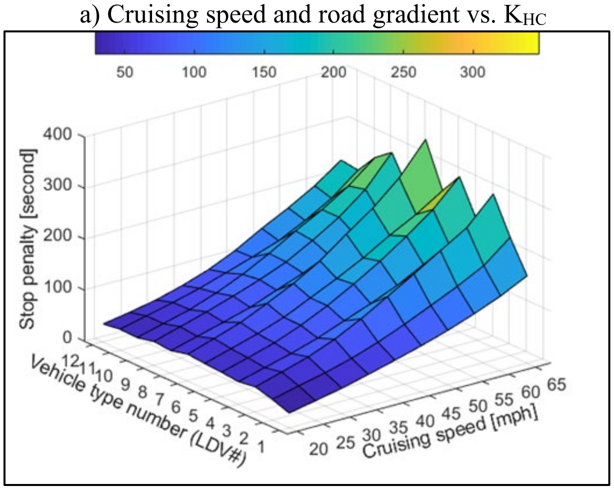

c) Cruising speed and vehicle type vs. K_{CO2}

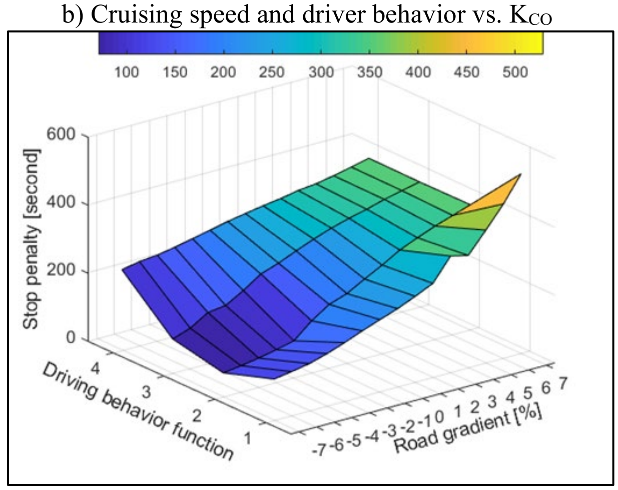

d) Road gradient and driver behavior vs. K_{NOx}

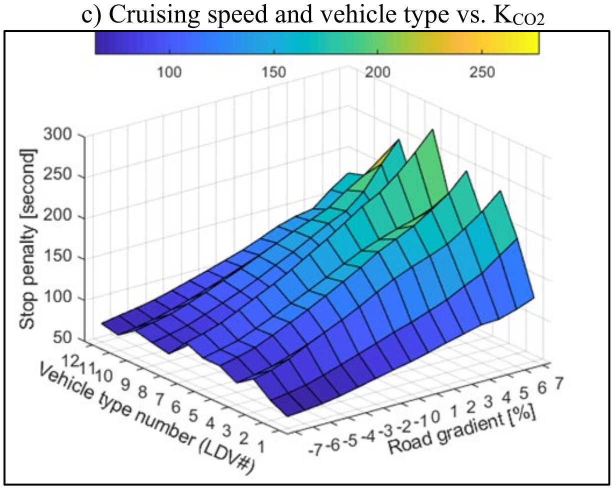

e) Road gradient and vehicle type vs. K_{CO2}

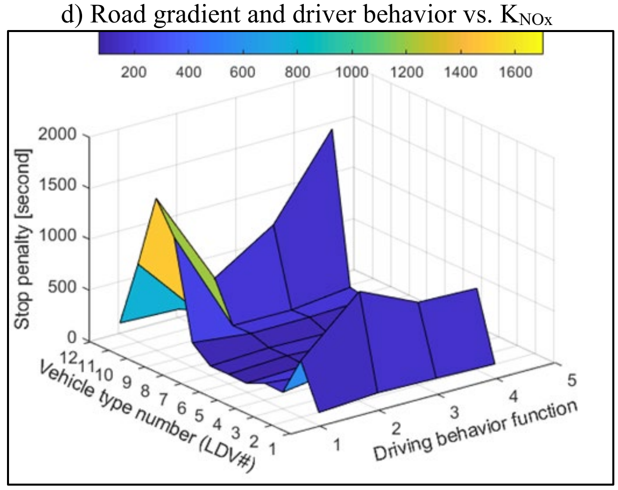

f) Driver behavior and vehicle type vs. K_{HC}

Figure 3.12 Relationships between stop penalty and its independent factors for various emissions.

Figure 3.12 and Figure 3.13 present representative results of the impact of the wind effect and the percentage of heavy vehicles in the fleet on the K_E under various cruising speeds and road gradients. As mentioned in previous sections, the analysis investigated the impact of wind effect only for the HDDVs; hence Figure 3.13a,b presents the change in the K_E of an HDDV. As expected, the wind speed and direction have shown that headwinds cause the HDDV to utilize more energy (which produces more fuel consumption and emissions) to overcome the wind blowing in the opposite direction. The findings in Figure 3.13c,d confirm a significant positive correlation between the percentage of HDDVs in the fleet and the K_E. Such a correlation becomes even more apparent under extremely high and low cruising speeds and grades.

The impact of the percentage of HDDVs on the K_E (shown in Figure 3.11b) suggests that the combined impact of this percentage with multiple factors will have a significant impact on the K_E. The impact is depicted in Figure 3.13c,d, and it is logical because LDVs and HDDVs have different engine sizes and technologies, which leads to various production rates of fuel consumption and emissions. The following section discusses the relationship between each factor and the K_E.

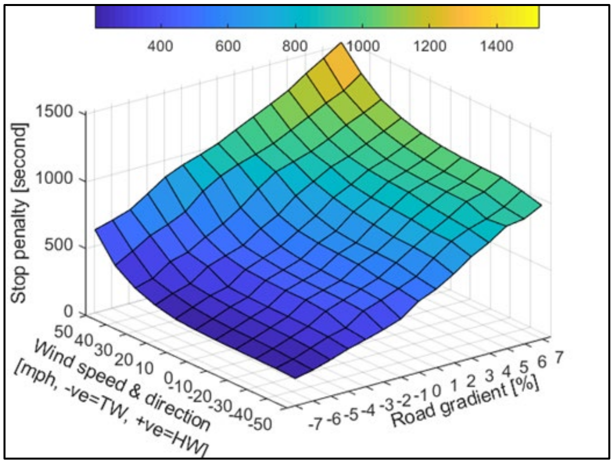

a) Wind and road gradient vs. K_{NOx}

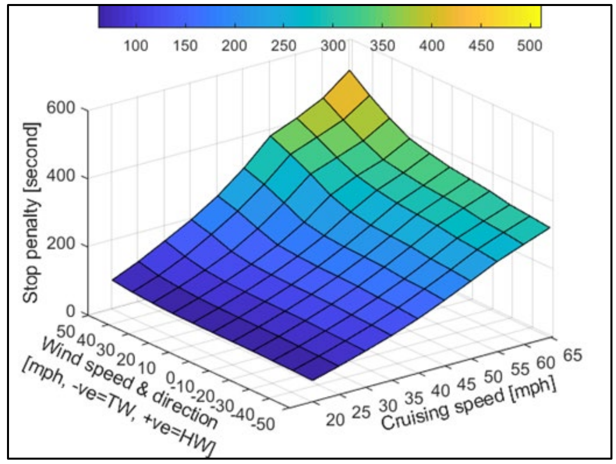

b) Wind and Cruising speed vs. K_{NOx}

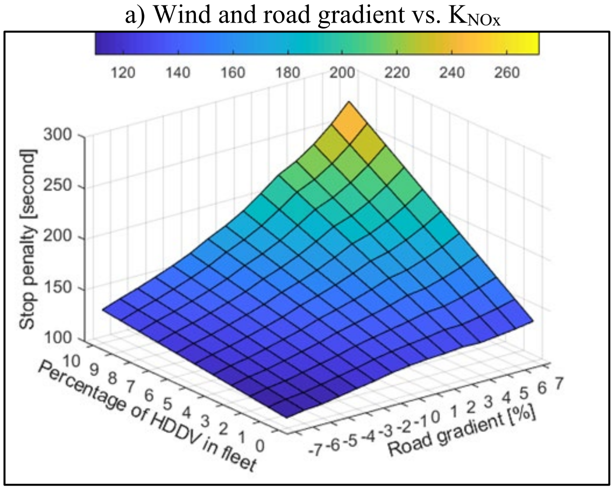

c) %HDDV in fleet and road gradient vs. K_{CO}

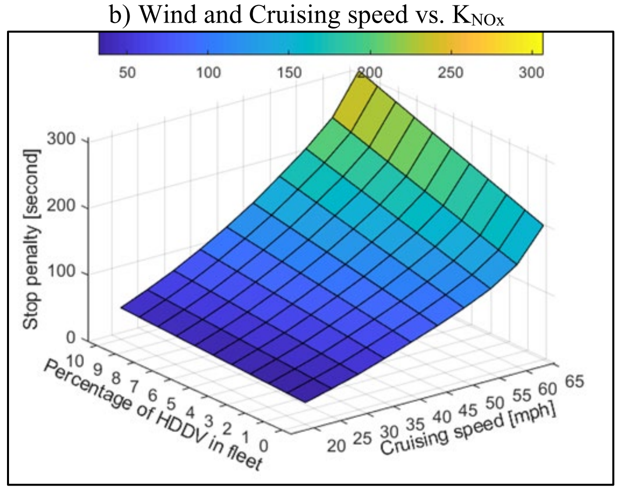

d) %HDDV in fleet and Cruising speed vs. K_{CO}

Figure 3.13 Relationships between stop penalty and wind effect and %of heavy vehicles for various emissions.

3.6 Discussion

Based on the ranges of the stop penalty, resulting from various factors shown in Figure 3.10, the main parameter that drives the K_E values (of various emission criteria) is the vehicle type. The impact of vehicle type does not seem to follow an easily identifiable pattern. On one side, the minimum K_{HC} and K_{CO} belong to normal emitting LDV (three-way catalyst, fuel-injected, > 50K miles, high power/weight ratio), as shown in Figure 3.10a. In contrast, the minimum K_{NOx}, K_{FC}, and K_{CO2} belong to normal emitting LDVs with no catalyst. Similarly, the maximum K_E of different emission criteria belongs to various vehicle types. Moreover, the K_{HC} and K_{CO} of some vehicles increase or remain constant with the decrease of K_{NOx}, K_{FC}, and K_{CO2}. Thus, it seems that reducing fuel consumption and CO_2, as generally adopted practices in the traffic community, may not lead to a tangible reduction in HC and CO. Previous studies have not recognized this inconsistency in the results. That can be explained, at least partially, by the different vehicle masses, engine powers, fuel used per engine's displacement, engine efficiency, and engine technologies used by vehicle manufacturers.

A question may arise concerning the high values of the K_{HC} and K_{NOx} for LDV 7, 9, 10, and 11, as shown in Figure 3.10a. The reason for such high values is the occasionally low emitting (approaching zero) CMEM's CO and NOx estimates, for those LDV types, during idling. These low emitting values significantly increase the K_E, according to Equation 3.7. However, it is not clear why CMEM resulted in such low estimates.

Figure 3.10b shows how the stop penalty fluctuates for HDDVs. Unexpectedly, it can be seen from Figure 3.10b that the K_{HC} and K_{NOx} have an inverse relationship with the K_{CO}, K_{FC}, and K_{CO2}. That can be easily seen in the transition in the curves from HDDV1 to HDDV2 and from HDDV2 to HDDV3. K_{CO}, K_{FC}, and K_{CO2} increased in the first transition while K_{HC} and K_{NOx} slightly decreased. The opposite happened in the second transition where K_{CO}, K_{FC}, and K_{CO2} decreased, K_{NOx} barely decreased for HDDV3, but K_{HC} has increased. These are all crucial findings to consider when computing the stop penalty, especially for fleets with a high proportion of heavy vehicles.

Indeed, decelerating and accelerating from/to higher cruising speeds requires more energy and emits more emissions, which explains higher K_E. The cruising speed is the second most significant parameter, and it has a positive exponential relationship with the K_E. This is mainly observed for CO, CO_2, fuel consumption, and at speeds higher than 50 mph, for HC and NOx, as shown in Figure 3.10c,d.

The observed significant increase in K_E with the increase in speed could be attributed to the cruising speed before or after stopping. These results depend on the emitting rate of a specific emission type during each phase of the stop. For example, Figure 3.2 shows that HC rates are higher for a specific vehicle type while decelerating, whereas CO_2 rates are the highest during accelerating. That should be a major concern when computing the stop penalty for left and right turn movements, as their cruising speeds before and after stopping are usually significantly different. Keeping in mind that emitting rates during various phases depends on the vehicle type, the impact of cruising speed on the K_E cannot be separated from the impact of the vehicle type.

The emissions generally increase when vehicles travel uphill and combat gravity. On the other hand, potential energy is added to the engine's kinematic energy when traveling downhill; thus, less emissions are produced on downhill terrains. The findings of this Chapter found that the relationship between road gradient and the LDVs K_E can be identified as linear for CO and NOx and second order polynomial for CO_2 and fuel consumption. A linear relationship can also be observed for the HC at grades between −7% and 2% (Figure 3.10e); however, K_{HC} decreases slightly and does not seem to be impacted by higher grades. That is attributed to the fact that HC estimation while idling is very sensitive to the increased engine load (Scora and Barth, 2006). Thus, resulting in lower K_{HC} variations (between 130 and 140 s) than the other emission criteria.

The impact of road gradient on the HDDVs K_E seems exponential (Figure 3.10f), with the K_{HC} and K_{FC} being the least and the most sensitive to grade increase, respectively. It is noted here that the HDDV categories in CMEM are for heavy trucks manufactured in the years between 1995 and 2000; thus, newer trucks may have lower K_E because of the new legislation released since then concerning reducing emissions. Nevertheless, it is still expected that HDDVs stop penalties will be significantly higher than those for LDVs.

Regarding driving behaviors, the results showed that the levels of accelerations and decelerations significantly impact the K_E. That is a logical and expected finding considering that individual driver's driving habits control the amount of fuel injected into the engine. The impact of driving behavior on the K_E does not follow a recognizable pattern and is not easily predictable, especially for LDVs, as shown in Figure 3.10g. For example, although function 1 has the lowest acceleration–deceleration values and resulted in the lowest K_{HC} and second lowest K_{CO}, it also had the highest K_{CO2} and K_{FC}. Interestingly, function 3 has the highest deceleration and resulted in the second-highest stop penalty for all emission types and fuel consumption. Such results indicate the importance of the deceleration phase duration despite the low emitting rate of most of the emission types during that phase. Figure 3.10h shows that the HDDVs stop penalty under various driving behaviors seemed to follow expected patterns, where the stop penalty increases with more aggressive (higher) accelerations. Such patterns could be seen clearly for K_{CO}, K_{NOx}, K_{FC}, and K_{CO2}. However, a much lower impact is observed for the K_{HC}. It is noted here that although the stochastic acceleration–deceleration functions developed in this Chapter were based on a large dataset, it is expected that the stop penalty could diversify more with a higher degree of stochasticity in driving behavior. Overall, these results indicate that further research is needed to better understand the impact of driving behavior on the K_E, especially for LDVs.

The results of wind effects have shown that the K_E increases linearly with the decrease of the tailwind speed and the increase of the headwind speed. For example, a 20-mph headwind could increase K_{CO} from 1150 seconds at no-wind conditions to 1300 s (Figure 3.11a). This difference is equal to 150 extra seconds of CO production while idling. In the opposite direction, a 20-mph tailwind could decrease K_{CO} by 40 seconds compared to its value at no-wind conditions. One can conclude that the excess emissions saved from a tailwind of a certain speed cannot recover the emission increases caused by a headwind of the same speed magnitude. It is noted here that the wind effect is most profound for trucks because of their large drag area against the airflow while moving. That does not mean that wind speed and direction will not impact LDVs stop penalties. However, such impact is left for future research due to the unavailability of emissions models to estimate fuel consumption and emissions under various wind speeds and directions for LDVs.

The impact of the proportion of heavy vehicles in the fleet is significant for most emission types and fuel consumption, as shown in Figure 3.11b. That finding is expected after observing the significant differences between stop penalties for each of the LDVs and HDDVs. Although the relationship between the percentage of HDDVs and the K_E is linear for all emissions and fuel consumption, the intensity (slope of the line) is noticeably different. The most variation caused by the percentage of heavy vehicles is observed for K_{FC} and K_{CO2}. The K_{CO} and K_{NOx} come in second and third place, respectively, whereas K_{HC} increases intangibly (1 second) with each 1% increase in the percent of HDDVs. These remarkable findings suggest that, on the one hand, reducing the production of CO, CO_2, and fuel consumption of a fleet relies on reducing those parameters from both LDVs and HDDVs. On the other hand, reducing HC and NOx depends much more on controlling those parameters from the LDVs.

Most of the results presented in Figure 3.10 and Figure 3.11 confirm that the emitting rate of CO_2 is strongly correlated with the fuel consumption rate. Hence their stop penalties are relatively similar under various operational conditions. That suggests that aiming to minimize either of them will minimize the other.

Although deriving the emissions-based stop penalty proposed in this Chapter is applicable for vehicles with Internal Combustion Engine (ICE), zero-emissions vehicles (electric vehicles) can still be combined with the ICE vehicles in the process of developing or optimizing signal timings plans using the proposed Environmental Performance Index. In such a case, the stopped delay and number of stops can be applied similarly to the ICE vehicles. However, the stop penalty can be used as the number of seconds of delay is equivalent to a stop-event (e.g., a widely used value of 10 seconds). Future research is needed to derive an energy-based stop penalty to include the impact of stops made by the emerging electrical vehicles.

This Chapter used a simulation-based investigation, the conclusions of which can be applied to any region. However, since the emissions model used in this Chapter is developed based on an American vehicular fleet, the results are highly applicable to the US fleet or any similar fleet. Although it is expected that the same investigation results in other regions would not deviate significantly from the results presented in this Chapter, it is recommended to use a relevant emissions model to the area of interest when computing the emissions-based stop penalty.

The findings of this Chapter are clear and can be summarized as follows: First, various emission types have different stop penalties; thus, unique Env-PI under the same conditions are in order. Thereby, minimizing a particular emission criterion may decrease but will not necessarily minimize another criterion. The exception is the minimization of fuel consumption which minimizes CO_2 because of their linear correlation. This finding does not support the claims of previous studies (Courage and Parapar, 1975; Li et al., 2004; Lv et al., 2013; Tan et al., 2017; Ding et al., 2019) that reported a reduction of an equal magnitude for all the emissions using the same objective function. Second, various operating conditions have a significant impact on the stop penalty. Thus, the stop penalty required to minimize a specific emission type on a particular link varies based on the link's vehicular, operational, topological, and external parameters. That means a link-based observation of traffic dynamics and geometry should be made if one optimizes signals to reduce emissions. Subsequently, those observations should be used to estimate the stop penalty for a specific emission type to be reduced when optimizing signal timings. It is crucial to note here that the findings presented in Figure 3.10, Figure 3.11, Figure 3.12, and Figure 3.13 are only representative of the entire findings of this Chapter. Hence, such figures are not adequate to estimate the K_E under the combined impact of multiple factors for various emission criteria. However, the presented figures can be used to estimate the K_E for the cases and emission types presented in them. Future research efforts to develop predictive models to estimate the K_E under the compound impact of various factors have already begun. Such predictive models are required to estimate the stop penalty under the combined impact of multiple real-world conditions. Once the K_E is estimated from the predictive models, it will be used in the proposed Env-PI objective function (Equation 3.8) to minimize sustainability metrics in signal timings optimization procedures. Future research should also include utilizing the Network Fundamental Diagram (NFD) to evaluate the impact of optimal signal plans developed using the Env-PI on the traffic conditions of the signalized corridor of interest, as outlined in (Alonso et al., 2017; Alonso et al., 2019).

3.7 Conclusions

Reducing emissions by optimizing traffic signals is challenging and requires a lot of work to quantify the various air emission criteria under various signal timing plans. However, reducing one type of emissions does not minimize other emissions, and it is likely to increase the delay. To solve this issue, this Chapter derived an emission type-based environmental objective function (called Env-PI) to minimize particular emission criteria. The Chapter also explained how the Env-PI is different for various emissions based on the emissions-based stop penalty, even under identical operating conditions. Furthermore, the present Chapter reveals the relationship between various operating conditions and the emissions-based stop penalty.

Emissions-based stop penalty data are generated using a set of full-factorial experiments and based on simulated traffic and emissions data. A real-world intersection has been modeled in Vissim to perform various experiments under different operating conditions. Vehicular trajectories from the field were used to develop acceleration–deceleration functions, which were utilized to represent various driving behaviors. The emissions model, CMEM, has been used to estimate the investigated emissions (HC, CO, NOx, and CO_2) and fuel consumption. A Vissim–Python–CMEM interface has been developed to speed up the experimental work and minimize errors.

The results reveal a significant relationship between the emissions-based stop penalty and the independent parameters, including the vehicle type, percentage of heavy vehicles, driver behavior, road gradient, cruising speed, and wind effect. Furthermore, the findings show that all the investigated independent parameters have a significant individual impact on the emissions-based stop penalty. The main parameters driving the variation in the stop penalty are the vehicle type and cruising speed, while the road gradient and driving behavior had a slightly lower impact.

Furthermore, the emissions-based stop penalty value differs for different emission criteria depending on their emitting rates during each stop's driving phase. Thus, this Chapter concluded that using the Env-PI with an accurate estimation of its stop penalty is vital to minimize emissions through optimizing traffic signals. This is especially true for urban communities suffering from specific polluting criteria, where such an Env-PI can be deployed to develop new signal retiming strategies or integrated into existing ones.

Finally, a few critical limitations need to be considered. First, this Chapter used the same acceleration–deceleration functions for both LDVs and HDDVs due to the lack of HDDVs trajectories from the field. Although this assumption is not perfect, it introduces a smaller error than using Vissim's default acceleration–deceleration functions. Second, the emissions model CMEM used in this Chapter was developed using a relatively old vehicular fleet. Therefore, future research is needed to accommodate these limitations. In addition to that, there is a need to conduct additional research to address the following problems: First, future research should incorporate more comprehensive sustainability measures (e.g., safety and noise). Second, the variability of stop profiles' emissions used to compute the emissions-based stop penalty should be further researched using variance estimation techniques. Finally, future research should focus on developing a health risk index based on optimal signal timings to minimize specific emission type and compare it to optimal signal plans to mitigate other types of emissions to help achieve sustainability of human beings.

4.0 Field-based Prediction Models for Stop Penalty in Traffic Signal Timing Optimization

This chapter has been published as:

Alshayeb, S., Stevanovic, A., & Park, B. B. (2021). Field-Based Prediction Models for Stop Penalty in Traffic Signal Timing Optimization. *Energies*, *14*(21), 7431.

Transportation agencies optimize signals to improve safety, mobility, and the environment. One commonly used objective function to optimize signals is the Performance Index (PI), a linear combination of delays and stops that can be balanced to minimize fuel consumption. The critical component of the PI is the stop penalty "*K*," which expresses a fuel consumption stop equivalency estimated in seconds of pure delay. This Chapter applies vehicular trajectory and fuel consumption data collected in the field, for a large fleet of modern vehicles, to compute the *K*-factor. The tested vehicles were classified into seven homogenous groups by using the k-prototype algorithm. Furthermore, multigene genetic programming (MGGP) is utilized to develop prediction models for the *K*-factor. The proposed *K*-factor models are expressed as functions of various parameters impacting its value, including vehicle type, cruising speed, road gradient, driving behavior, idling fuel consumption, and the deceleration duration. A parametric analysis is carried out to check the developed models' quality in capturing the individual impact of the included parameters on the *K*-factor. The developed models showed an excellent performance in estimating the *K*-factor under multiple conditions. Future research shall evaluate the findings using field-based *K* values in optimizing signals to reduce fuel consumption.

4.1 Introduction

Emissions of greenhouse gases (GHG) are a significant public concern due to their association with the ongoing climate change (McMichael et al., 1996; Hannah, 2021). The leading cause of this problem is the combustion of fossil fuels. With 24% of total U.S. GHG emissions, light-medium- and heavy-duty vehicles and trucks are among the most significant contributors (EPA, 2019a). The negative impact of vehicular fuel consumption is not limited to environmental concerns, but it extends to affect human health by increasing the concentration of some harmful pollutants (e.g., particulate matters) (Pope et al, 2002). One of the primary sources of excess fossil fuel consumption in the transportation sector is the stop-and-go events (Rakha and Ding, 2003) that occur primarily at intersections because they involve high traffic density and crossing of two or more roads.

Traffic signals are one of the most used devices to control the flows of traffic at intersections. Since early in the history of retiming traffic signals, several studies have proved that adjusting retiming signals is one of the most valuable techniques to reduce fuel consumption (Bauer, 1975; Courage and Parapar, 1975; Cohen and Euler, 1978). That is usually done by reducing the number of stops, which decreases fuel consumption caused by unnecessary deceleration-acceleration events. Thereby, traffic signal optimization has been recognized as a policy that can help mitigate vehicular fuel consumption and emissions (Robertson et al, 1980; Akcelik, 1981). However, stops and fuel consumption minimization might lead to a significant increase in delay (Robertson et al, 1980; Park et al., 2009; Stevanovic at al., 2015).

Thus, one of the very important, early research achievements in traffic signal control was the development of the Performance Index (PI) (Robertson, 1969)—an objective function for optimization of traffic signal timings. Researchers recognized the PI as a way to reduce unnecessary (stop-related) fuel consumption without a substantial increase in delay (Robertson et al, 1980). The PI, expressed in Equation 4.1, is a linear combination of delay (*D*) (seconds) and the number of stops (*S*), with a weighting factor (*K*) (also known as 'stop penalty') (seconds) given to a single stop. The variable *K* refers to the number of seconds of delay during which a waiting vehicle consumes the same amount of fuel consumed when making a full stop.

$$PI = D + K \times S \tag{4.1}$$

With the passage of time, the concept of the PI has become one of the central performance measures to optimize traffic signals. Nowadays, some of the widely used signal timing optimization programs (e.g., Synchro) use the PI as the primary objective function for the optimization, not so much to reduce fuel consumption, but as a way to find a balance between two of the most crucial performance measures at signalized intersections, delays and stops (David and John, 2006; PTV Vistro, 2014). Such optimization programs usually use a very low value for *K* (e.g., 10 seconds), which has been shown not to be appropriate if the goal is to minimize fuel consumption at signalized intersections (Courage and Parapar, 1975; Robertson et al, 1980; Akcelik, 1981).

Several studies have attempted to compute the *K*-factor, where each study used a unique approach (Courage and Parapar, 1975; Robertson et al, 1980; Akcelik, 1981; Stevanovic et al., 2021). The first serious discussions and analyses of the *K*-factor emerged in 1975 by Courage and Parapar (Courage and Parapar, 1975). They computed the *K*-factor by dividing the fuel consumption of a complete stop (containing the fuel consumed during deceleration, idling, and acceleration modes) by the fuel consumption of 1-hr of idling time transformed to one second, as expressed in Equation 4.2. This approach is mainly problematic because Courage and Parapar did not distinguish between fuel consumption caused by the action of stopping (deceleration and acceleration modes) and fuel consumption associated with pure delay during idling (referred to as stopped delay hereafter) at the signal.

$$K = 3600 \times \frac{F_s}{F_I} \tag{4.2}$$

Where:

F_S – fuel consumed in a complete stop (gallon).

F_I – fuel consumed by 1-h idling (gal/hour).

3600 – a conversion factor.

Robertson et al, 1980 evaluated the influence of several values of *K* on the delay and fuel consumption. The authors demonstrated that a *K* value of 20 s could reduce fuel consumption without a substantial increase in delay. Unlike Courage and Parapar, 1975, Akcelik, 1981 differentiated between fuel consumption during deceleration-acceleration modes and fuel consumption caused by the stopped delay. He calculated the *K*-factor by dividing the fuel consumption during deceleration-acceleration modes by the fuel rate while idling at the signal (stopped delay) (Equation 4.3).

$$K = 3600 \times \frac{F_s — F_I \times d_s — F_I \times d_h}{F_I} \tag{4.3}$$

Where:

F_S – fuel consumed in a complete stop (liter).

F_I – fuel consumed by 1-h idling (liter/hour).

d_s – stopped delay (hour).

d_h – delay caused by deceleration-acceleration action (hour).

It is worth noting here that the *K*-factor reported elsewhere (Courage and Parapar, 1975; Robertson et al, 1980; Akcelik, 1981) has only been computed based on macroscopic fuel consumption estimates. Such low-resolution fuel consumption measures did not provide accurate computations of the *K*-factor. A recent study by Stevanovic et al., 2021 proposed an analytical model (described in Section 4.2) to compute the *K*-factor by making a complete distinction between the fuel consumption caused by the deceleration-acceleration event (stopping action) and fuel consumed while idling (zero speed).

Despite these great efforts, the literature has not estimated the *K*-factor based on very representative field datasets collected for a large number of various vehicles whose fuel consumptions may vary. Moreover, none of the previous studies developed a prediction model to estimate the *K*-factor based on multiple contributing factors (e.g., speed, grade, and vehicle type). This study bridges these gaps in the state-of-the-art by using vehicular trajectories and fuel consumption data from a large fleet of contemporary vehicles (the dataset was collected in 2017) to compute the *K*-factor. Hence, this research represents the most trustworthy attempt to estimate the *K*-factor for a representative fleet. Furthermore, this Chapter develops a series of predictive models for the *K*-factor by utilizing the computed stop penalties from the field based on high-resolution fuel consumption measurements. The models developed in this Chapter could then be used to predict *K* values for various movements at signalized intersections under different operating conditions. Those conditions are vehicle type, cruising speed, road gradient, driving behavior, idling fuel consumption, and the deceleration duration.

The rest of the Chapter is divided into seven sections. The first section gives a brief overview of the computation procedure for the *K*-factor as proposed in (Stevanovic et al., 2021). The second section presents the factors that impact the *K*-factor, which are investigated in this Chapter. The field data collection is briefly described in the third section. Section four explains data preparation, classifying the tested vehicles into homogenous categories, and processing the vehicular trajectory data. Information on the development and application of seven predictive models is provided in section five. Finally, the summary findings and conclusions are presented in sections 6 and 7, respectively.

4.2 Overview of the Stop Penalty Derivation

The stop penalty needed to reduce fuel consumption was derived based on the fuel consumed during the three driving modes of a complete stop at signalized intersections. These modes are deceleration, idling, and acceleration. An example of field vehicular trajectory of those modes is shown in Figure 4.1a. The change in speed during those modes can be represented by a Cruising Speed Stop Profile (CSSP), as displayed in Figure 4.1b. Cruising speeds before deceleration and after acceleration are not necessarily equal. In fact, field data processing, discussed in Section 4.5.3, showed that it is rare that a vehicle decelerates from a particular cruising speed and accelerates back to the exact original speed. The reality is that the cruising speed after accelerating can be lower or higher than the original cruising speed before stopping. Figure 4.1c depicts changes in acceleration during a stop event. Finally, the instantaneous fuel consumption changes over time during a CSSP are demonstrated in Figure 4.1d. The total fuel consumption of a CSSP is formulated in Equation 4.4 (Stevanovic et al., 2021), where all units are identical and can be in gallons, liters, or grams:

$$FC_{CSSP} = FC_D + FC_I + FC_A \tag{4.4}$$

Where:

FC_{CSSP} – total fuel consumed during a CSSP.

FC_D – fuel consumed during the deceleration mode.

FC_I – fuel consumed during the idling mode.

FC_A – fuel consumed during the acceleration mode.

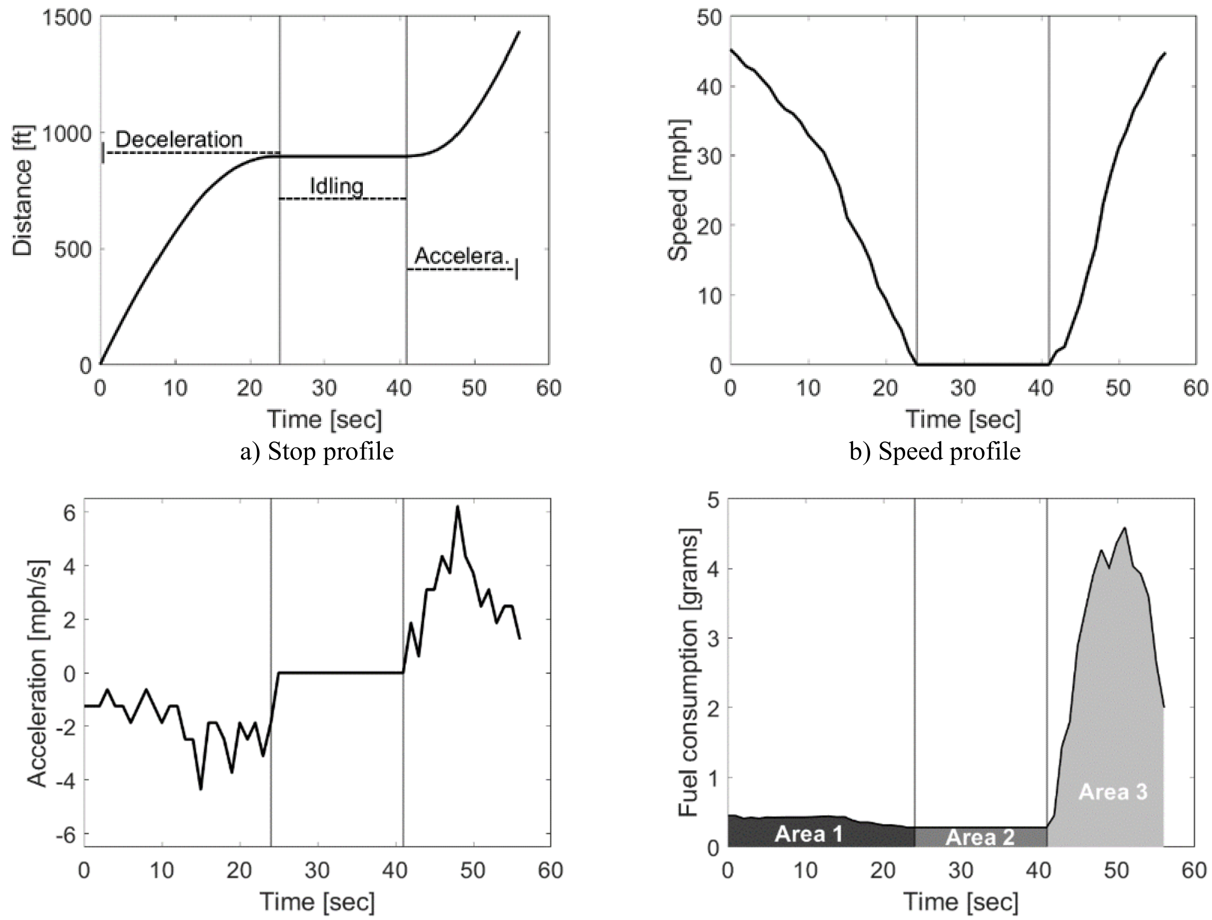

a) Stop profile

b) Speed profile

c) Acceleration profile

d) Field fuel consumption profile

Figure 4.1 Dynamics and kinematics of a stopped vehicle.

The *K*-factor is the number of seconds of delay that consume the same amount of fuel consumed by a stopping event. Hence, it is crucial to separately identify extra fuel consumed during a stopping event (deceleration and acceleration modes), represented as FC_{DA} ($FC_D + FC_A$), from what is consumed during the stopped delay, represented as FC_I. Thus, it can be said that FC_{DA} is equal to a constant (K_e) multiplied by the FC_I, as expressed in Equation 4.5.

$$FC_{DA} = K_e \cdot FC_I \tag{4.5}$$

By rearranging Equation 4.5, the unitless constant (K_e) can be denoted as shown below:

$$K_e = \frac{FC_{DA}}{FC_I} \tag{4.6}$$

The stopped delay varies based on the length of the red interval for a given phase. So, for this reason, the FC_I is divided by the total idling time (T_I) in seconds, as shown in Equation 4.7. This step is important to assign the number of seconds of stopped delay equivalent to a stopping event, which is the stop penalty (*K*-factor). The PI (Equation 4.1) can then be called FC-PI (since it is derived to reduce FC) and is expressed as shown in Equation 4.8.

$$K = \frac{FC_{DA}}{\frac{FC_I}{T_I}} = \frac{FC_{DA} \cdot T_I}{FC_I} \tag{4.7}$$

$$FC - PI = \sum_{i=1}^{n} D_i + \frac{(FC_{DA} \cdot T_I)_i}{(FC_I)_i} \cdot S_i \tag{4.8}$$

Where:

D_i – stopped delay on link i (seconds).

S_i – total stops on link i.

n – number of links in the network or links included in the optimization process.

4.3 Factors Impacting Stop Penalty

It is apparent from Equation 4.7 that the *K*-factor depends significantly on the operating conditions that impact the fuel consumption during the deceleration, idling, and acceleration modes of a stopping event. Such primary conditions include vehicle type, proportion of heavy vehicles in the fleet (because of their heavy masses), driving behavior, road gradient, cruising speed, and aerodynamic effect. The individual and combined impacts of all the previously mentioned conditions on the stop penalty, based on simulation results, were documented elsewhere (Alshayeb et al., 2021a; Alshayeb et al., 2021b). However, the impact of two additional factors (idling fuel consumption rate (FC_I/T_I) and deceleration duration (T_D)) was not examined in the previous studies. On the one hand, higher fuel consumption rates (FC_I/T_I) result in lower *K* values, as it can be concluded from Equation 4.7. On the other hand, a longer deceleration duration causes a higher *K* value because the excess fuel consumption during the deceleration phase depends on the duration of the deceleration process, which depends on several factors, including the driver's behavior and the traffic dynamics of the vehicle(s) in front of the stopping vehicle. Thus, regardless of how small the fuel consumption (per unit of time) during deceleration is, longer deceleration times mean more fuel consumed.

Therefore, the predictive models developed in this Chapter are based on the combined impact of various vehicle types, cruising speeds, road gradients, driving behaviors (acceleration-deceleration rates), fuel consumption rate during idling, and deceleration durations. Besides their profound effect on the *K*-factor, these factors were chosen because they can be (mostly) acquired from the vehicular trajectories recorded via On-board diagnostics (OBD) readers in the field. It is worth mentioning that for cruising speed, road gradient, and driving behavior parameters, attention was given for the acceleration side of those parameters (e.g., speed after accelerating, grade while accelerating, and acceleration itself). That is because the same parameters during deceleration have an insignificant impact on the stop penalty, as discussed in Section 4.6.2.

4.4 Collection of Field Data

This Chapter investigates the stop penalty by utilizing a dataset provided by the Department of Energy (DOE) (Department of Energy, 2021) and collected by the Idaho National Lab (INL, 2021). The dataset includes vehicular trajectories of field trips lasting for 1850 hours and covering 41,385 miles of various urban arterials in Michigan, which offers a wide range of collected fuel consumption rates under different operating conditions. InMetrics telemetry On-board diagnostics (OBD) recorder from ISAAC instruments (InMetrics telemetry, Ohio, United States) (Driver-Centric Fleet Management Solutions, 2021), combined with a Global Positioning System (GPS) module, was installed in the tested vehicles, and used to collect the field data. Although the OBD recorder can sample over 40 distinctive parameters with a frequency of up to 10 Hz, only eight parameters were included in the dataset. This Chapter focused on the following parameters: latitude, longitude, altitude, speed, and mass airflow, and the last one was used to compute fuel consumption (more details below). The process of collecting the data with a sample of the utilized parameters are shown in Figure 4.2.

This field dataset was chosen because it contains many CSSPs, it includes stops on uphill and downhill roadway sections, it has a fleet consisting of many vehicle types, and it encompasses various drivers with different driving behaviors. These characteristics made this dataset suitable to test the impact of various operating conditions on the *K*-factor. The following section discusses the preparation of field data that was followed to achieve the goal of the Chapter.

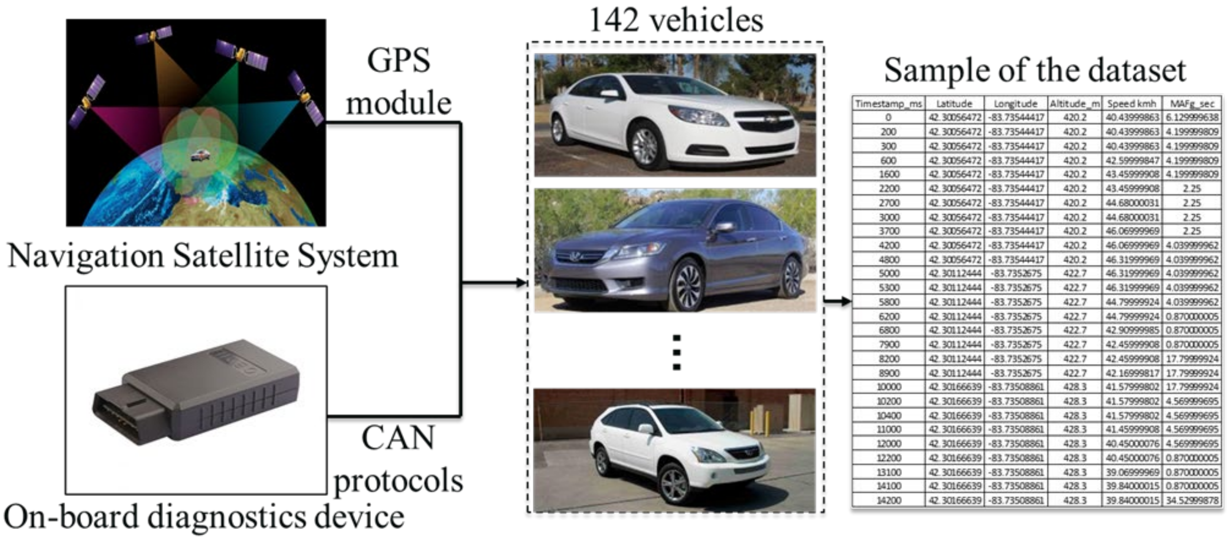

Timestamp_ms	Latitude	Longitude	Altitude_m	Speed kmh	MAFg_sec
0	42.30056472	-83.73544417	420.2	40.43999863	6.129999638
200	42.30056472	-83.73544417	420.2	40.43999863	4.199999809
300	42.30056472	-83.73544417	420.2	40.43999863	4.199999809
600	42.30056472	-83.73544417	420.2	42.59999847	4.199999809
1600	42.30056472	-83.73544417	420.2	43.45999908	4.199999809
2200	42.30056472	-83.73544417	420.2	43.45999908	2.25
2700	42.30056472	-83.73544417	420.2	44.68000031	2.25
3000	42.30056472	-83.73544417	420.2	44.68000031	2.25
3700	42.30056472	-83.73544417	420.2	46.06999969	2.25
4200	42.30056472	-83.73544417	420.2	46.06999969	4.039999962
4800	42.30056472	-83.73544417	420.2	46.31999969	4.039999962
5000	42.30112444	-83.7352675	422.7	46.31999969	4.039999962
5300	42.30112444	-83.7352675	422.7	46.31999969	4.039999962
5800	42.30112444	-83.7352675	422.7	44.79999924	4.039999962
6200	42.30112444	-83.7352675	422.7	44.79999924	0.870000005
6800	42.30112444	-83.7352675	422.7	42.90999985	0.870000005
7900	42.30112444	-83.7352675	422.7	42.45999908	0.870000005
8200	42.30112444	-83.7352675	422.7	42.45999908	17.79999924
8900	42.30112444	-83.7352675	422.7	42.16999817	17.79999924
10000	42.30166639	-83.73508861	428.3	41.57999802	17.79999924
10200	42.30166639	-83.73508861	428.3	41.57999802	4.569999695
10400	42.30166639	-83.73508861	428.3	41.57999802	4.569999695
11000	42.30166639	-83.73508861	428.3	41.45999908	4.569999695
12000	42.30166639	-83.73508861	428.3	40.45000076	4.569999695
12200	42.30166639	-83.73508861	428.3	40.45000076	0.870000005
13100	42.30166639	-83.73508861	428.3	39.06999969	0.870000005
14100	42.30166639	-83.73508861	428.3	39.84000015	0.870000005
14200	42.30166639	-83.73508861	428.3	39.84000015	34.52999878

Figure 4.2 Field data collection process.

4.5 Data Preparation

The DOE provided the dataset as a giant Comma-separated values (CSV) file; hence, it was necessary to divide the entire dataset into smaller subsets for easier handling. Each subset included trajectories for a single tested vehicle. Prior to commencing the data preparation, tested vehicles were classified into homogenous groups based on their properties that impact fuel consumption, especially based on vehicular engine sizes. The purpose of the classification was to combine the stop penalties computed for similar vehicles in one group as it is formidable to present the results for each vehicle. Following this step, a Python code was developed to extract all the CSSPs for each tested vehicle (discussed in Section 4.5.3) and determine the following parameters for each CSSP, cruising speeds, (i) right before decelerating and (ii) right after the end of accelerating; grades while decelerating and accelerating; idling fuel consumption rate; duration of deceleration stage; acceleration. In the end, the stop penalty was computed for all extracted CSSPs individually using Equation 4.7 and fuel consumption estimates recorded in the field.

4.5.1 Vehicle Classification

This section presents the vehicle clustering process. For the reader's convenience, Table 4.1 summarizes the notation used in this subsection.

Table 4.1 Nomenclature.

Variable	Description
C	Total cost function of the k-prototype algorithm
l	Number of clusters
i	Cluster
C_i^r	Cost of assigning numerical objects in cluster i
C_i^c	Cost of assigning categorical objects in cluster i
$WCSS$	Within-Cluster Sum of Squares
x_{ij}^r	Numerical object number j in cluster i
q_i^r	Mean point of the centroid of cluster (i)
n_r	Number of numerical objects in each cluster i
q_{ij}^c	Categorical prototype number j in cluster i
n_c	Number of categorical objects in cluster i
C_j	Set of all unique values in the categorical attribute j
LDV	Light-Duty Vehicle
LDT	Light-Duty Truck

A total of 177 vehicle models with various Internal Combustion Engines (ICEs) were tested during the DOE field data collection campaign, including many vehicular styles (e.g., 2-Door, 4-Door, passenger van, minivan, and pickup). Examples of the vehicles included 1996 Toyota Corolla sedan, 2000 Ford Truck Windstar van, 2003 Lexus GS 300, 2006 Honda Civic, Audi A4 Quattro, 2014 Hyundai Tucson, and Mazda CX-3. The 2012 Ford Truck F250 Crew 4 × 4 was the heaviest and the most powerful vehicle with an 8-DSL 6.7 L T/C engine, while the 2014 Toyota

Yaris with 4-FI 1.5 L engine was the lightest and one of the least powerful vehicles. More information about the tested vehicles is given in Appendix C. Classifying the tested vehicles is a fundamental procedure that is required when dealing with fuel consumption and the *K*-factor concepts. This is because the amount of vehicular fuel consumption and the *K*-factor depend significantly on vehicle characteristics, such as vehicle make, year of manufacture, engine technology, engine size, and vehicle mass. This Chapter categorizes vehicles on two levels, (i) based on its size and purpose, a vehicle is either an LDV or an LDT (this classification level is similar to how the state of art fuel consumption models such as the Comprehensive Modal Emission Model CMEM, Virginia Tech microscopic (VT-Micro) model, and Virginia Tech Comprehensive Power-based Fuel Consumption Model (VT-CPFM) categorize their tested vehicles), and (ii) based on vehicular operating characteristics that impact fuel consumption, and such classification is done by using the k-prototype algorithm (Huang, 1996).

The k-means algorithm is efficient for classifying various datasets, thus widely utilized for many data mining applications (Hartigan and Wong, 1979; Yadav and Sharma, 2013). The major drawback of the k-means is that it is primarily limited to numeric data because it minimizes the Euclidean distance measured between data points and means of clusters (Huang, 1996). In contrast, the k-prototype algorithm is a data-mining technique that clusters objects with numeric and categorical attributes based on and with the same efficiency as the k-means paradigm (Huang, 1996). The k-prototype method dynamically updates the k-prototypes to maximize the intra-cluster similarity of objects. The object similarity measure is derived from both numeric and categorical attributes. Thus, the k-prototype algorithm was utilized in this study to classify the 177 tested vehicles into seven categories that were similar in operating characteristics impacting fuel consumption. The classification process was based on a 177-by-n matrix that included several vehicle attributes, including the vehicle class, vehicle year, engine size and technology, and vehicle mass. The k-prototype algorithm aims at minimizing a total cost function (C) (Huang, 1996):

$$C = \sum_{i=1}^{l} C_i^r + C_i^c \tag{4.9}$$

The first term of the total cost function is the total cost on all numerical objects (C_i^r) in cluster *i*. C_i^r is represented by the within-cluster sum of squares (*WCSS*), which is often defined as the Euclidean distance sum of squares between each object (x_{ij}^r) and the mean point (q_i^r) of the centroid of cluster (*i*), as expressed in Equations 4.10 and 4.11.

$$\sum_{i=1}^{l} C_i^r = WCSS = \sum_{i=1}^{l} \sum_{j=1}^{n_r} \left(x_{ij}^r - q_i^r\right)^2 \tag{4.10}$$

$$q_i^r = \frac{\sum_{j=1}^{n_r} x_{ij}^r}{n_r} \tag{4.11}$$

The second term of Equation 4.9 (C_i^c) is represented as the number of mismatches between an object and each cluster prototype (q_{ij}^c) of cluster (*i*), which can be represented as follows:

$$\sum_{i=1}^{l} C_i^c = \sum_{i=1}^{l} \sum_{j=1}^{n_c} n_c \left(1 - p(q_{ij}^c \in C_j | i)\right) \tag{4.12}$$

Where:

C_j – a set of all unique values in the categorical attribute j.

$p(q_{ij}^c \in C_j | l)$ – the probability of categorical prototype (q_{ij}^c) occurring in cluster *i*.

Hence, C in Equation 4.9 can be rewritten as:

$$C = \sum_{i=1}^{l} \sum_{j=1}^{n_r} \left(x_{ij}^r - q_i^r\right)^2 + \gamma \sum_{i=1}^{l} \sum_{j=1}^{n_c} n_c \left(1 - p(q_{ij}^c \in C_j | i)\right) \tag{4.13}$$

Where γ is a weight for categorical attributes for cluster l. Such weight is introduced to avoid favoring either type of attribute (numerical or categorical). The selection of a γ value was recommended in (Huang, 1996) as the average standard deviations of numeric attributes. It should be noted that categorical values are unitless, whereas the numerical values follow the unit of the attribute being clustered.

The k-prototype algorithm was applied to the data by using the Python programming language, allowing the user to input categorical and numerical vehicular characteristics for each tested vehicle to cluster vehicles into somewhat homogenous groups. When clustering the vehicles, all tested vehicles were initially divided into LDVs and LDTs because, as discussed earlier, LDVs and LDTs have significantly different fuel consumption characteristics. The number of LDV and LDT groups is determined by using the 'Elbow method'. The Elbow method (Figure 4.3) uses the quality of clustering performance as a function of the number of groups to select a point at the elbow of the curve that indicates the optimum number of groups. From the result of the Elbow method in Figure 4.3, one can observe that four and three groups are suggested for LDVs and LDTs, respectively. Therefore, all tested vehicles were classified into seven groups identified as LDV1, LDV2, LDV3, LDV4, LDT1, LDT2, and LDT3.

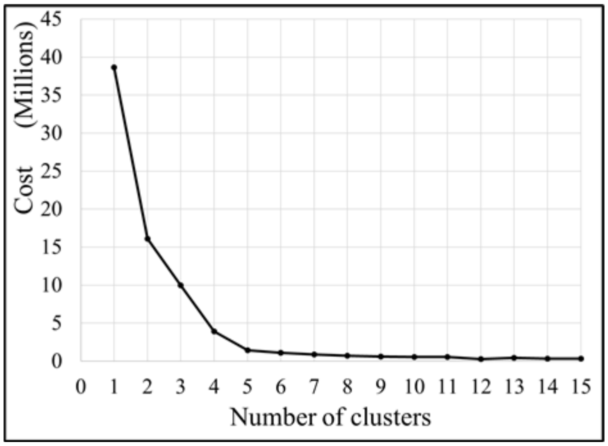

a) Light-Duty vehicles

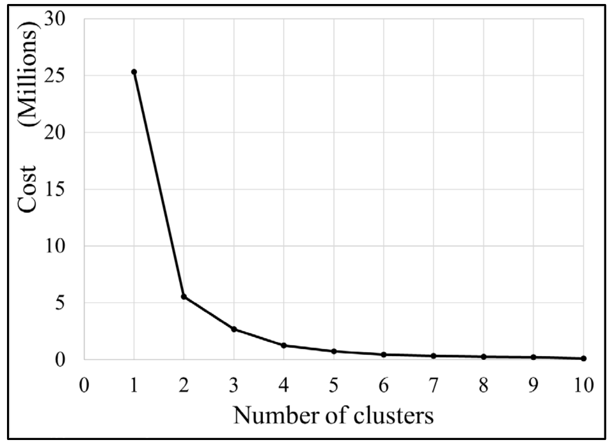

b) Light-Duty trucks

Figure 4.3 Determine optimal number of vehicle groups using the Elbow method.

4.5.2 Instantaneous Fuel Consumption Rates

Given that the OBD recorder provides the mass air flow (MAF) along with a timestamp, instantaneous fuel consumption rates can be derived from the recorded MAF (An et al., 1997; Park et al, 2013). Specifically, the instantaneous fuel consumption rates (gram/second) were computed by using the MAF records, under the assumption that the stoichiometric (aka air-fuel) ratio is 14.7 (Hillier and Coombes, 2004). The instantaneous fuel consumption can then be calculated using Equation 4.14. It should be noted that using a constant air-fuel ratio is not 100% accurate because the petroleum mixture will run lean or rich, depending on the power required by the engine (Hillier and Coombes, 2004; Park et al, 2013). Therefore, fuel consumption estimates from Equation 4.14 include a certain level of error. Although the air-fuel ratio can range from 6.1 to 20.1 for a gasoline engine (Hillier and Coombes, 2004), the vehicle's catalytic converter and its management system work together to keep the stoichiometric ratio at 14.7. Therefore, assuming a stoichiometric ratio of 14.7 in this Chapter is expected to have an insignificant impact on fuel consumption estimates, as shown in other studies (An et al., 1997; Park et al, 2013), which are later used to compute the K-factor, as discussed in the following subsections.

$$FC = \frac{a}{s} \tag{4.14}$$

Where:

FC – the fuel consumption (grams/second).

a – the mass air flow “MAF” (grams/second).

s – the stoichiometric ratio equals to 14.7.

4.5.3 Cruising Speeds and CSSPs

The next step was to detect and extract CSSPs, for each tested vehicle, from the entire vehicular trajectories. Such a step started by detecting zero speeds (idling time) and then determining the two cruising speeds of a stop event. First, the cruising speed before starting the deceleration phase (referred to as initial speed hereafter), and second, the cruising speed after the accelerating phase (referred to as final speed hereafter). The initial speed is defined as the maximum speed at which a stopping vehicle starts to decelerate to zero speed. Similarly, the final speed is the maximum speed reached after accelerating before the vehicle reaches its initial speed or starts decelerating again. The initial and final speed definitions were used to develop a Python (Python Software Foundation, Haarlem, Netherlands) code to determine and extract each CSSPs from the vehicular trajectory data.

Initial data processing showed that some vehicles decelerating from an initial speed do accelerate for a short time (<2 s) before decelerating to zero. The opposite situation can happen during accelerating, where accelerating vehicles can decelerate for a short time due to queuing and then continue accelerating to their cruising speed. Therefore, the developed code accounted for such inconsistencies and determined the actual initial and final speeds to extract CSSPs.

After the initial and final speeds were determined for each CSSPs, the next step was to determine idling fuel consumption rate, decelerations and accelerations, deceleration's duration, and road gradients. Idling fuel consumption rate is defined as an average fuel consumption in grams/second during idling. Deceleration and acceleration are the rates of change in velocities from initial speed to zero and zero to the final speed, respectively. The following subsection explains the grade computation during the deceleration and acceleration phases.

4.5.4 Road Gradient

Road gradient during the deceleration mode was computed as an average value based on the difference in altitude between the point of initial speed and the point at which the vehicle reaches a zero speed. Similarly, the road gradient during the acceleration mode was computed based on the difference in altitude between the starting acceleration point (at zero speed) to the point at which the vehicle reaches its final speed.

Initial observation of the data showed that the altitude data are missing for several tested vehicles. Moreover, resolutions of some of the altitude data may not be sufficiently accurate for computational purposes. Thus, the missing altitude data of higher resolution were acquired, when needed, from the National Elevation Dataset available from the U.S. Geological Survey (an agency in the US Department of the Interior) (National Geospatial PROGRAM, 2021) based on recorded latitude and longitude coordinates in the field.

Finally, the stop penalty was computed for all CSSPs from the field using Equation 4.15, which results from substituting Equations 4.7 and 4.14.

$$K = \frac{\left[\frac{a}{s}\right]_{DA}}{\frac{\left[\frac{a}{s}\right]_{I}}{T_I}} = \frac{\left[\frac{a}{s}\right]_{DA} \cdot T_I}{\left[\frac{a}{s}\right]_{I}} \tag{4.15}$$

As mentioned previously, a recent simulation-based study (Alshayeb et al., 2021a) investigated the individual impact of multiple operating conditions (e.g., cruising speed and road gradient) on the *K*-factor (Figure 4.4). The study concluded that the *K*-factor varies significantly under various conditions. Thus, the *K*-factor should be a function of multiple factors. To achieve that, the following subsection explains the development of a series of predictive models to estimate the *K*-factor, considering the simultaneous impact of various factors.

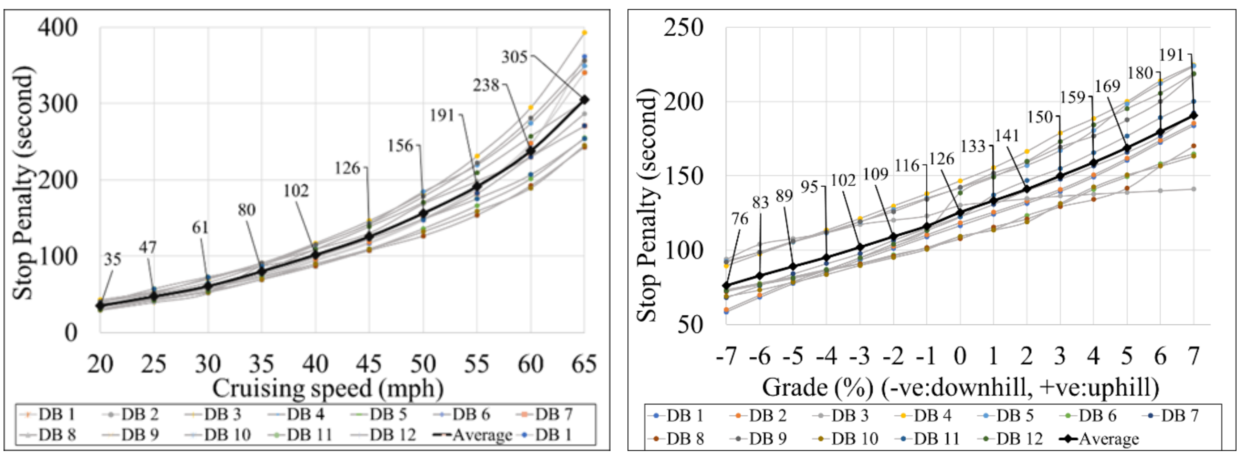

a) Light-Duty vehicles

b) Light-Duty trucks

Figure 4.4 Impact of various speeds, grades, and driving behaviors (DB) on the *K*-factor.

4.6 Machine Learning (ML) Models

ML techniques have been used extensively in various transportation applications. This section presents an evolutionary computation (EC) technique to estimate the *K*-factor based on various operating conditions, such as vehicle type, cruising speed, road gradient, driving behavior, idling fuel consumption, and deceleration duration.

4.6.1 Multigene Genetic Programming

An EC method was used in this Chapter because of two primary reasons, (i) EC models converge faster than a typical ML (e.g., neural network), and (ii) explicit mathematical formulations of the relationship between the *K*-factor and its independent factors can be derived (Koza et al., 1992; Martínez-Ballesteros, 2010; Roy et al., 2010; Zhang et al., 2021). The EC technique used in this Chapter is called multigene genetic programming (MGGP). In MGGP, a single GP individual (program) is derived from a few genes, each of which is a tree expression (Koza et al., 1992; Zhang et al., 2021). Each model evolved by MGGP is a weighted linear combination of the outputs from a few GP trees. The trees are called "genes." Figure 4.5 and Equation 4.16 show a typical 2-gene program evolved by MGGP. The inputs of the model are *x2*, *x5*, and *x8*. Several functions can be used for the evolution process (e.g., ×, −, +, Log, and √). The model is linear in the parameters for the coefficients β_0, β_1, and β_2 despite using nonlinear terms. As it is seen from Figure 4.5, the evolved model is a linear combination of nonlinear transformations of the predictor variables. Two important MGGP parameters that need significant attention are the maximum allowable number of genes and maximum tree depth. Restricting the tree depth mainly results in generating more compact models. The products of MGGP are profoundly nonlinear equations, reached after forming millions of preliminary models through a complex evolutionary process (Gandomi and Alavi, 2012). As described in previous sections, field data is used to generate the MGGP models, consisting of thousands of *K* values for a wide range of operating condition scenarios.

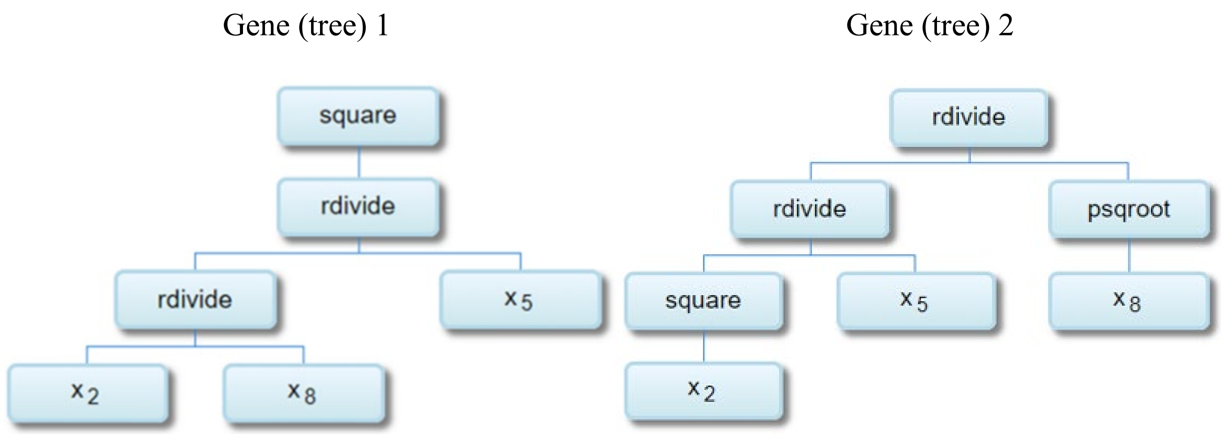

Figure 4.5 Typical 2-gene program evolved by MGGP with a maximum tree depth of 4.

$$y = \beta_0 + \beta_1 \sqrt{\frac{x_2 \cdot x_5}{x_8}} + \beta_2 \frac{{x_5}^2 \cdot \sqrt{x_8}}{x_5} \tag{4.16}$$

4.6.2 Development of MGGP Models

The initial inputs (or independent variables) included eight parameters for the training of the MGGP models, with the output (or dependent variable) being the stop penalty. Those independent variables are initial-final speeds, deceleration-acceleration grades, idling fuel consumption rates, deceleration-acceleration values, and the deceleration durations. Table 4.2 presents the input parameters with their minimum and maximum values. The vehicle type was also considered the ninth variable (to impact the stop penalty) by developing seven individual MGGP models for the seven vehicular groups described in the data preparation section. A few dozen of preparatory runs were conducted to determine the impactful input variables on the stop penalty. The outcomes revealed that decelerating grades and deceleration itself had an insignificant effect on the stop penalty. Accordingly, the MGGP models (seven models, one for each vehicular group) were developed by using only the six remaining variables, as given in Equation 4.17.

$$K = f(S_D, S_A, G_A, FC_I, T_D, A) \tag{4.17}$$

Where:

S_D – decelerating (initial) speed (mph).

S_A – accelerating (final) speed (mph).

G_A – accelerating grade (%).

FC_I – idling fuel consumption rate (gram/second).

T_D – decelerating duration (second).

A – acceleration (ft/sec^2).

CSSPs for each vehicle group were randomly partitioned into training, testing, and validation datasets based on the proportions 60%, 20%, and 20%, respectively. The best-performed models on the training and testing data were also assessed using a new (validation) dataset. GPTIPS toolbox (Searson et al., 2010), a free access MGGP training tool developed in MATLAB (MathWorks, Natick, Massachusetts, USA), was used to create the prediction models. Seven models were developed for the stop penalty, four for LDVs and three for LDTs. Table 4.3 shows the final attributes setting for the MGGP as recommended in previous studies (Koza et al., 1992; Roy et al., 2010; Zhang et al., 2021).

Table 4.2 Values of the input parameters used in the training sets.

Input Parameter	LDV1 Model		LDV2 Model		LDV3 Model		LDV4 Model		LDT1 Model		LDT2 Model		LDT3 Model	
	Min	Max	Min	Max	Min	Max	Min	Max	Min	Max	Min	Max	Min	Max
S_D (mph)	9.32	74.56	9.32	65.24	9.32	60.27	9.32	74.56	9.32	74.56	9.32	55.92	10.56	57.17
S_A (mph)	9.32	75.19	9.32	70.21	9.32	55.92	9.32	72.7	9.32	66.49	9.32	59.65	9.32	59.65
G_A (%)	−13.67	13.16	−13.43	12.08	−13.29	13.69	−12.8	15.28	−9.54	8.55	−10.48	8.65	−6.36	11.49
FC_I (gram/sec)	0.09	1.2	0.09	1.314	0.1	1.18	0.1	1.17	0.09	1.21	0.09	0.98	0.1	1.04
T_D (sec)	1.7	30	1.4	30	3.1	30	0.6	30	1.3	30	2.3	30	2.6	33.5
A_r (ft/sec^2)	0.28	37.97	0.39	36.45	0.1	22.02	0.16	36.45	0.24	30.38	0.59	22.78	0.3	9.11

Table 4.3 Optimal MGGP attributes setting.

Attribute*	Options/value
Function set	+, -, x, /, log, sqrt, square
Population size	800
Number of generations	500
Maximum number of genes allowed in an individual	6
Maximum tree depth	4
Tournament size	80
Tournament type	Pareto (probability = 1)
Elite fraction	0.7
Number of inputs	8
Constants range	[-10 10]
Complexity measure	Node count

Coefficient of determination (R^2) and the root-mean-squared error (*RMSE*) were employed to judge the performance of the introduced models. *RMSE* and R^2 equations are expressed in Equations 4.18 and 4.19.

$$RMSE = \sqrt{\frac{\sum_{j=1}^{n}(C_i - E_i)^2}{n}} \tag{4.18}$$

$$R^2 = \left(\frac{\sum_{j=1}^{n}(C_i - \bar{C})(E_i - \bar{E})}{\sqrt{\sum_{j=1}^{n}(C_i - \bar{C})^2 \sum_{j=1}^{n}(E_i - \bar{E})^2}} \right)^2 \tag{4.19}$$

Where:

C_i – computed *K*-factor for the j^{th} output.

p_i – estimated *K*-factor for the j^{th} output.

$\bar{C}$ – average computed *K*-factor.

$\bar{E}$ – average estimated *K*-factor.

n – sample size.

Equations 4.20-4.26 in Table 4.4 represent the stop penalty under various operating conditions for each vehicle group (LDV1, LDV2, LDV3, LDV4, LDT1, LDT2, and LDT3). These models were developed using (6188, 2604, 1379, 4073, 1588, 888, and 225) and (2063, 869, 460, 1358, 530, 269, and 75) sets of training and testing data, respectively.

Table 4.4 Mathematical formulations of the MGGP models.

Model	Equation #
LDV1	
$K_{LDV1} = \frac{1.321e-2 \cdot S_D{}^2 \cdot T_D + 0.3979 \cdot T_D{}^2 - 5.102 \cdot FC_I \cdot T_D}{FC_I \cdot T_D} + \frac{1.608 \cdot S_D + 0.2311 \cdot S_D \cdot T_D + 4.966e-3 \cdot S_D{}^2 \cdot G_A \cdot T_D + 3.073e-2 \cdot S_D{}^2 \cdot FC_I \cdot T_D + 7.796e-3 \cdot S_A \cdot S_D \cdot T_D}{FC_I \cdot T_D \cdot A}$	(4.20)
LDV2	
$K_{LDV2} = \frac{S_D{}^2 \cdot [8.426\times10^{15} \cdot (G_A + FC_I) + 4.229\times10^{16}] \cdot 4.337\times10^{-19}}{FC_I \cdot A} + \frac{4.235\times10^{-22}[FC_I \cdot S_A{}^2 \cdot T_D{}^2 \cdot 6.245\times10^{19} \cdot S_D{}^2 + 8.126\times10^{20} \cdot T_D + 2.781\times10^{22} \cdot FC_I - 1.44\times10^{22} \cdot FC_I \cdot log(\|A\|)]}{FC_I \cdot A}$	(4.21)
LDV3	
$K_{LDV3} = \frac{3.341e-4 \cdot FC_I \cdot (S_A + S_D)}{G_A{}^2} - \frac{1.11\times10^{-15}[3.904\times10^{15} \cdot T_D - 2.643\times10^{15} \cdot S_D + 2.972\times10^{14} \cdot S_D \cdot T_D]}{T_D} + \frac{8.674\times10^{-19} \cdot [4.58\times10^{17} \cdot FC_I \cdot T_D + 6.994\times10^{15} \cdot S_D{}^2 \cdot G_D + 2.46\times10^{16} \cdot S_D{}^2 \cdot T_D - 6.994\times10^{15} \cdot S_D \cdot G_D \cdot T_D]}{G_A \cdot T_D}$	(4.22)
LDV4	

Table 4.4 (continued).

$$K_{LDV4} = \frac{0.01948 \cdot {S_D}^2 \cdot A^3 - FC_I \cdot S_D \cdot 0.01757}{FC_I \cdot A^4} - \frac{6.345 \cdot FC_I + 0.2576 \cdot T_D + 0.008612 \cdot {S_D}^2 + 4.518 \times 10^{-6} \cdot A^2 \cdot FC_I \cdot {T_D}^2 + \frac{0.0025 \cdot {S_D}^2 \cdot G_A}{\sqrt{(|A|)}}}{FC_I} \tag{4.23}$$

LDT1

$$K_{LDT1} = \frac{8.674e{-19} \cdot S_D \cdot (1.574e14 \cdot S_A \cdot {G_A}^2 + 1.574e14 \cdot S_A \cdot S_D \cdot G_A + 7.553e17)}{(FC_I \cdot A)} - \frac{\left(8.314e{-3} \cdot {S_D}^2 \cdot {FC_I}^2 \cdot {T_D}^2 + 8.977 \cdot {S_D}^2 \cdot FC_I + 5.725e3 \cdot {FC_I}^2 + 2.983 \cdot (S_A \cdot FC_I \cdot T_D) + 4.946 \cdot T_D\right) \cdot 1.694e{-3}}{{FC_I}^2} \tag{4.24}$$

LDT2

$$K_{LDT2} = \frac{1.059e{-3} \cdot S_A \cdot {S_D}^2 \cdot {FC_I}^3 + G_A \cdot \log(|T_D|) \cdot {S_D}^2 \cdot {FC_I}^2 \cdot 0.002112 + 0.5789 \cdot S_D \cdot {FC_I}^2}{(FC_I)^3 \cdot A} - \frac{0.0002673 \cdot S_D - 0.01809 \cdot {S_D}^2 \cdot {FC_I}^2 - 2.792 \cdot {FC_I}^2 \cdot \sqrt{(|T_D|)} + 9.811 \cdot {FC_I}^3}{{FC_I}^3} \tag{4.25}$$

LDT3

$$K_{LDT3} = \frac{3.006e{-2} \cdot {S_D}^2}{G_A} + 0.4344 \cdot FC_I \cdot T_D - 0.003328 \cdot (S_A + S_D + FC_I + T_D)^2 + \frac{13.16}{G_A} + \frac{\left(5.023 \times 10^{15} (S_A + S_D + G_D)\right) \cdot 4.441 \times 10^{-16}}{T_D} + \frac{(G_D\left(-1 \cdot {G_D}^2 + \frac{S_D}{G_A}\right) \cdot 0.2658}{T_D} - 39.4 \tag{4.26}$$

4.7 Results and Discussion

4.7.1 Models Training, Testing, and Validation

Figure 4.6 and Figure 4.7 present the performance indices of the MGGP models on the training, testing, and validation datasets. As seen, the MGGP models have an excellent fitting and high coefficient of determination represented by R^2 values of more than 0.96. It is important to note that the same training datasets (for the seven-vehicle groups) were used to develop multivariate linear regression models. The obtained R^2 values were less than 0.35 for most of those regression models. Such poor performance of the conventional multivariate linear regression models can be explained by limitations of such statistical regression techniques. In most cases, the best linear or nonlinear models developed using the commonly used statistical approaches are obtained after controlling a few equations established in advance. Thus, such models cannot efficiently consider the interactions between the dependent and independent variables.

On the other hand, MGGP introduced completely new characteristics and traits and directly derived correlations without assuming prior forms of existing relationships. Figure 4.8 shows a simple summary example of a run in GPTIPS. The upper part and lower part of Figure 4.8 show the $\log_{10}$ value of the best RMSE and the mean RMSE achieved over the generations of a run. It is worth mentioning that the $\log_{10}$ value of the RMSE is the error metric that GPTIPS attempts to minimize over the training data.

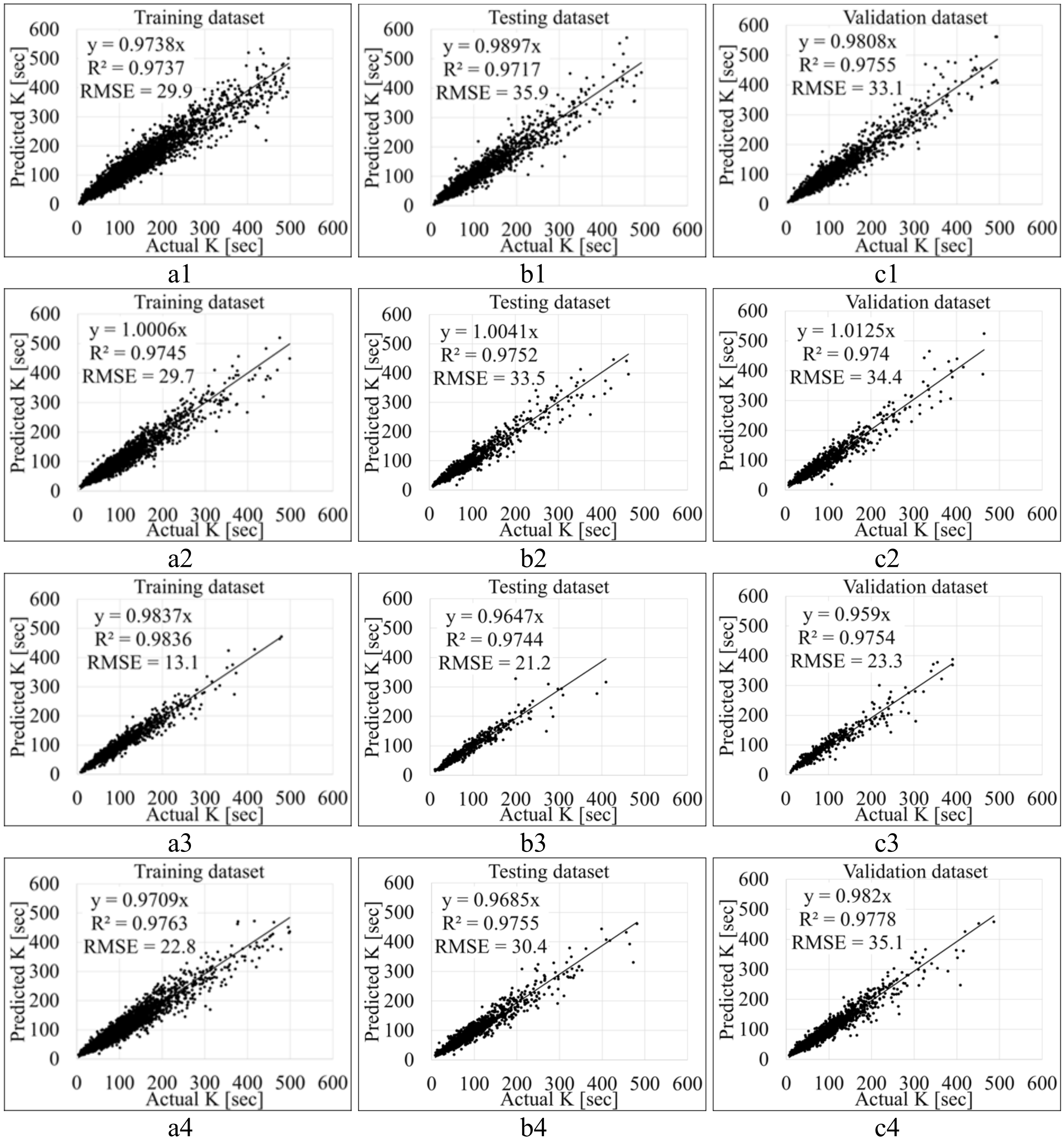

Figure 4.6 Predicted versus computed stop penalty of Ligh-duty vehicle (LDV) groups: (1) LDV1, (2) LDV2, (3) LDV3, (4) LDV4, (a) training data, (b) testing data, (c) validation data.

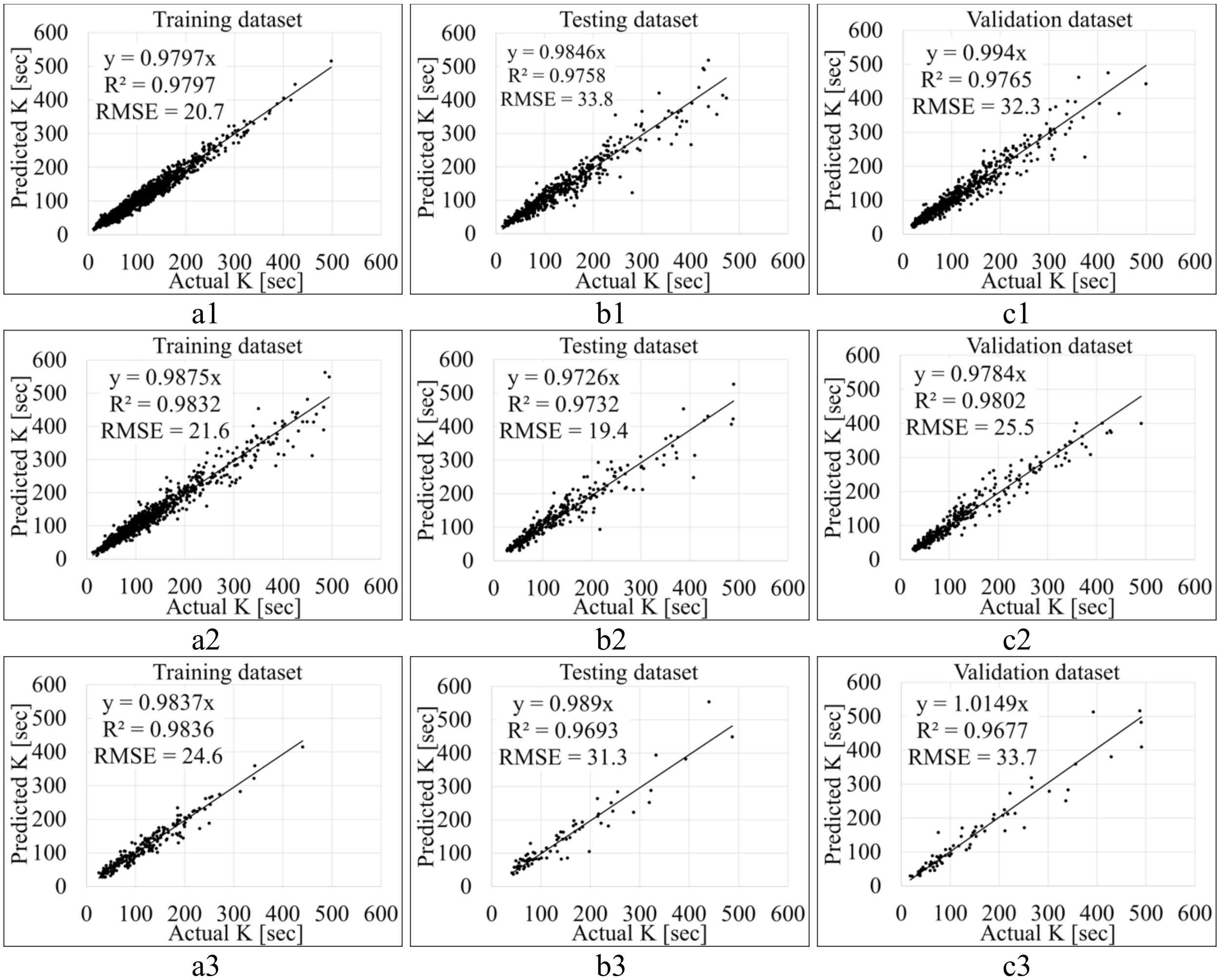

Figure 4.7 Predicted versus computed stop penalty of Light-duty truck (LDT) groups: (1) LDT1, (2) LDT2, (3) LDT3, (a) training data, (b) testing data, (c) validation data.

Figure 4.9 visualizes an example of the training procedure for minimizing the error and simplifying the complexity of the MGGP models during the evolutionary process. The green dots represent the Pareto front of models in terms of model performance and complexity. Blue Xs represent non-Pareto models. The red circled dot represents the best model in the population based on the R^2 value on the training data. The final model for each vehicle group was selected based on two criteria, accuracy and model complexity. The developed models are validated with a fresh dataset to evaluate the generalization capability of the developed models. Figure 4.6(c1)–(c4) and Figure 4.7(c1)–(c3) show the acceptable performance of the models for the validation data.

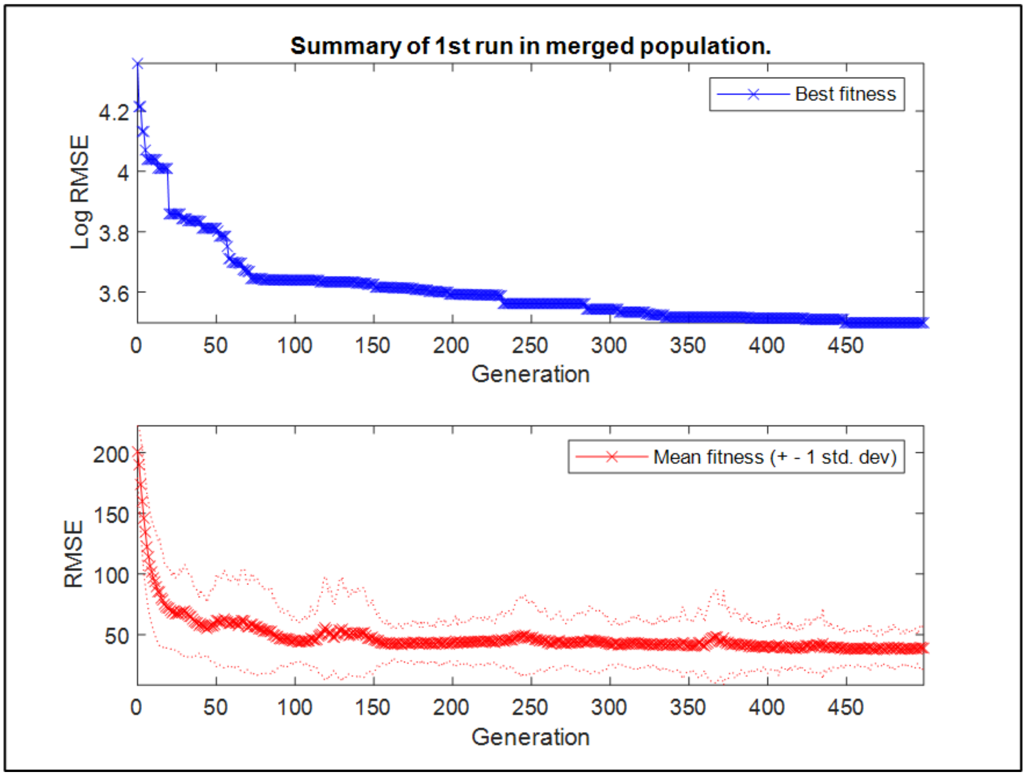

Figure 4.8 Example of a run summary shows reduction in RMSE with the number of generations.

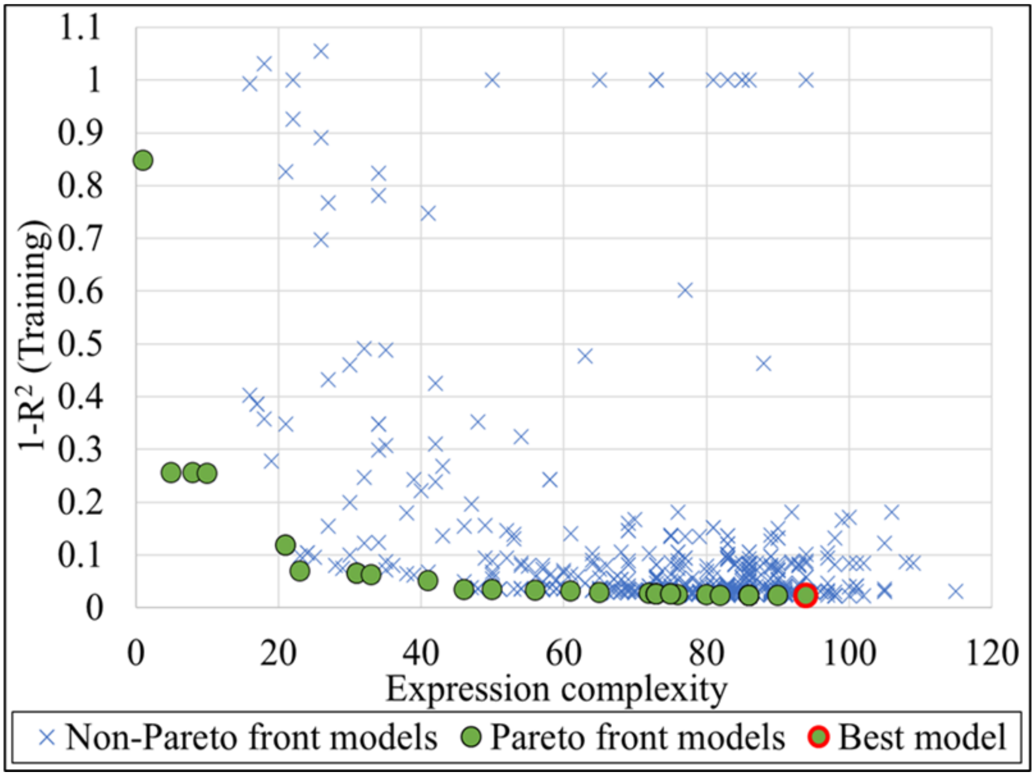

Figure 4.9 Example of the fluctuations in the training error while searching for the best model.

4.7.2 Parametric Analysis

A parametric analysis was performed to investigate the impact of the tested independent factors on the stop penalty and to investigate the robustness of the developed models. This analysis was done by varying one parameter within a practical range, while other parameters were kept constant at their average values. Figure 4.10 shows the results of the parametric study for the best models. Figure 4.10 shows that all the studied factors had a significant impact on the value of the stop penalty. Some conditions (such as the final speed and idling fuel consumption rate) had a much more significant impact than the others (e.g., initial speed).

Figure 4.10 shows that the LDT groups had larger *K* values than those of the LDVs'. The difference in *K* value between LDT and LDV groups is most remarkable for the initial speed, accelerating grade, deceleration duration, and acceleration. The same difference is still observed for the other factors but with a smaller margin. Such findings can be mainly attributed to the vehicles' masses, where heavier vehicles, represented by the LDTs, require more fuel (thus higher *K* value) than the lighter vehicles (LDVs) to operate under the same conditions of a stop event. On average and under various operating conditions, *K* values of LDTs were ~1.2–3 times higher than those of LDVs. It is expected that heavy-duty diesel vehicles (HDDVs) would have an even higher *K* value. It can also be observed from Figure 4.10 that the *K* value differs internally among the individual LDV and LDT groups. For instance, *K* values for LDV1 in Figure 4.10a range from 70–85 s, while LDV4′s range starts from 67–75 s. Thus, when computing the *K* value, it is crucial to pay considerable attention to the percentage of various vehicle types arriving at signalized intersections.

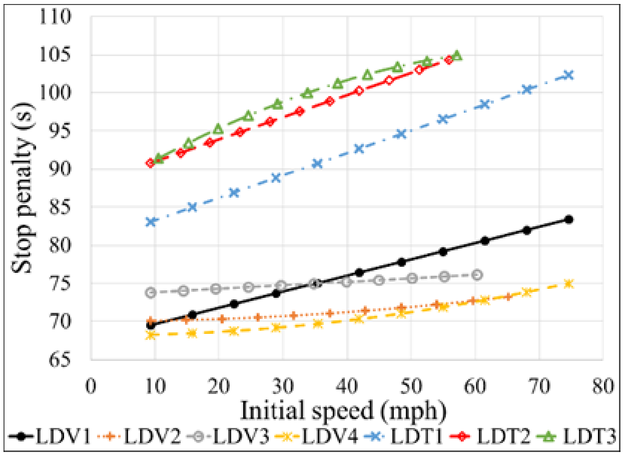

a) Initial speed vs. stop penalty

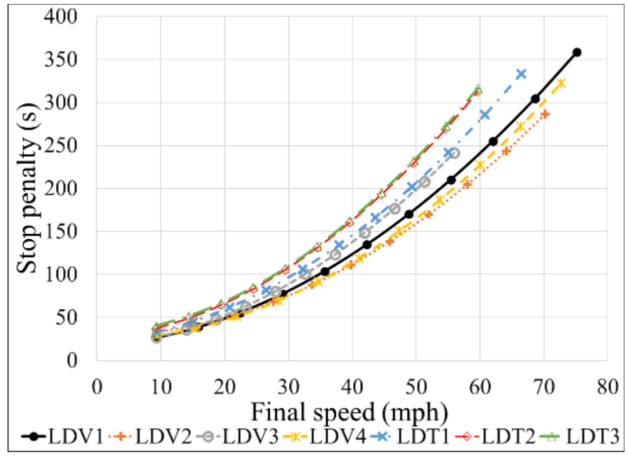

b) Final speed vs. stop penalty

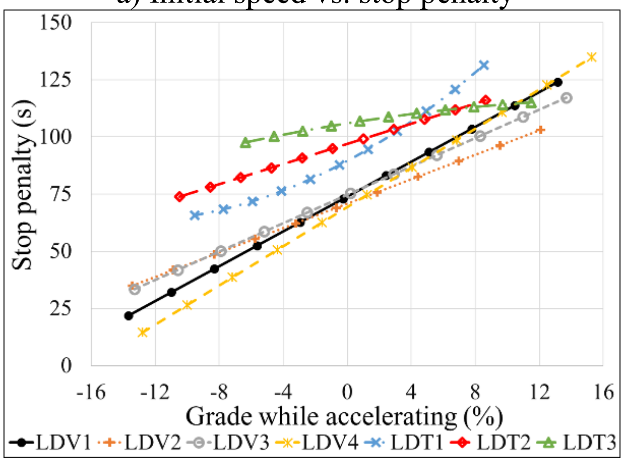

c) Accelerating grade vs. stop penalty

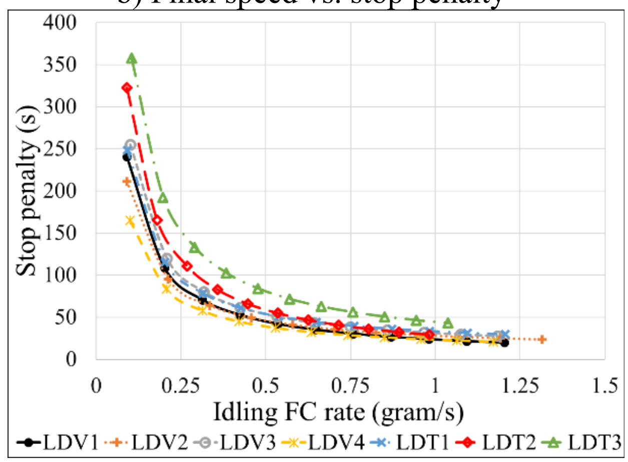

d) Idling fuel consumption rate vs. stop penalty

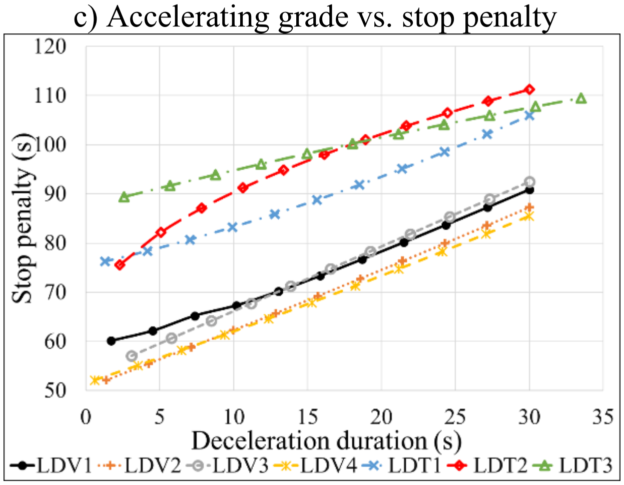

e) Accelerating grade vs. stop penalty

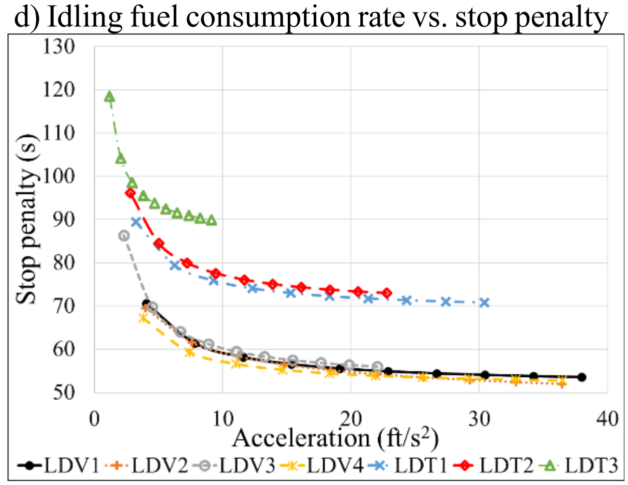

f) Idling fuel consumption rate vs. stop penalty

Figure 4.10 Parametric analysis of the developed models.

As shown in Figure 4.10a,b, the *K*-factor shows approximately linear and exponential relationships with the increase of the initial and final speeds, respectively. A comparison of the two relationships shows that the final speeds impact the *K* value much more than the initial speeds. As a result, various initial and final speeds lead to a *K* value between 67–105 and 15–350 s, respectively, for various vehicle types. The difference in the two ranges for the initial and final speeds is attributed to the fact that the amount of fuel consumed during acceleration is far larger than its counterpart during deceleration. Such a difference is important to be taken into account when computing the *K*-factor for left and right turns because, in those cases, initial and final speeds are often very different.

Regarding the grades, the findings show that grades during deceleration have a negligible impact on the *K*-factor, as mentioned in the previous sections. On the other hand, the road gradient on the acceleration side is found to correlate linearly with the *K*-factor. It is interesting to note that all seven models developed in this study cover a wide range of accelerating grades which can be as low as −13.5% and as high as 15% for most LDVs. In contrast, narrower ranges (−6% to 8%) were conducted for the LDTs, as shown in Table 4.2.

One of the most important findings of this study reveals an approximately quadrinomial relationship between idling fuel consumption rate and *K*-factor (Figure 4.10d). Such a relationship results in a *K* value of more than 250 s for some vehicle types at low idling fuel consumption rates. Most vehicles included in this Chapter had an idling fuel consumption rate range between 0.1–1 g/s. There could be several reasons for such a wide range of idling fuel consumption rates, and engine size, mass, and ambient temperature are the most important ones. Since it is not easy to identify the idling fuel consumption rate for all vehicles stopping at signalized intersections, it is recommended that operating agencies use distributions of idling rates based on various vehicle types, various times of the day, and various climates zones.

Despite its minimal impact on the *K*-factor, it was necessary to show the relationship between fuel consumption during deceleration and the stop penalty. It is worth noting that the deceleration fuel consumption is highly unpredictable, as it depends on the driver's characteristics (e.g., driving behavior and perception reaction time), geometrical characteristics of intersections, and the interactions (while breaking) with other vehicles. This Chapter used deceleration durations to represent the deceleration fuel consumption. Figure 4.10e demonstrates that deceleration duration impacts the stop penalty linearly.

Surprisingly, higher accelerations were found to reduce the stop penalty, as illustrated in Figure 4.10f. This finding was unexpected and suggested that maybe the acceleration duration (required to reach the final speed) is more impactful than the aggressiveness of accelerating. This is speculated because higher accelerations require a shorter time to reach a particular speed. Therefore, caution and engineering judgment must be applied until further research is conducted because the findings of the impact of acceleration on the stop penalty might not be generalized or transferable to other datasets with the field vehicular trajectories.

4.7.3 Comparison of Stop Penalties from Various Studies

As mentioned in the introduction, only a few studies have computed the stop penalty, either by using fuel consumption collected in the field or consumption estimates from simulated vehicular trajectories. This subsection discusses the stop penalty values from various studies (Courage and Parapar, 1975; Akcelik, 1981; Robertson et al. 1980; David and Johm, 2006;

Stevanovic et al., 2021; Alshayeb et al., 2021a) to address how the outcomes of this Chapter may improve practices and policies when optimizing signal timings in urban corridors.

Considering that most of the evaluated studies report only the cruising speed (as a factor associated with the reported stop penalties), Figure 4.11 shows (with my best effort as data from various studies may not be 100% consistent) a set of relationships between the stop penalty and cruising speed from seven sources, MGGP models developed in this Chapter; "Synchro"—a widely used signal timing optimization tool (David and Johm, 2006); field-based stop penalties reported by Courage and Parapar, 1975, Akcelik, 1981, Stevanovic et al., 2021, and Robertson et al. 1980; simulation-based stop penalties from Alshayeb et al., 2021a.

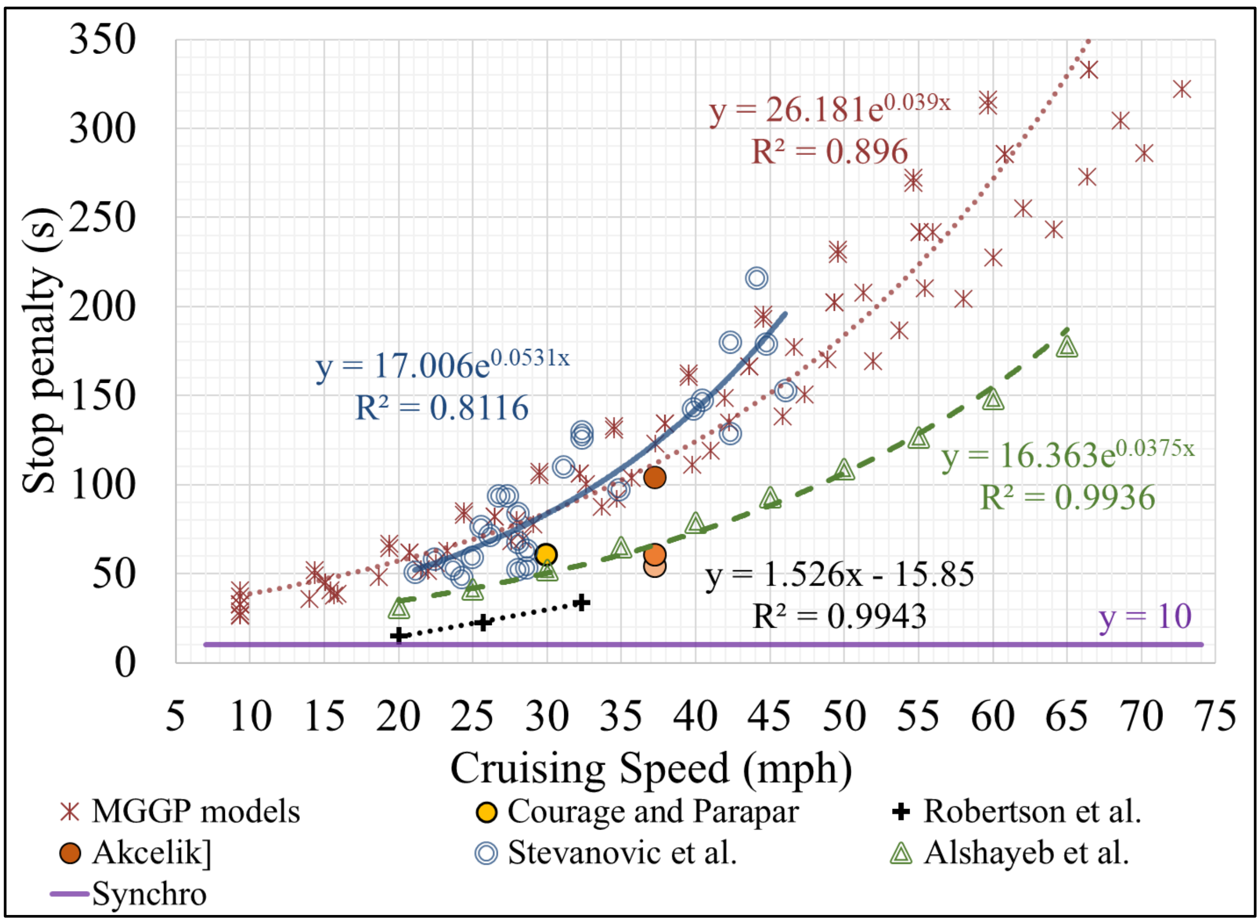

Figure 4.11 Stop penalty vs. cruising speed from various studies.

Figure 4.11 shows that various studies show different trends, where most of them point to a positive impact of the speed on stop penalty. To be more precise, the studies can be classified, according to their trends, into two groups, (i) studies that report constant stop penalties (Courage and Parapar, 1975; Akcelik, 1981; David and Johm, 2006) and (ii) studies that define the stop penalty as a function of—at least—the speed (field data covered in this research, Robertson et al. 1980; Stevanovic et al., 2021; Alshayeb et al., 2021a). The following paragraphs discuss in detail the results shown in Figure 4.11.

Courage and Parapar, 1975 were among the first to report a single stop penalty value (60 seconds) using fuel consumption measurements of a mixed fleet with a cruising speed of 30 mph and level grade, as reported by Claffey, 1971. Akcelik, 1981 derived the stop penalties for three fleet distributions, one consisting exclusively of light vehicles, another of heavy vehicles, and one composite fleet with 10% of heavy vehicles, which resulted in K values of 54, 104, and 60 s, respectively. Those three stop penalty values are shown in Figure 4.11 as orange dots with various color intensities for a cruising speed of 37 mph. Reporting the speed at which the stop penalty was computed in both studies (Courage and Parapar, 1975; Akcelik, 1981) indicates that the authors of those studies were aware of the importance of cruising speed on the stop penalty. However, the same studies did not collect field fuel consumption data for various vehicle types and other important factors (e.g., idling rate, grade), and for that reason, their reported stop penalties would not reflect the impact of those conditions.

Based on fuel consumption measurements from Robertson et al. 1980, stop penalties show a positive linear trend with the cruising speed. However, that study also did not cover a wide range of cruising speeds (only three speeds) and was based on macroscopic fuel consumption measurements. Thus, the MGGP results seem to be more reliable because they were based on high-resolution fuel consumption measurements and covered a wide range of speeds.

Although a recent study by Stevanovic et al., 2021 was conducted under some limitations (e.g., utilized a single vehicle, utilized a single driver, limited speed range of ~20–45 mph), the stop penalties from the MGGP models showed that the findings from Stevanovic et al., 2021 are still quite valid. However, the MGGP models were still based on a much larger data set that includes many different vehicles and drivers and covers a much broader range of speeds (~10–75 mph).

When comparing the MGGP stop penalties with those from the simulation models (Alshayeb et al., 2021a), Figure 4.11 shows that both data series depict the same trend (stop penalty correlates positively with the cruising speed), but it seems that the simulation-based stop penalties underestimate those from the field (e.g., either from this study or the results from Alshayeb et al., 2021a. On the other hand, Figure 4.12, which compares the field and simulated stop penalties as functions of the road gradient, shows that the simulated data overestimated the field values. There could be several reasons for such differences between the field and simulated stop penalties (for both speeds and grades). One is the difference in the fuel consumption idling rate, which ranges from 0.1 to 1.3 g/second in the field, whereas the range is smaller in the simulation (~0.20–0.6 g/second). Or it could be that tested vehicle types in the field are very different from evaluated vehicle types in the simulation.

It is important to note that none of the previous studies, except for the one with simulated data (Alshayeb et al., 2021a), reported the impact of other factors (excluding cruising speed) on the stop penalty. The simulation-based study (Alshayeb et al., 2021a) covered the effect of multiple factors on the stop penalty, which are 15 vehicle types (make year 1990–2000), driving behavior represented by acceleration-deceleration functions, road gradient while accelerating (−7% to 7%, as shown in Figure 4.12), cruising speed (assuming equal speed before and after stopping), and aerodynamic effect from the wind. It is also noted that the simulation-based study (Alshayeb et al., 2021a) did not develop a prediction model to estimate the stop penalty considering various factors—it simply derived bivariate relationships between each individual factor (while other have been kept constant) and the stop penalty. In comparison to that study with simulated data, this work developed MGGP models that cover more than 170 modern vehicle types (1996–2017), driving behavior with higher resolution by separately including the deceleration and acceleration times, a larger range of road gradients (while accelerating) (~−14% to 14%), a broader range of cruising speeds, etc. Finally, the MGGP models are not bivariate—they represent multivariate correlations between the stop penalty (as dependent variable) and all of the listed impact factors.

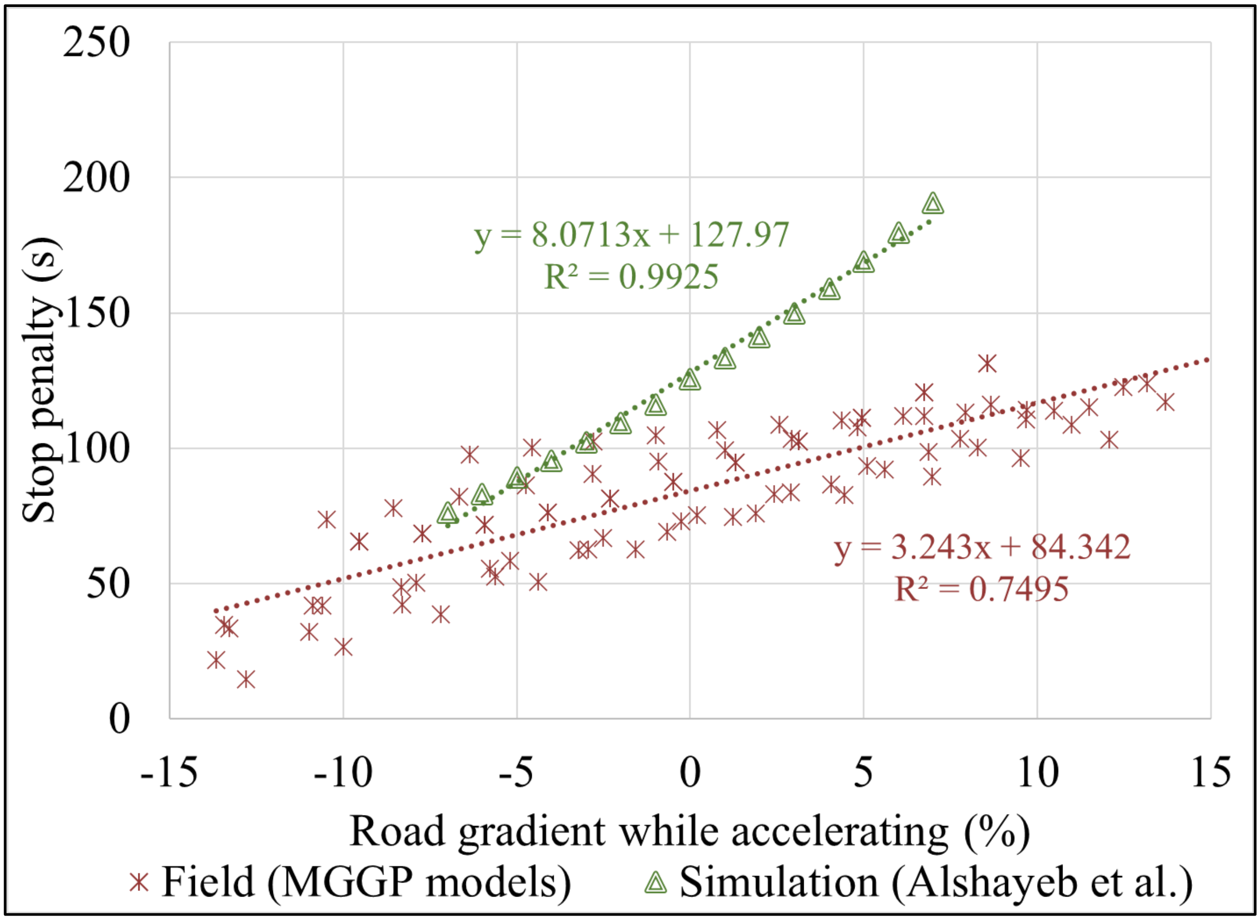

Figure 4.12 Stop penalty vs. road gradient from the field and simulation.

Based on the previous discussion, the major unique features of the MGGP models can be summarized as follows:

- The models were developed using high-resolution fuel consumption measurements, unlike Courage and Parapar, 1975, Akcelik, 1981, and Robertson et al., 1980 whose fuel consumption measurements were not of the same accuracy.
- Fuel consumption measurements were collected in the field, unlike Alshayeb et al., 2021a, whose stop penalties were simulation-based.

- Large number of LDVs and LDTs were included, whereas most previous studies used less than three vehicles.
- The tested fleet consisted of modern vehicles, whereas tested vehicles in the previous studies, except for Stevanovic et al., 2021 are old for contemporary standards.
- Tested vehicles covered long distances, resulting in a significantly larger dataset than those used in the previous studies.
- The models cover multiple factors impacting the stop penalty (vehicle type, cruising speed, road gradient, fuel consumption idling rate, driving behavior, and decelerating duration), whereas most of the previous studies investigated only the impact of the cruising speed.

While transportation agencies in different regions in the US can utilize the developed models because they included a large fleet of commonly driven vehicles on US roads, it is unknown whether the *K*-factor might vary for various locations. However, it is expected that this will be the case, as the *K*-factor depends on the operating conditions of each specific area. For example, an area could have a large percentage of elderly or youthful population, whose driving behaviors are quite different. Thus, the *K* values for such a location can be significantly different from a demographically well-balanced area. Consequently, further research is needed to develop regional *K* values for multiple distinctive regions. That can be done by collecting floating vehicle data, including fuel consumption in the field, especially for critical signalized corridors in the region, or by modeling the operating conditions of those distinctive regions in traffic simulation and fuel consumption models and designing proper experiments to derive *K* values.

Another future research should utilize the emerging basic safety message (BSM) data from connected vehicles to calibrate the developed models. Further, in a fully vehicular connected traffic environment, the BSM data can be used to compute the current *K* value for each network movement and use such a value for real-time adjustment of traffic timing parameters. Finally, the BSM data can also be used to derive the *K*-factor based on user satisfaction instead of equivalent fuel consumption. In such a case, the *K*-factor is expected to be lower at movements where drivers may be more inclined to wait longer or be stopped more frequently (e.g., side streets) than at movements where drivers expect good progression (e.g., through movement on the major street).

4.8 Conclusions and Future Research

This Chapter had two major objectives, (i) to assess the impact of the major operating conditions (vehicle type, cruising speed, road gradient, idling fuel consumption rate, deceleration duration, and driving behavior) on the stop penalty (*K*-factor) using vehicular trajectories and fuel consumption estimates collected from the field, and (ii) to develop valid EC models, namely MGGP, to formulate the stop penalty as a factor of various operating conditions.

An extensive real-world dataset from the field was used to develop predictive models for seven vehicular groups classified in this Chapter. The performance of the developed models was evaluated by using testing and validation datasets. The models developed achieved high accuracy for the training, testing, and validation datasets.

A parametric study was also carried out to investigate the impact of the investigated factors on the stop penalty and to ensure the robustness of the developed models. The parametric study revealed that the stop penalty is positively correlated with all of the factors studied. Specifically, initial speed, grade while accelerating, and deceleration duration have linear relationships with the stop penalty, whereas the idling fuel consumption rates and accelerations have quadrinomial ones. Lastly, final speed seemed to impact the stop penalty exponentially. These findings suggest that, in general, the stop penalty is not a low constant value as widely thought in the traffic signal optimization community.

An implication of this Chapter is the possibility of feasibly computing the *K*-factor by using the models developed in this study. It is recommended that traffic agencies should implement fuel consumption-based stop penalties in their signal timing optimization practices. Such implementation can be as simple as changing the value of *K* when optimizing signals using Synchro—or integrating the PI with correctly computed stop penalty as the objective function when optimizing signal timings utilizing various optimization techniques (e.g., genetic algorithm).

One limitation of the current Chapter is that it does not analyze the impact of some other important factors affecting the stop penalty (e.g., pavement type and ambient temperature) due to their unavailability in the field dataset. However, this research has identified a few questions that require further investigation. Most importantly, a future study should investigate the actual applicability of various *K*-values (especially $K > 250$ s) for different movements of signalized intersections on the reduction of fuel consumption and other performance measures (e.g., progression and delay). In addition, one could develop a microscopic level ML model and evaluate and validate the performance of such a microscopic model. One could also integrate a vehicle dynamics model to consider vehicle throttle and braking levels to assure more accurate fuel consumption and emissions estimates. This would be particularly important when connected and automated vehicles are considered.

5.0 Optimizing of Traffic Signal Timings Based on FC-PI - a Surrogate Measure for Fuel Consumption

Optimizing signal timings is an effective way to reduce sustainability metrics (e.g., fuel consumption and emissions). Historically, traffic agencies have retimed signal timings to improve traffic mobility performance measures (e.g., delay). However, optimizing signal timings to reduce delay does not necessarily mitigate sustainability measures. This Chapter introduces a new approach that integrates a traffic microsimulation software, a fuel consumption surrogate measure, and a stochastic genetic algorithm. This approach optimizes signal timings to reduce the surrogate measure of fuel consumption and thereby reducing sustainability metrics. In addition, multiple optimization scenarios are evaluated to identify the impact of heavy vehicles' presence in the fleet on the resulted signal timings and fuel consumption savings. A 13-intersection arterial on Washington Street in Chicago network served as a case study. Optimized signal timings delivered solutions that balanced both sustainability and mobility. Compared to initial signal timings, the estimated fuel consumption saving was 2.7% under normal conditions with no heavy vehicles. The saving reaches up to 5.7% when many heavy vehicles exist on the side streets. Most of the improvements came without significant worsening of traffic mobility efficiency, which shows the possibility of a fair trade-off between mobility and sustainability. All optimization scenarios showed that a slightly longer cycle length than the one implemented in the field is required to reduce fuel consumption. Further investigation is needed to evaluate the approach under various operational conditions (e.g., road gradients) and draw a general conclusion of the importance of utilizing the proposed surrogate measure through signal timings optimizations on sustainability metrics.

5.1 Introduction

Fuel consumption negatively impacts the environment (EPA, 2019e), health (Hall, 1996), and the economy (Yin and Lawphongpanich, 2006; Koonce and Rodegerdts, 2008) by inducing global climate change, reducing the quality of life by causing diseases (e.g., respiratory, nervous, and cardiovascular diseases), and causing inflation due to increasing oil prices. The traffic congestion problem in metropolitan areas and rapid urbanization of rural areas are leading causes of excess fossil fuels combustion (Cai et al., 2009; Sharma et al., 2010). Signalized intersections are one of the primary sources of extra vehicular fuel consumption (Rakha and Ding, 2003). They involve enormous traffic volumes, deceleration-acceleration events, and long idling times to accommodate the conflicts caused by intersecting multiple traffic streams. Moreover, the presence of unsustainable operational conditions (e.g., large percentage of heavy vehicles, high road gradients, high cruising speeds) increases extra fuel consumption at those intersections (Alshayeb et al., 2021a). Hence, it is crucially important to use the most efficient countermeasures to mitigate traffic congestion seeking more sustainable transportation systems.

Traffic signals are recognized to have a fundamental role in reducing congestion at signalized intersections (Gartner et al., 1991; Park et al., 1999; Stevanovic et al., 2015). Traditionally, researchers and practitioners have put much effort into developing signal timings that reduce motorists' delays (travel time) and stops (e.g., Robertson and Bretherton, 1991; Stevanovic et al., 2007; Christofa et al., 2016). However, a few studies have shown that minimizing delay does not necessarily minimize stops (Robertson et al., 1981; Park et al., 2009; Hitchcock and Gayah, 2018). Considering that fuel consumption is highly correlated with the stops (Rakha and Ding, 2003), signal timing plans that minimize delay do not necessarily lead to an optimal reduction in fuel consumption, as indicated in several studies (e.g., Park et al., 2009; Stevanovic et al., 2009; Liao, 2013). Therefore, a tradeoff between stops and fuel consumption on one side and delay on the other side is needed to generate sustainable signal timings.

Balancing between delay and fuel consumption in traffic signals optimization begun in the 1970s (Bauer, 1975; Courage and Parapar, 1975; Cohen and Euler, 1978). However, at that time, traffic signal timing tools were macroscopic and not very accurate in their estimation of the mobility (e.g., delay) and sustainability (e.g., fuel consumption) performance measures. That is attribute to the fact that such tools do not capture individual acceleration traces required to estimate fuel consumption and emissions accurately. The past few decades have seen several studies that used microscopic traffic simulation and fuel consumption models to minimize fuel consumption and emissions by developing sustainable signal timings (Park et al., 2009; Stevanovic et al., 2009; Kwak et al, 2012; Zhang et al., 2013). Such studies usually utilized heuristic optimization approaches (e.g., genetic algorithm 'GA'), which led to near-optimal signal timing, to accommodate the complex nature of microscopic traffic simulations and fuel consumption models (Park et al., 2009). The integration of optimization methods, traffic simulation, and fuel consumption and emissions models is a complex process, and such optimization models require processing of every vehicular trajectory, which makes them very computationally expensive (Osorio, C., & Nanduri, 2015). Additionally, such integrations are infeasibly implementable in the field because of the difficulty of estimating sustainability metrics (fuel consumption and emissions) from a particular site in the field. More importantly, previous studies rarely included the combined effects of multiple factors that impact sustainability metrics in the field (e.g., road grade, percentage of heavy vehicles in the fleet).

This Chapter attempts to fill the above-mentioned gaps by proposing a method that optimizes traffic signal timings to reduce sustainability metrics by minimizing the fuel consumption Performance Index (FC-PI), proposed by Stevanovic et al., 2021, as a surrogate measure for fuel consumption. The Chapter starts by investigating the potential fuel savings obtained when using the FC-PI under normal conditions of a real-world test site. Such normal conditions mean that the operating conditions impacting sustainability metrics (e.g., percentage of heavy vehicles in the fleet and road gradients) are considered as they are in the field, where their presence is very minor. Furthermore, to illustrate benefits of the proposed approach under more diverse scenarios, the authors developed two artificial scenarios and optimized FC-PI to reduce fuel consumption. The percentage of heavy vehicles in the fleet was altered in both modeled scenarios as one of the most important operating conditions impacting sustainability metrics. All of the optimization scenarios in this Chapter were performed using the integration of a GA optimization (Retime) (Stevanovic et al., 2007) and a microscopic simulation model (Vissim) (PTV Vissim, 2020).

The rest of the Chapter is organized as follows. The second section first reviews the most notable studies that optimized signal timing parameters to minimize sustainability metrics, and second provides an overview of the FC-PI derivation. The third section presents the proposed methodology. The case study used to apply the methodology is explained in the fourth section. Section five depicts the evaluations and thoroughly discusses the results. Finally, conclusions and recommendations are given in the last section.

5.2 Literature Review

The petroleum shortages in the early 1970s have attracted researchers to investigate adjusting signal timings to minimize extra fuel consumption caused by unnecessary stops.

Although earlier studies have revealed that mobility and sustainability measures can be reduced using the same cycle length, minimizing the latter requires implementing a longer cycle length than the one needed to minimize the former (Bauer, 1975; Courage and Parapar, 1975; Cohen and Euler, 1978; Akcelik, 1980; Robertson et al., 1981). Thus, the following batch of relevant studies focused on converting the signal control formulations into an optimization problem to balance between mobility and sustainability measures (Al-Khalili and El-Hakeem, 1984; Al-Khalili, 1985; Reljic et al., 1992; Penic and Upchurch, 1992; Liao and Machemehl, 1998). The last two decades have seen a large and growing body of literature discussing optimization of traffic signal control timings. For brevity, this section first reviews the most notable signal control optimization studies whose primary goal was to reduce fuel consumption and vehicular emissions. Second, the FC-PI derivation is presented.

5.2.1 Related Work

Considering that there are various operating factors (e.g., cruising speed) that impact fuel consumption and emissions at signalized intersections, each of the reviewed studies included one or more of those factors. Moreover, the reviewed studies have utilized various optimization techniques, macroscopic and microscopic traffic simulation models, and fuel consumption and emission models to optimize traffic signals. To review as many aspects of each study as possible, the studies were reviewed from five perspectives: i) the included operating factors in the optimization problem. The factors included in the review are: vehicle type, percentage of heavy vehicles, road gradient, and cruising speed. Those factors were specifically chosen because they have a profound impact on the sustainability metrics, as shown in previous studies (Stevanovic et al., 2021; Alshayeb et al., 2021b). ii) fidelity of the fuel consumption and emissions data used in the optimization process. iii) the size of the tested network. iv) the reported fuel consumption and emissions saving (%). v) the traffic simulation and optimization programs used to test the proposed optimization models.

Table 5.1 shows the studies that utilized high-resolution (second-by-second) fuel consumption and emissions estimates as well as the factors included in each study. Referring to Table 5.1, 16 out of 24 studies have used microscopic sustainability metrics estimates. Those 16 studies are considered more accurate than the rest because they captured the instantaneous change in cruising speed, which is the second impactful factor on sustainability metrics after vehicle type (Alshayeb et al., 2021b) and the only factor included by all studies, as shown in Table 5.1.

Prior commencing discussion about vehicle type, it should be brought up that there are two major vehicular classification. First, high-level classification which groups vehicles into Light-duty vehicles (LDVs) and heavy-duty diesel vehicles (HDDVs). The fleet distribution column in Table 5.1 reflects whether the study included the two categorize in the high-level classification. Second, low-level (more detailed) classification, which groups vehicles into subordinate to the LDVs and HDDVs. The vehicle type column in Table 5.1 reflects whether the study used multiple types of LDVs and documented the specifications of the utilized LDVs. Although vehicle type is the most impactful factor on sustainability metrics, only 3 studies clearly documented the use of both LDVs and HDDVs. Moreover, many studies did not precisely report the specification of the vehicle type(s) included in their case studies. Such lack of documentation of the tested vehicle types adds some sort of ambiguity to the results, which prevents a meaningful comparison between various studies. Regarding road gradient, none of the previous studies included the impact of the road gradient, even though several studies documented significant impact for the percentage of grade on the sustainability metrics (Boriboonsomsin and Barth, 2009; Gallus et al., 2017).

Table 5.1 Data fidelity and factors used in the reviewed studies.

Study	High resolution data	Impactful factors on fuel consumption and emissions			
		Vehicle type	Fleet distribution	Grade	Cruising speed
Li et al. (2004)	✗	✗	✗	✗	✓
Oda et al. (2004)	✗	✗	✗	✗	✓
Stevanovic et al. (2009)	✓	✓	✗	✗	✓
Park et al. (2009)	✓	✗	✗	✗	✓
Ma and Nakamura (2010)	✗	✓	✓	✗	✓
Li et al, (2011)	✓	✗	✗	✗	✓
Kwak et al. (2012)	✓	✗	✗	✗	✓
Zhang et al. (2013)	✗	✗	✗	✗	✓
Lv et al. (2013)	✓	✗	✗	✗	✓
Liao (2013)	✓	✗	✗	✗	✓
Ma et al, (2014)	✓	✓	✓	✗	✓
Khalighi and Christofa (2015)	✗	✓	✓	✗	✓
Osorio and Nanduri (2015)	✓	✓	✗	✗	✓
Stevanovic et al. (2015)	✓	✓	✗	✗	✓
Ubiergo et al, (2016)	✓	✓	✗	✗	✓
Han et al. (2016)	✗	✗	✗	✗	✓
Tan et al. (2017)	✓	✗	✗	✗	✓
Yu et al, (2018)	✓	✗	✗	✗	✓
Ding et al. (2019)	✓	✓	✗	✗	✓
Liu et al, (2019)	✓	✗	✗	✗	✓
Abudayyeh et al, (2021)	✗	✗	✗	✗	✓
Yang et al, (2021)	✓	✗	✗	✗	✓
Ma et al, (2021)	✓	✗	✗	✗	✓
This Chapter	✓	✓	✓	✓	✓

Table 5.2 summarizes the benefits reported by the reviewed studies when reducing sustainability metrics. It can be observed from Table 5.2 that 13 studies optimized signals for emissions only. It should be noted here that the emission types (CO, CO_2, HC, and NOx) shown in Table 5.2 are the most commonly reported emissions by the reviewed studies. One can also see from Table 5.2 that some studies reported savings only for fuel consumption or emissions, whereas other studies reported savings for all sustainability metrics. Moreover, five studies combined all emissions in the same saving percentage range. Such results are not supported by studies that reported a unique saving percentage for each sustainability metric. Hence, one of the contributions of this Chapter is confirming one of the two types of results. Table 5.2 also shows that various

studies reported that fuel consumption saving can vary significantly. Such saving can be lower than 1% and can reach up to 40.9% when signal timing plans generated by some of the proposed optimization models are compared to signal timing plans obtained from Synchro and TRANSYT (well-known and widely used signal timings optimization tools). However, studies that have reported low savings in the sustainability metrics seem more accurate and acceptable. Such studies were mainly based on high-resolution data, which captures the vehicle's phase operations on a second-by-second basis. Another logical reason for such a statement is that savings of more than 10% seem to be too high and difficult to accept when the underlying methodology lacks the necessary fidelity and data resolution. That excludes studies where a certain percentage of connected and autonomous vehicles (CAVs) are included in the tested fleet because of the advantages provided through the connectivity between such vehicles and the traffic signals (Ubiergo et al, 2016; Yu et al, 2018; Liu et al, 2019; Ma et al, 2021).

Table 5.2 Saving (%) in sustainability metrics as documented by various studies.

Study	Network size	Saving in fuel consumption and vehicular emissions				
		FC	CO	CO_2	VOC (HC)	NOx
Li et al. (2004)	Isolated intersection	-	2.9	-	2.7	1.05
Oda et al. (2004)	Three arterial roads	-	-	6.7	-	-
Stevanovic et al. (2009)	14 signalized intersections	1-1.5	-	1.4	-	-
Park et al. (2009)	4 signalized intersections	5.5-8.7	3.5-17.5	5.8-8.3	3.7-14.1	4.9-16.3
Ma and Nakamura (2010)	Isolated intersection	-	-	-	-	30.4
Li et al, (2011)	Isolated intersection	-	7.3	26.4	27.8	12.3
Kwak et al. (2012)	4 signalized intersections	20.3	7.8	20.5	15.3	20.6
Zhang et al. (2013)	5 signalized intersections	-	8	-	-	-
Lv et al. (2013)	Isolated intersection	-	2-11	2-11	2-11	2-11
Liao (2013)	Isolated intersection and an arterial	2.2-40.9	-	-	-	-
Ma et al, (2014)	Isolated intersection	2.4-5.34	14.6-15.6	-	13.5	7.4
Khalighi & Christofa (2015)	Isolated intersection	-	-	-	2.5-4.4	3.6-7.6
Osorio and Nanduri (2015)	9 signalized intersections	-	-	9.7	14.3	23.6
Stevanovic et al. (2015)	5 signalized intersections	4.5	-	-	-	-
Ubiergo et al, (2016)	Isolated intersection	2-20	1-14	2.6-20	-	3.1-22
Han et al. (2016)	3 signalized intersections	-	-	-	2-2.1	-
Tan et al. (2017)	Isolated intersection	-	50	50	50	50
Yu et al, (2018)	Isolated intersection	-	-	1.9-49.3	-	-
Ding et al. (2019)	4 signalized intersections	-	7	-	7	7
Liu et al, (2019)	Isolated intersection	2.2-29	-	-	-	-
Abudayyeh et al, (2021)	24 signalized intersections	-	-	5-8	-	-
Yang et al, (2021)	6 signalized intersections	3.9-7.4	-	-	-	-
Ma et al, (2021)	Isolated intersection	10-30	-	-	-	-
This Chapter	12 signalized intersections	2.7-5.7	1.1-1.5	2.6-5.4	1.2-2.5	1.6-5.5

Figure 5.1 presents the reviewed studies with their deployed traffic models or simulation programs with the fuel consumption and emission models utilized in each study. The traffic simulation or models (the first column from the left) is connected with the studies (the second column from the left) and the fuel consumption and/or emission model (the third column from the left), which have been used in the optimization process to assess the performance of the optimal signal timing plans.

The following research gaps were identified from the above reviewed studies:

1. Several studies did not use high resolution sustainability metrics estimates. Such high-resolution data have shown superiority over aggregated (averaged) data (Dobrota et al., 2019). Moreover, few studies included the fuel consumption of fully

stopped vehicles and vehicles that passed the intersection on the cruising speed (without slowing down), ignoring vehicles with deceleration-acceleration events. Thus, one could question the accuracy of those studies, especially that they suffer from several other gaps defined below.

2. Most of the previous studies did not include the impact of vehicular distribution (e.g., percentage of HDDVs in the fleet) in the optimization process. Also, they used various LDV types with no proper documentation of their specifications. Thus, it is difficult to determine the impact of the presence of heavy vehicles on the optimization results.
3. The impact of topological conditions (e.g., grade) were completely neglected. This gap can have significant negative impacts on the optimization results. For example, the optimizer might generate a 'so-called' optimal signal plan for level-terrain conditions on all links in the optimized corridor or network, whereas -in fact- many links in the optimized network have a certain slope. In such cases, the generated optimal signal plan is not actually optimal.
4. The fact that researchers deployed large number of various combinations of traffic simulation programs, fuel consumption and emissions models, and optimization techniques, has led to a variety of reported results. Thus, it is almost impossible to meaningfully compare all studies and determine a factual range of savings based on fixed (or range of fixed) conditions and standards.

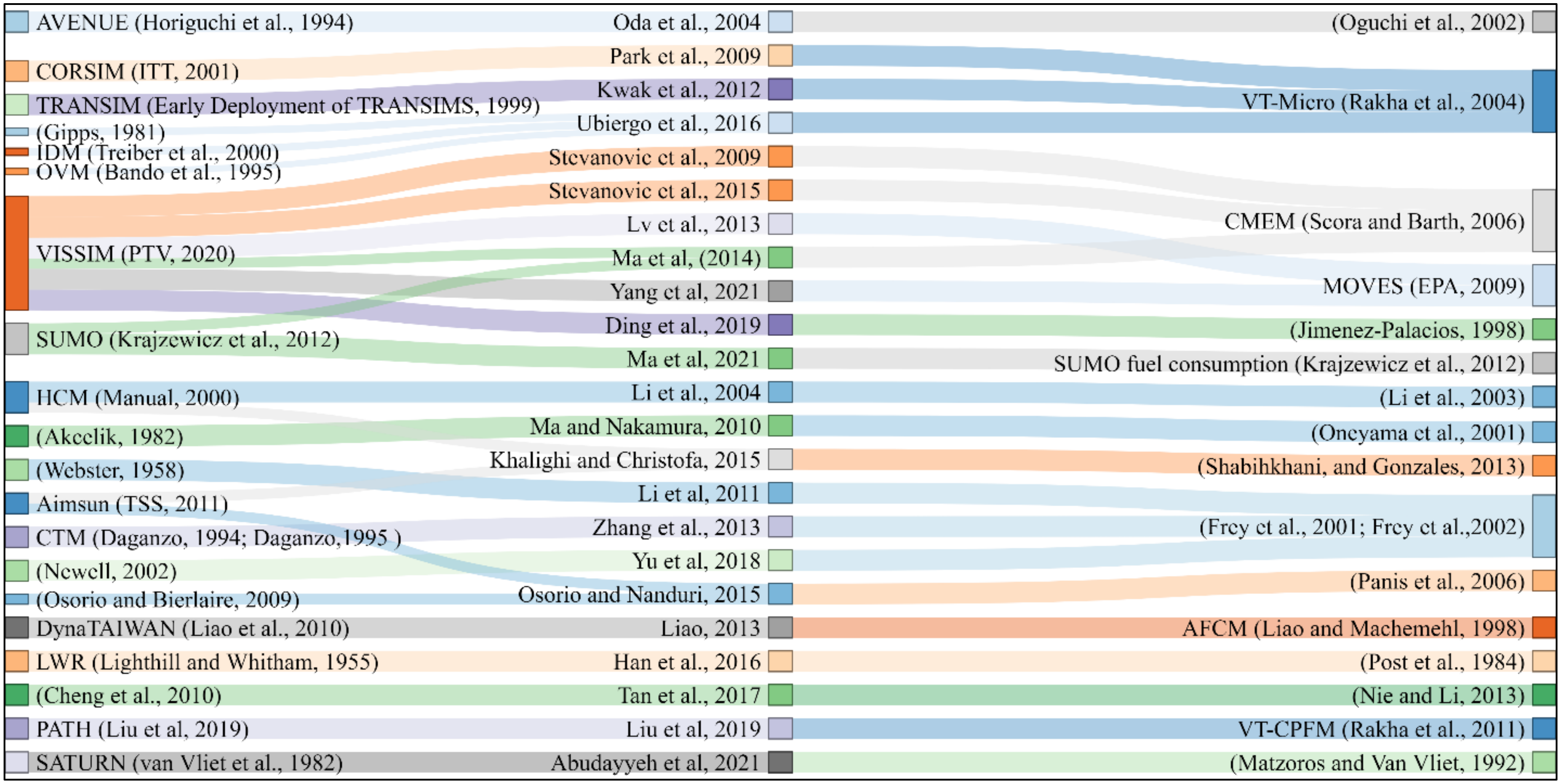

Figure 5.1 Connections between studies, traffic programs, and fuel consumption/emissions models.

5. Most of the reviewed studies have used one hypothetical intersection or small networks (less than four intersections) to test the proposed optimization tools. Nevertheless, testing a new framework or methodology on such small networks is not adequate to ensure that the proposed framework or methodology works on complex urban networks.
6. Although most of the proposed methods have shown promising results in reducing sustainability metrics by optimizing signals, many of the proposed methods are time-consuming and computationally expensive. Moreover, most of the signal optimization techniques and their alternatives of reinforcement learning approaches (e.g., Zhu et al., 2015; Aslani et al., 2017; Yoon et al., 2021; Li et al., 2021) introduced by the previous studies are not adopted by transportation agencies, partially, because of their complexity. Thus, there is a need to use an objective function which can be feasibly integrated in the most used signal timing optimization tools in practice (e.g., Synchro, Vistro, TRANSYT-7F).
7. Most of the recent studies proposed optimization models for mixed vehicular fleets (CAVs and human driven vehicles) (e.g., Stevanovic et al., 2017), which need a relatively long time to be implemented in the field. Further, many studies are undertaken for fully autonomous vehicles conditions. Such studies are only applicable when 100% of the vehicular fleet is CAVs. Therefore, there is an urgent need, originated by the accelerating change in the climate, to more short-term technologies based on today’s average vehicles, traffic signals, and the optimization tools utilized by transportations agencies.

Therefore, this Chapter attempts to fill the above-mentioned gaps by optimizing traffic signal timings of 12 signalized intersections modeled, calibrated, and validated in the microscopic traffic simulation software Vissim. A GA optimization (Retime), which was proved to generate near-optimal solutions (Stevanovic et al., 2007; Stevanovic et al., 2009; Stevanovic et al., 2015), is deployed in this Chapter to generate optimal signal plans. Two of the default vehicle types (one LDV and one HDDV) defined in the widely used and accepted Comprehensive Modal Emission Model (CMEM) are used in the relevant scenarios investigated in this Chapter. Road gradients were computed for all movements in the network and included in the FC-PI computation (Section 5.3.3). The Chapter uses the surrogate measure for fuel consumption "FC-PI" as the main objective function to be enhanced in the optimization process. This measure was derived based on the principles of the traditional Performance Measure (PI) (Robertson, 1969), as discussed in the following subsection. Using such a surrogate measure speeds up the optimization process because it does not require estimating sustainability metrics for each possible solution (signal plan).

5.2.2 Overview of FC-PI

One of the first attempts to reduce fuel consumption through retiming signals was conducted by Robertson et al., 1980 using the Performance Index (PI) (Robertson, 1969), shown in Equation 5.1. This PI is a linear relationship between delay and the number of stops at a specific link. The critical component of the PI is a weighting factor '*K*' multiplied by the number of stops to give each stop an equivalent number of seconds in terms of delay; hence it is also known as the "stop penalty." Since its development, several studies have confirmed the excellent efficiency of the PI in improving mobility metrics (e.g., Chiou, 1999; Papatzikou and Stathopoulos, 2015). Moreover, several studies used similar objective functions to the PI to address both mobility and sustainability metrics (e.g., Li et al., 2004; Oda et al., 2004). However, this was not always done consistently, and the selected objectives are not always distinctive enough. Also, it does not seem that newer studies made full use of the traditional PI, which has proven to be effective in earlier studies. Thus, recent research on the *K*-factor was carried out to derive a new fuel consumption Performance Index (FC-PI) based on the original PI (Stevanovic et al., 2021). This FC-PI defines the stop penalty as the number of seconds of delay (idling phase) that consume the same amount of fuel consumed during a stopping event (deceleration-acceleration phases). The interesting aspect of such a definition is that the *K* value for individual links (or movements) can be computed based on different factors (e.g., vehicle type, cruising speeds, and road gradient) impacting fuel consumption. Hence, one can use the FC-PI as a surrogate measure to the actual fuel consumption estimates to optimize traffic signal timing plans.

$$PI = \sum_{i=1}^{n} D_i + K \cdot C_i \tag{5.1}$$

Where:

D_i – is an average delay in pcu_s-hours per hour on the i^{th} link (or movement) of the network.

C_i – is an average number of pcu_s stops per second on the i^{th} link (or movement) of the network.

n is the number of links or movements included in the optimization.

K is the weighting factor, which was defined for a stop-event in (Stevanovic et al., 2021) as:

$$K = \frac{(FC_D + FC_A) \cdot T_I}{FC_I} \tag{5.2}$$

Where:

FC_D – fuel consumed during the deceleration phase.

FC_I – fuel consumed during the idling phase.

FC_A – fuel consumed during the acceleration phase; [gallons, liters, or grams].

T_I – total idling time in seconds.

Figure 5.2 shows the changes in cruising speed and fuel consumption during a complete stop (decelerating from 40-mph-idling for 10 seconds-accelerating to 45-mph) for LDV (Figure 5.2a)) and HDDV (Figure 5.2b)). It is important to mention that Figure 5.2 was developed based on simulated trajectories from Vissim and fuel consumption estimates from CMEM. Also, the LDV and HDDV used are LDV-category 4 (Car, Normal Emitting, Three-Way Catalyst, fuel injected, >50k miles, Low Power/Weight) and HDDV-category 7 (HDD 1999-2000, 4-stroke, Elec. Fl, Normal Emitting) in CMEM, respectively (Scora and Bath, 2006). Two primary observations are apparent from Figure 5.2. First, the time taken by an HDDV to decelerate from a certain speed to zero and then accelerate to a specific cruising speed is significantly longer than the time needed by an LDV to achieve the same dynamics. Second, fuel consumption rate of an HDDV is higher than that of an LDV for all modes of a stop (deceleration-idling-acceleration). That is especially seen during the acceleration mode. Thus, it is expected that the *K*-factor of an HDDV is larger than that of an LDV under identical operating conditions because of the above-mentioned observations. That means that the *K*-factor for a particular movement (*i*), which can be computed as the average of all *K*s computed for all stops (*m*) at that movement as shown in Equation 5.3, changes proportionally to the percentage of HDDVs in the fleet.

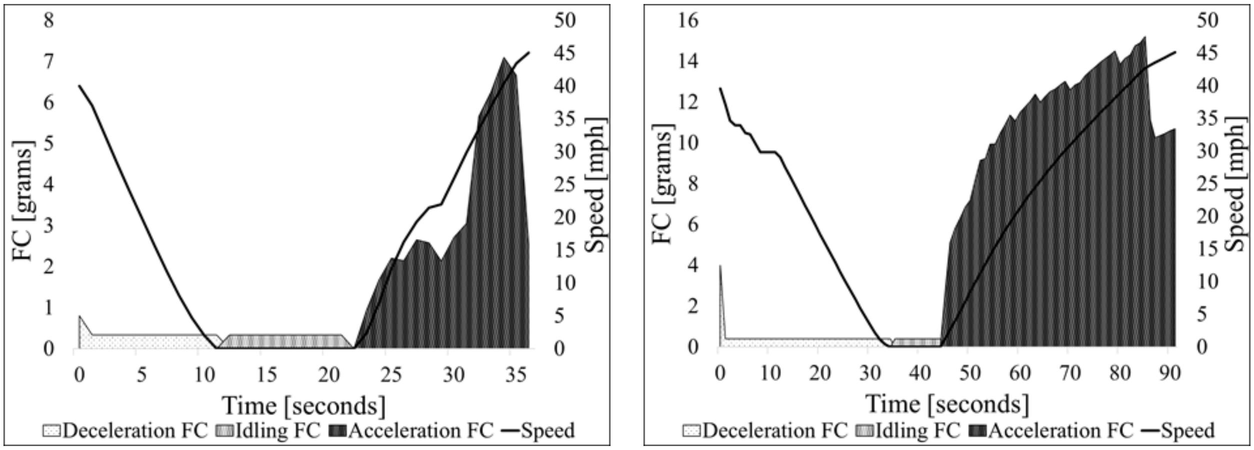

a) LDV b) HDDV

Figure 5.2 Dynamics and kinematics of complete stops made by two types of vehicles.

$$K_i = \frac{\sum_{j=1}^{m} \frac{(FC_D + FC_A)_j \cdot T_{I_j}}{FC_{I_j}}}{m} \tag{5.3}$$

Based on Equation 5.3, the relationship between *K*s on various movements, when adjusted by signal timings, would impact how the entire intersection performs in terms of the consumed fuel. A similar statement could be made for the entire network. Therefore, an FC-PI for a number of movements *n*, and a given analysis period (e.g., an hour) for an intersection or a network can be expressed as:

$$FC - PI = \sum_{i=1}^{n} D_i + \left(\frac{\sum_{j=1}^{m} \frac{(FC_D + FC_A)_j \cdot T_{I_j}}{FC_{I_j}}}{m} \right)_i \cdot S_i \tag{5.4}$$

Where:

D_i – is the total stopped delay at movement *i*.

S_i – is the total number of stops at movement *i*.

It is noted here that n can be the total number of movements at an intersection and in the network when computing the FC-PI for an intersection or the entire network, respectively. However, the movements (n) included in the computation of FC-PI do not have to cover all movements at an intersection or the network. For example, less important movements (e.g., left turns or those with very low traffic volumes) could be excluded, when calculating the FC-PI. The following section discusses the methodology of integrating the values of the K-factor based on fuel consumption estimates from CMEM with the GA optimization program (Retime) and the traffic simulation software program (Vissim).

5.3 Methodology

The methodology started by computing the K-factor for each movement in the case study investigated in this Chapter (Section 5.3.3). The next step was to integrate the K values into the adopted online optimization tool Retime, which was also interfaced with Vissim microscopic simulation. This Chapter tested the use of the FC-PI in the optimization on three scenarios – normal field conditions and two artificial conditions developed to show the importance of heavy vehicles when developing signal plans to reduce fuel consumption and emissions. Minimizing the FC-PI was the primary objective function for all of the three optimizations. The Chapter then evaluated the impact of the newly developed signal plans on mobility and sustainability metrics, namely, delay, number of stops, throughput, latent demand, fuel consumption, and four air pollutants (HC, CO, CO_2, and NOx). In summary, this Chapter conducts multiple optimizations with one objective function under three different operational conditions, as described in the following subsections.

5.3.1 Vissim Microscopic Traffic Simulation Model

This Chapter selects the microscopic simulation model PTV Vissim (PTV Vissim, 2020) to serve as a stochastic traffic model that suits the stochastic nature of the GA optimization. Vissim has been recognized in the traffic community for its friendliness and the ability to model the most implemented traffic signal controllers in the US. Vissim was used in this study at two stages for each of the three performed optimizations as follows:

1. Generate second-by-second vehicular trajectories, including timestamp, speed, and acceleration-deceleration traces to compute the *K*-factor before starting the optimization process.
2. Provide the mobility measures, stopped delay, and stops for each possible solution (set of signal plans) provided from the optimization tool to compute the FC-PI for that solution.

Finally, the vehicular trajectories of the best-optimized model (set of signal plans) for each scenario were extracted from Vissim and used to evaluate the fuel consumption and emissions improvements.

5.3.2 CMEM Microscopic Fuel Consumption and Emissions Model

CMEM (Scora and Bath, 2006) is a power-demand model that estimates fuel consumption and emissions based on various components (e.g., vehicle engine, grades, and vehicle mass) that are correlated with the vehicles' fuel consumption and emissions production. In this Chapter, CMEM is used to:

1. Estimate fuel consumption measures to compute the *K*-factor of all movements using stop profiles trajectories extracted from the base case (with unoptimized signal plans) simulation model of all three scenarios evaluated in this Chapter.
2. Evaluate the improvements in vehicular fuel consumption and emissions of the best set of signal timing plans (the ones with minimum FC-PI). This evaluation was performed by developing a Vissim-Python-CMEM interface that processes vehicular trajectories from Vissim in CMEM, providing the total fuel consumption and emissions.

It is worth noting that previous studies have calibrated, and validated sustainability metrics estimates from CMEM and indicated that CMEM generates acceptable fuel consumption estimates not only for California vehicular fleet for the US general fleet (Barth et al., 2001; Rakha et al., 2003). Hence, calibration efforts for CMEM were not made in this Chapter, instead, two default vehicle types were used in the Chapter. Those vehicle types are: i) Car (LDV), Normal Emitting, Three-Way Catalyst, fuel injected, >50k miles, Low Power/Weight, and ii) HDDV 1999-2000, 4-stroke, Elec. Fl, Normal Emitting. It is worth emphasizing here that this methodology, unlike other studies, does not estimate fuel consumption and emissions for every possible solution provided by the Retime during the optimization. Instead, the improvement is only measured for the optimal set of signal timings (of each scenario), once the optimization is completed. This approach is time-efficient because it significantly reduces the evaluation run time of each generation in the optimization.

5.3.3 Computation of Stop Penalty

The *K* factors were computed by running the base case model for each of the three scenarios before starting the optimization process. As shown in Figure 5.3, the vehicular trajectories (FZP file) from Vissim were processed in Python to extract the stop profiles' trajectories of all stopped vehicles at each movement. Those trajectories were then processed in CMEM to estimate second-by-second fuel consumption measures during each stop's driving phase (deceleration, idling, acceleration). The fuel consumption estimates in each phase were then used to apply Equation 5.2 and compute the *K*-factor for each stop. Once *K*-factor is calculated for all stops individually, Equation 5.3 was applied to compute the *K*-factor for every intersection movement. The final *K* value for each movement included the impact of four operating factors which are:

1. Vehicle type (two types were used as mentioned in the previous subsection).
2. Fleet distribution: two optimization scenarios include 15% HDDVs in the fleet on specific movements. Thus, as mentioned earlier, movements with such a significant percentage of heavy vehicles had noticeably higher *K* values due to those vehicles' higher fuel consumption footprints.
3. Road grade which was modeled in both Vissim and CMEM to capture its impact on the dynamics (acceleration and deceleration) and kinematics (fuel consumption) of the vehicle, respectively.
4. Cruising speed which was taken from Vissim and used as the main input for the power-demand module in CMEM to estimate fuel consumption. Finally, the movements' *K* factors were integrated into the Retime algorithm to compute the FC-PI for the entire network (Equation 5.4) for every solution provided by the optimization process.

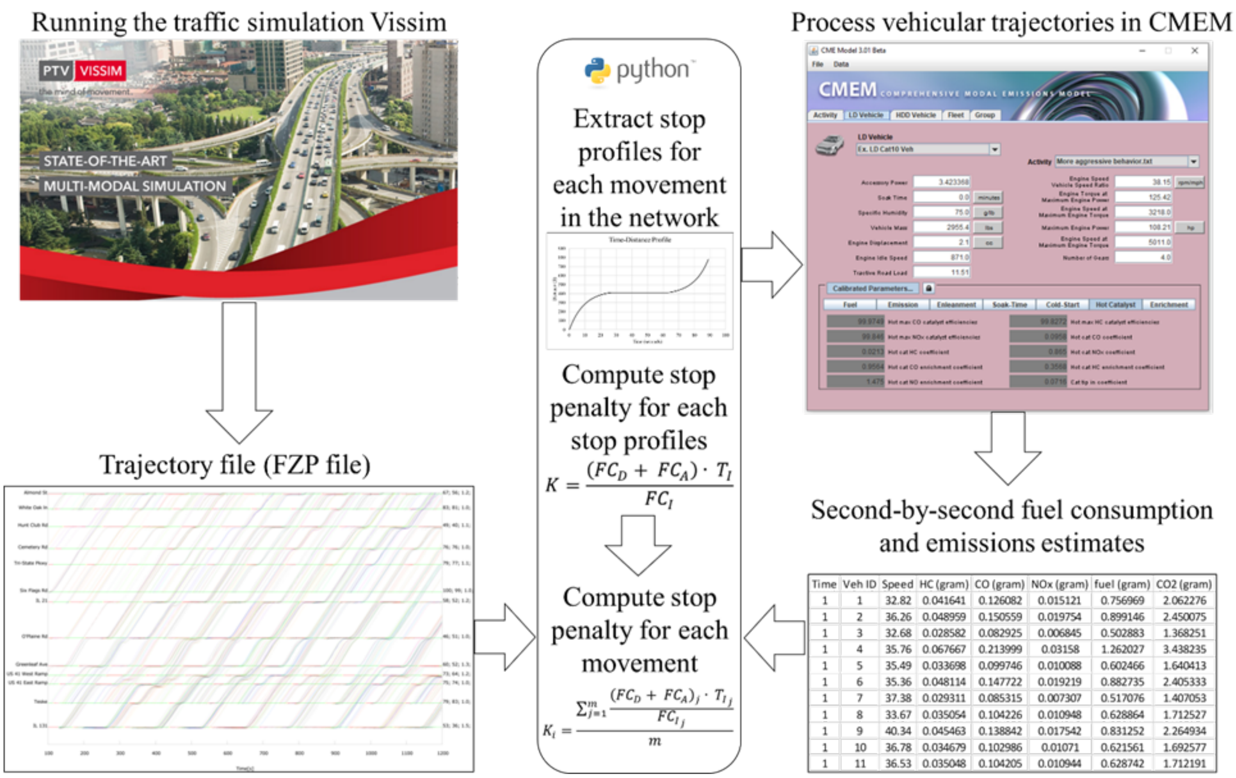

Figure 5.3 Connection between Vissim, Python, and CMEM.

5.3.4 Retime Optimization Tool

Retime optimization tool is an online signal timing optimization program that utilizes VISSIM microscopic simulation to evaluate signal timings proposed by the stochastic nature of the GA. The general structure of Retime is similar to other GAs formulations, and it is well documented elsewhere (Stevanovic et al., 2007). The Retime uses VISSIM's input and output files to compute the FC-PI and provide a new set of signal plans to be evaluated. The fundamental part of the Retime is inspired by the natural selection and evolution of the current population (Holland, 1992). The Retime can be used to optimize basic signal timing parameters (e.g., cycle length, offsets, splits, and phase sequence) by finding signal timing plans which can reduce the FC-PI through a predefined number of generations. Retime was extended to accommodate the needs of this Chapter, including functionalities to enable optimization of signal settings to minimize the FC-PI for the entire network. The FC-PI is computed based on different *K* values defined for each movement before starting the optimization process. Also, the program was revised to fit the current cloud version of Vissim, which improved run time of each evaluation. Algorithm 1 shows a basic step-description of Retime operations process used in this Chapter.

Algorithm 1. Description of the genetic algorithm optimization coded in Retime optimization tool.

Step 0:Initializing
G, total number of generations
T, total number of timing plans per generation
i, current number of population
$i = 0$
Generation of initial population p^i of timing plans tp^k, $\forall k \in [1,\ldots,T]$

- Read initial timing plan tp^1 from field Vissim files
- Generate tp^k, $\forall k \in [2,\ldots,T]$

Step 1:Evaluating Population
Evaluation of $tp^k \in p^i$, $\forall k \in [1,..T]$

- Write tp^k to Vissim files (on the main VM)
- Transfer Vissim files to cloud (to one of the temporary created VMs)
- Simulate and evaluate tp^k
- Transfer evaluation results back to the main VM
- Calculate $FCIC\text{-}PI^k$ by applying the following formula for $\forall$ intersection, $\forall$ movement and $\forall$ vehicle class:
  $FCIC\text{-}PI^k$ = ∑(stoppedDelayTotal+stopPenalty*stopsTotal)*numOfVehPerClass/*numOfVehiclesOverall*
- Calculate $fitness^k$ while applying penalty if $externalQueue^k$ reached the limit

Step 2:Testing Termination Criteria
$fitness^b = \max(fitness^1, \ldots, fitness^T)$
IF ($i = G$)
Stop and RETURN $tp^b \in p^i$
ELSE
GO TO Step 3
Step 3:Generating New Population
$i = i + 1$
Generation of new population p^i

- Select a couple of timing plans from p^{i-1} based on their fitnesses (e.g., probabilities to be selected for mating)
- Generate a new couple of timing plans through GA-operations (crossover and mutation)
- Continue generating the rest of the p^i by repeating the previous two steps until the required number of timing plans is created

GO TO Step 1

5.3.5 Retime Stochastic Optimizations

Signal timings optimization process in this research aimed at minimizing the FC-PI as the main objective function for three scenarios as follows:

- **Scenario 1** represents the actual normal operational conditions from the field. The normal field conditions put a very low focus on any of the operational conditions that could have a large impact on the fuel consumption as documented in other studies (Alshayeb et al., 2021a) (e.g., similar speeds for most movements, level-terrain, and low percentage of heavy vehicles). Consequently, it is very difficult in such cases to show distinctive advantage of using the FC-PI as an objective function over some other conventional objective functions. For this reason, two hypothetical scenarios (2 and 3) were proposed to include at least one major factor that would give FC-PI a chance to show its potential. Such an impact was found through a higher percentage of heavy vehicles in the fleet distribution. In those hypothetical scenarios more weight (higher *K* values) was added to the movements with higher percentage heavy vehicles.
- **Scenario 2** assumes increased percentage of heavy vehicles (from 0% to 15%), but only in the vehicular distribution of the side streets. This increase was applied only for 4-leg intersections and only through movements saw increase in heavy vehicle traffic. It was intended that this scenario gives higher weight on side street traffic and open side-street greens more as a mean to reduce fuel consumption of such heavily loaded truck movements. For example, a common PI (which consists only of delays and stops) would not pick up such a change as delays and stops do not contain information about heavy truck producing extra fuel consumption, while the

FC-PI is ‘equipped’ to do so through an additional ‘knowledge’ embedded in specific *K* factors (of heavy-traffic side-street movements).

- **Scenario 3** also increases the percentage of heavy vehicles in the vehicular distribution but this time it was done for the Westbound direction of the major road. Similar to the second scenario, percentage of heavy vehicles was set to 15%. It is noted here that those 15% of heavy vehicles travel across the entire corridor in westbound direction, thus representing a heavy traffic route.

Each optimization run started with the same initial set of signal timing plans from the field. Each optimization scenario was based on the evaluation of FC-PI accumulated during 60 min of simulation time. An additional 15-min for the warm-up was added to achieve steady-state traffic conditions in the tested arterial. Each optimization had a minimum of 50 generations, where 20 signal timing plans were operated through GA procedures for each generation. It is note here that the optimizations were stopped once the number of generations reached 50 and the algorithm stopped finding better solutions. The optimizations performed in this Chapter included modifications of cycle lengths, splits, and offsets without changing the sequence of the phases as the government agency responsible for this corridor prefers to have leading left-turns on all of the signals. It is worth noting here that a few initial 15-minute optimizations were conducted to test the process and capture any inconsistencies. Once all of the optimization parameters were tuned in, the full-hour optimizations were performed. It is also important to mention that the optimization processes used some additional constraints that ensure that modifying signal timings does not leave any traffic outside of the network.

5.4 Case Study

This section presents the case study implemented in this research to demonstrate best the impact of developing optimized traffic signal plans to minimize the FC-PI under the three proposed scenarios.

5.4.1 Building, Calibrating, and Validating Vissim Model

The arterial network representing Washington Street (Lake A22), located in Lake County, Chicago, IL, United States, was chosen as a test site to optimize signal timings for minimal fuel consumption using the FC-PI as the objective function. The arterial consists of 13-signalized intersections and has an average annual daily traffic that ranges from 21,000 to 28,000. The test site shown in Figure 5.4 starts from Almond Rd (west) and lasts to N Green Bay Rd (east), which is designated as IL-131.

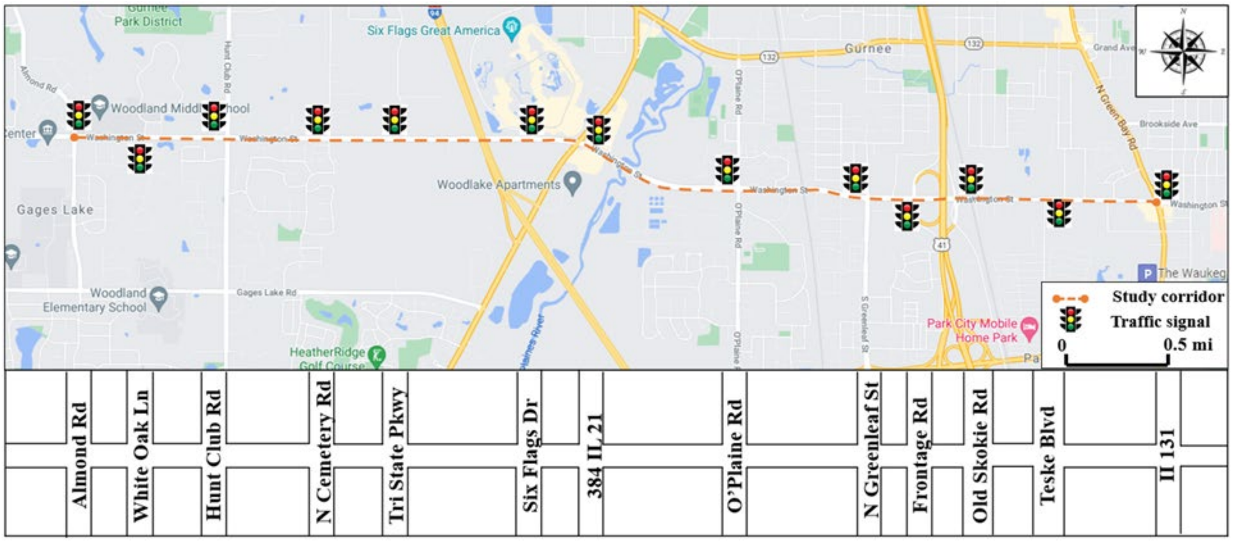

Figure 5.4 Study area of Washington Street.

Data collection efforts were required to provide necessary inputs to build the microsimulation model and develop various performance measures for the calibration and validation of the Vissim model. Such data included traffic volumes, traffic signal timing sheets, turning movement counts, saturation flow rates, travel times, detectors' locations, intersections' layouts. The data were either collected through remote access to Lake County, Division of Transportation (LC DOT) cameras, and LC DOT Automated Traffic Signal Performance Measures (ATSPM) software platform or were obtained directly from the LC DOT. The developed Vissim microsimulation model resembles field traffic conditions observed on Washington Street during the PM peak period (15:30-16:30). The signal controllers in the field are either ASC/3, Cobalt, or Siemens signal controllers. The Vissim model for the test site was prepared in Vissim 2020 by importing a Synchro model obtained from the LC DOT. Subsequently, manual adjustments were made to correct the geometry of the imported model according to more relevant information from the field.

Simulation models used in signal timing optimization studies should reflect the traffic characteristic in the field to the greatest possible extent. Traffic volumes, saturation flow rate, and travel times are the most used measures to calibrate and validate such models. However, microscopic fuel consumption models mainly estimate vehicular fuel consumption estimates using acceleration, deceleration and driving speed. Thus, realistic driving characteristics such as speed and acceleration patterns are required to compute an accurate *K*-factor. Several parameters can be adjusted, for calibration purposes, in Wiedeman 74 model used in Vissim (Wiedeman, 1974). Most of those parameters have minor impact on the saturation flow, acceleration, speed and travel time. Hence, the most relevant parameters that were adjusted in preparing this testbed are summarized in Table 5.3.

Table 5.3 Most impactful parameters adjusted in Vissim for calibrating the testbed modeled in Vissim.

Traffic characteristic	Parameter in Vissim (PTV Vissim, 2020)
Traffic volume	Vehicle input and static routing decisions
Time and distance headways	Additive part of safety distance and Multiplicative part of safety distance
Following variation	Look ahead and back distances, and speed and acceleration behavior during recovery from speed breakdown
Lane change	Maximum and accepted decelerations
Speed	desired speed distribution
Acceleration and deceleration	desired deceleration and acceleration functions

Traffic volumes and routing decisions were coded to represent turning movement counts from the field. The volumes were collected from the cameras on the modeled intersections of Washington Street. In a few cases, where a camera of a particular intersection in the field, does not cover all movements at that intersection, the most recent turning movement counts were used instead. The cameras were also used to calibrate the saturation flow rate which was determine on various intersections and segments by determining the time and distance headways. The saturation flow was modeled in Vissim by combining the parameters Additive part of safety distance and Multiplicative part of safety distance. Following variation and lane change parameters were adapted and adjusted systematically to obtain better calibration and validation results.

Vissim defines speed as a distribution between minimum and maximum speeds (PTV Vissim, 2020). The traffic speeds on the Washington Street (the major street) were modeled based on free-flow travel times (measured through Waze application) between intersections. Speed limits in the field were the bases to model speeds for the signalized side streets because travel times were not available for those streets. Subsequently, the desired speed distributions in Vissim were gradually adjusted for each segment (link between two intersections) to represent the speeds from the field.

Vissim defines the desired acceleration and deceleration values as distribution functions of the current speed known as desired acceleration–deceleration functions (PTV Vissim, 2020). Both acceleration–deceleration functions for each vehicle type are defined using three curves representing the minimum, median, and maximum possible acceleration–deceleration values at different speeds. Developing those functions requires enormous number of field vehicular trajectories covering a wide range of speed. Collecting such trajectories is costly and time-consuming task. Hence, realistic acceleration–deceleration functions developed in previous study based on a large trajectories' dataset collected in Michigan was used for the current testbed (Alshayeb et al., 2021c). Utilizing those functions from a different location than the testbed might result in differences between simulated accelerations and decelerations and those happening in the field. However, such differences can be considered insignificant compared to the differences that would be introduced if the default acceleration–deceleration functions were used. That is because the default acceleration–deceleration functions in VISSIM are based on an older dataset from Europe, as indicated by previous studies (Wilmink et al., 2009; Jie et al., 2013), whereas the testbed is in the US.

Simulated traffic volumes per movement were compared with their counterparts from the field to measure the calibration quality. Once the calibration was completed, the model was validated against average green times. The model calibration results are shown in Figure 5.5a), which shows that the field traffic volumes are highly correlated with modeled volumes for the same period.

The correlation between field average green times per phase (collected from the ATSPM platform) and average green times per phase obtained from the Vissim output file (.lsa file) are utilized to validate the model built in Vissim. The validation results of average green times are shown in Figure 5.5b). To further validate the model, link travel times from the field (Waze) were compared with the travel times from the model. The results of travel times validation are presented in Figure 5.5c) and Figure 5.5d) for the eastbound (EB) and westbound (WB) directions, respectively. The validation results of the modeled travel times, against their counterparts from the field, showed a strong resemblance between the modeled and the field values. In summary, the calibration and validation results for the modeled period show that the model strongly reflects the field conditions; hence it is ready to be used for testing the signal timings optimization scenarios.

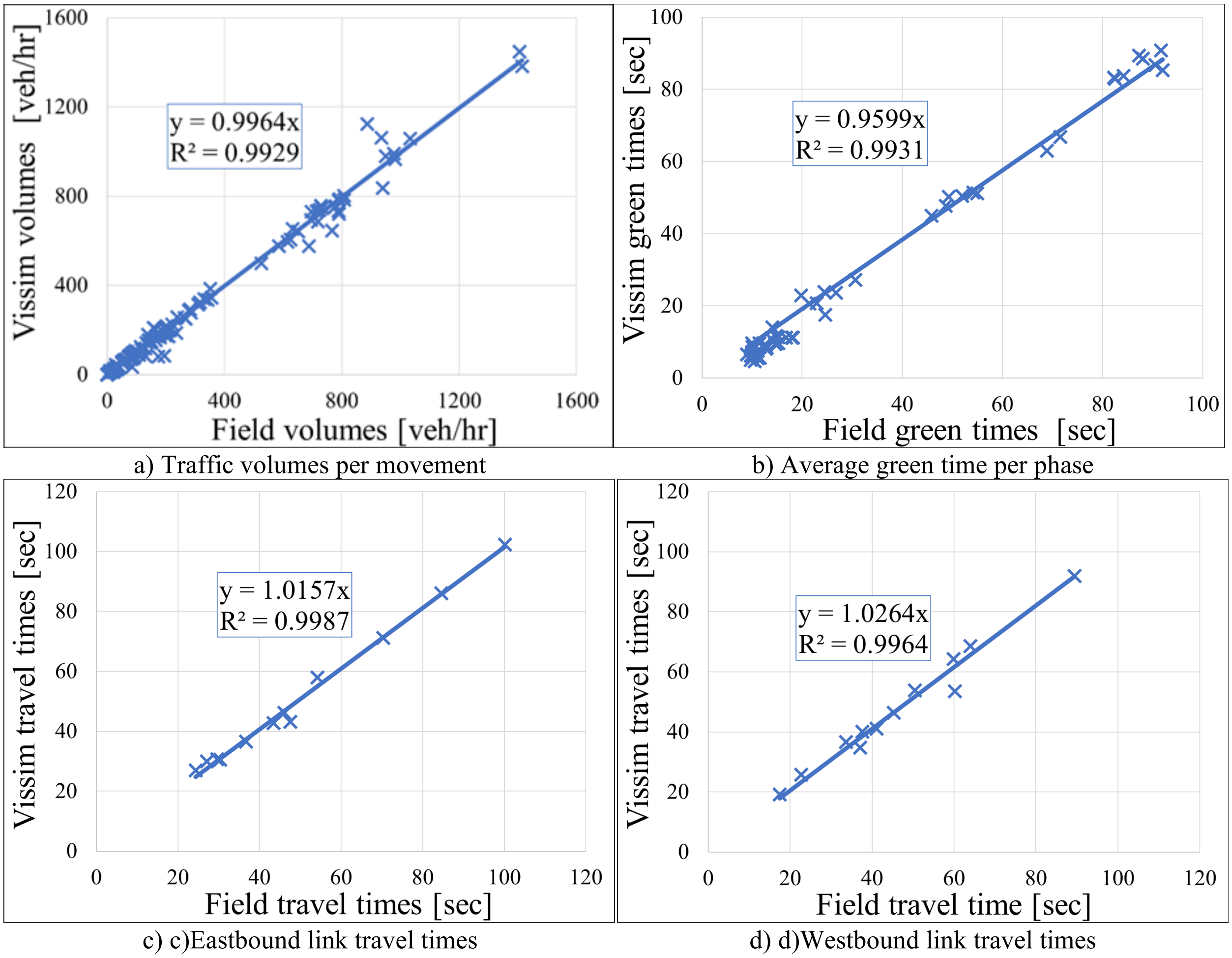

Figure 5.5 Calibration and validation results of the Vissim model.

5.5 Results and Discussion

The convergences of FC-PI optimizations for the three scenarios are shown in Figure 5.6a), which demonstrates how the best FC-PI vary over the number of generations. It appears that the optimization runs for Scenario 1 converged after 62 generations, whereas the optimization runs for scenarios 2 and 3 converged after 21 and 12 generations, respectively.

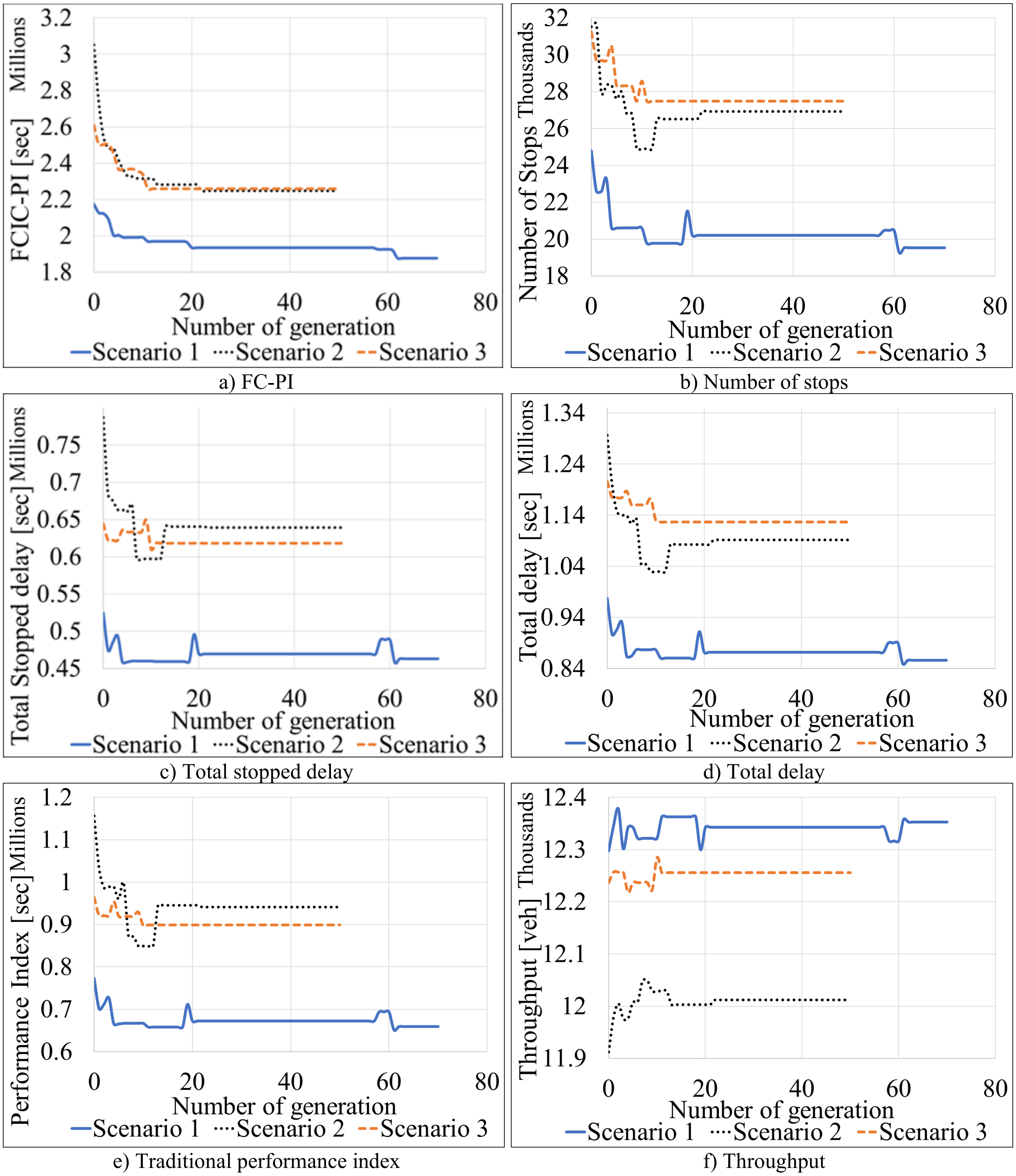

Figure 5.6 Performance Measure (PM) Charts – PMs through Optimization.

Two clear observations can be made from Figure 5.6a). First, the FC-PI value at the start of the optimization (number of generations = zero) is significantly different for the three scenarios. Second, scenarios 2 and 3 had relatively similar convergence patterns, whereas scenario 1 resulted in a quite different pattern. Both of these two observations can be attributed to the high stop penalty values for the heavy vehicles in scenarios 2 and 3. It is worth noting that *K*-factor for heavy vehicles was ~5 times higher than the *K*-factor for the light-duty vehicles. It appears that the presence of heavy vehicles with their high values of *K*-factor can play a significant role in the minimization of the FC-PI.

The rest of the charts in Figure 5.6 show how various performance measures change during various generations of the optimization processes. As expected, the FC-PI was continually reduced (not necessarily in each generation, but whenever a better solution was found) as the optimizations progressed. However, improving the FC-PI did not necessarily constantly improve some of the other performance measures. For example, the conventional Performance Index, delays, and stops (shown in Figure 5.6) increased for some generations, while the FC-PI was decreased.

These inconsistencies in the behavior of various performance measures can likely be explained with a notion that stops with a high value of the stop penalty (*K*) played a significant role in the optimization process. Thus, while the PI considered each stop to be worth the same the FC-PI would take in consideration more those stops whose *K* value was higher. It is also interesting to mention that some optimizations ended up with higher throughputs than those achieved with the initial signal timings, as shown in Figure 5.6f). This means that the final solution was able to process more vehicles (which also means more fuel consumed), and it certainly did not keep significant number of vehicles outside of the network.

One of the most interesting ways to interpret the results is to observe a Pareto chart (shown in Figure 5.7), illustrating delays and stops as a pair of potentially conflicting performance measures during the optimization. The dashed lines represent the path of the optimal solutions during the optimization process. Such a line starts with a suboptimal combination of stops and delays and keeps moving towards the lower-left corner of the chart, where both stops and delays are minimal. The dashed line usually ends at one of the points on the red line (Pareto Front), which connects all of the stops-delays combinations where one cannot further improve one performance measure (e.g., stops) without worsening the other (e.g., delay). The fact that the final solution in Figure 5.7 does not fall on the Pareto Front (red line) is also indication that the FC-PI, as an objective function, takes 'something else' in consideration and not only delays and stops; that 'something else' is fuel consumption footprint of various stops (e.g., of those experienced by heavy vehicles).

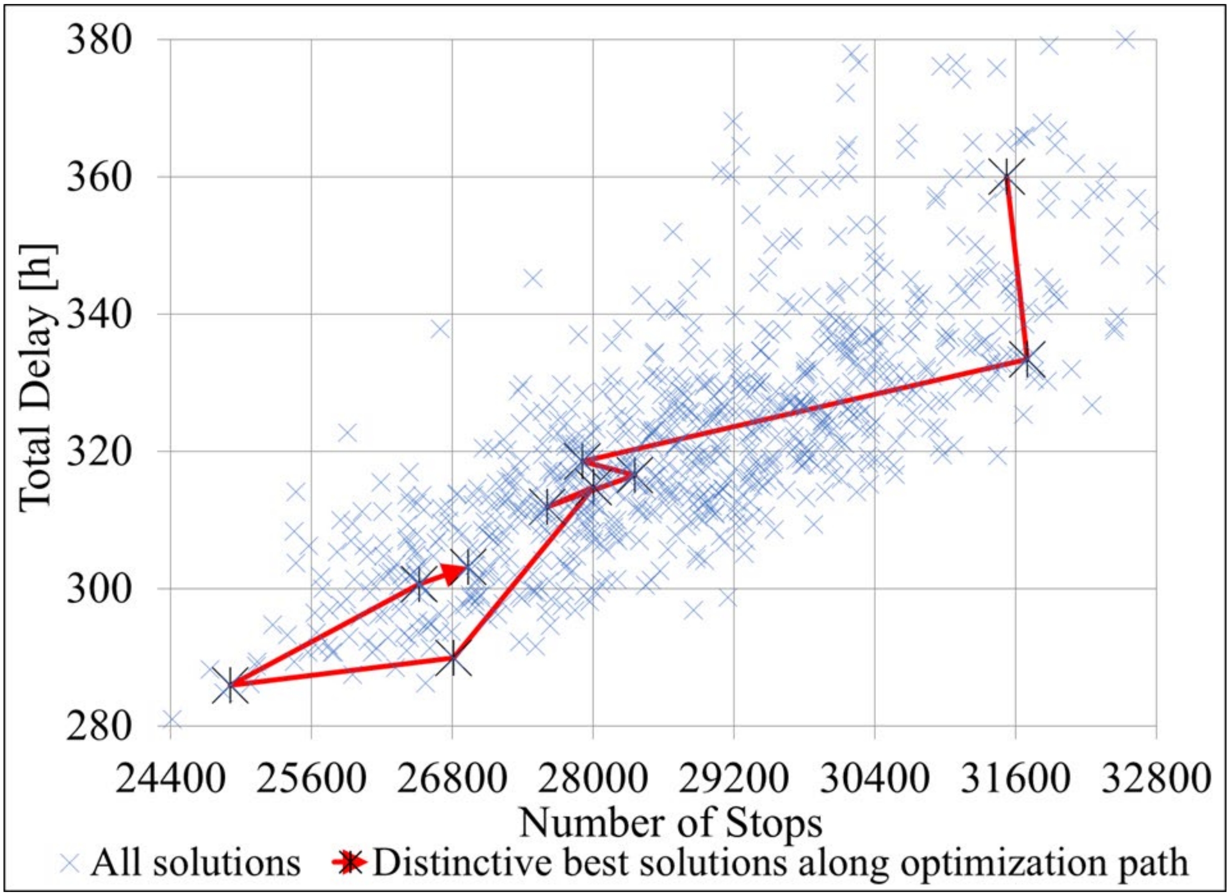

Figure 5.7 Pareto Chart – Trade-off between delay and stops for Scenario 2.

When it comes to the changes in signal timings which are being made as the results of the optimization processes, it is clear from Figure 5.8 that all of the three optimizations scenarios led to higher cycle lengths. More specifically, scenarios 1, 2, and 3 show that the cycle length should be increased from 110 seconds to 128, 119, and 117 seconds, respectively. All charts in Figure 5.8 show two values (encircled in red and green), representing cycle lengths before and after the optimization. The value encircled with green color is for the intersection of Washington Street and IL-131 where the cycle length is 125 seconds. This cycle length remains constant as IL-131 signal is not included in the optimization because it is not coordinated with the rest of the signals. The point encircled in red represents a value for all other coordinated signals. Other points in Figure 5.8 represents the other signal timings parameters (offsets, splits) whose changes cannot be interpreted so easily.

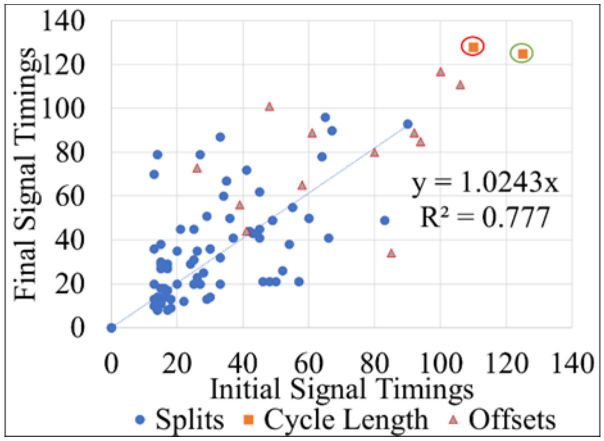

a) Scenario 1

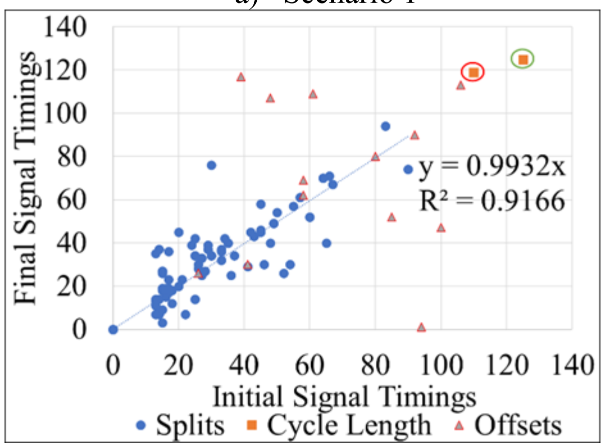

b) Scenario 2

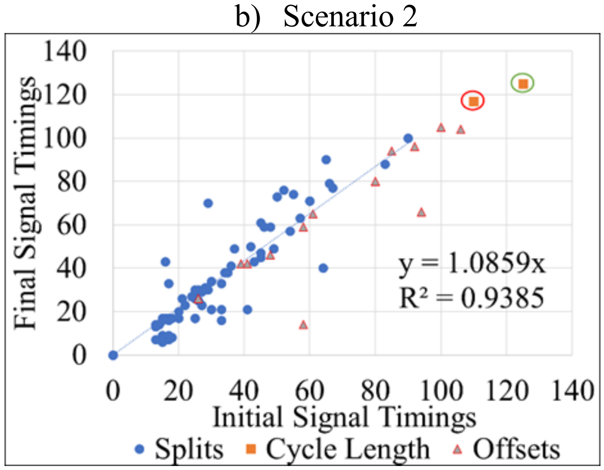

c) Scenario 3

Figure 5.8 Initial vs. final signal timing parameters.

Once the optimizations were completed, the base case and the best model of each tested scenario were used to conduct 50 random-seeded Vissim runs. This step was needed to consider variability in the stochastic nature of traffic in Vissim. Table 5.4 summarizes the results of 50 simulation runs. While the mobility measures (e.g., delay and number of stops) in Table 5.4 were obtained directly from Vissim, the fuel consumption and emissions were estimated by using the CMEM model based on individual vehicular trajectories.

It is expected that optimizing traffic signal timings by minimizing the FC-PI should result in lower fuel consumption and emissions with improved, or similar, mobility performance measures, too. However, the FC-PI consists of both stopped delay and number of stops with their weightings (based on the *K*-factors); hence, there might be trade-offs in the optimizations between delay and fuel consumption and emissions savings.

The improvements in FC-PI gained for the three optimized scenarios are 13.68%, 26.28%, and 13.42% for scenarios 1, 2, and 3, respectively. However, these 14-26% improvements in FC-PI do not necessarily translate to a 14-26% reduction in estimated fuel consumption, when such fuel consumptions are calculated by processing individual vehicular trajectories in CMEM. When processing second-by-second trajectories from Vissim in CMEM, an average improvement of 2.7%, 5.7%, and 3.4% was observed in the estimated fuel consumption for scenarios 1, 2, and 3, respectively. While these improvements are still significantly high, it is apparent that the improvements observed on the FC-PI side are different from the savings in fuel consumption.

Table 5.4 Mobility, fuel consumption, and emissions results from 50-run tests.

Performance measure	Statistics	Scenario 1			Scenario 2			Scenario 3		
		Base case	Optimized	Mean Difference %	Base case	Optimized	Mean Difference %	Base case	Optimized	Mean Difference %
Total Delay (hr)	Mean	270.4	315.6	16.72	307.7	274.3	-10.85	358	313.5	-12.43
	SD	15.8	10.9		17.1	15.3		17.6	17.4	
Stops	Mean	24618	28488	15.72	27011	25821	-4.41	31858	28124	-11.72
	SD	2402	1561		2358	2390		1778	2377	
Stopped Total Delay (hr)	Mean	149.9	188	26.17	166.5	148.9	-10.57	218.1	167.4	-23.25
	SD	10.6	8.3		11.6	10.2		13.5	11.7	
Throughput (veh)	Mean	12197	11919	-2.28	12187	12185	0	11850	12163	2.64
	SD	45	59		60	55		59	61	
Latent Demand (veh)	Mean	14.7	16.3	10.88	89.5	88	-1.68	15.2	17.2	13.15
	SD	21.7	23.3		39.5	34.9		20.1	21.3	
Fuel consumption (g/mile)	Mean	105.24	102.44	-2.66	155.19	146.76	-5.69	142.88	138.17	-3.3
	SD	1.15	1.132		2.58	1.921		2.68	2.424	
HC (g/mile)	Mean	0.83	0.82	-1.2	0.79	0.77	-2.53	0.8	0.79	-1.25
	SD	0.005	0.005		0.006	0.005		0.004	0.004	
CO (g/mile)	Mean	6.64	6.57	-1.05	6.72	6.62	-1.49	6.51	6.43	-1.23
	SD	0.068	0.063		0.077	0.066		0.072	0.064	
NOx (g/mile)	Mean	0.64	0.63	-1.56	1.76	1.68	-4.54	1.45	1.37	-5.52
	SD	0.007	0.007		0.05	0.041		0.051	0.048	
CO_2 (g/mile)	Mean	320.67	312.23	-2.63	482.45	456.57	-5.36	442.21	428.25	-3.16
	SD	3.621	3.546		8.33	6.211		8.596	7.771	

SD = Standard deviation. Gray shading indicates 95% significant change. Negative mean difference = improvement in the performance. Positive mean difference = degradation in the performance.

A set of one-tailed Student t-tests, with a confidence level of 99%, was performed to document the statistical significance of the change in performance measures resulting from the optimized signal plans (compared with the base case signal plans). Results in Table 5.4 show that improvements in fuel consumption and emissions were all statistically significant with (p-value < 0.05). The t-tests on the mobility measures showed that most changes were insignificant statistically (p-value > 0.05). Thus, one can conclude that the optimal signal plans developed in this study achieved an excellent balancing between sustainability and mobility measures.

The following bullet points provide some potential causes for the differences in the improvements between FC-PI and fuel consumption:

- Benefits achieved in FC-PI do not linearly translate into reduced fuel consumption.

In the overall game of who to stop more – side-street or main-street vehicles, it seems that stopping slower side-street vehicles (side-street speeds are usually lower) may reduce fuel consumption (because accelerating back to higher speed costs more in terms of fuel consumption). However, that also means that letting faster vehicles drive (without stopping) will consume more fuel than if slower vehicles are let go. This simply comes from the fact that faster vehicles (almost always) consume more fuel than slower vehicles. This is especially apparent when fuel consumed is not expressed as a solo performance measure but when it is normalized per mile of travel. So, in this balancing process, when deciding to whom to give more green time (main-street (faster) vehicles or side-street (slower) vehicles), one should not account only for the costs of stopping the traffic but also for the costs of letting the traffic go.

Figure 5.9 and Figure 5.9 shed more light on this phenomenon, which may not be intuitively comprehended (unless related numbers and charts are presented). For example, Figure 5.9a), Figure 5.9b), and Figure 5.9c) show stop profiles of stopped and non-stopped vehicles at three various speeds (20 mph, 45 mph, and 65 mph) when traversing the same distance (distances are not same for various cruising speeds, but they are the same for stopped and non-stopped vehicles of the same cruising speed). Figure 5.9d), Figure 5.9e), and Figure 5.9f) present the fuel consumption profile for each stop profile shown in Figure 5.9a), Figure 5.9b), and Figure 5.9c), respectively. Finally, Figure 5.10 shows the fuel consumption for all of the stop profiles in Figure 5.9, in addition to the stop penalty of the stopped vehicle at each cruising speed.

By comparing stopped vehicles (at various cruising speeds), one can observe that stopping a vehicle while driving at 20-mph costs ~26.5 grams of fuel compared to ~4.3 grams of fuel if the same vehicle is not stopped. This means that the fuel consumption of a non-stopped vehicle (at this speed) is approximately 16% of the fuel consumption of a stopped vehicle. Looking at the corresponding fuel consumption values for the 45-mph trajectories, one can find that the fuel consumption of a non-stopped vehicle constitutes 27% of the fuel consumption of a stopped vehicle. This means that the total fuel consumption is higher if a 45-mph vehicle is stopped than if a 20-mph vehicle is stopped, but it also means that if the 45-mph vehicle is let go, it will consume more fuel than if the 20-mph vehicle is let go. That essentially proves that not all of the benefits from non-stopping faster vehicles (which is logical to do) could be translated into equivalent fuel consumption savings. The same trend is even further accentuated if one considers vehicles traveling at higher cruising speeds (e.g., at 65-mph, a non-stopped vehicle consumes a whole 32% of a stopped vehicle).

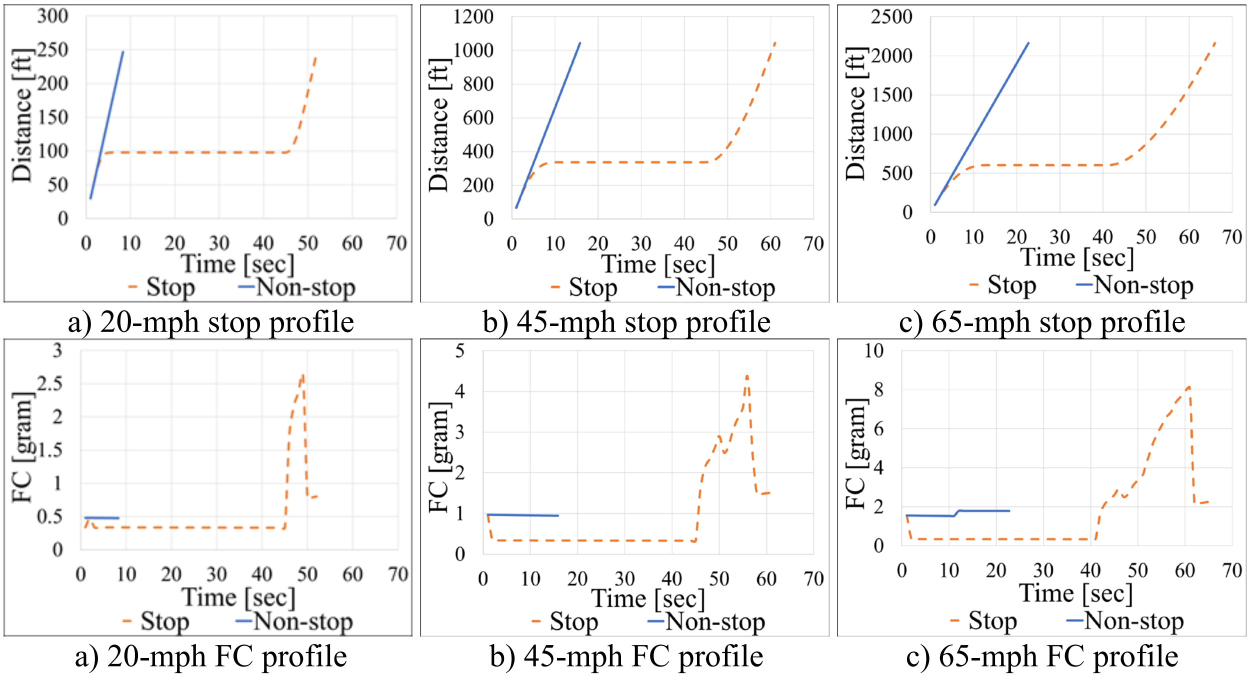

Figure 5.9 Stop and fuel consumption (FC) profiles of stopped vs non-stopped vehicular trajectories.

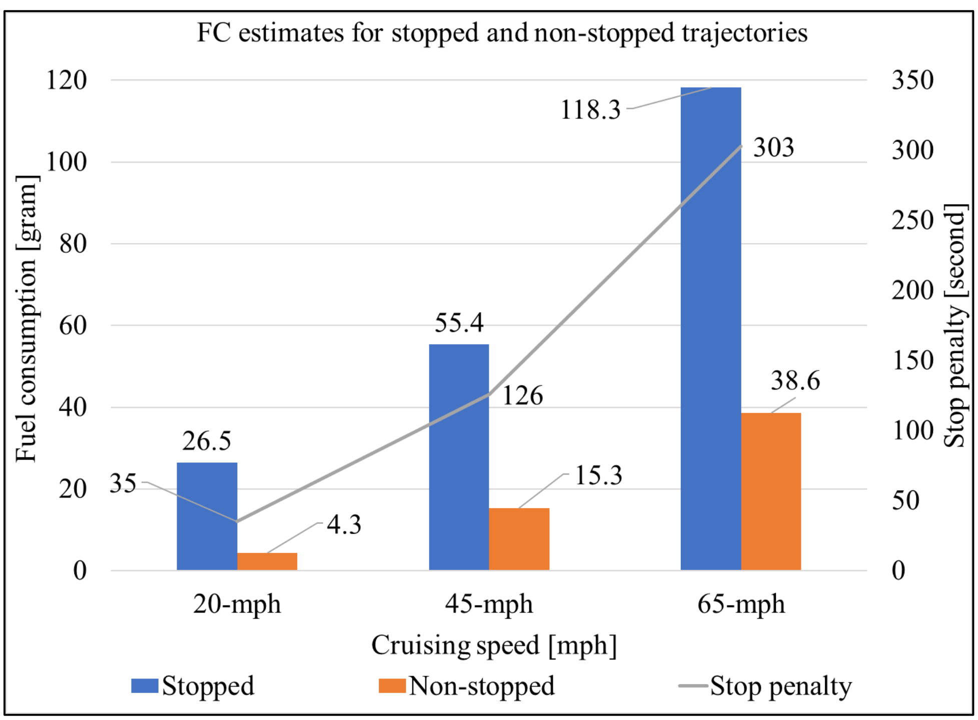

Figure 5.10 Fuel consumption of stopped vs non-stopped vehicular trajectories.

- Traffic is much heavier on the Washington St. than on the side streets.

The FC-PI is an excellent performance measure to find a proper balance between stops and delays at various traffic movements with different driving conditions (e.g., cruising speeds) and comparable traffic volumes. So, for example, in a case where the major and minor streets have speed limits of 45-mph and 30-mph, respectively, minimizing the FC-PI will mean reducing more stops on the 45-mph street because it is more beneficial in terms of the fuel consumption.

However, having much more traffic on the major street (when compared to the minor street) means that by providing more green time to the main street we will reduce many more stops (than if more green is given to the side-street), just because the major street carries much heavier traffic. So, from that perspective, the significance of higher weights given to the main-street stops is secluded by the fact that the main streets carry much more traffic (and get such weights 'naturally').

- Special factors that could theoretically have a significant role are insignificant in practice.

As mentioned in the introduction, recent research demonstrated that various factors have a significant impact on fuel consumption and the *K*-factor. Such impact was apparent in the optimization results of Scenarios 2 and 3, which had a large percentage of heavy vehicles compared to the 1st Scenario. However, other operating conditions at Washington St. are not 'extreme' enough to show the benefits of using the FC-PI, which is developed to balance variations in those conditions. For example, road gradient was shown to have a high impact on fuel consumption, but there are few places in Washington street with very moderate grades, making the impact of grades insignificant. An identical driving behavior was assumed for all of the roadways (for all of the movements) because one cannot easily observe the difference in driving behavior at the tested corridor (at least not with conventional data). Finally, all movements were assumed to have the same vehicle types because there were not significant differences in vehicle fleets at various intersection movements.

- Washington Street already has decent signal timings.

Analysis of arrivals on green percentages shows that the Washington Street already has decent signal timings, and it seems that the entire system is well-maintained (this was also confirmed by the LC DOT staff). It should be also noted that the signal timings on Washington Street were optimized relatively recently (in 2016) and that the optimization of the FC-PI in this study still provided a 2.7% improvement based on the current conditions.

5.6 Conclusions and Future Research

This Chapter aimed to present a new approach to integrate traffic simulation, fuel consumption surrogate measure, and signal timing optimization tools to optimize signal timings under various operating conditions. The proposed approach seeks to achieve a minimal amount of fuel consumption while improving or maintaining the efficiency of traffic signals. The Chapter also presented a case study of a network consisting of 13 signalized intersections in Chicago, Illinois, as the test site. For this corridor, three optimization scenarios were completed to determine the fuel consumption saving obtained using the surrogate objective function under normal conditions and a high percentage of heavy vehicles, for certain intersection movements. Based on the results and observed findings, the following conclusions are reached:

The FC-PI seems to be a reliable surrogate objective function for fuel consumption when used for optimization of the traffic signal timings. This novel PI combines conventional traffic performance measures (stopped delay and number of stops) with a set of factors that represent the fuel consumption weights for each stop.

Using the FC-PI saves a significant computation time that other approaches must endure because it does not require fuel consumption estimates from post-processing vehicular trajectories when optimizing signal timings. Hence, such the FC-PI can be practical for regular optimizations of signal timings.

The reduction achieved in FC-PI throughout the optimization does not linearly translate into reduced fuel consumption. There could be several reasons for that, as discussed in the Chapter. Despite of this non-linearity, the FC-PI provided a moderate improvement in fuel consumption.

The surrogate objective function used in the optimization resulted in a minimum saving of 2.7% in fuel consumption with a little degradation in the mobility performance measures compared to the base case signal timings. Such savings were significantly increased to 5.7% (accompanied with significant improvements in the mobility measures) when the impact of a high percentage of heavy vehicles in the fleet was considered in the optimization.

Future research should investigate how well FC-PI captures the impact of other factors (e.g., road gradients and driving behaviors). Also, the savings of the emissions showed that various air pollutants, except CO_2, are not linearly correlated with fuel consumption. Thus, further research is needed to investigate the differences between the signal optimizations when stop penalties are based on the fuel consumption estimates and those derived based on various emission' estimates.

More research is also required to apply the proposed methodology on various networks under multiple factors impacting fuel consumption and emissions. Finally, this Chapter utilized stop penalties computed from simulated vehicles; such penalties should be validated based on fuel consumption measurements from the field.

6.0 Impact of Deceleration-Acceleration Events on Excess Fuel Consumption at Signalized Intersections

6.1 Introduction

The increasing traffic demand and limits of existing transportation network infrastructure have significantly increased the use of fossil fuels in recent years, which have resulted in consequential harmful impacts to human health and contributions to climate change (McMichael et al, 1996). Intersections along urban arterials contribute significantly to increased fuel consumption because they entail long idling times and many deceleration-acceleration events (e.g., stops), which are the primary cause of excess fuel consumption and emissions at intersections (Rakha and Ding, 2003).

Traffic signals are one of the most common ways used to spatially and temporally allocate conflicting traffic streams at intersections. Thus, several studies have evaluated the performance of traffic signals from an environmental perspective (e.g., impact on fuel consumption) (Robertson et al., 1980; Stevanovic et al., 2009; Park et al, 2009; Kwak et al, 2012). Further, many of these studies proved that optimizing signal timings is a cost-effective way to reduce excess fuel consumption and emissions at signalized intersections, which is fundamentally done by reducing stop-and-go events and idling times.

Most previous studies (e.g., Robertson 1980; Stevanovic et al., 2009) focused on reducing the number of complete (full) stops, where a vehicle decelerates from a cruising speed to zero and then accelerates back to its original cruising speed. However, high traffic demands cause near-saturated and oversaturated conditions, which result in deceleration-acceleration events (aka partial stops) happening before (or after) a complete stop; or even more than one complete stop could be made by the same vehicle while traveling through the intersection. Such Deceleration-Acceleration Events (referred to as DAEs hereafter) can contribute significantly to the excess fuel consumption. For example, decelerating from a cruising speed to a lower speed (without necessarily coming to a complete stop), and then accelerating back to the original speed is also an event that contributes to increased fuel consumption due to traffic signal operations. In fact, a complete stop is just an extreme case of a DAE, when a vehicle decelerates to zero speed before accelerating to its original cruising speed.

The depth and practicality of previous signal timing optimization studies are usually impacted by the objective function (performance measures) utilized in the optimization process (Alshayeb et al., 2021b). Nowadays, new signal performance measures have emerged (with use of modern detection technologies), which are based on high-resolution (e.g., 10 Hz) data. One such, recently developed, performance measure is the Environmental Performance Index (Env-PI) (Alshayeb et al., 2021b). The Env-PI can be feasibly implemented in signal timing optimizations because it has been derived similarly to an older Performance Index (PI), one of the most widely accepted objective functions in signal optimization practice (Roberston, 1969). The Env-PI is a linear combination of delays and stops with a K-factor (aka stop penalty) that assigns a weight for each stop as an equivalent delay, from the perspective of either fuel consumption or vehicular emissions. Thus, the Env-PI serves as a surrogate measure for fuel consumption (or other types of emissions) and can be used to find a balance between delay and sustainability metrics (e.g., fuel consumption). The critical key of the Env-PI is the stop penalty, which is a function of various operating conditions (e.g., cruising speed, grade, vehicle type, driver's aggressiveness) that impact the fuel consumption and emissions estimates during a stop-event.

Although a few studies already estimated impact of the stop penalties (Alshayeb et al., 2021a; 2021b; 2021c), such estimations included only complete stops. Thus, they have resulted in Env-PIs which may not be accurate in congested conditions, because the methodology does not account for all other DAEs (e.g., partial stops). Such an inaccuracy could be further increased if all DAEs are treated as complete stops, with corresponding full-stop FC penalties.

Thus, the objective of this Chapter is to address such a problem by proposing a methodology to integrate the impact of DAEs and Multiple consecutive DAEs (MDAEs) on fuel consumption in the estimation of the Env-PI. Since this Chapter uses only fuel consumption estimates, the Env-PI will be referred to as Fuel Consumption-PI (FC-PI) hereafter.

6.2 Methodology

To illustrate the impact of DAEs on fuel consumption, Figures 1a) and 1b) present simulated trajectories of a DAE45-0 (DAE from a cruising speed of 45-mph to zero and then back to 45-mph), and a DAE45-15 (DAE from a cruising speed of 45-mph to 15-mph and then back to 45-mph), respectively. It can be seen from Figure 1c) that in the case of the DAE45-0, the vehicle decelerated from 45-mph to zero and waited for some time before accelerating back to 45-mph; whereas for the DAE45-15 the vehicle decelerated to 15-mph and instantly started accelerating to 45-mph, as shown in Figure 1d). Such changes in deceleration and acceleration resulted in different deceleration-acceleration profiles, as shown in Figures 1e) and 1f), which further required different amounts of fuel during each event, as shown in Figures 1g) and 1h). Considering that the fuel consumption shown in Figures 1g) and 1h) is given in grams/second, the total fuel consumed (in grams) during a DAE is represented by the area under the curve. Using that concept, the total fuel consumption for the DAE45-0 is ~52 grams, whereas it is ~43 grams for the DAE45-15. Thus, the difference in fuel consumption between the DAE45-0 and the DAE45-15 is ~9 grams. According to such difference, one can conclude that all of DAEs contribute to some excess fuel consumption, but the magnitude of that contribution is dictated by the difference of the initial (before decelerating) and final (after accelerating) cruising speeds during a DAE (in addition to the vehicle type and other factors). It is worth noting that the comparison above did not include the idling fuel consumption for the DAE45-0 to ensure consistency.

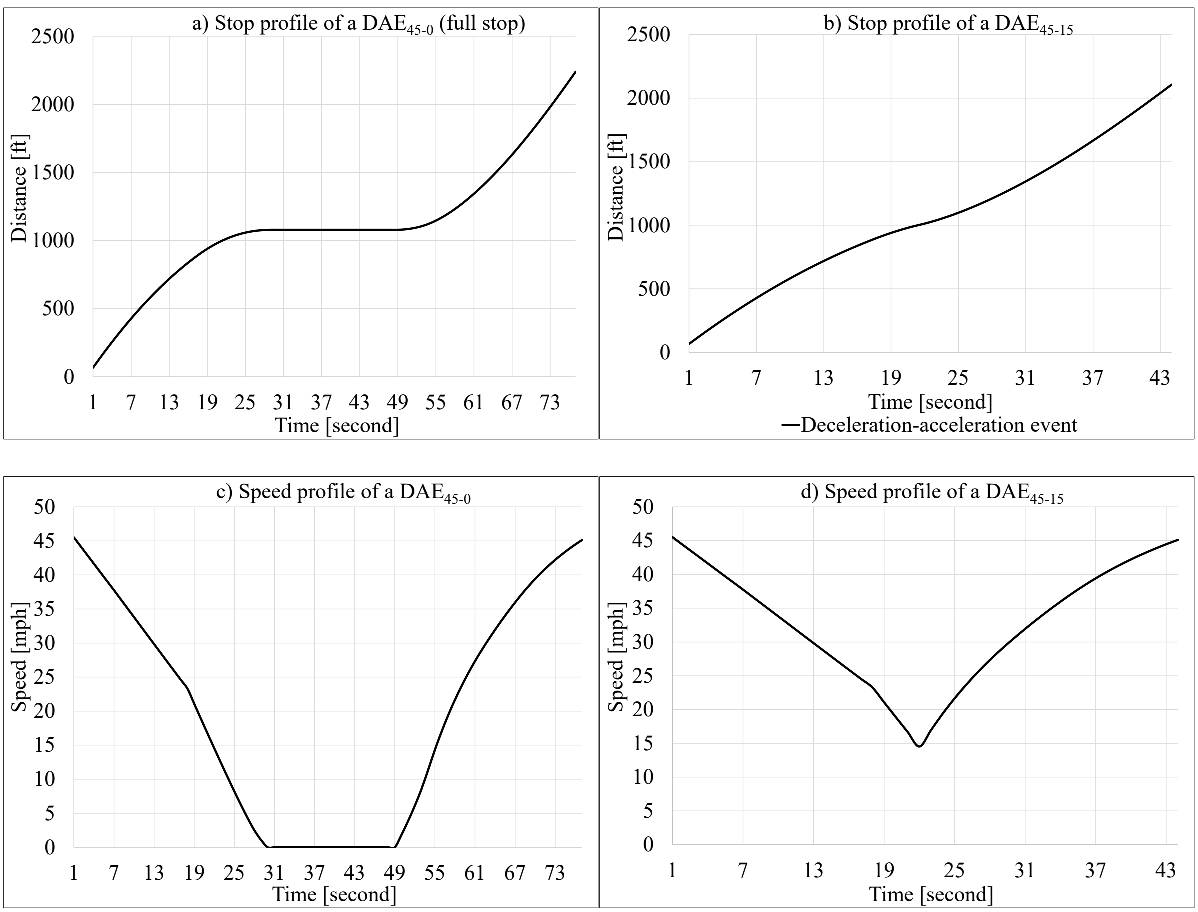

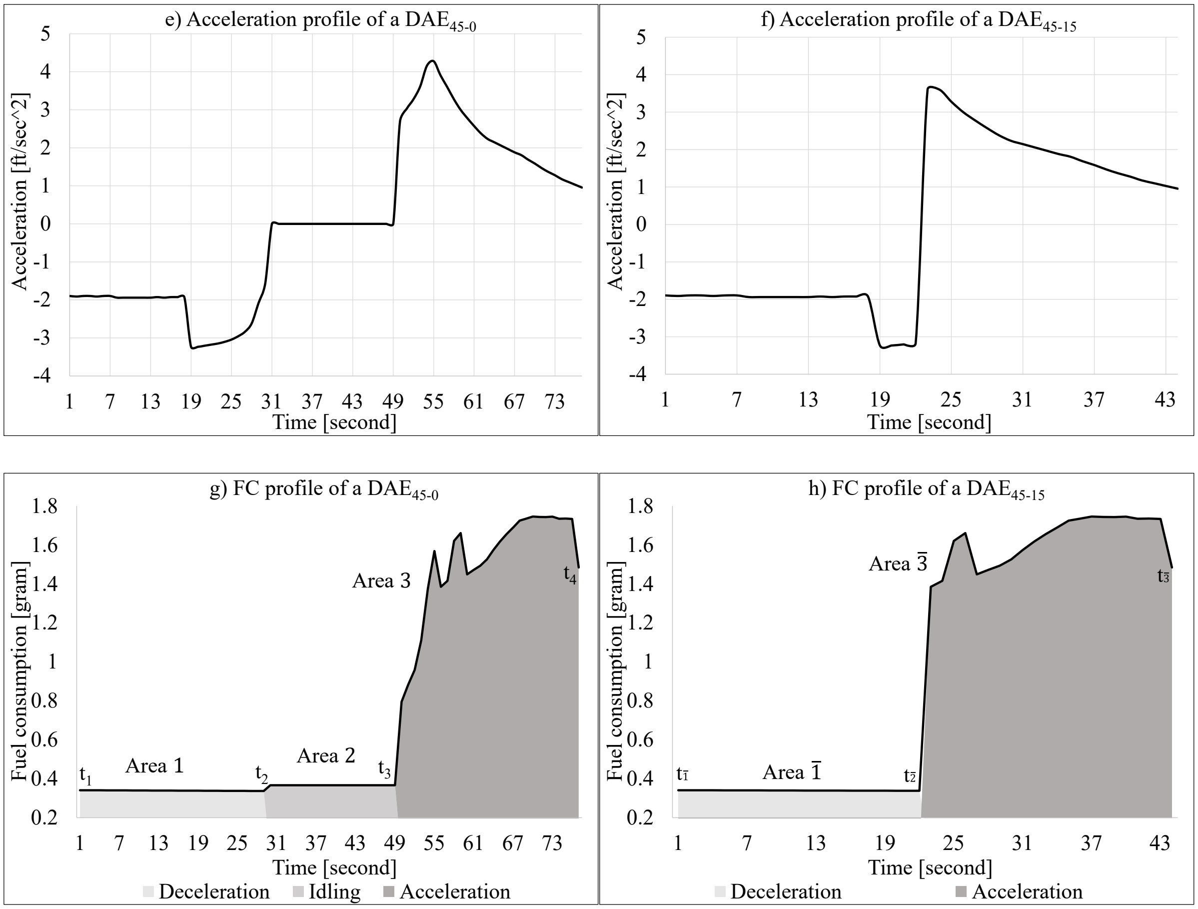

Figure 6.1 The dynamic and kinematic differences a $DAE_{45\text{-}0}$ (complete stop) vs $DAE_{45\text{-}15}$ (partial stop).

The FC-PI objective function was derived by Stevanovic et al. 2021 as:

$$FC - PI = \sum_{i=1}^{n} D_i + K_i \cdot S_i = \sum_{i=1}^{n} D_i + \left(\frac{FC_D + FC_A}{\frac{FC_I}{T_I}} \right)_i \cdot S_i \tag{6.1}$$

Where:

D_i – Stopped delay [seconds] at movement i.

K_i – Stop penalty [seconds] at movement i.

S_i – Number of complete stops ($DAE_{CS\text{-}0}$) at movement i.

DAE$_{CS-0}$ – Deceleration-acceleration event from a Cruising Speed *CS* to zero and then back to *CS*.

FC_D- Total fuel consumption during decelerating for DAE$_{CS-0}$ [grams].

FC_A- Total fuel consumption during accelerating for DAE$_{CS-0}$ [grams].

FC_I- Total fuel consumption during idling for DAE$_{CS-0}$ [grams].

T_I- Total duration of idling for DAE$_{CS-0}$ [seconds].

N – Total number of movements (or intersections) included in the optimization.

It is noticeable from Equation 6.1 that only complete stops are included in the computation the FC-PI. Such a practice leads may lead to inaccurate estimation of the excess fuel consumption in the congested traffic conditions. Specifically, it leads to underestimated FC-PI because of excluding DAEs that do not represent complete stops. Therefore, this Chapter proposes that such DAEs are accounted for through a DAE penalty ($K_{DAE_{CS-j}}$ – event penalty for a DAE from a cruising speed (*CS*) to speed *j*.). Such a DAE penalty is computed as a percentage of the K_i of a complete stop, which is characterized in this study as $K_{DAE_{CS-0}}$ – event (stop) penalty for a DAE from a cruising speed (*CS*) to speed 0. This percentage is a ratio of the amount of fuel consumed during the deceleration and acceleration modes of a $K_{DAE_{CS-j}}$ and the one consumed by $K_{DAE_{CS-0}}$ during the same modes (as shown by Equation 6.2). By utilizing integration to estimate the areas shown in Figures 1g) and 1h), the $K_{DAE_{CS-j}}$ can be expressed as:

$$K_{DAE_{CS-j}} = \frac{\int_{t_{\bar{1}}}^{t_{\bar{2}}} F_r(t) \cdot dt + \int_{t_{\bar{2}}}^{t_{\bar{3}}} F_r(t) \cdot dt}{\int_{t_1}^{t_2} F_r(t) \cdot dt + \int_{t_3}^{t_4} F_r(t) \cdot dt} \times K_{DAE_{CS-0}} \qquad (6.2)$$

Where:

F_r – Fuel rate [gram/second].

$t_{\bar{1}}$ – Start deceleration time for DAE_{CS-j} [second].

$t_{\bar{2}}$ – End deceleration time and start acceleration time for DAE_{CS-j} [second].

$t_{\bar{3}}$ – End acceleration time for DAE_{CS-j} [second].

t_1 – Start deceleration time for DAE_{CS-0} [second].

t_2 – End deceleration time for DAE_{CS-0} [second].

t_3 – Start acceleration time for DAE_{CS-0} [second].

t_4 – End acceleration time for DAE_{CS-0} [second].

In this study the *Fr* was estimated using the Comprehensive Modal Emission Model (CMEM), in which case the areas under the curve can be approximated by using an appropriate discretization, where *FC* is fuel consumption:

$$\begin{aligned} K_{DAE_{CS-j}} &= \frac{\sum_{t=t_{\bar{1}}}^{t_{\bar{2}}} FC + \sum_{t=t_{\bar{2}}}^{t_{\bar{3}}} FC}{\sum_{t=t_1}^{t_2} FC + \sum_{t=t_3}^{t_4} FC} \times K_{DAE_{CS-0}} \\ &= \frac{\sum_{t=t_{\bar{1}}}^{t_{\bar{3}}} FC}{\sum_{t=t_1}^{t_2} FC + \sum_{t=t_3}^{t_4} FC} \times K_{DAE_{CS-0}} \end{aligned} \tag{6.3}$$

It is crucial to note that there could exist multiple DAEs depending on the cruising speed and the reduction in speed caused by traffic signal and other vehicles. considering that the adjusted FC-PI ($\overline{FC - PI_i}$) for movement *i* can be expressed as shown in Equation 6.4.

$$\overline{FC - PI_i} = D_i + \left(\sum_{j=0}^{N} K_{DAE_{CS-j}} \cdot E_{DAE_{CS-j}} \right)_i \tag{6.4}$$

Where:

D_i – Stopped delay at movement *i* [second].

N – Total number of DAE levels.

$E_{DAE_{CS-j}}$ – Number of DAEs from a cruising speed (*CS*) to speed *j*.

Substituting Equation 6.3 in Equation 6.4 results in the following equation:

$$\overline{FC-PI}_i = D_i + \left(\sum_{j=0}^{N} \left(\frac{\sum_{t=t_{\bar{1}}}^{t_{\bar{3}}} FC}{\sum_{t=t_1}^{t_2} FC + \sum_{t=t_3}^{t_4} FC} \times K_{DAE_{CS-0}} \right)_j \cdot E_{DAE_{CS-j}} \right)_i \tag{6.5}$$

Finally, the adjusted $\overline{FC-PI}$ for the whole network can be represented as shown in Equation 6.6, where *n* is the total number of movements (or intersections) included in the optimization.

$$\overline{FC-PI} = \sum_{i=1}^{n} D_i + \left(\sum_{j=0}^{N} \left(\frac{\sum_{t=t_{\bar{1}}}^{t_{\bar{3}}} FC}{\sum_{t=t_1}^{t_2} FC + \sum_{t=t_3}^{t_4} FC} \times K_{DAE_{CS-0}} \right)_j \cdot E_{DAE_{CS-j}} \right)_i \tag{6.6}$$

The figure below shows the stop, speed, acceleration, and fuel consumption profiles of a vehicle passing through a signalized intersection under oversaturated conditions. It can be observed from Figure 2b) that the vehicle experienced Multiple DAEs (MDAEs), some of which were complete stops, before accelerating back to its original cruising speed. In such situations, the concept shown in Equations 6.2 and 6.3 can be also applied to compute the MDAE penalty (K_{MDAE}), as shown in Equation 6.7. The K_{MDAE} can be then treated as one of the events *j* in the Equation 6.6.

$$K_{\text{MDAE}} = \frac{FC_D + FC_A}{\sum_{t=t_1}^{t_2} FC + \sum_{t=t_3}^{t_4} FC} \times K_{DAE_{CS-0}} \tag{6.7}$$

Where:

FC_D – Total fuel consumption for all DAEs in a MDAE during deceleration.

FC_D – Total fuel consumption for all DAEs in a MDAE during acceleration.

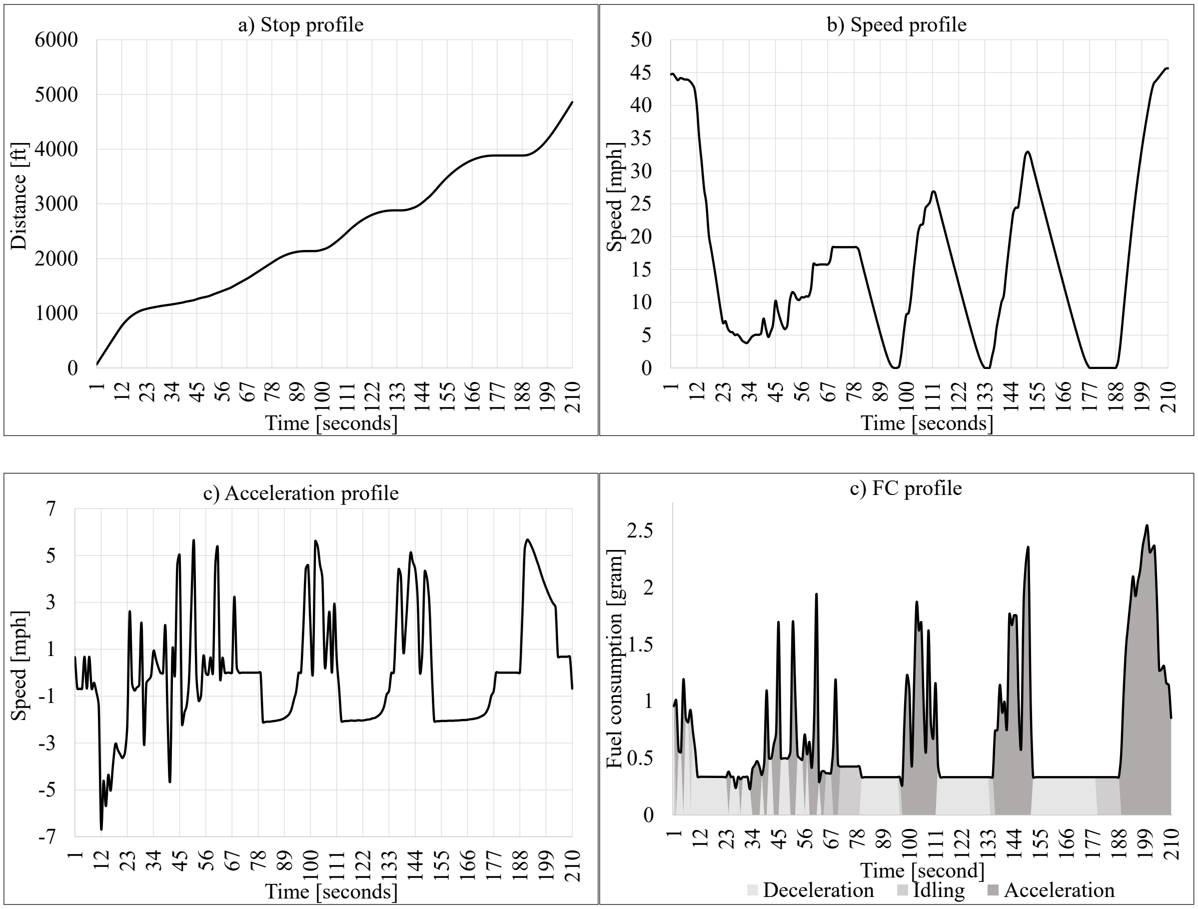

Figure 6.2 The dynamic and kinematic of a sequence of DAEs on oversaturated signalized intersection approach.

7.0 Summary, Conclusions, and Future Directions

The overarching theme of this research is to develop a framework for traffic signal timing optimization to reduce sustainability metrics. Specifically, this research developed a family of environmental performance measures to be used in signal timing optimization to minimize fuel consumption and vehicular emissions. The first Chapter defined the problem statement, goal, and objectives of the research. Summaries and conclusions of the rest of the chapters are presented below.

The second Chapter argued that the stop penalty (*K*-factor), used to balance between delay and number of stops in terms of fuel-consumption equivalency, as used in one of the most popular objective functions in the signal retiming practice, is a function of multiple operational conditions and not a constant value as mistakenly recognized by our current signal retiming practice. Obviously, the *K*-factor dependency on several operational conditions suggests that the *K*-factor will most likely be different for various approaches of each signalized intersection. That is because each approach at a signalized intersection has unique operational conditions. Thus, having a better understanding of the factors that cause the major observed variations in the *K* value will lead to better signal optimization results. The following concluding remarks have been reached:

- Operational conditions during stop-and-go events at traffic signals significantly impact excess fuel consumption caused by such stops. The findings have shown that all of the six investigated factors significantly impact fuel consumption, which results in different *K* values.
- Stop penalty for various LDVs ranges between 118-second to 132-second except for LDV with GVW>8500lbs, which results in a stop penalty twice as high as those

of other LDVs. These results may indicate that the fuel consumption is more sensitive to the vehicle's mass than the fuel/engine type. Such a conclusion may also be reached by observing the stop penalties of HDDVs, which resulted in ~9-15 times higher values than the average stop penalty from the LDVs.

- An increase of 1% of HDDVs in the fleet distribution adds extra 11 seconds of equivalent delay from the fuel consumption perspective. Similarly, a 1% uphill gradient adds up to ~11 seconds of fuel consumption-equivalent delay if a vehicle is stopped on uphill terrain.
- When accelerating from a stop-line at a signalized intersection, an aggressive driving behavior can increase the fuel consumption of a stopping vehicle by up to 42-seconds of equivalent waiting-idling time, when compared to a "normal" acceleration behavior.
- The increase of fuel consumption and the *K* with an increase of cruising speed seems to follow an exponential trend. For the most common speed limits on urban arterials (35-45 mph), a stop-and-go event from-and-to a cruising speed of 45-mph (common for major arterials) costs 46 seconds more (of equivalent fuel consumption during idling) than a stop for a vehicle traveling at a cruising speed of 30-mph (e.g., common for side-streets).
- Wind can significantly increase or decrease the stop penalty of HDDV. The findings show that the stop penalty for trucks facing significant headwinds could be increased by up to 970 seconds compared to a no-wind conditions. Thus, this should be seriously considered for signalized intersections of the roadways with frequent and heavy winds and a high percentage of HDDVs.

Chapter 3 derived an emission type-based environmental objective function (called Env-PI) to minimize particular emission criteria. The Chapter also explained how the Env-PI is different for various emissions based on the emissions-based stop penalty, even under identical operating conditions. Furthermore, the Chapter 3 reveals the relationship between various operating conditions and the emissions-based stop penalty.

Emissions-based stop penalty data were generated using a set of full-factorial experiments and based on simulated traffic and emissions data. A real-world intersection has been modeled in Vissim to perform various experiments under different operating conditions. Vehicular trajectories from the field were used to develop acceleration–deceleration functions, which were utilized to represent various driving behaviors. The emissions model, CMEM, has been used to estimate the investigated emissions (HC, CO, NOx, and CO_2) and fuel consumption. A Vissim–Python–CMEM interface has been developed to speed up the experimental work and minimize errors.

The results reveal a significant relationship between the emissions-based stop penalty and the independent parameters, including the vehicle type, percentage of heavy vehicles, driver behavior, road gradient, cruising speed, and wind effect. Furthermore, the findings show that all the investigated independent parameters have a significant individual impact on the emissions-based stop penalty. The main parameters driving the variation in the stop penalty are the vehicle type and cruising speed, while the road gradient and driving behavior had a slightly lower impact.

Furthermore, the emissions-based stop penalty value differs for different emission criteria depending on their emitting rates during each stop's driving phase. Thus, Chapter 3 concluded that using the Env-PI with an accurate estimation of its stop penalty is vital to minimize emissions through optimizing traffic signals. This is especially true for urban communities suffering from specific polluting criteria, where such an Env-PI can be deployed to develop new signal retiming strategies or integrated into existing ones.

This Chapter paved the road for multiple future research directions which included, first, to incorporate other comprehensive safety and environmental measures (e.g., conflicts and noise level). Second, the variability of stop profiles' emissions, used to compute the emissions-based stop penalty, should be further researched by using variance estimation techniques. Finally, future research should focus on developing a health-risk index, based on optimal signal timings, to minimize specific emission type to help achieve sustainability of human environment.

Chapter 4 covered two major objectives, (i) to assess the impact of the major operating conditions (vehicle type, cruising speed, road gradient, idling fuel consumption rate, deceleration duration, and driving behavior) on the stop penalty (*K*-factor) using vehicular trajectories and fuel consumption estimates collected from the field, and (ii) to develop valid evolutionary computation models, namely multi-gene genetic programming (MGGP), to formulate the stop penalty as a function of various operating conditions.

An extensive real-world dataset from the field was used to develop predictive models for seven vehicular groups classified in this Chapter. The performance of the developed models was evaluated by using testing and validation datasets. The developed models achieved high accuracy for the training, testing, and validation datasets.

A parametric study was also carried out to investigate the impact of multiple factors on the stop penalty, and to ensure the robustness of the developed models. The parametric study revealed that the stop penalty is positively correlated with all of the investigated factors. Specifically, initial speed, grade while accelerating, and deceleration duration have linear relationships with the stop penalty, whereas the idling fuel consumption rates and accelerations have quadrinomial relationships. Lastly, the final speed seemed to impact the stop penalty exponentially. These findings suggest that, in general, the stop penalty is not a low constant value as widely thought, and currently, used in the traffic signal optimization community.

An implication of this Chapter is the possibility to compute the *K*-factor by using the models developed in this Chapter. It is recommended that traffic agencies implement fuel consumption-based stop penalties in their signal timing optimization practices. Such implementation can be as simple as changing the value of *K* when optimizing signals using Vistro, or by integrating the PI with correctly computed stop penalty as the objective function when optimizing signal timings utilizing various optimization techniques (e.g., genetic algorithm).

One limitation of the current research in this Chapter is that it does not analyze the impact of some other important factors affecting the stop penalty (e.g., pavement type and ambient temperature) due to their unavailability in the field dataset. Future research should address the impact of such factors. Another future study should also integrate a vehicle dynamics model to consider vehicle throttle and braking levels to assure more accurate fuel consumption and emissions estimates. This would be particularly important when connected and automated vehicles are considered.

Chapter 5 aimed to present a new approach to integrate traffic simulation, fuel consumption surrogate measure (FC-PI), and signal timing optimization tools to optimize signal timings under various operating conditions. The proposed approach seeks to achieve a minimal amount of fuel consumption while maintaining the efficiency of traffic signals. The Chapter also presented a case study of a corridor consisting of 13 signalized intersections in suburbs of Chicago, Illinois, as the test site. For this corridor, three optimization scenarios were completed to determine the fuel consumption savings obtained using the surrogate objective function (under normal conditions and a high percentage of heavy vehicles, for certain intersection movements). Based on the results and observed findings, the following conclusions were reached:

- The FC-PI seems to be a reliable surrogate objective function for fuel consumption when used for optimization of the traffic signal timings. This novel PI combines conventional traffic performance measures (stopped delay and number of stops) with a set of factors that represent the fuel consumption weights for each stop.
- Using the FC-PI saves a significant computation time that other approaches must endure because it does not require fuel consumption estimates from post-processing vehicular trajectories when optimizing signal timings. Hence, such the FC-PI can be practical for regular optimizations of signal timings.
- The reduction achieved in FC-PI throughout the optimization does not linearly translate into reduced fuel consumption. There could be several reasons for that, as discussed in the Chapter. Despite of this non-linearity, the FC-PI provided a moderate improvement in fuel consumption.
- The surrogate objective function used in the optimization resulted in a minimum saving of 2.7% in fuel consumption with a little degradation in the mobility performance measures compared to the base case signal timings. Such savings were significantly increased to 5.7% (accompanied with significant improvements in the mobility measures) when the impact of a high percentage of heavy vehicles in the fleet was considered in the optimization.

Future research should investigate how well FC-PI captures the impact of other factors (e.g., road gradients and driving behaviors). Also, the savings of the emissions showed that various air pollutants, except CO_2, are not linearly correlated with fuel consumption. Thus, further research is needed to investigate the differences between the signal optimizations when stop penalties are based on the fuel consumption estimates and those derived based on various emission' estimates. More research is also required to apply the proposed methodology on various networks under multiple factors impacting fuel consumption and emissions. Finally, this Chapter utilized stop penalties computed from simulated vehicles; such penalties should be validated based on fuel consumption measurements from the field.

Chapter 6 illustrated the impact of deceleration-acceleration events (DAEs) on the stop penalty and proposed a methodology to integrate their impact to the Env-PI. Future research needed to publish this Chapter includes developing an estimation methodology for various DAE levels under certain conditions. The research should also quantify the impact of those DAE levels on the excess fuel consumption estimates and compare it to the impact of complete stops for various cruising speeds and vehicle types. Finally, the research should compare the Env-PIs computed with and without the impact of DAEs.

In summary, it is recommended that traffic agencies should implement fuel consumption-based stop penalties in their signal timing optimization practices. The stop penalty should be computed by using the developed field-based prediction models because they represent the current vehicular fleet operating in the field.

This research derived stop penalty for vehicles with Internal Combustion Engine (ICE) that stays running during idling. Future research is needed to propose a methodology to derive a stop penalty for vehicles with technology that shuts the engines down during the idling phase at intersections. Such research can be based on the premise that those vehicles do not turn off their engines as soon as the stop occurs, but it takes a second or two before the engine shuts off. Similarly, when releasing the brake, the engine idles for a second or two before the actual acceleration starts. In addition to account for a full environmental impact of such operations one would also need to consider extra 'hot starts' of the engine, which may be equivalent to 5-7 seconds of idling fuel consumed. Thus, the methodology developed in this research can still be used to compute the stop penalty, but more weight is expected to be given to stops than to the stopped delay.

Future research should also propose an energy-based stop penalty to include the impact of stops made by the emerging zero-emission vehicles (e.g., electric vehicles). Until then, practitioners can still combine such emerging vehicles with the ICE vehicles in the process of developing or optimizing signal timings plans using the proposed Environmental Performance Index.

Appendix A Impact of Various Levels of Operating Conditions on Sustainability Metrics

Appendix A.1 Fuel Consumption

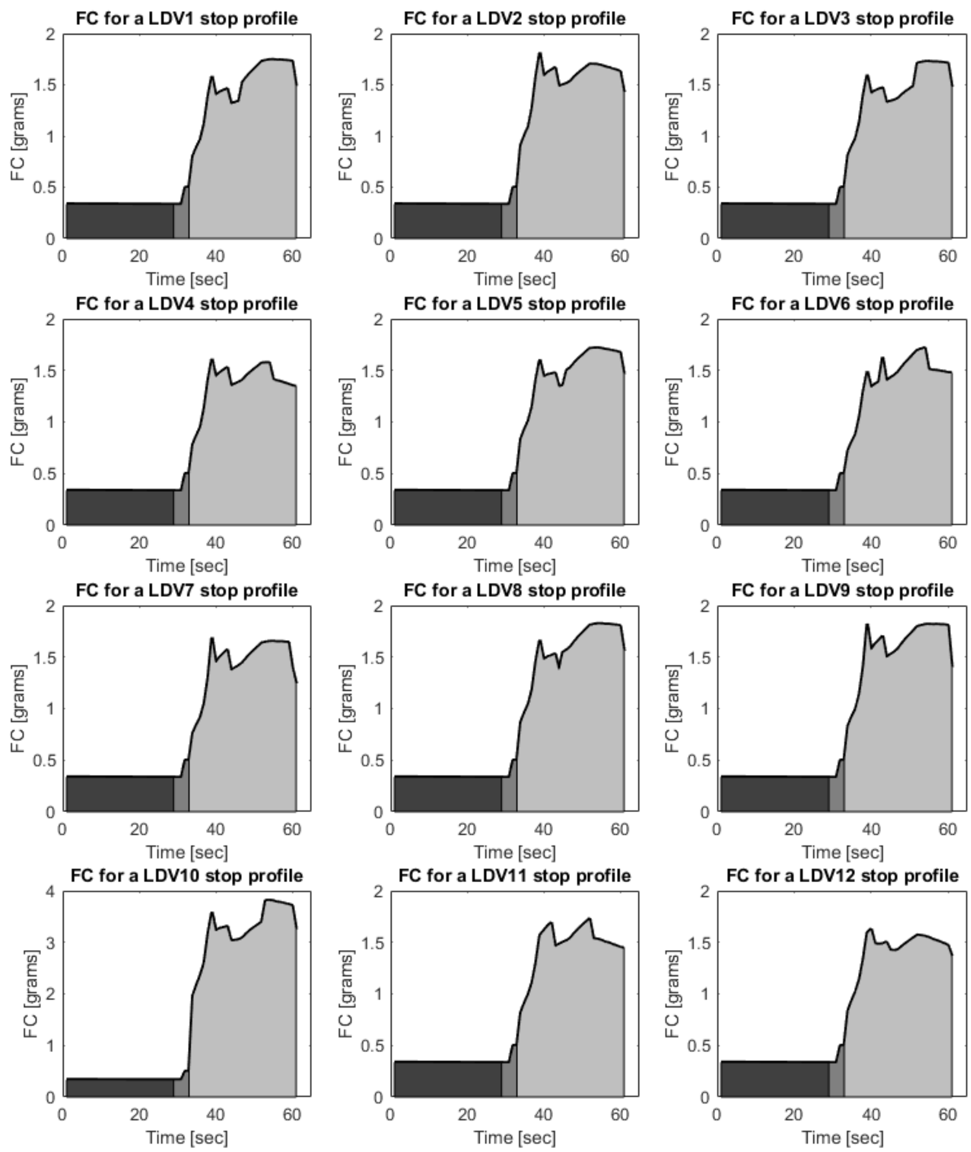

Appendix Figure 1 Light-Duty Vehicle type.

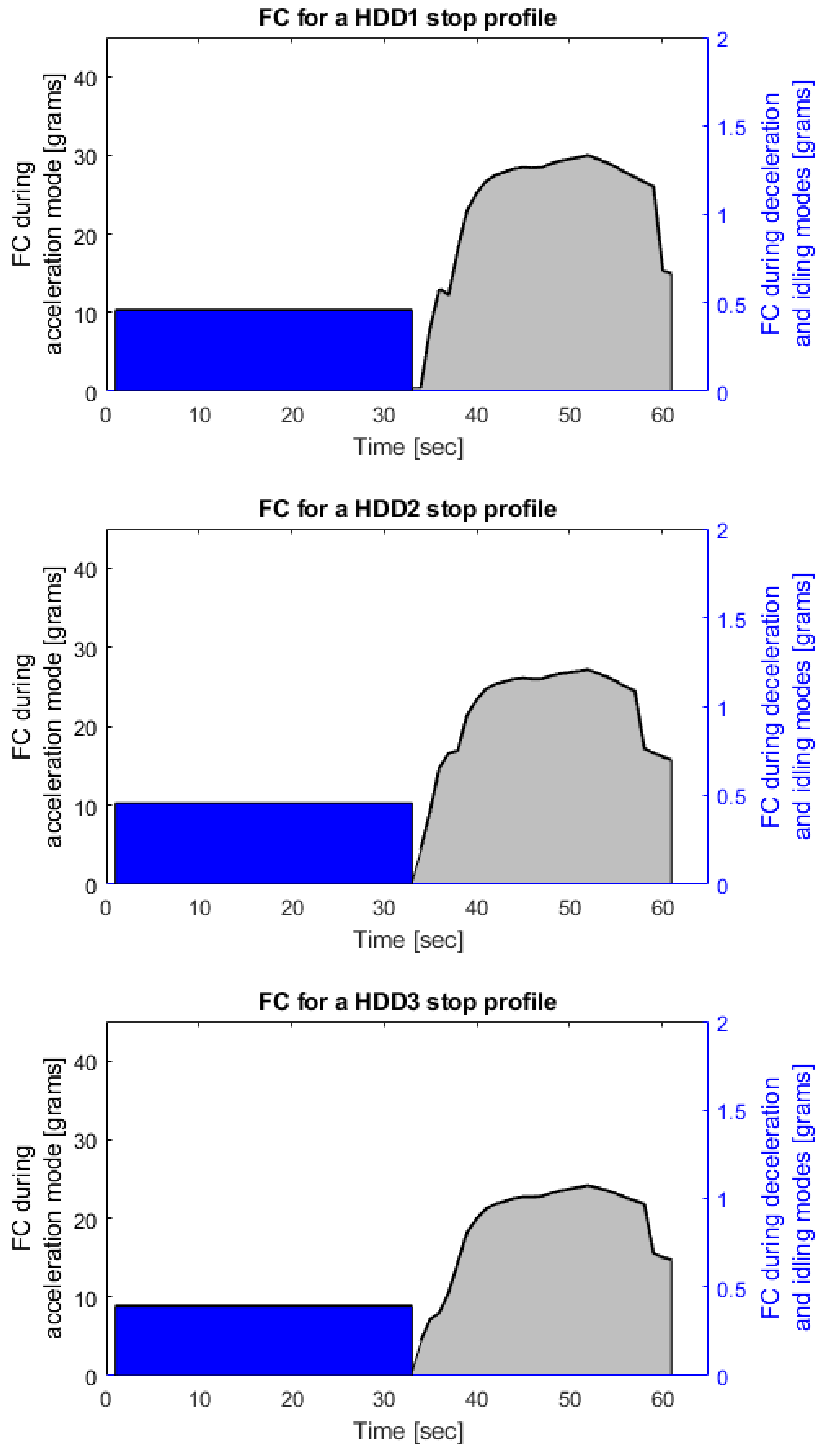

Appendix Figure 2 Heavy-Duty Diesel Vehicle type.

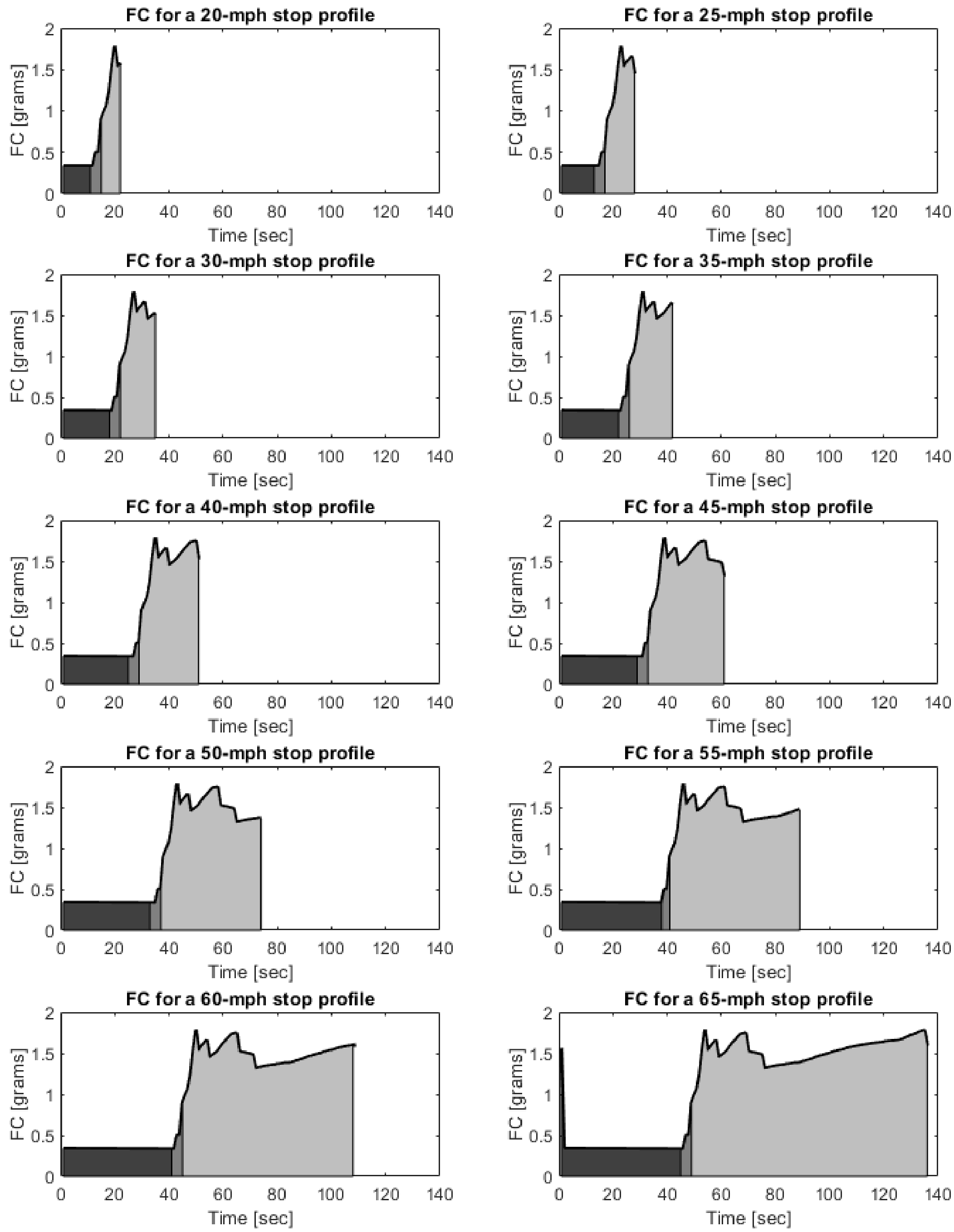

Appendix Figure 3 Cruising speed.

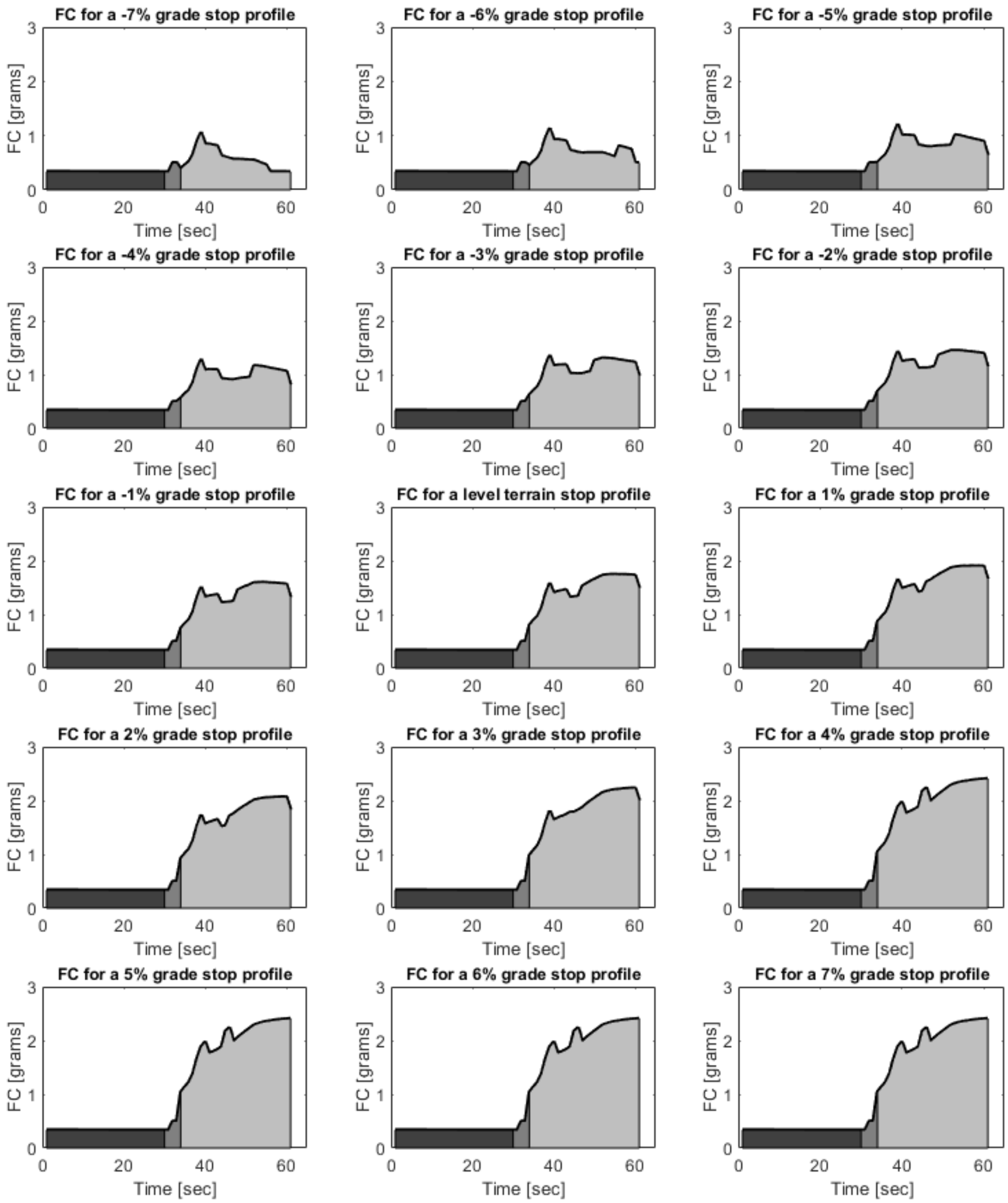

Appendix Figure 4 Road Gradient.

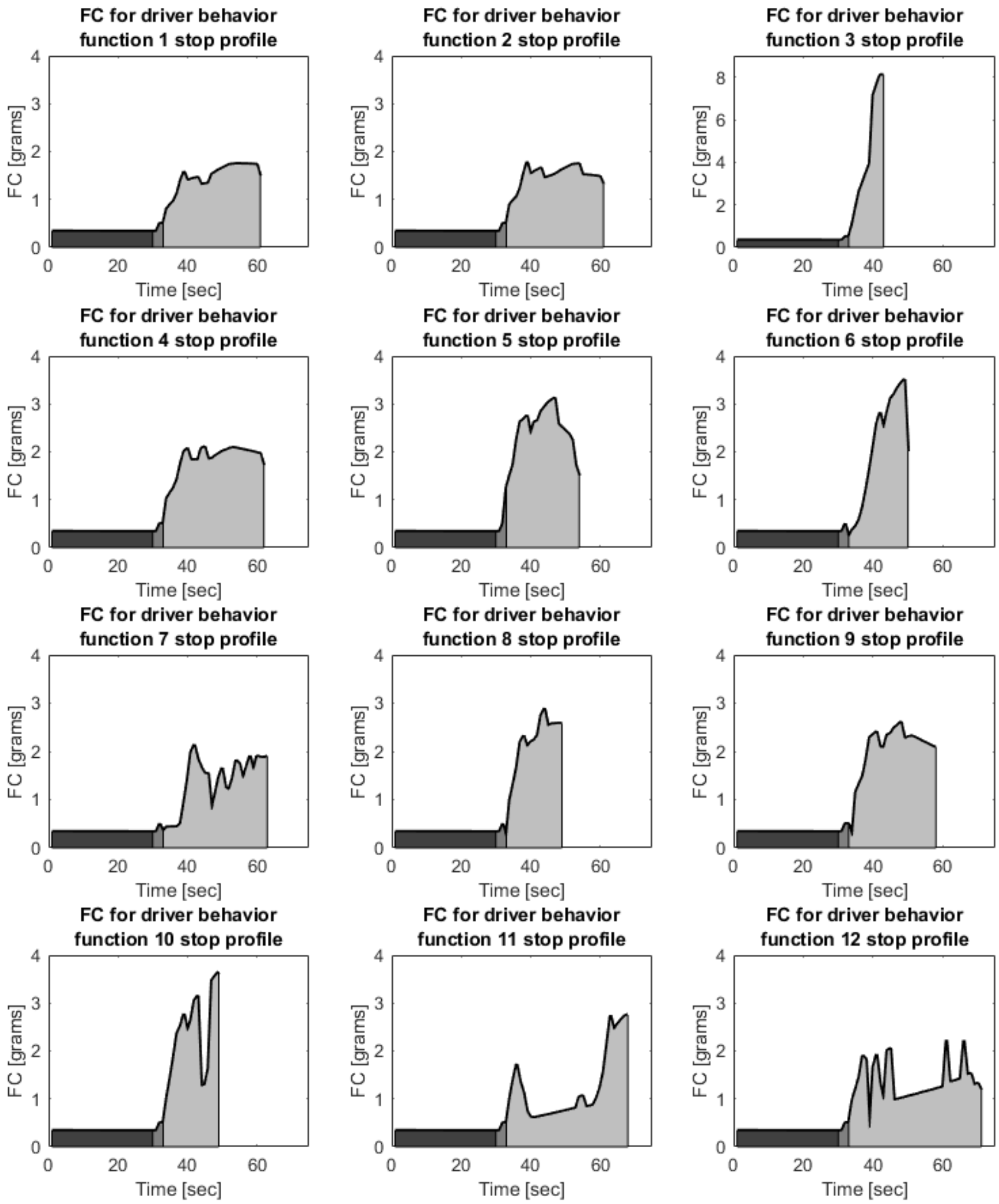

Appendix Figure 5 Driving Behavior.

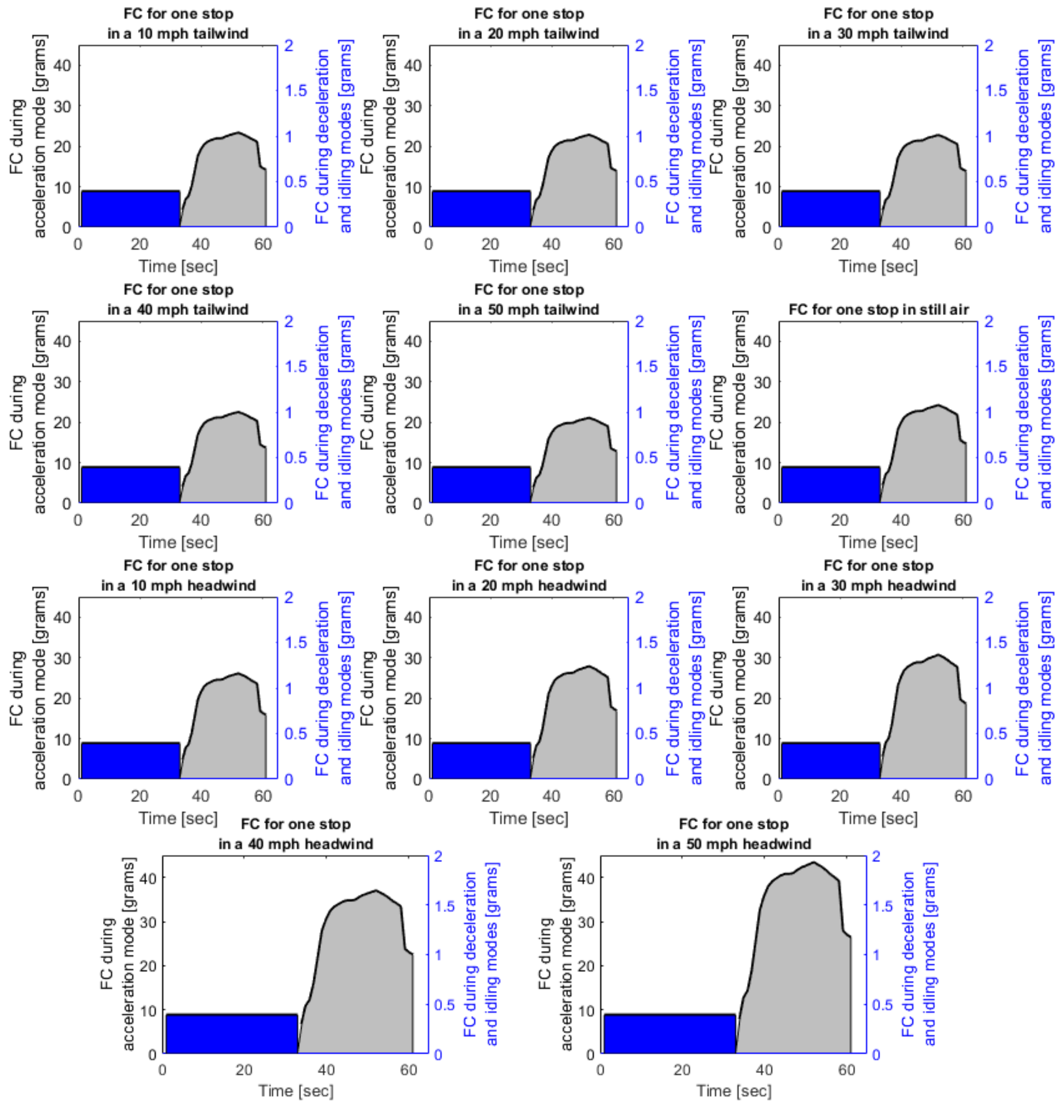

Appendix Figure 6 Wind Effect.

Appendix A.2 Emissions

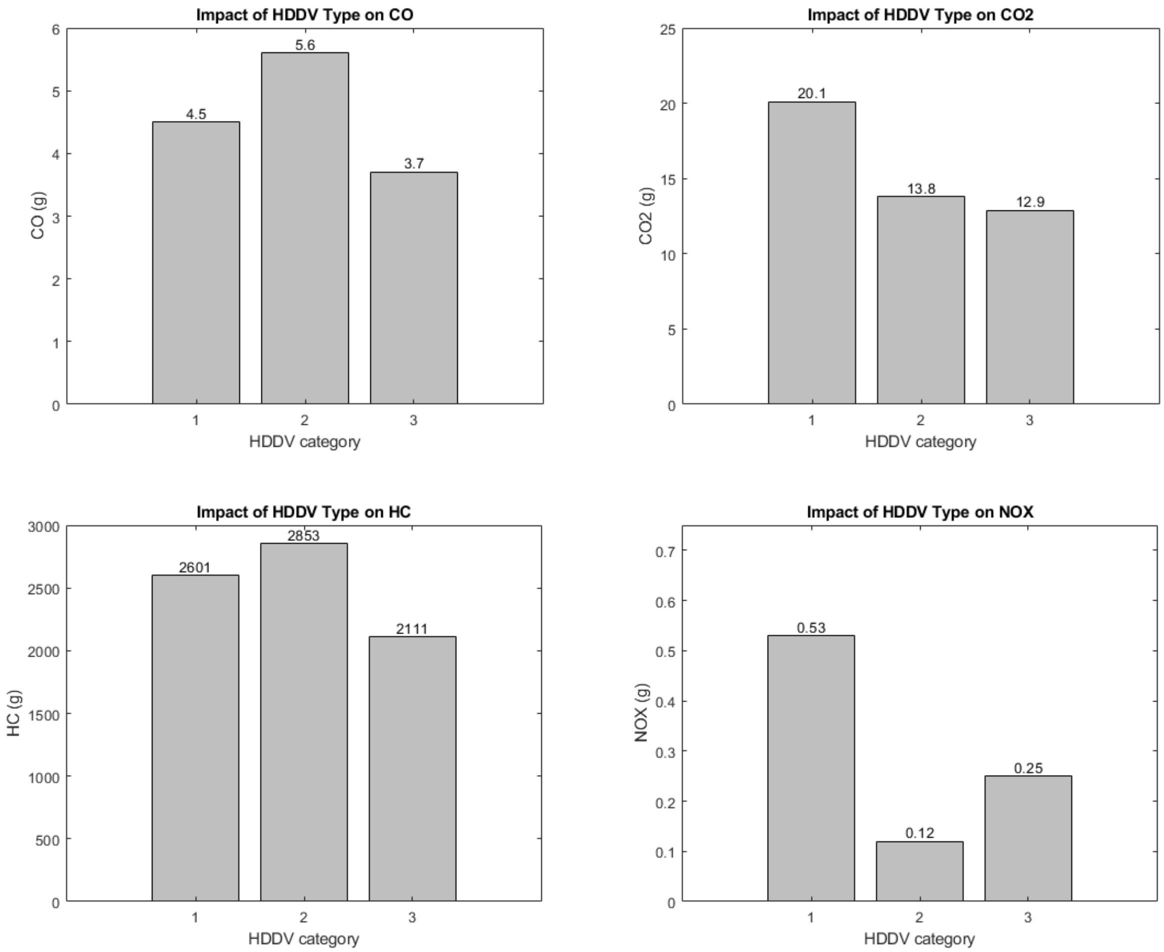

Appendix Figure 7 Impact of HDD vehicle type on emissions.

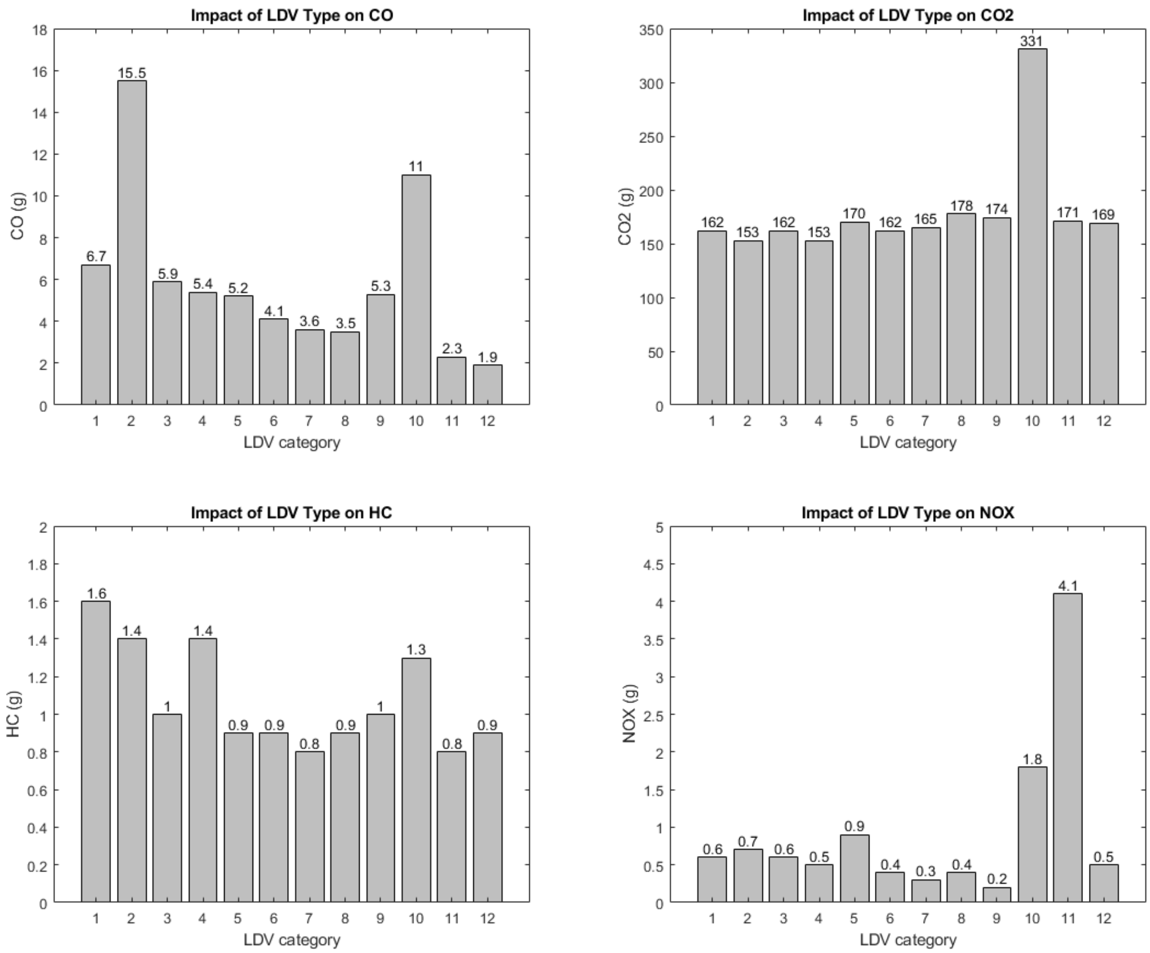

Appendix Figure 8 Impact of LDV vehicle type on emissions.

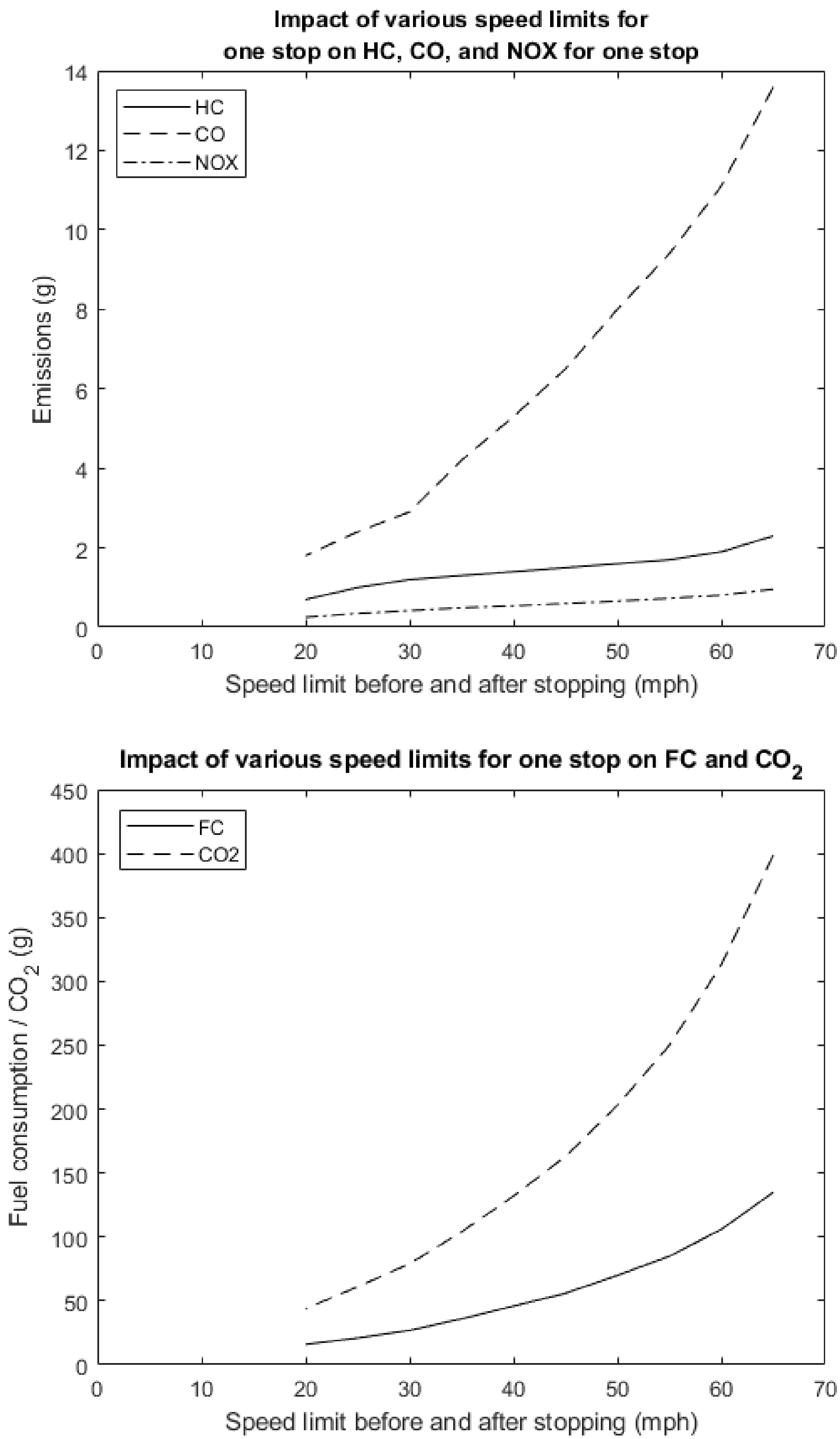

Appendix Figure 9 Impact of cruising speed on emissions.

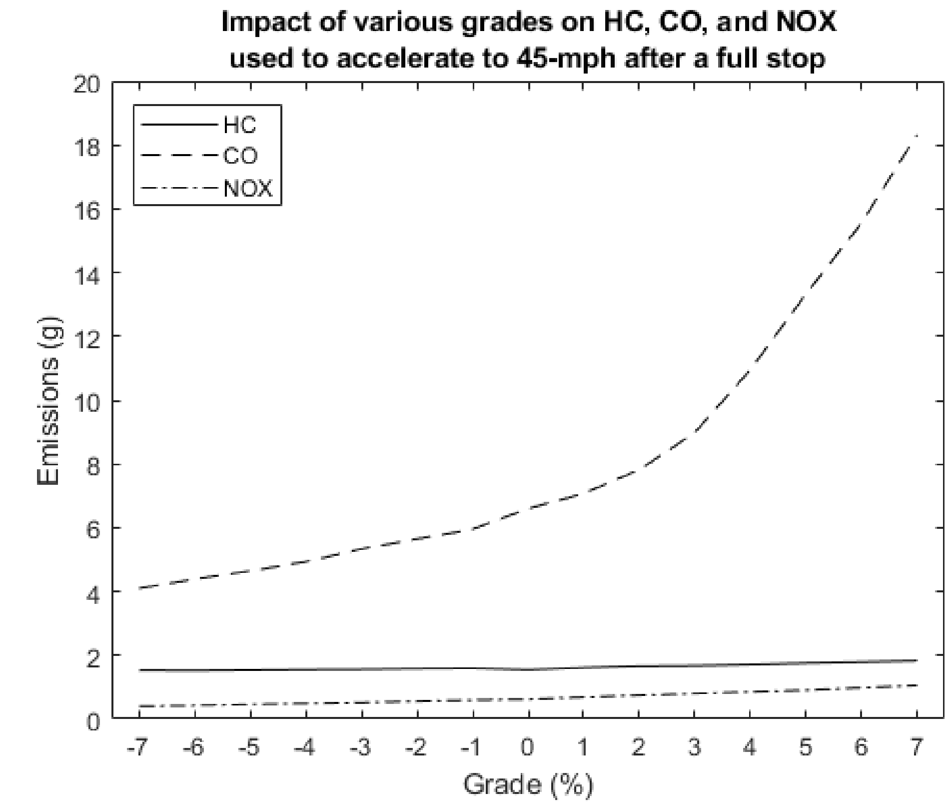

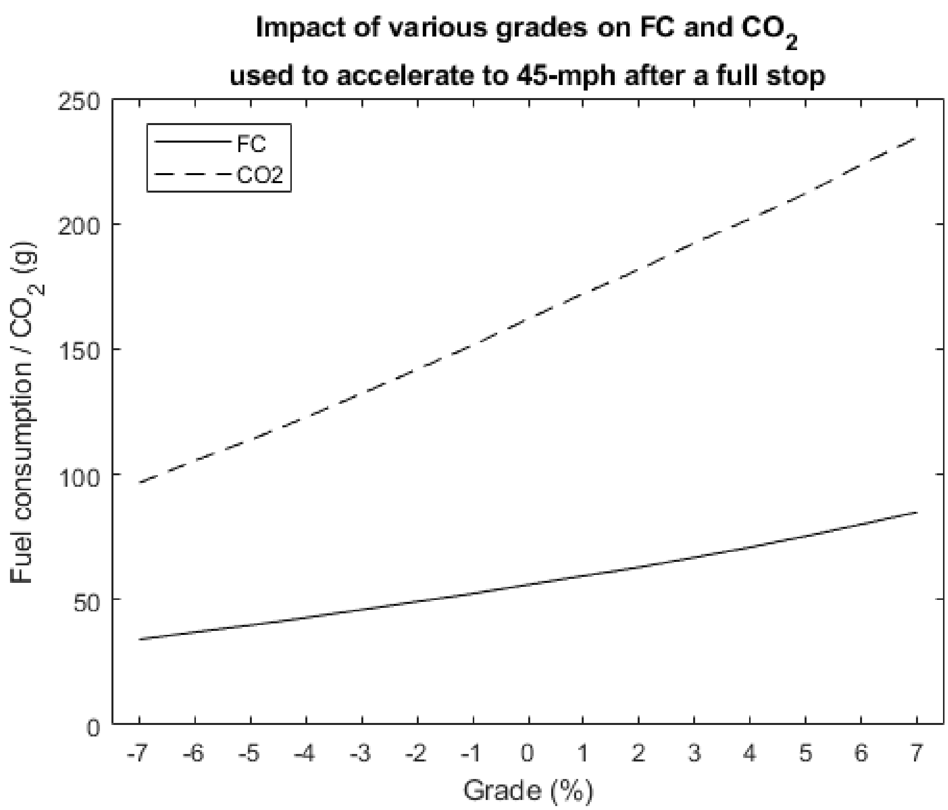

Appendix Figure 10 Impact of road gradient on emissions.

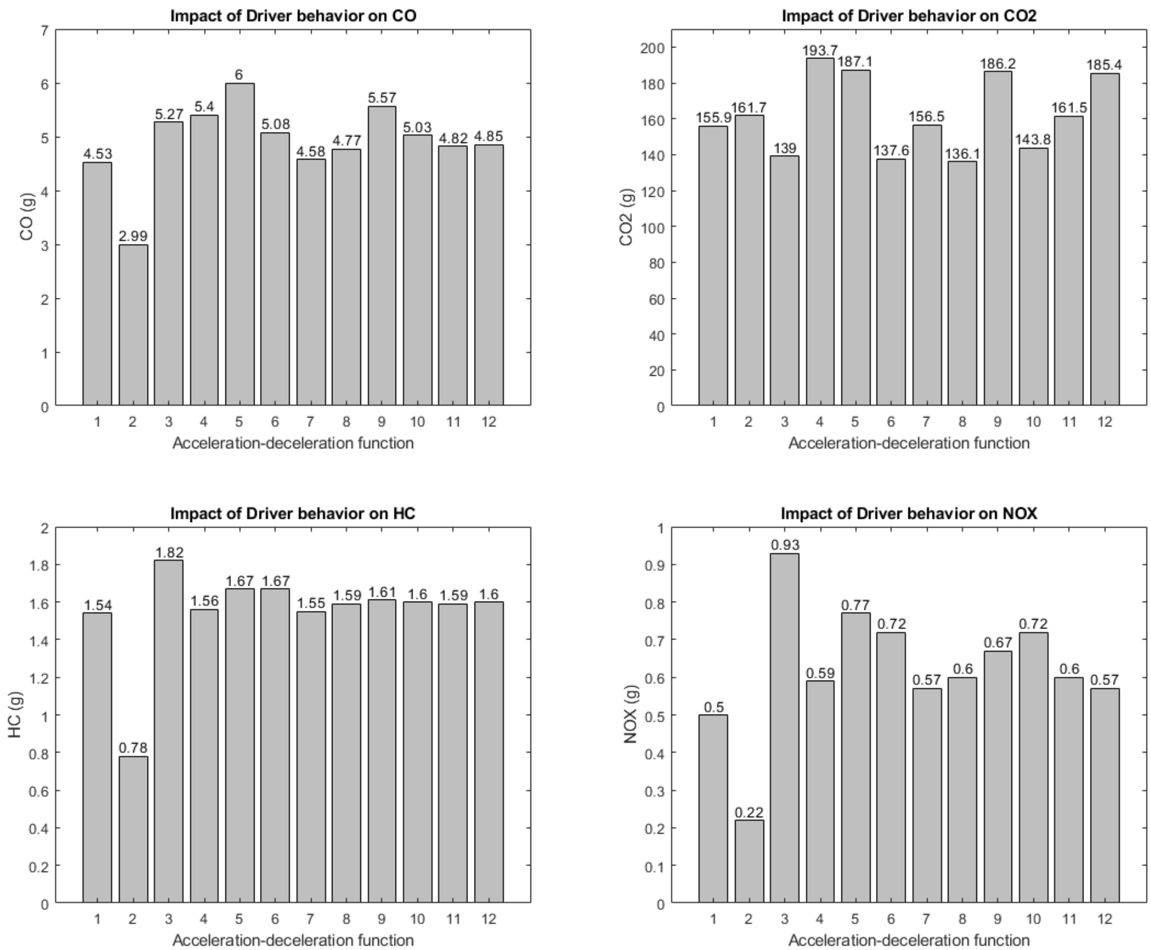

Appendix Figure 11 Impact of driving behavior on emissions.

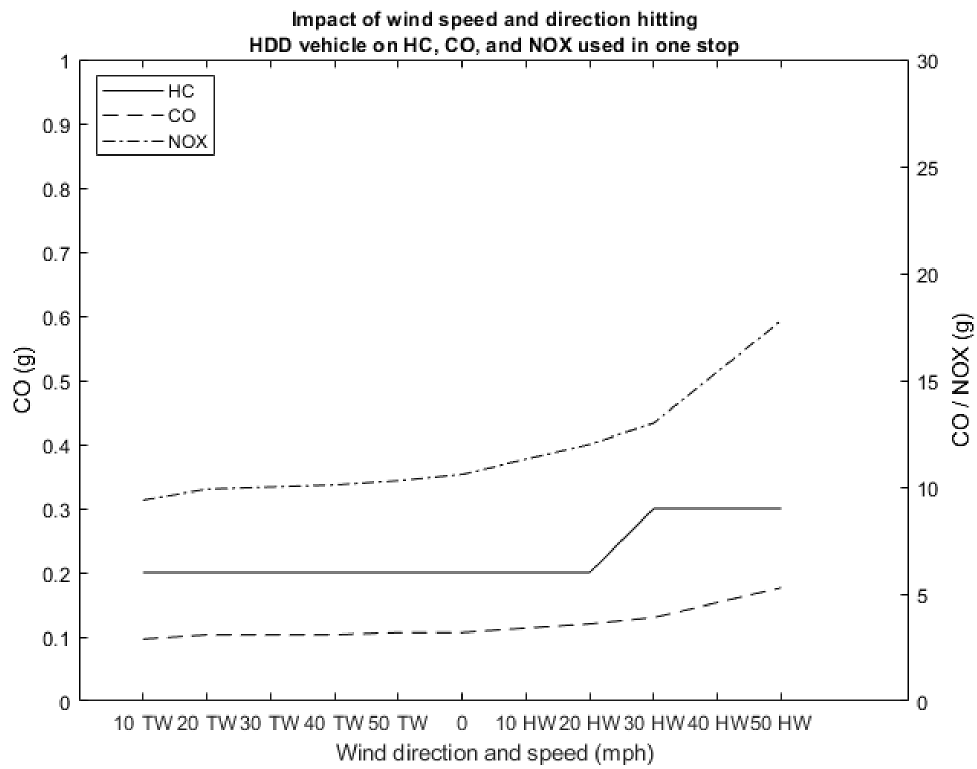

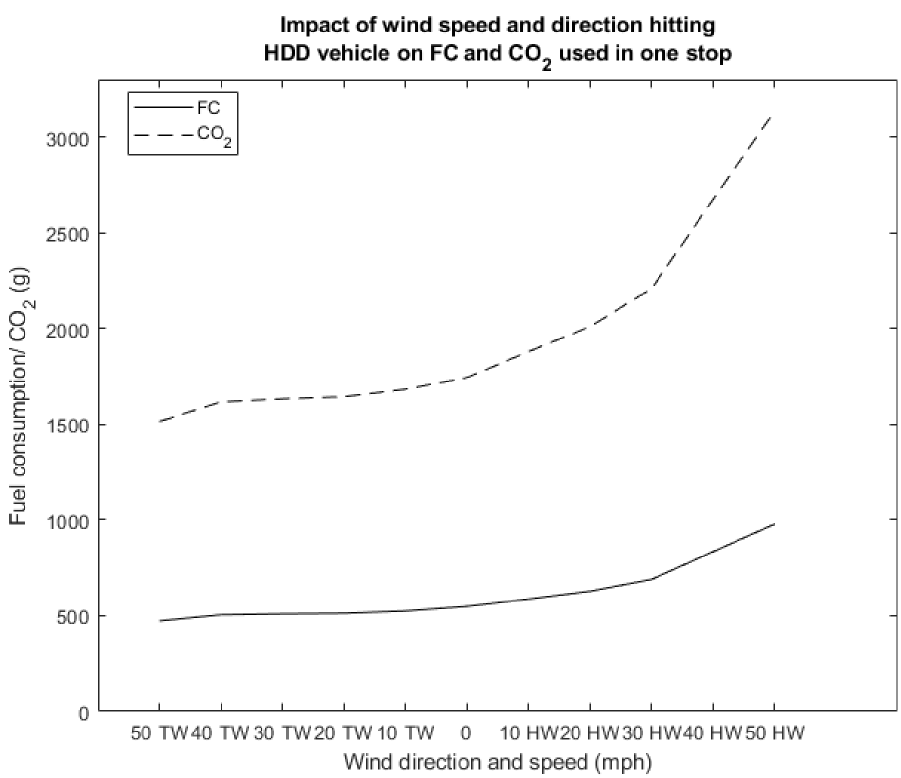

Appendix Figure 12 Impact of HDD vehicle type on emissions.

Appendix B Combined Impact of Various Sustainability Metrics on the Stop Penalty

Appendix B.1 Light Duty Vehicles

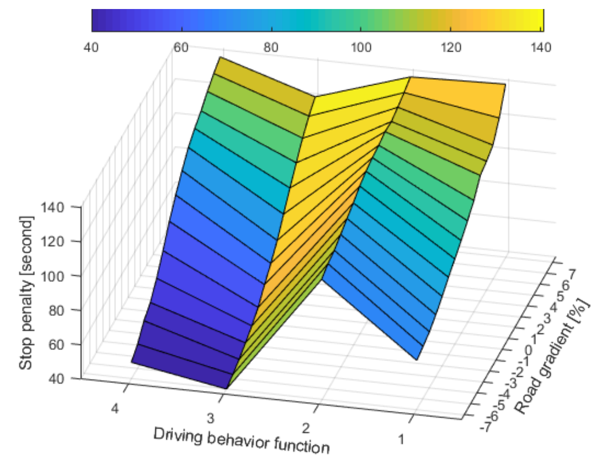

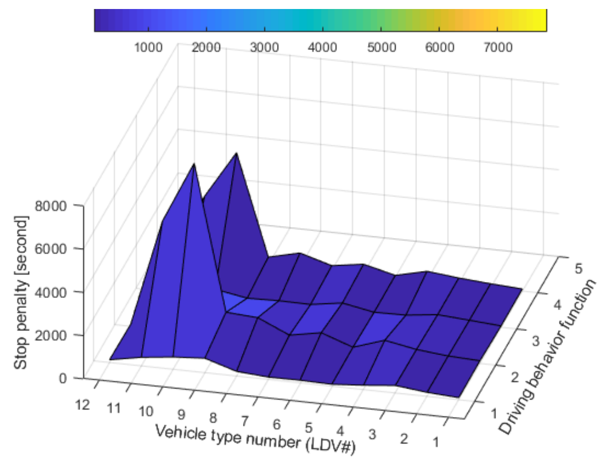

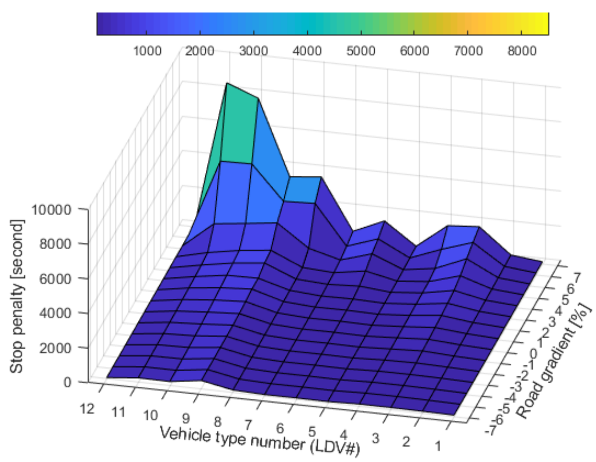

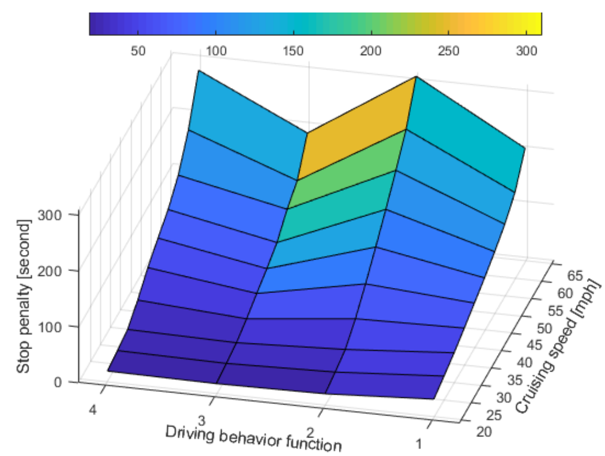

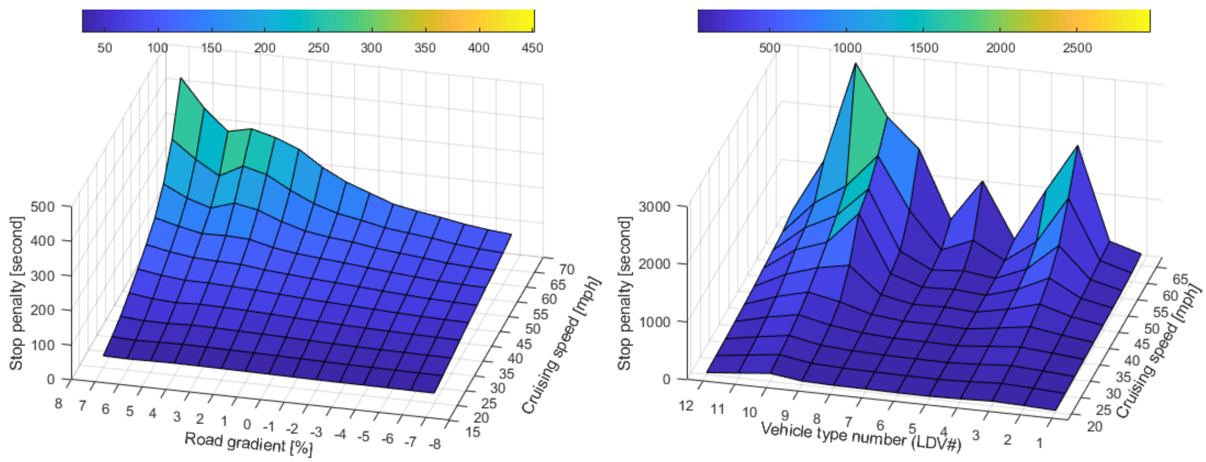

Appendix Figure 13 CO LDV results

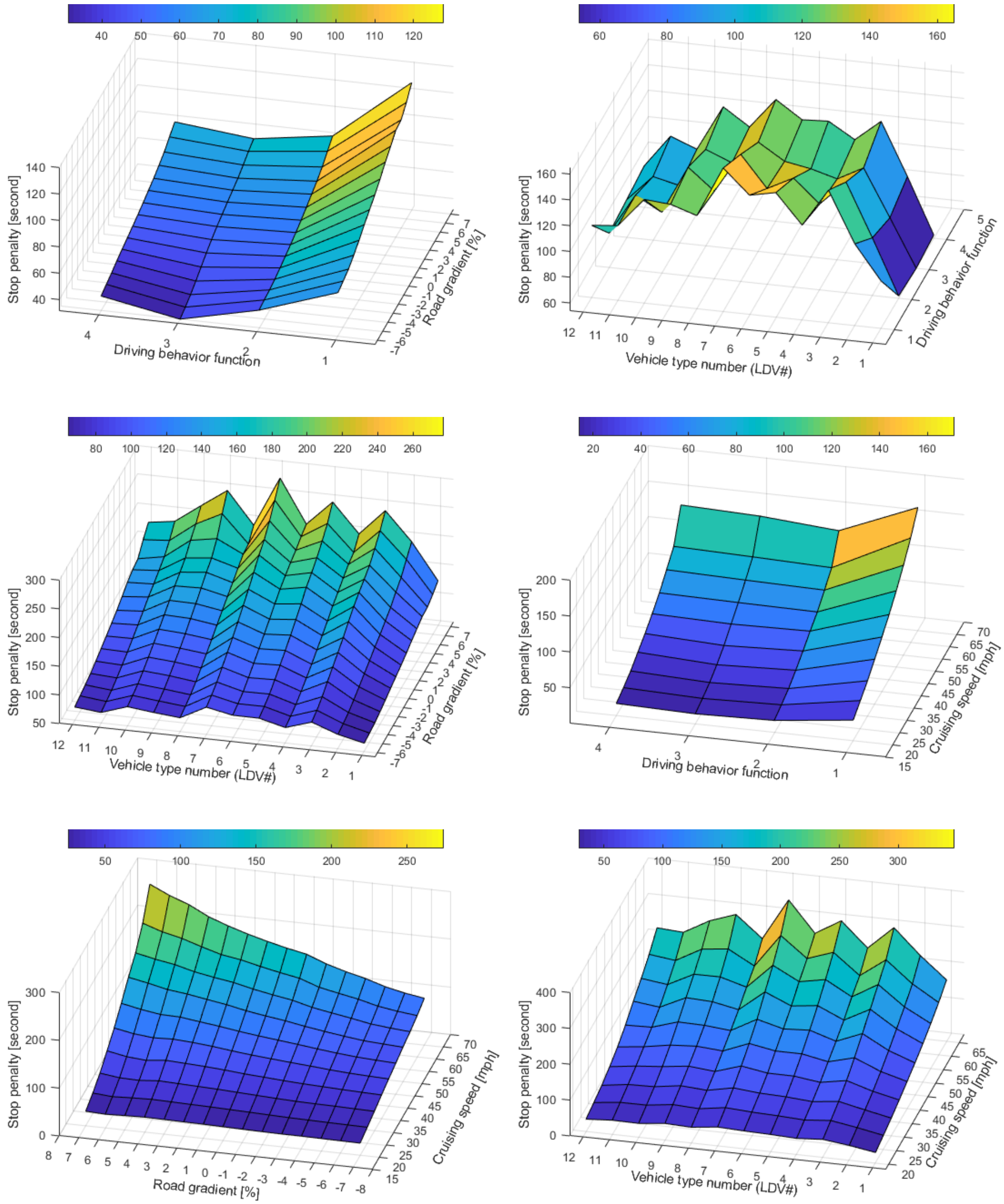

Appendix Figure 14 CO_2 LDV results.

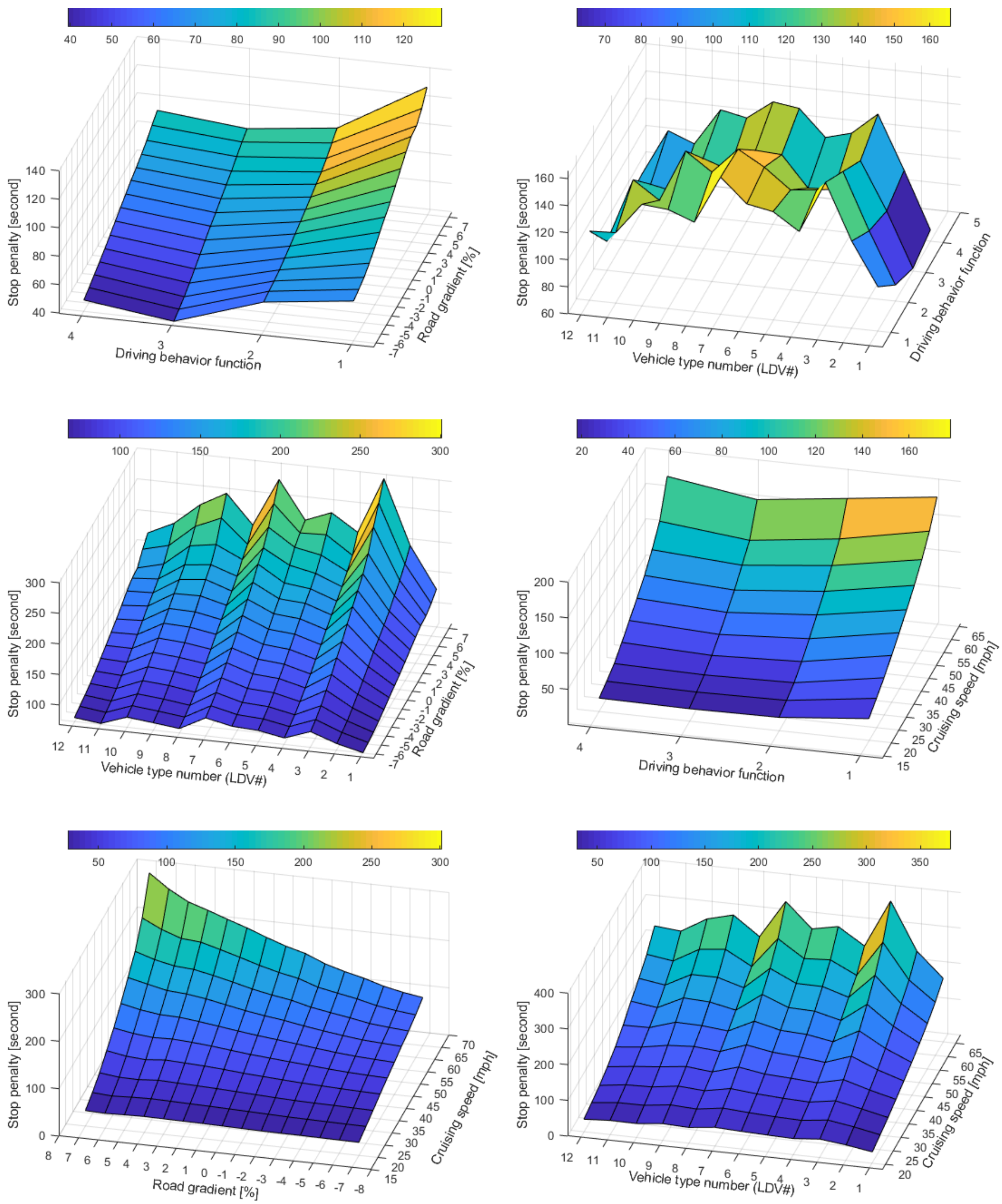

Appendix Figure 15 FC LDV results

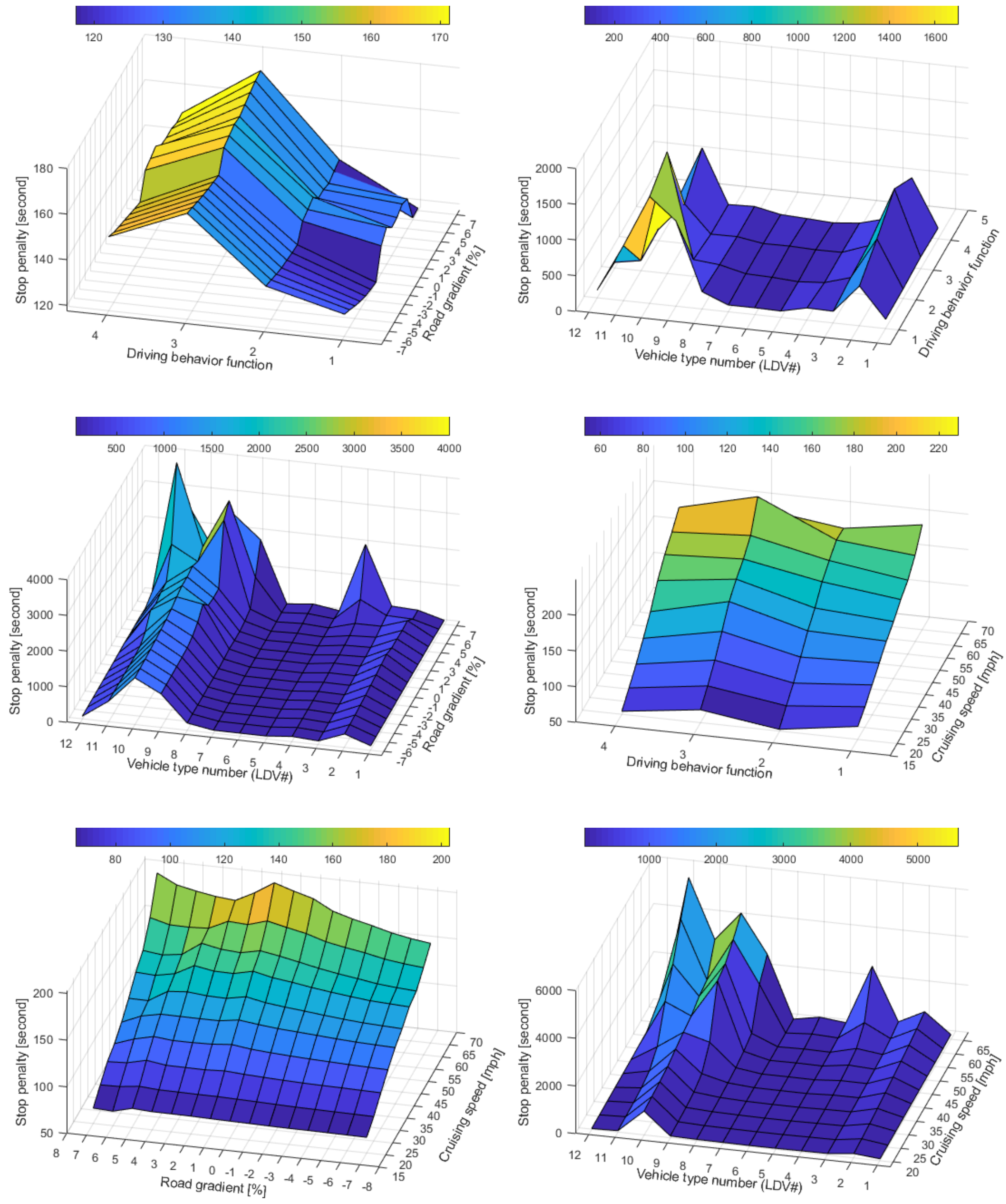

Appendix Figure 16 HC LDV results

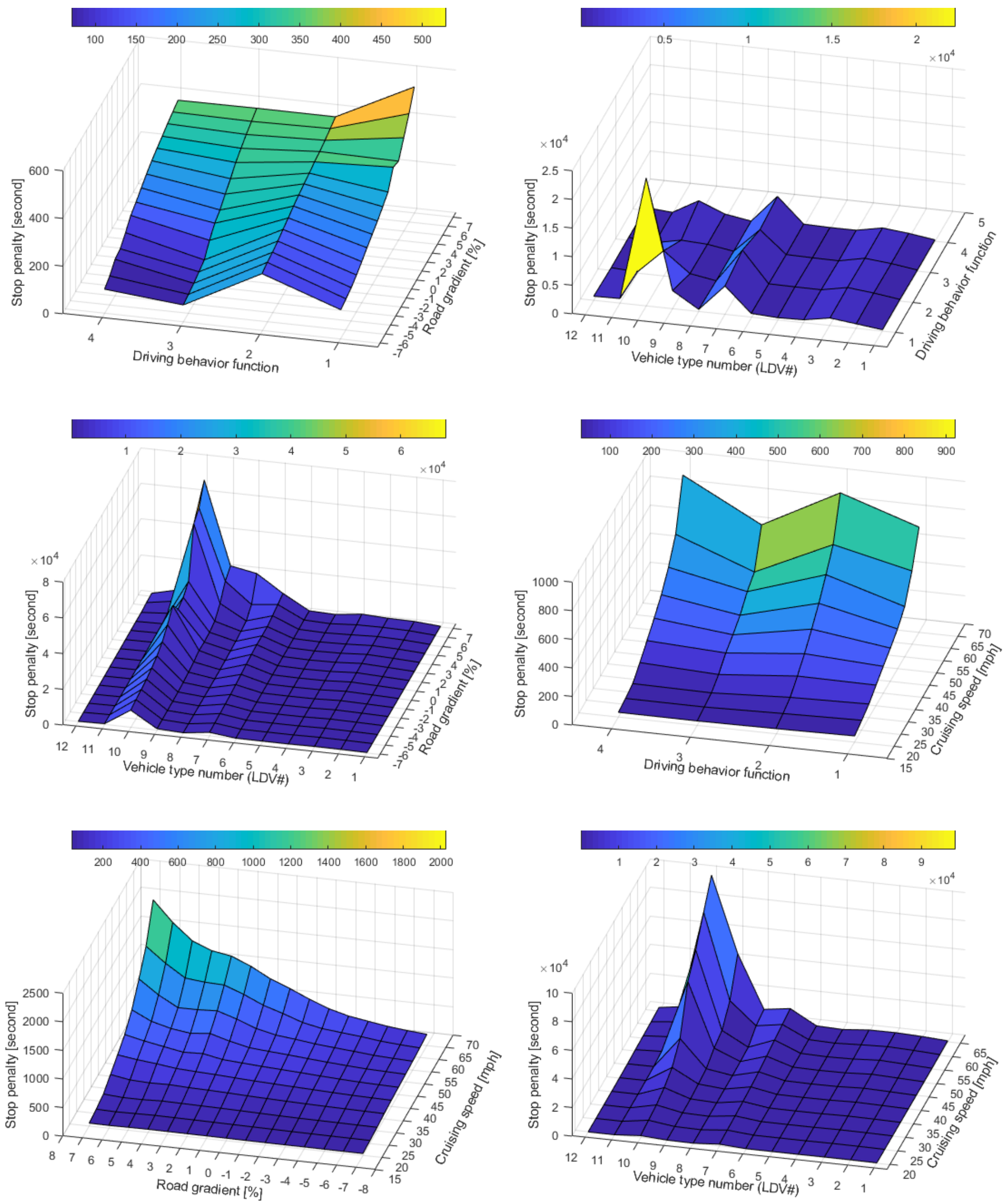

Appendix Figure 17 NOx LDV results

Appendix B.2 Heavy Duty Diesel Vehicles

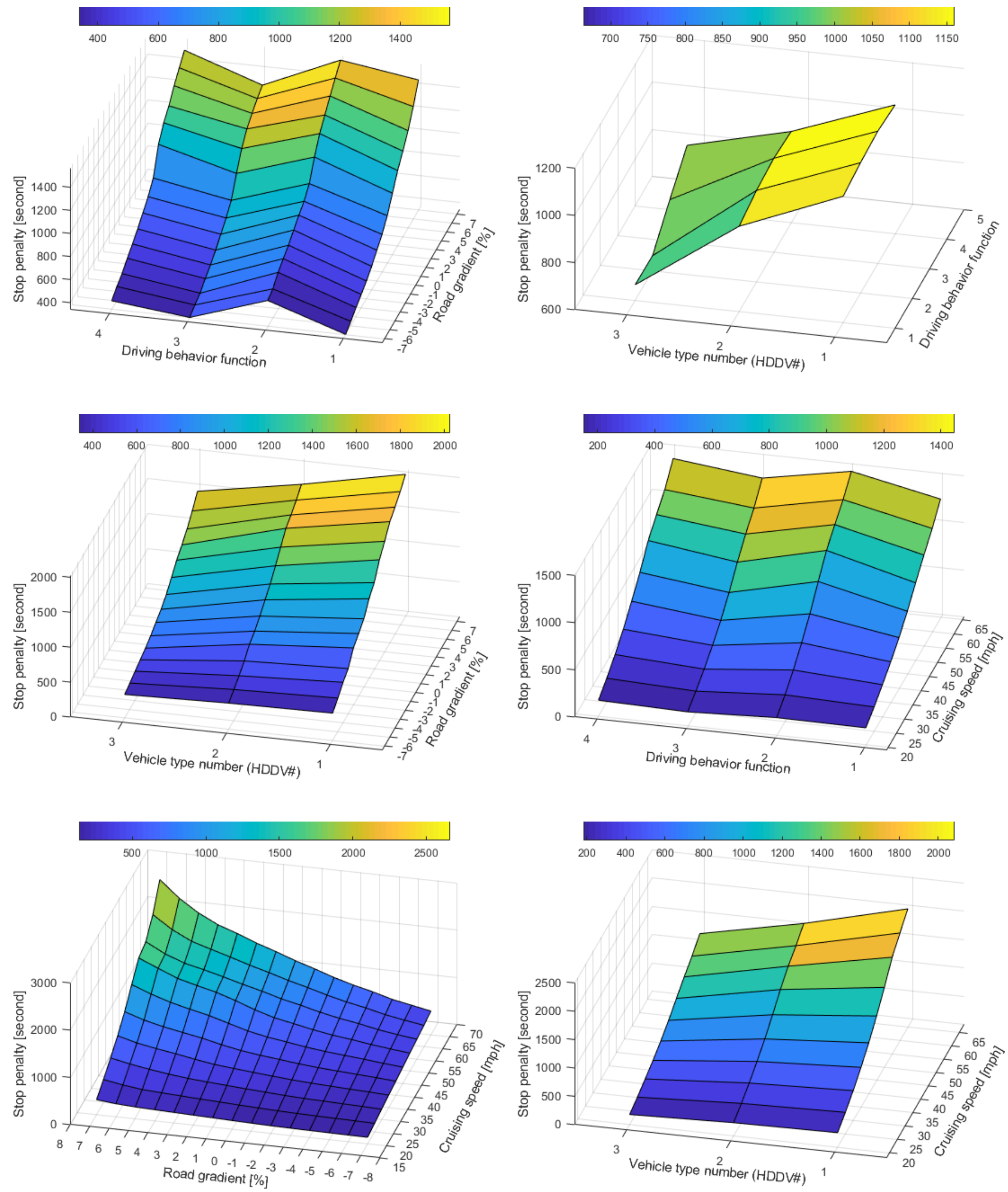

Appendix Figure 18 CO HDDV results

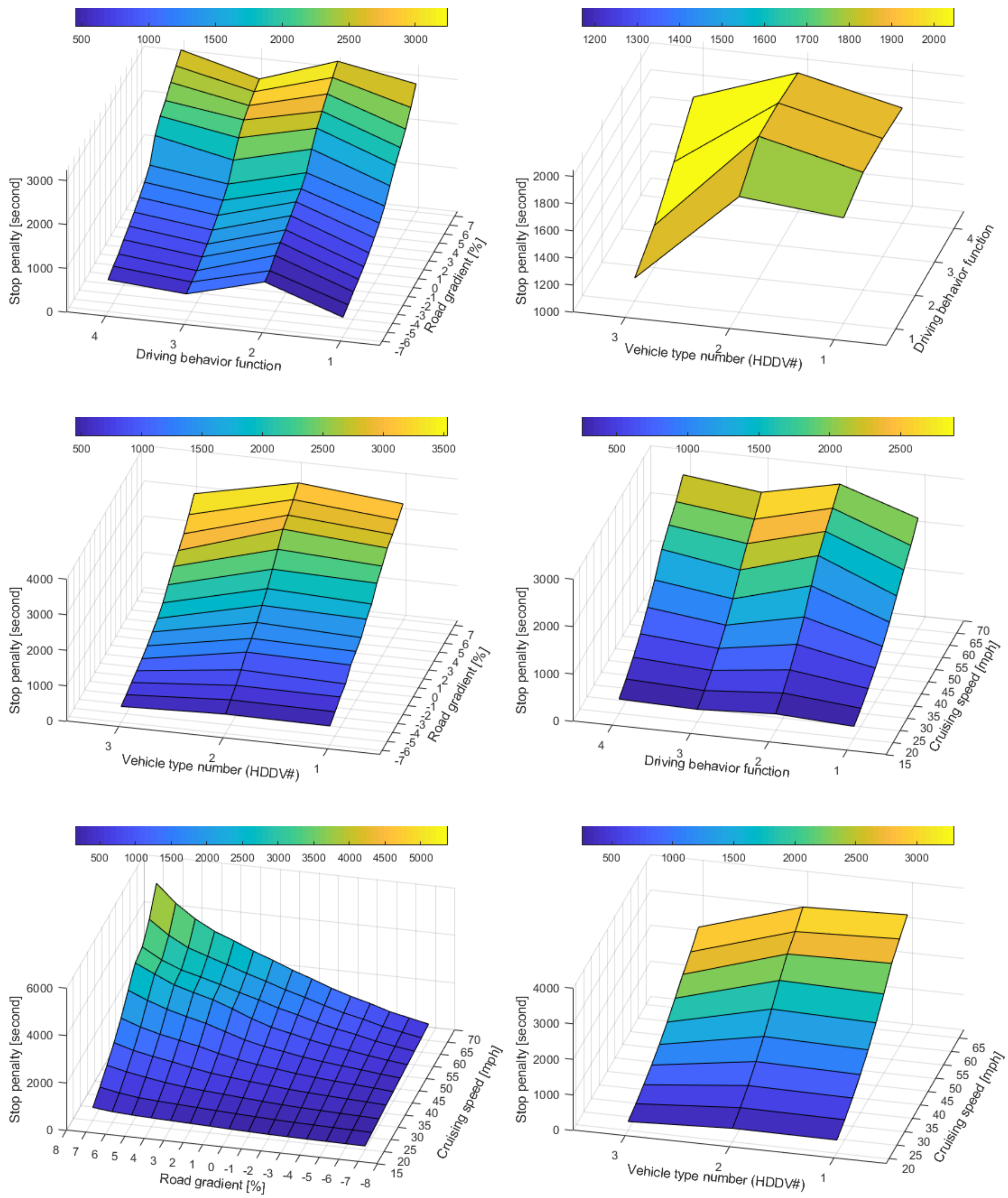

Appendix Figure 19 CO_2 HDDV results

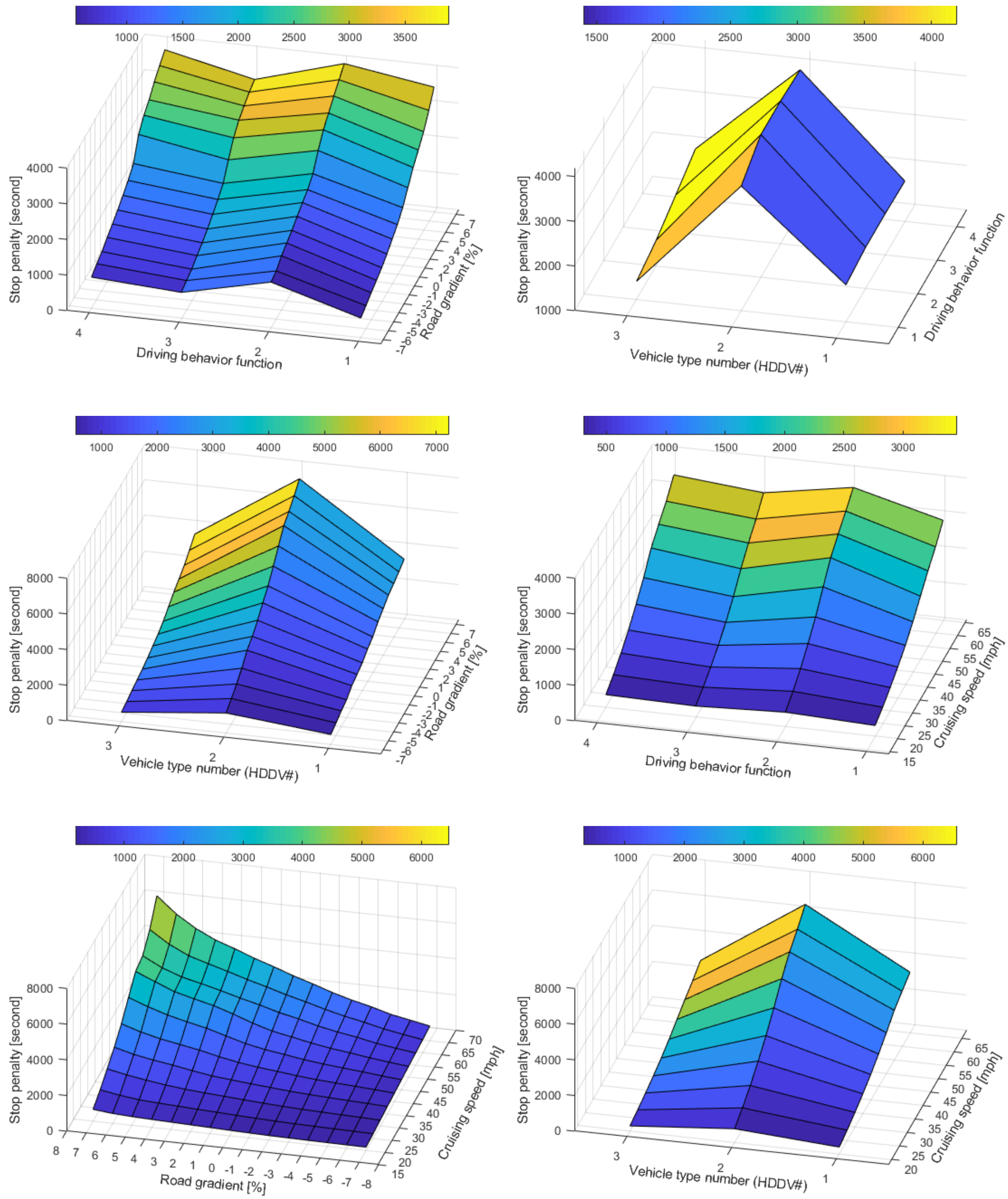

Appendix Figure 20 FC HDDV results

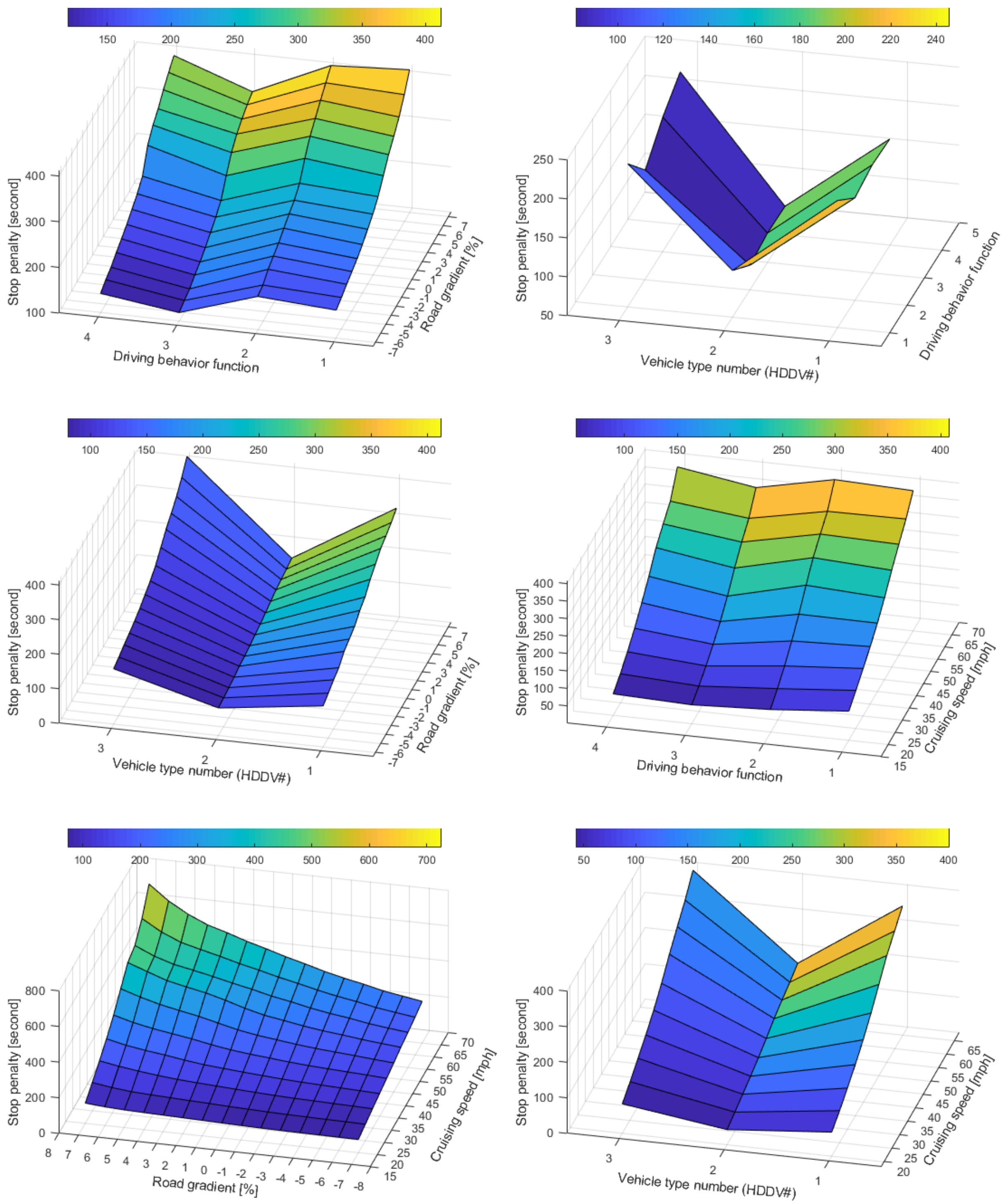

Appendix Figure 21 HC HDDV results

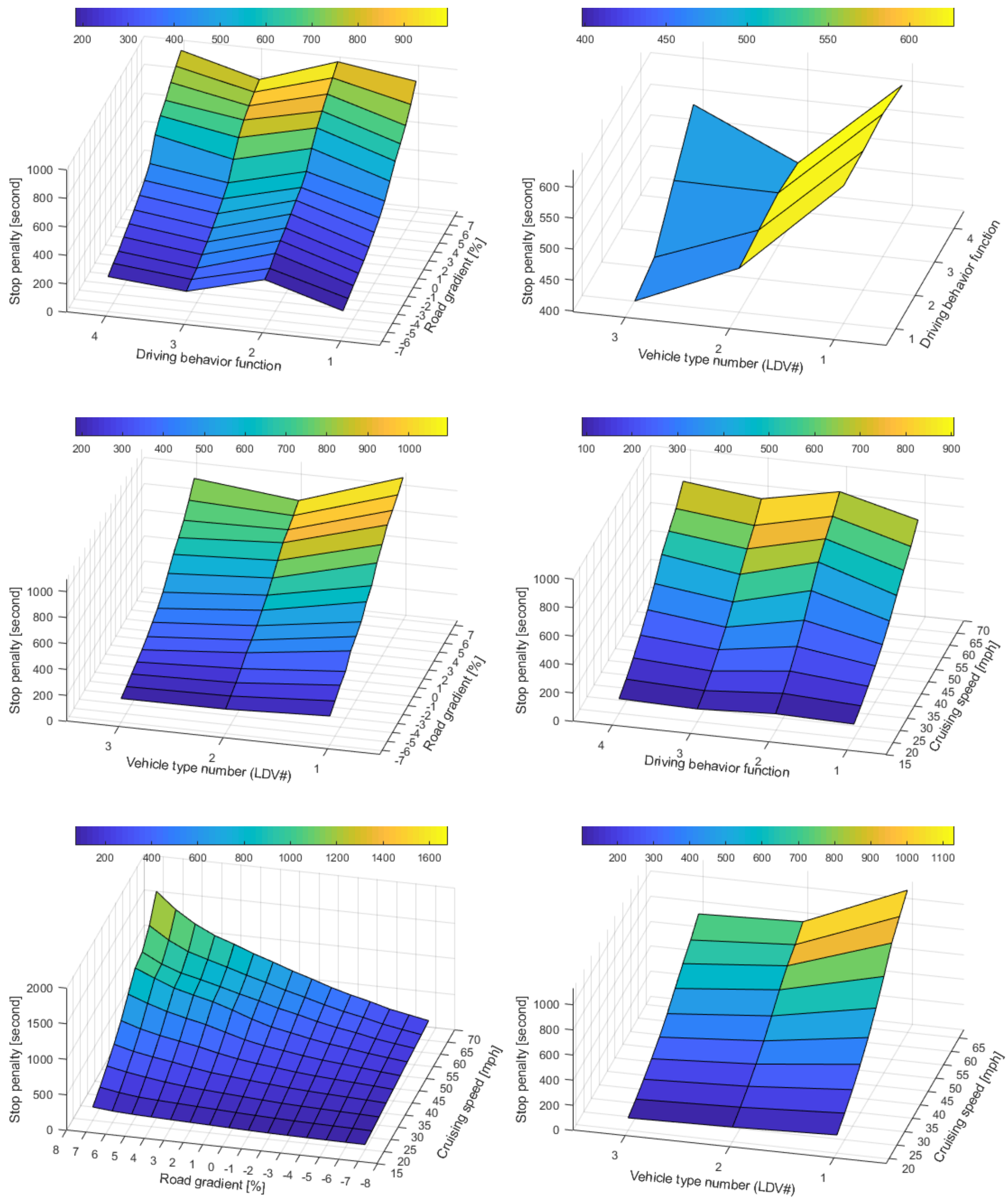

Appendix Figure 22 NOx HDDV results

Appendix C Characteristics of Tested Vehicles in Chapter 4

Appendix Table 1 Characteristics of tested vehicles

Vehicle No.	Groups	Year	Make	Series	Model	Class	Style	Engine	Weight	Wheelbase	Length	Width	Height
1	LDV1	2015	CADILLAC	ATS 4D 4WD	LUXURY	MIDSIZE	LUXURY	4-FI 2.0L T/C	3542	109.3	182.8	71.1	55.9
2	LDV1	2005	CHEVROLET	IMPALA 4D	NO DATA	LARGE	4 DOOR	6-FI 3.4L	3465	110.5	200	73	57.3
3	LDV1	2015	HONDA	CR-V 4D 4WD	EX-L	SMALL	UTILITY	4-FI 2.4L	3479	103.1	179.4	71.6	65.1
4	LDV1	2016	TOYOTA	AVALON 4D	XLE/PREM/TOURING/LTD	LARGE	4 DOOR	6-FI 3.5L	3461	111	195.3	72.2	57.5
5	LDV1	2012	HONDA	CR-V 4D 4WD	EX-L	SMALL	UTILITY	4-FI 2.4L	3426	103.1	178.3	71.6	65.1
6	LDV1	2011	TOYOTA	RAV4 4D 2WD	4 CYL	SMALL	UTILITY	4-FI 2.5L	3360	104.7	178.7	71.5	66.3
7	LDV1	2011	TOYOTA	RAV4 4D 4WD	LIMITED 4 CYL	SMALL	UTILITY	4-FI 2.5L	3494	104.7	178.7	71.5	66.3
8	LDV1	2013	CHEVROLET	MALIBU 4D (NEW)	1LT	MIDSIZE	4 DOOR	4-FI 2.5L	3393	107.8	191.3	73	57.6
9	LDV1	2015	SUBARU	OUTBACK SW 4WD W/EYESGHT	2.5I LIMITED VDC NAVI	MIDSIZE	STATION WAGON	4-FI 2.5L	3609	108.1	189.6	72.4	66.1
10	LDV1	2014	HONDA	CR-V 4D 4WD	EX-L	SMALL	UTILITY	4-FI 2.4L	3426	103.1	178.3	71.6	65.1
11	LDV1	2015	HONDA	CR-V 4D 4WD	LX	SMALL	UTILITY	4-FI 2.4L	3479	103.1	179.4	71.6	65.1
12	LDV1	2016	TOYOTA	RAV4 4D 4WD	LE (LUX. EDN)	SMALL	UTILITY	4-FI 2.5L	3570	104.7	181.1	72.6	65.4
13	LDV1	2008	CHEVROLET	IMPALA 4D	LS	LARGE	4 DOOR	6-FI 3.5L FLEX FUEL	3555	110.5	200.4	72.9	58.7
14	LDV1	2005	TOYOTA	HIGHLANDER 4D 4WD	NO DATA	MIDSIZE	UTILITY	4-FI 2.4L	3750	106.9	184.6	71.9	67.9
15	LDV1	2011	TOYOTA	RAV4 4D 4WD	LIMITED 4 CYL	SMALL	UTILITY	4-FI 2.5L	3494	104.7	178.7	71.5	66.3
16	LDV1	2011	CHEVROLET	MALIBU 4D (NEW)	LS	MIDSIZE	4 DOOR	4-FI 2.4L	3432	112.3	191.8	70.3	57.1
17	LDV1	2016	MAZDA	CX-5 4D 4WD	GRAND TOURING	SMALL	UTILITY	4-FI 2.5L	3589	106.3	178.7	72.4	65.7
18	LDV1	2010	FORD	FUSION 4D 2WD	SE	MIDSIZE	4 DOOR	4-FI 2.5L	3285	107.4	190.6	72.2	56.9
19	LDV1	2004	LEXUS	ES 330 4D	NO DATA	MIDSIZE	LUXURY	6-FI 3.3L	3400	107.1	191.1	71.3	57.3
20	LDV1	2010	TOYOTA	RAV4 4D 4WD	4 CYL	SMALL	UTILITY	4-FI 2.5L	3494	104.7	178.7	71.5	66.3
21	LDV1	2016	HONDA	CR-V 4D 4WD	EX-L	SMALL	UTILITY	4-FI 2.4L	3479	103.1	179.4	71.6	65.1
22	LDV1	2009	MERCURY	MARINER 4D 4WD	PREMIER	SMALL	UTILITY	6-EFI 3.0L	3493	103.1	174.7	71.1	67.9
23	LDV1	2010	CHEVROLET	MALIBU 4D (NEW)	2LT	MIDSIZE	4 DOOR	6-FI 3.6L	3415	112.3	191.8	70.3	57.1
24	LDV1	2011	CHEVROLET	MALIBU 4D (NEW)	LS	MIDSIZE	4 DOOR	4-FI 2.4L	3432	112.3	191.8	70.3	57.1
25	LDV1	2002	HYUNDAI	SANTA FE 4D 2WD	GLS/LX	SMALL	UTILITY	6-FI 2.7L	3494	103.1	177.2	72.7	66
26	LDV1	2003	LEXUS	GS 300 4D 2WD	NO DATA	LARGE	LUXURY	6-FI 3.0L	3649	110.2	189.2	70.9	55.9
27	LDV1	2007	SUZUKI	GRAND VITARA 4D 4X2	HARDTOP	SMALL	UTILITY	6-FI 2.7L	3452	103.9	176	71.3	66.3
28	LDV1	2008	SUBARU	OUTBACK SW 4WD	2.5I/L.L.BEAN NAVI	MIDSIZE	STATION WAGON	4-FI 2.5L	3350	105.1	189	69.7	61.6

Appendix Table 1 (continued).

29	LDV1	2016	SUBARU	FORSTR 4D 4WD W/EYESGHT	2.5I PREMIUM VDC	SMALL	UTILITY	4-FI 2.5L	3395	103.9	180.9	70.7	66.4
30	LDV1	2007	HONDA	CR-V 4D 4WD	LX	SMALL	UTILITY	4-FI 2.4L	3501	103.1	178	71.6	66.1
31	LDV1	2006	SUBARU	LEGACY SW 4WD	2.5I LIMITED/SP.ED.	MIDSIZE	STATION WAGON	4-FI 2.5L	3305	105.1	188.7	68.1	58.1
32	LDV1	2015	SUBARU	FORESTER 4D 4WD	2.5I PREMIUM VDC	SMALL	UTILITY	4-FI 2.5L	3296	103.9	180.9	70.7	66.4
33	LDV1	2015	NISSAN	ROGUE SELECT 4D 2WD	NO DATA	SMALL	UTILITY	4-FI 2.5L	3287	105.9	183.3	70.9	66.3
34	LDV1	2014	SUBARU	LEGACY 4D 4WD	2.5I PREMIUM VDC	MIDSIZE	4 DOOR	4-FI 2.5L	3315	108.3	187.2	71.7	59.3
35	LDV1	2014	NISSAN	810/MAXIMA SEDAN	3.5 S/3.5 SV	MIDSIZE	4 DOOR	6-FI 3.5L	3550	109.3	190.6	73.2	57.8
36	LDV1	2017	SUBARU	OUTBACK SW 4WD W/EYESGHT	2.5I LIMITED VDC NAVI	MIDSIZE	STATION WAGON	4-FI 2.5L	3622	108.1	189.6	72.4	66.1
37	LDV1	2011	SUBARU	OUTBACK SW 4WD	2.5I PREMIUM VDC	MIDSIZE	STATION WAGON	4-FI 2.5L	3386	107.9	188.2	71.7	65.7
38	LDV1	2010	FORD	FUSION 4D 2WD	SE	MIDSIZE	4 DOOR	4-FI 2.5L	3285	107.4	190.6	72.2	56.9
39	LDV1	2015	CHEVROLET	MALIBU 4D (NEW)	1LT	MIDSIZE	4 DOOR	4-FI 2.5L	3393	107.8	191.5	73	57.6
40	LDV1	2009	HONDA	CR-V 4D 4WD	EX-L	SMALL	UTILITY	4-FI 2.4L	3501	103.1	177.9	71.6	66.1
41	LDV1	2009	MITSUBISHI	GALANT 4D 2WD	ES SPORT	MIDSIZE	4 DOOR	4-FI 2.4L	3395	108.3	191.1	72.4	57.9
42	LDV1	2008	SATURN	AURA 4D	XE	MIDSIZE	4 DOOR	6-FI 3.5L	3528	112.3	190	70.3	57.6
43	LDV1	2007	MERCURY	MONTEGO 4D 2WD	PREMIER	LARGE	4 DOOR	6-EFI 3.0L	3680	112.9	200.7	74.5	60
44	LDV1	2013	HONDA	CR-V 4D 4WD	EX-L	SMALL	UTILITY	4-FI 2.4L	3426	103.1	178.3	71.6	65.1
45	LDV1	2011	VOLKSWAGEN	TIGUAN 4D 4WD	2.0T 4MOTION S/SE/SEL	SMALL	UTILITY	4-FI T/C 2.0L	3631	102.5	174.3	71.2	66.3
46	LDV1	2009	PONTIAC	VIBE SW 4WD	AWD	SMALL	STATION WAGON	4-FI 2.4L	3295	102.4	171.1	69.5	62.8
47	LDV1	2005	CHEVROLET	MALIBU MAXX 5D	LS	MIDSIZE	STATION WAGON	6-FI 3.5L	3458	112.3	187.8	69.8	58.1
48	LDV1	2015	SUBARU	OUTBACK SW 4WD W/EYESGHT	2.5I PREMIUM VDC	MIDSIZE	STATION WAGON	4-FI 2.5L	3609	108.1	189.6	72.4	66.1
49	LDV1	2016	SUBARU	OUTBACK SW 4WD W/EYESGHT	3.6R LIMITED VDC NAVI	MIDSIZE	STATION WAGON	6-FI 3.6L	3609	108.1	189.6	72.4	66.1
50	LDV1	2015	SUBARU	FORESTER 4D 4WD	2.5I VDC	SMALL	UTILITY	4-FI 2.5L	3296	103.9	180.9	70.7	66.4
51	LDV1	2010	AUDI	A4 QUATTRO 4D 4WD (NEW)	2.0T PRESTIGE	MIDSIZE	LUXURY	4-FI 2.0L T/C	3626	110.6	185.2	71.9	56.2
52	LDV1	2004	CHEVROLET	MALIBU MAXX 5D	LS	MIDSIZE	STATION WAGON	6-FI 3.5L	3458	112.3	187.8	69.8	59.1
53	LDV1	2013	CHEVROLET	MALIBU 4D (NEW)	2LT ECO	MIDSIZE	4 DOOR	4-FI 2.4L	3393	107.8	191.3	73	57.6
54	LDV1	2008	HONDA	CR-V 4D 4WD	LX	SMALL	UTILITY	4-FI 2.4L	3501	103.1	177.9	71.6	66.1
55	LDV1	2009	HONDA	CR-V 4D 4WD	EX	SMALL	UTILITY	4-FI 2.4L	3501	103.1	177.9	71.6	66.1
56	LDV1	2017	SUBARU	FORESTER 4D 4WD	2.5I PREMIUM VDC	SMALL	UTILITY	4-FI 2.5L	3322	103.9	181.5	70.7	66.4
57	LDV1	2012	SUBARU	OUTBACK SW 4WD	2.5I LIMITED VDC	MIDSIZE	STATION WAGON	4-FI 2.5L	3386	107.9	188.2	71.7	63.9
58	LDV2	2014	FORD	FOCUS 4D	SE	SMALL	4 DOOR	4-FI 2.0L	2907	104.3	178.5	71.8	57.7
59	LDV2	2016	SUBARU	IMPREZA SW 4WD	2.0I SPORT LIMITED VDC	SMALL	STATION WAGON	4-FI 2.0L	2955	104.1	173.8	68.5	57.7
60	LDV2	2006	VOLKSWAGEN	NEW JETTA 4D	2.5	MIDSIZE	4 DOOR	5-FI 2.5L	3230	101.5	179.3	70.1	57.4
61	LDV2	2012	CHEVROLET	CRUZE 4D	2LS	SMALL	4 DOOR	4-FI 1.8L FLEX FUEL	3102	105.7	181	70.7	58.1
62	LDV2	2005	TOYOTA	CAMRY 4D 2WD	STD/LE/XLE/SE	MIDSIZE	4 DOOR	4-FI 2.4L	3108	107.1	189.2	70.7	58.3
63	LDV2	2007	HONDA	ACCORD 4D	SE	MIDSIZE	4 DOOR	4-FI 2.4L	3124	107.9	191.1	71.6	57.2
64	LDV2	2012	FORD	FOCUS 5D	SE	SMALL	STATION WAGON	4-FI 2.0L	2920	104.3	171.6	71.8	57.7
65	LDV2	2015	SUBARU	XV CROSSTREK SW 4WD	2.0I PREMIUM VDC	SMALL	STATION WAGON	4-FI 2.0L	3109	103.7	175.2	70.1	63.6
66	LDV2	2009	SUBARU	FORESTER 4D 4WD	2.5X LIMITED VDC	SMALL	UTILITY	4-FI 2.5L	3250	103	179.5	70.1	65.9
67	LDV2	2006	HONDA	ACCORD 4D	EX	MIDSIZE	4 DOOR	4-FI 2.4L	3128	107.9	191.1	71.6	57.2
68	LDV2	2001	SATURN	LS 4D	L300	MIDSIZE	4 DOOR	6-FI 3.0L	2944	106.5	190.4	68.5	56.4
69	LDV2	2003	CHEVROLET	MALIBU 4D	LS	MIDSIZE	4 DOOR	6-FI 3.1L	3106	107	190.4	69.4	56.2

Appendix Table 1 (continued).

70	LDV2	2008	KIA	OPTIMA 4D (NEW)	NO DATA	MIDSIZE	4 DOOR	6-FI 2.7L	3142	107.1	186.4	71.1	58.3
71	LDV2	2013	CHEVROLET	CRUZE 4D	LS	SMALL	4 DOOR	4-FI 1.8L FLEX FUEL	3082	105.7	181	70.7	58.1
72	LDV2	2015	HONDA	ACCORD 4D	EX	MIDSIZE	4 DOOR	4-FI 2.4L	3192	109.3	191.4	72.8	57.7
73	LDV2	2012	NISSAN	SENTRA 4D	NO DATA	SMALL	4 DOOR	4-FI 2.0L	2906	105.7	179.8	70.5	59.5
74	LDV2	2012	FORD	FOCUS 4D	SE	SMALL	4 DOOR	4-FI 2.0L	2907	104.3	178.5	71.8	57.7
75	LDV2	2016	BUICK	ENCORE 4D 2WD	LEATHER	SMALL	LUXURY UTILITY	-FI 1.4L T/C FLEX FUE	3237	100.6	168.4	69.9	65.2
76	LDV2	2001	NISSAN	810/MAXIMA SEDAN	GXE/SE/GLE	MIDSIZE	4 DOOR	6-EFI 3.0L	3186	108.3	190.5	70.3	56.5
77	LDV2	2014	CHEVROLET	CRUZE 4D	1LT	SMALL	4 DOOR	4-FI 1.4L T/C	3082	105.7	181	70.7	58.1
78	LDV2	2006	TOYOTA	MATRIX SW 4WD	STD/XR	SMALL	STATION WAGON	4-FI 1.8L	2943	102.4	171.3	69.9	60.6
79	LDV2	2014	FORD	FOCUS 4D	SE	SMALL	4 DOOR	4-FI 2.0L	2907	104.3	178.5	71.8	57.7
80	LDV2	2016	HONDA	HR-V 4D 4WD	LX	MINI	UTILITY	4-FI 1.8L	3062	102.8	169.1	69.8	63.2
81	LDV2	2008	TOYOTA	CAMRY 4D 2WD	CE/LE/XLE/SE	MIDSIZE	4 DOOR	4-FI 2.4L	3263	109.3	189.2	71.7	57.9
82	LDV2	2016	CHEVROLET	CRUZE LIMITED 4D	1LT	SMALL	4 DOOR	4-FI 1.4L T/C	3084	105.7	181	70.7	58.1
83	LDV2	2013	CHEVROLET	CRUZE 4D	1LT	SMALL	4 DOOR	4-FI 1.4L T/C	3082	105.7	181	70.7	58.1
84	LDV2	2013	HONDA	ACCORD 4D	LX	MIDSIZE	4 DOOR	4-FI 2.4L	3192	109.3	191.4	72.8	57.7
85	LDV2	2005	TOYOTA	CAMRY 4D 2WD	STD/LE/XLE/SE	MIDSIZE	4 DOOR	4-FI 2.4L	3108	107.1	189.2	70.7	58.3
86	LDV2	2004	TOYOTA	CAMRY 4D 2WD	STD/LE/XLE/SE	MIDSIZE	4 DOOR	4-FI 2.4L	3086	107.1	189.2	70.7	57.9
87	LDV2	2005	KIA	OPTIMA 4D	NO DATA	MIDSIZE	4 DOOR	6-FI 2.7L	3281	106.3	185.8	71.5	55.5
88	LDV2	2009	FORD	FUSION 4D 2WD	SE	MIDSIZE	4 DOOR	4-FI 2.3L	3181	107.4	190.2	72.2	57.2
89	LDV2	2013	HONDA	ACCORD 4D	EX	MIDSIZE	4 DOOR	4-FI 2.4L	3192	109.3	191.4	72.8	57.7
90	LDV2	2005	MERCEDES-BENZ	C CLASS 4D 2WD	230	MIDSIZE	LUXURY	4-FI S/C 1.8L GAS	3250	106.9	178.2	68	55.1
91	LDV2	2011	TOYOTA	CAMRY 4D 2WD	STD/LE/XLE/SE	MIDSIZE	4 DOOR	4-FI 2.5L	3263	109.3	189.2	71.7	57.9
92	LDV3	2008	SATURN	OUTLOOK 4D 2WD	XR	LARGE	UTILITY	6-FI 3.6L	4700	118.9	201.1	78.9	69.9
93	LDV3	2002	TOYOTA	TUNDRA PU AC CAB 4X2	SR5 V8	LARGE	PICKUP	8-FI 4.7L	4088	128.3	217.5	75.2	70.7
94	LDV3	2015	TOYOTA	SIENNA VAN 2WD	XLE/LIMITED V6 5D	VERY LARGE	MINIVAN	6-FI 3.5L	4375	119.3	200.2	78.1	68.9
95	LDV3	2012	HONDA	ODYSSEY VAN (NEW)	EXL/EXL-N/EXL-R	VERY LARGE	MINIVAN	6-FI 3.5L	4337	118.1	202.9	79.2	68.4
96	LDV3	2010	TOYOTA	SIENNA VAN 4WD	XLE/XLE LIMITED 5D	VERY LARGE	MINIVAN	6-FI 3.5L	4515	119.3	201	77.4	68.9
97	LDV3	2016	TOYOTA	HIGHLANDER 4D 4WD	XLE V6	MIDSIZE	UTILITY	6-FI 3.5L	4398	109.8	191.1	75.8	68.1
98	LDV3	2004	MERCURY	MONTEREY VAN	NO DATA	VERY LARGE	MINIVAN	6-EFI 4.2L	4340	120.8	201.5	76.6	68.8
99	LDV3	2016	HONDA	ODYSSEY VAN (NEW)	EX	VERY LARGE	MINIVAN	6-FI 3.5L	4396	118.1	202.9	79.2	68.4
100	LDV3	2007	HONDA	ODYSSEY VAN (NEW)	EX-L	VERY LARGE	MINIVAN	6-FI 3.5L	4384	118.1	201	77.1	68.8
101	LDV3	2015	HONDA	ODYSSEY VAN (NEW)	EXL/EXL-N/EXL-R	VERY LARGE	MINIVAN	6-FI 3.5L	4396	118.1	202.9	79.2	68.4
102	LDV3	2011	LEXUS	RX 350 4D 4WD	NO DATA	MIDSIZE	LUXURY UTILITY	6-FI 3.5L	4343	107.9	187.8	74.2	67.7
103	LDV3	2008	TOYOTA	SIENNA VAN 4WD	LE 5D	VERY LARGE	MINIVAN	6-FI 3.5L	4398	119.3	201	77.4	68.9
104	LDV3	2017	LEXUS	RX 350 4D 4WD	NO DATA	MIDSIZE	LUXURY UTILITY	6-FI 3.5L	4387	109.8	192.5	74.6	67.7
105	LDV3	2006	LEXUS	RX 330 4D 4WD	NO DATA	MIDSIZE	LUXURY UTILITY	6-FI 3.3L	4065	106.9	186.2	72.6	66.1
106	LDV3	2007	TOYOTA	SIENNA VAN 2WD	XLE/XLE LIMITED 5D	VERY LARGE	MINIVAN	6-FI 3.5L	4270	119.3	201	77.4	68.9
107	LDV3	2007	TOYOTA	SIENNA VAN 4WD	LE 5D	VERY LARGE	MINIVAN	6-FI 3.5L	4515	119.3	201	77.4	68.9
108	LDV4	2009	HONDA	FIT SW	SPORT	MINI	STATION WAGON	4-FI 1.5L	2489	98.4	161.6	66.7	60
109	LDV4	2010	TOYOTA	COROLLA SEDAN 2WD	STD/S/LE/XLE	SMALL	4 DOOR	4-FI 1.8L	2723	102.4	178.7	69.3	57.7
110	LDV4	2010	HONDA	CIVIC 4D	LX	SMALL	4 DOOR	4-FI 1.8L	2630	106.3	177.3	69	56.5

Appendix Table 1 (continued).

111	LDV4	2005	FORD	FOCUS 4D	ZX4	SMALL	4 DOOR	4-FI 2.0L PZEV	2697	102.9	175.2	66.7	56.8
112	LDV4	2006	HONDA	CIVIC 4D	EX	SMALL	4 DOOR	4-FI 1.8L	2628	106.3	176.7	69	56.5
113	LDV4	2006	MAZDA	3 4D	I	SMALL	4 DOOR	4-FI 2.0L	2685	103.9	178.3	69.1	57.7
114	LDV4	2009	HONDA	FIT SW	SPORT NAVI	MINI	STATION WAGON	4-FI 1.5L	2489	98.4	161.6	66.7	60
115	LDV4	2007	HONDA	CIVIC 4D	LX	SMALL	4 DOOR	4-FI 1.8L	2628	106.3	176.7	69	56.5
116	LDV4	1998	MAZDA	626 SEDAN	DX/LX	MIDSIZE	4 DOOR	4-FI 2.0L	2798	105.1	186.8	69.3	55.1
117	LDV4	2006	HONDA	CIVIC 4D	LX	SMALL	4 DOOR	4-FI 1.8L	2628	106.3	176.7	69	56.5
118	LDV4	2010	FORD	FOCUS 4D	SE	SMALL	4 DOOR	4-FI 2.0L	2623	102.9	175	67.8	58.6
119	LDV4	2004	PONTIAC	VIBE SW 2WD	NO DATA	SMALL	STATION WAGON	4-FI 1.8L	2700	102.4	171.9	69.9	62.2
120	LDV4	2010	FORD	FOCUS 2D	SE	SMALL	2 DOOR	4-FI 2.0L	2588	102.9	175	67.9	58.6
121	LDV4	2010	FORD	FOCUS 4D	SE	SMALL	4 DOOR	4-FI 2.0L	2623	102.9	175	67.8	58.6
122	LDV4	2014	TOYOTA	YARIS 5D	L/LE/SE	MINI	4 DOOR	4-FI 1.5L	2315	98.8	153.5	66.7	59.4
123	LDV4	2009	TOYOTA	COROLLA SEDAN 2WD	STD/LE/XLE	SMALL	4 DOOR	4-FI 1.8L	2723	102.4	178.7	69.3	57.7
124	LDV4	2004	HYUNDAI	ELANTRA 4D	GLS/GT	SMALL	4 DOOR	4-FI 2.0L	2635	102.7	178.1	67.9	56.1
125	LDV4	2011	NISSAN	VERSA 5D	1.8 S/1.8 SL	SMALL	4 DOOR	4-FI 1.8L	2693	102.4	169.1	66.7	60.4
126	LDV4	2013	HONDA	FIT SW	NO DATA	MINI	STATION WAGON	4-FI 1.5L	2496	98.4	161.6	66.7	60
127	LDV4	2015	HONDA	CIVIC 4D	LX	SMALL	4 DOOR	4-FI 1.8L	2754	105.1	179.4	69	56.5
128	LDV4	2006	FORD	FOCUS 4D	ZX4	SMALL	4 DOOR	4-FI 2.0L PZEV	2636	102.9	175.2	66.7	56.9
129	LDV4	2009	FORD	FOCUS 4D	SE	SMALL	4 DOOR	4-FI 2.0L	2623	102.9	175	67.8	58.6
130	LDV4	2007	FORD	FOCUS 4D	ZX5 HATCHBACK	SMALL	4 DOOR	4-FI 2.0L PZEV	2636	102.9	175.2	66.7	56.9
131	LDV4	2017	CHEVROLET	CRUZE 4D	LS	SMALL	4 DOOR	4-FI 1.4L T/C	2835	106.3	183.7	70.5	57.4
132	LDV4	2014	TOYOTA	COROLLA SEDAN 2WD	L/LE/S	SMALL	4 DOOR	4-FI 1.8L	2800	106.3	182.6	69.9	57.3
133	LDV4	2006	PONTIAC	VIBE SW 2WD	NO DATA	SMALL	STATION WAGON	4-FI 1.8L	2701	102.4	171.9	69.9	62.2
134	LDV4	2005	PONTIAC	VIBE SW 2WD	NO DATA	SMALL	STATION WAGON	4-FI 1.8L	2701	102.4	171.9	69.9	62.2
135	LDV4	2009	FORD	FOCUS 4D	SES	SMALL	4 DOOR	4-FI 2.0L	2623	102.9	175	67.8	58.6
136	LDV4	2010	FORD	FOCUS 4D	S	SMALL	4 DOOR	4-FI 2.0L	2623	102.9	175	67.8	58.6
137	LDV4	2012	HONDA	FIT SW	SPORT	MINI	STATION WAGON	4-FI 1.5L	2496	98.4	161.6	66.7	60
138	LDV4	2017	HONDA	FIT SW	EX	MINI	STATION WAGON	4-FI 1.5L	2513	99.6	160	67	60
139	LDV4	2015	NISSAN	VERSA 4D	1.6 S/S PLUS/SV/SL	SMALL	4 DOOR	4-FI 1.6L	2363	102.4	175.4	66.7	59.6
140	LDV4	2006	HONDA	CIVIC 4D	EX	SMALL	4 DOOR	4-FI 1.8L	2628	106.3	176.7	69	56.5
141	LDV4	2005	NISSAN	SENTRA 4D	NO DATA	SMALL	4 DOOR	4-FI 1.8L	2513	99.8	177.5	67.3	55.5
142	LDT1	2017	HEVROLET TRUC	EQUINOX 4D 2WD	LT/FLEET	MIDSIZE	UTILITY	4-FI 2.4L	3777	112.5	187.8	72.5	66.3
143	LDT1	2010	HEVROLET TRUC	HHR SW 2WD	LS	SMALL	STATION WAGON	4-FI 2.2L FLEX FUEL	3155	103.6	176.2	69.1	62.5
144	LDT1	1999	HEVROLET TRUC	ASTRO EXT CG VAN 4X2	TRUCK	LARGE	ARGO / PASSENGER VA	6-FI 4.3L	3887	111.2	189.8	77.5	74.9
145	LDT1	2011	HEVROLET TRUC	EQUINOX 4D 4WD	2LT	MIDSIZE	UTILITY	6-FI 3.0L FLEX FUEL	3929	112.5	187.8	72.5	66.3
146	LDT1	2010	FORD TRUCK	ESCAPE 4D 4WD	XLT	SMALL	UTILITY	4-FI 2.5L	3504	103.1	174.7	71.1	67.8
147	LDT1	2017	HEVROLET TRUC	EQUINOX 4D 2WD	LS	MIDSIZE	UTILITY	4-FI 2.4L	3777	112.5	187.8	72.5	66.3
148	LDT1	2007	FORD TRUCK	ESCAPE 4D 2WD	XLT	SMALL	UTILITY	4-FI 2.3L	3156	103.2	174.9	70.1	67.9
149	LDT1	2010	GMC TRUCK	TERRAIN 4D 2WD	SLT1	MIDSIZE	UTILITY	6-FI 3.0L	3798	112.5	185.3	72.8	66.3
150	LDT1	2006	HEVROLET TRUC	HHR SW 2WD	LT	SMALL	STATION WAGON	4-FI 2.4L	3155	103.5	176.2	68.1	61.5
151	LDT1	2016	HEVROLET TRUC	EQUINOX 4D 2WD	LT	MIDSIZE	UTILITY	4-FI 2.4L	3777	112.5	187.8	72.5	66.3

Appendix Table 1 (continued).

152	LDT1	2012	HEVROLET TRUC	EQUINOX 4D 2WD	1LT	MIDSIZE	UTILITY	4-FI 2.4L	3777	112.5	187.8	72.5	66.3
153	LDT1	2012	FORD TRUCK	ESCAPE 4D 2WD	XLT	SMALL	UTILITY	4-FI 2.5L	3229	103.1	174.7	71.1	67.9
154	LDT1	2014	FORD TRUCK	EDGE 4D 2WD	SPORT	MIDSIZE	UTILITY	6-FI 3.7L	3999	111.2	184.2	76	67
155	LDT1	2017	HEVROLET TRUC	EQUINOX 4D 2WD	LT/FLEET	MIDSIZE	UTILITY	4-FI 2.4L	3777	112.5	187.8	72.5	66.3
156	LDT1	2000	FORD TRUCK	WINDSTAR VAN	SEL	VERY LARG	MINIVAN	6-FI 3.8L	3890	120.7	200.9	75.2	65.6
157	LDT1	2017	HEVROLET TRUC	EQUINOX 4D 2WD	LT/FLEET	MIDSIZE	UTILITY	4-FI 2.4L	3777	112.5	187.8	72.5	66.3
158	LDT1	2006	FORD TRUCK	ESCAPE 4D 4WD	LIMITED	SMALL	UTILITY	6-EFI 3.0L	3347	103.2	174.9	70.1	67.6
159	LDT1	2017	HEVROLET TRUC	EQUINOX 4D 2WD	PREMIER	MIDSIZE	UTILITY	4-FI 2.4L	3777	112.5	187.8	72.5	66.3
160	LDT2	2016	HEVROLET TRUC	TRAVERSE 4D 2WD	LS	LARGE	UTILITY	6-FI 3.6L	4713	118.9	203.7	78.5	69.9
161	LDT2	2004	FORD TRUCK	F150 SUPER PU 4X2 (NEW)	STYLESIDE	LARGE	PICKUP	8-FI 4.6L	4993	132.5	218	78.9	73.1
162	LDT2	2014	FORD TRUCK	EXPLORER 4D 4X4	XLT	MIDSIZE	UTILITY	6-FI 3.5L	4610	112.6	197.1	78.9	71
163	LDT2	2002	GMC TRUCK	YUKON 4D 4X2 (NEW)	NO DATA	LARGE	UTILITY	8-FI 4.8L	4875	116	198.8	78.8	76.7
164	LDT2	2012	FORD TRUCK	FLEX 4D 2WD	SEL	MIDSIZE	UTILITY	6-FI 3.5L	4448	117.9	201.8	75.9	68
165	LDT2	2017	GMC TRUCK	ACADIA 4D 4WD	SLE2	MIDSIZE	UTILITY	6-FI 3.6L	4156	112.5	193.6	75.4	68.7
166	LDT2	2011	FORD TRUCK	FLEX 4D 2WD	SEL	MIDSIZE	UTILITY	6-FI 3.5L	4471	117.9	201.8	75.9	68
167	LDT3	2013	GMC TRUCK	SIERRA 2500 4X4 NEW	NO DATA	VERY LARG	PICKUP	8-4V/FI 6.0L	5962	133.7	225	80	77.6
168	LDT3	2013	GMC TRUCK	SIERRA 2500 4X4 NEW	NO DATA	VERY LARG	PICKUP	8-4V/FI 6.0L	5962	133.7	225	80	77.6
169	LDT3	2009	GMC TRUCK	YUKON 4D 4X4 (NEW)	SLE	LARGE	UTILITY	8-FI 5.3L FLEX FUEL	5536	116	202	79	77
170	LDT3	2013	HEVROLET TRUC	SLVRDO 1500 CR 4X4 NEW	NO DATA	LARGE	PICKUP	8-FI 4.8L	5410	143.5	230	80	73.7
171	LDT3	2013	GMC TRUCK	SAVANA CG VAN 2500 4X2	NO DATA	LARGE	ARGO / PASSENGER VA	8-FI 4.8L	5291	135	224	79.2	81.5
172	LDT3	2014	FORD TRUCK	F150 SUPER PU 4X4 (NEW)	SUPER CAB	LARGE	PICKUP	8-EFI 5.0L	6016	133.3	220.6	86.3	78.5
173	LDT3	2010	GMC TRUCK	YUKON XL 1/2T 4D 4X2	SLT	VERY LARG	UTILITY	8-FI 5.3L FLEX FUEL	5621	130	222.4	79.1	76.8
174	LDT3	2004	HEVROLET TRUC	SUBURBAN 1/2T 4D 4X4	4-WHEEL DRIVE	VERY LARG	UTILITY	8-FI 5.3L FLEX FUEL	5219	130	219.3	78.9	75.4

Bibliography

"Brian" Park, B., Yun, I., & Ahn, K. (2009). Stochastic optimization for sustainable traffic signal control. *International journal of sustainable transportation*, *3*(4), 263-284.

Abudayyeh, D., Nicholson, A., & Ngoduy, D. (2021). Traffic signal optimisation in disrupted networks, to improve resilience and sustainability. *Travel Behaviour and Society*, *22*, 117-128.

Ahn, K., Rakha, H., Trani, A., & Van Aerde, M. (2002). Estimating vehicle fuel consumption and emissions based on instantaneous speed and acceleration levels. *Journal of transportation engineering*, *128*(2), 182-190.

Akcelik, R. (1981). Fuel efficiency and other objectives in traffic system management. *Traffic Engineering and Control*, *22*(2), 54-65.

Akcelik, R. (1982). New approximate expressions for delay, stop rate and queue length at isolated signals.

Ali, M. S., Kitali, A. E., Kodi, J. H., Alluri, P., & Sando, T. (2021). Safety impacts of transit signal priority using a full Bayesian approach. Transportation research record, 2675(11), 1189-1204.

Ali, M. S., Kitali, A. E., Kodi, J., Alluri, P., & Sando, T. (2022). Quantifying the Safety Benefits of Transit Signal Priority Using Full Bayes Before–After Study. Journal of Transportation Engineering, Part A: Systems, 148(1), 04021102.

Al-Khalili, A. J. (1985). Urban traffic control—A general approach. *IEEE transactions on systems, man, and cybernetics*, (2), 260-271.

Al-Khalili, A., & El-Hakeem, A. K. (1984). A computer control system for minimization of fuel consumption in urban traffic network. In *IEEE Real Time Systems Symposium* (pp. 249-254).

Alonso, B., Ibeas, Á., Musolino, G., Rindone, C., & Vitetta, A. (2019). Effects of traffic control regulation on Network Macroscopic Fundamental Diagram: A statistical analysis of real data. *Transportation Research Part A: Policy and Practice*, *126*, 136-151.

Alonso, B., Pòrtilla, Á. I., Musolino, G., Rindone, C., & Vitetta, A. (2017). Network Fundamental Diagram (NFD) and traffic signal control: First empirical evidences from the city of Santander. *Transportation research procedia*, *27*, 27-34.

Alshayeb, S., Stevanovic, A., & Dobrota, N. (2021b). Impact of Various Operating Conditions on Simulated Emissions-Based Stop Penalty at Signalized Intersections. *Sustainability*, *13*(18), 10037.

Alshayeb, S., Stevanovic, A., & Effinger, J. R. (2021a). Investigating impacts of various operational conditions on fuel consumption and stop penalty at signalized intersections. *International Journal of Transportation Science and Technology*.

Alshayeb, S.; Stevanovic, A.; Park, B; (2022c) Field-based Prediction Models for Stop Penalty in Traffic Signal Timing Optimization. In Proceedings of the 101st Annual Meeting of the Transportation Research Board, Washington, DC, USA.

Alzoubaidi, A. R., Alzoubaidi, M., Ismaiel Abu Mahfouz, T., Alkhamis, F. F. S. A. (2021a), M. Virtual Desktop Infrastructure in Higher Education Institution: An Application of Home and Mobile Computing Environment.

Alzoubaidi, M., Molan, A. M., & Ksaibati, K. (2021b). Comparing the efficiency of the super diverging diamond interchange to other innovative interchanges'. *Simulation Modelling Practice and Theory*, *106*, 102174.

An, F., Barth, M., Norbeck, J., & Ross, M. (1997). Development of comprehensive modal emissions model: operating under hot-stabilized conditions. *Transportation Research Record*, *1587*(1), 52-62.

Arafat, M., Hadi, M., Hunsanon, T., & Amine, K. (2021a). Stop sign gap assist application in a connected vehicle simulation environment. *Transportation research record*, *2675*(9), 1127-1135.

Arafat, M., Hadi, M., Raihan, M. A., Iqbal, M. S., & Tariq, M. T. (2021b). Benefits of connected vehicle signalized left-turn assist: Simulation-based study. *Transportation Engineering*, *4*, 100065.

Ardalan, T., Kaisar, E. I., & Tabassum, A. Operation and Safety Analysis of Turbo-roundabout and Conventional Intersections on Freight Movements 2. 6th International Symposium on Highway Geometric Design.

Aslani, M., Mesgari, M. S., & Wiering, M. (2017). Adaptive traffic signal control with actor-critic methods in a real-world traffic network with different traffic disruption events. *Transportation Research Part C: Emerging Technologies*, *85*, 732-752.

Bando, M., Hasebe, K., Nakayama, A., Shibata, A., & Sugiyama, Y. (1995). Dynamical model of traffic congestion and numerical simulation. *Physical review E*, *51*(2), 1035.

Banister, D. (2008). The sustainable mobility paradigm. *Transport policy*, *15*(2), 73-80.

Barth, M., An, F., Younglove, T., Scora, G., Levine, C., Ross, M., & Wenzel, T. (2000). The development of a comprehensive modal emissions model. *NCHRP Web-only document*, *122*, 25-11.

Barth, M., Malcolm, C., Younglove, T., & Hill, N. (2001). Recent validation efforts for a comprehensive modal emissions model. *Transportation Research Record*, *1750*(1), 13-23.

Bauer, C. S. (1975). Some energy considerations in traffic signal timing. *Traffic Engineering*, *45*(2).

Boriboonsomsin, K., & Barth, M. (2009). Impacts of road grade on fuel consumption and carbon dioxide emissions evidenced by use of advanced navigation systems. *Transportation Research Record*, *2139*(1), 21-30.

Cai, M., Yin, Y., & Xie, M. (2009). Prediction of hourly air pollutant concentrations near urban arterials using artificial neural network approach. *Transportation Research Part D: Transport and Environment*, *14*(1), 32-41.

Cheng, Y., Qin, X., Jin, J., & Ran, B. (2010, January). An exploratory shockwave approach for signalized intersection performance measurements using probe trajectories. In *89th Annual Meeting of Transportation Research Board*.

Chiou, S. W. (1999). Optimization of area traffic control for equilibrium network flows. *Transportation Science*, *33*(3), 279-289.

Christofa, E., Ampountolas, K., & Skabardonis, A. (2016). Arterial traffic signal optimization: A person-based approach. *Transportation Research Part C: Emerging Technologies*, *66*, 27-47.

Claffey, P. J. (1971). Running costs of motor vehicles as affected by road design and traffic. *NCHRP Report*, (111).

Claffey, P. J. (1976). *Passenger car fuel conservation* (No. FHWA/Pl-77/009 Final Rpt.).

Cohen, S. L., & Euler, G. (1978). *Signal cycle length and fuel consumption and emissions* (No. HS-025 846).

Courage, K. G., & Parapar, S. M. (1975). Delay and fuel consumption at traffic signals. *Traffic Engineering*, *45*(11).

Croce, A. I., Musolino, G., Rindone, C., & Vitetta, A. (2021). Estimation of travel demand models with limited information: Floating car data for parameters' calibration. *Sustainability*, *13*(16), 8838.

Daganzo, C. F. (1994). The cell transmission model: A dynamic representation of highway traffic consistent with the hydrodynamic theory. *Transportation Research Part B: Methodological*, *28*(4), 269-287.

Daganzo, C. F. (1995). The cell transmission model, part II: network traffic. *Transportation Research Part B: Methodological*, *29*(2), 79-93.

Dart, O. K., & Mann, L. (1978). Potential Energy Conservation in Louisiana's Cities through Traffic Engineering Measures. In *48th Annual Meeting of the Institute of Transportation Engineers, Atlanta, GA* (pp. 300-309).

David, H.; John, A. (2006). Synchro Studio 7 User Guide; Trafficware, Ltd.: Houston, TX, USA, pp. 4–6.

Department of Energy, (2021), Available online: https://www.energy.gov/ (accessed on 1 September 2021).

Ding, S., Chen, X., Yu, L., & Wang, X. (2019). Arterial Offset Optimization Considering the Delay and Emission of Platoon: A Case Study in Beijing. *Sustainability*, *11*(14), 3882.

Dobrota, N., & Stevanovic, A. (2021a). Modelling of Delay for Protected/Permitted Left Turning Vehicles using Multigene Genetic Programming.

Dobrota, N., Stevanovic, A., & Mitrovic, N. (2020). Development of assessment tool and overview of adaptive traffic control deployments in the US. *Transportation research record*, *2674*(12), 464-480.

Dobrota, N., Stevanovic, A., & Mitrovic, N. (2021b). Modifying Signal Retiming Procedures and Policies by Utilizing High-Fidelity Modeling with Medium-Resolution Traffic Data. *Transportation Research Record*, 03611981211055668.

Dobrota, N., Stevanovic, A., & Mitrovic, N. (2022). A novel model to jointly estimate delay and arrival patterns by using high-resolution signal and detection data. *Transportmetrica A: Transport Science*, 1-33.

Dobrota, N., Stevanovic, A., Mitrovic, N., & Chowdhury, S. E. (2019). *Signal Retiming Based on Comprehensive Field Data Analysis and High-Fidelity Simulation Modeling* (No. 19-03340).

Driver-Centric Fleet Management Solutions [Internet]. ISAAC Instruments. (2021). [updated 2021 Jul 9 cited 2021 Jul 22]. Available online: https://isaacinstruments.com/en/ (accessed on 3 November 2021).

Early Deployment of TRANSIMS. (1999, August). https://web.archive.org/web/20100527134930/http://tmip.fhwa.dot.gov/resources/clearinghouse/docs/issue_paper/issue_paper.pdf

El-Shawarby, I., Ahn, K., & Rakha, H. (2005). Comparative field evaluation of vehicle cruise speed and acceleration level impacts on hot stabilized emissions. *Transportation Research Part D: Transport and Environment*, *10*(1), 13-30.

EPA, (2019a), Us transportation sector greenhouse gas emissions 1990-2017 https://www.epa.gov/greenvehicles/fast-facts-transportation-greenhouse-gas-emissions; (accessed on 12/14/2020)

EPA, (2019b), Environmental Protection Agency. History of Air Pollution. Available online: https://www.epa.gov/air-research/historyair-pollution (accessed on 15 July 2021).

EPA, (2019c), Environmental Protection Agency. How Does PM Affect Human Health? Available online: https://www3.epa.gov/region1/airquality/pm-human-health.html (accessed on 4 June 2021).

EPA, (2019d), Environmental Protection Agency. Transportation Sector Emissions. Available online: https://www.epa.gov/ghgemissions/sources-greenhouse-gas-emissions#transportation (accessed on 4 June 2021).

EPA, (2019e), Environmental Protection Agency. Smog, Soot, and Other Air Pollution from Transportation. Available online: https://www.epa.gov/transportation-air-pollution-and-climate-change/smog-soot-and-local-air-pollution (accessed on 4 June 2021).

EPA, (2019f), Environmental Protection Agency. Carbon Pollution from Transportation. Available online: https://www.epa.gov/transportation-air-pollution-and-climate-change/carbon-pollution-transportation (accessed on 4 June 2021).

EPA, (2019g), Environmental Protection Agency. Air Pollution Emissions Overview. Available online: https://www3.epa.gov/airquality/ emissns.html (accessed on 4 June 2021).

EPA, (2019h), Environmental Protection Agency. Basic Information about Carbon Monoxide (CO) Outdoor Air Pollution. Available online: https://www.epa.gov/co-pollution/basic-information-about-carbon-monoxide-co-outdoor-air-pollution#Effects (accessed on 4 June 2021).

EPA, (2019i), Environmental Protection Agency. Overview of Greenhouse Gases. Available online: https://www.epa.gov/ghgemissions/overview-greenhouse-gases#carbon-dioxide (accessed on 4 June 2021).

EPA, (2019j), Environmental Protection Agency. Effects of Acid Rain. Available online: https://www.epa.gov/acidrain/effects-acid-rain (accessed on 4 June 2021).

EPA, (2019k), Environmental Protection Agency. Basic Information about NO2. Available online: https://www.epa.gov/no2-pollution/basic-information-about-no2#Effects (accessed on 4 June 2021).

EPA, (2019l), Environmental Protection Agency. Ground-Level Ozone Basics. Available online: https://www.epa.gov/ground-levelozone-pollution/ground-level-ozone-basics (accessed on 4 June 2021).

Fisher, R. A. (1992). The arrangement of field experiments. In *Breakthroughs in statistics* (pp. 82-91). Springer, New York, NY.

Frey, H. C., Rouphail, N. M., Unal, A., & Colyar, J. D. (2001). *Emissions reduction through better traffic management: An empirical evaluation based upon on-road measurements* (No. FHWA/NC/2002-001).

Frey, H. C., Unal, A., & Chen, J. (2002, February). Recommended strategy for on-board emission data analysis and collection for the new generation model. In *Proceedings of the 12th CRC On-Road Vehicle Emissions Workshop, San Diego, CA*.

Frey, H. C., Unal, A., Rouphail, N. M., & Colyar, J. D. (2003). On-road measurement of vehicle tailpipe emissions using a portable instrument. *Journal of the Air & Waste Management Association*, *53*(8), 992-1002.

Gallus, J., Kirchner, U., Vogt, R., & Benter, T. (2017). Impact of driving style and road grade on gaseous exhaust emissions of passenger vehicles measured by a Portable Emission Measurement System (PEMS). *Transportation Research Part D: Transport and Environment*, *52*, 215-226.

Gamboa-Rosales, N. K., Celaya-Padilla, J. M., Hernandez-Gutierrez, A. L., Moreno-Baez, A., Galván-Tejada, C. E., Galván-Tejada, J. I., ... & López-Robles, J. R. (2020). Visualizing the Intellectual Structure and Evolution of Intelligent Transportation Systems: A Systematic Analysis of Research Themes and Trends. *Sustainability*, *12*(21), 8759.

Gandomi, A. H., & Alavi, A. H. (2012). A new multi-gene genetic programming approach to nonlinear system modeling. Part I: materials and structural engineering problems. *Neural Computing and Applications*, *21*(1), 171-187.

Gartner, N. H., Assman, S. F., Lasaga, F., & Hou, D. L. (1991). A multi-band approach to arterial traffic signal optimization. *Transportation Research Part B: Methodological*, *25*(1), 55-74.

Gates, B. (2021). *How to avoid a climate disaster: the solutions we have and the breakthroughs we need*. Knopf.

Gavric, S., Sarazhinsky, D., Stevanovic, A., & Dobrota, N. (2022, January). Evaluation of Pedestrian Timing Treatments for Coordinated Signalized Intersections. In *Proceedings of the Transportation Research Board 101st Annual Meeting, Washington, DC, USA* (pp. 9-13).

Gipps, P. G. (1981). A behavioural car-following model for computer simulation. *Transportation Research Part B: Methodological*, *15*(2), 105-111.

Gordon, R. L. (2010). *Traffic signal retiming practices in the United States* (Vol. 409). Transportation Research Board.

Hall, J. V. (1996). Assessing health effects of air pollution. *Atmospheric environment*, *30*(5), 743-746.

Han, K., Liu, H., Gayah, V. V., Friesz, T. L., & Yao, T. (2016). A robust optimization approach for dynamic traffic signal control with emission considerations. *Transportation Research Part C: Emerging Technologies*, *70*, 3-26.

Hancock, M. W., & Wright, B. (2013). A policy on geometric design of highways and streets. *American Association of State Highway and Transportation Officials: Washington, DC, USA*.

Hannah, L. (2021). *Climate change biology*. Academic Press.

Hartigan, J. A., & Wong, M. A. (1979). Algorithm AS 136: A k-means clustering algorithm. *Journal of the royal statistical society. series c (applied statistics)*, *28*(1), 100-108.

Heide, C. H., & Mohazzabi, P. (2013). Fuel economy of a vehicle as a function of airspeed: the concept of parallel corridors. *International Journal of Energy and Environmental Engineering*, *4*(1), 1-7.

Hillier, V. A. W., & Coombes, P. (2004). *Hillier's fundamentals of motor vehicle technology*. Nelson Thornes.

Hirokazu Kato, et al. (2002). Emission estimation model based on vehicle driving mode for the purpose of environmental evaluation of improved traffic measures. in JSCE 30th, 135-141.

Hitchcock, O., & Gayah, V. V. (2018). Methods to reduce dimensionality and identify candidate solutions in multi-objective signal timing problems. *Transportation Research Part C: Emerging Technologies*, *96*, 398-414.

Holland, J. H. (1992). Genetic algorithms. *Scientific american*, *267*(1), 66-73.

Horiguchi, R., Katakura, M., Akahane, H., & Kuwahara, M. (1994, August). A development of a traffic simulator for urban road networks: AVENUE. In *Proceedings of VNIS'94-1994 Vehicle Navigation and Information Systems Conference* (pp. 245-250). IEEE.

Huang, Z. (1997, February). Clustering large data sets with mixed numeric and categorical values. In *Proceedings of the 1st pacific-asia conference on knowledge discovery and data mining,(PAKDD)* (pp. 21-34).

Hull Grasso, S., Barnes, P., & Chavis, C. (2020). Bike Share Equity for Underrepresented Groups: Analyzing Barriers to System Usage in Baltimore, Maryland. *Sustainability*, *12*(18), 7600.

Hurley, J. W., & Ball, R. P. (1979). Evaluation of Energy-Based Signal Settings for Traffic-Actuated Control. *Modeling and Simulation*, *10*.

Husch, D., Albeck, J., (2006). Synchro Studio 7 User Guide. Trafficware. 522, p.

INL, (2021), Idaho National Laboratory. Available online: https://inl.gov/ (accessed on 1 September 2021).

Iqbal, M. S., Ardalan, T., Hadi, M., & Kaisar, E. I. (2021a). *Developing Guidelines for Implementing Transit Signal Priority (TSP) and Freight Signal Priority (FSP) Using Simulation Modeling and Decision Tree Algorithm* (No. TRBAM-21-03266).

Iqbal, S., Ardalan, T., Hadi, M., & Kaisar, E. (2021b). Developing Guidelines for Implementing Transit Signal Priority and Freight Signal Priority Using Simulation Modeling and a Decision Tree Algorithm. *Transportation Research Record*, 03611981211057528.

ITT Industries, Inc. (2001). CORSIM Reference Manual: Version 5.0. Colorado Springs, CO: Systems Division and ATMS R&D and Systems Engineering Program Team, ITT Industries.

Jie, L., Van Zuylen, H., Chen, Y., Viti, F., & Wilmink, I. (2013). Calibration of a microscopic simulation model for emission calculation. *Transportation Research Part C: Emerging Technologies*, *31*, 172-184.

Jimenez-Palacios, J. L. (1998). Understanding and quantifying motor vehicle emissions with vehicle specific power and TILDAS remote sensing. *Massachusetts Institute of Technology*.

Kaisar, E. I., Liu, D., & Ardalan, T. (2019). Evaluation of truck tonnage estimation methodologies.

Karam, A., & Hegner Reinau, K. (2021). Evaluating the Effects of the A-Double Vehicle Combinations If Introduced to a Line-Haul Freight Transport Network. *Sustainability*, *13*(15), 8622.

Khalighi, F., & Christofa, E. (2015). Emission-based signal timing optimization for isolated intersections. *Transportation Research Record*, *2487*(1), 1-14.

Kodi, J. H., Kitali, A. E., Ali, M. S., Alluri, P., & Sando, T. (2021). Estimating safety impacts of adaptive signal control technology using a full Bayesian approach. Transportation Research Record, 2675(11), 1168-1179.

Koonce, P., & Rodegerdts, L. (2008). *Traffic signal timing manual* (No. FHWA-HOP-08-024). United States. Federal Highway Administration.

Koza, J. R., & Koza, J. R. (1992). *Genetic programming: on the programming of computers by means of natural selection* (Vol. 1). MIT press.

Krajzewicz, D., Erdmann, J., Behrisch, M., & Bieker, L. (2012). Recent development and applications of SUMO-Simulation of Urban MObility. *International journal on advances in systems and measurements*, *5*(3&4).

Kwak, J., Park, B., & Lee, J. (2012). Evaluating the impacts of urban corridor traffic signal optimization on vehicle emissions and fuel consumption. *Transportation Planning and Technology*, *35*(2), 145-160.

Li, J. Q., Wu, G., & Zou, N. (2011). Investigation of the impacts of signal timing on vehicle emissions at an isolated intersection. *Transportation Research Part D: Transport and Environment*, *16*(5), 409-414.

Li, X. G., Yu, L., & Wang, W. (2003, January). Derivation of emission factors for Nanjing, China using MOBILE5. In *Proceeding of the 82nd Annual Meeting of Transportation Research Board (CD-ROM), TRB paper* (pp. 03-2913).

Li, X., Li, G., Pang, S. S., Yang, X., & Tian, J. (2004). Signal timing of intersections using integrated optimization of traffic quality, emissions and fuel consumption: a note. *Transportation Research Part D: Transport and Environment*, *9*(5), 401-407.

Li, Z., Yu, H., Zhang, G., Dong, S., & Xu, C. Z. (2021). Network-wide traffic signal control optimization using a multi-agent deep reinforcement learning. *Transportation Research Part C: Emerging Technologies*, *125*, 103059.

Liao, T. Y. (2013). A fuel-based signal optimization model. *Transportation Research Part D: Transport and Environment*, *23*, 1-8.

Liao, T. Y., & Machemehl, R. B. (1998). Development of an aggregate fuel consumption model for signalized intersections. *Transportation research record*, *1641*(1), 9-18.

Liao, T. Y., Hu, T. Y., Chen, L. W., & Ho, W. M. (2010). Development and empirical study of real-time simulation-based dynamic traffic assignment model. *Journal of transportation engineering*, *136*(11), 1008-1020.

Lighthill, M. J., & Whitham, G. B. (1955). On kinematic waves II. A theory of traffic flow on long crowded roads. *Proceedings of the Royal Society of London. Series A. Mathematical and Physical Sciences*, *229*(1178), 317-345.

Lighthill, M. J., & Whitham, G. B. (1955). On kinematic waves II. A theory of traffic flow on long crowded roads. *Proceedings of the Royal Society of London. Series A. Mathematical and Physical Sciences*, *229*(1178), 317-345.

Liu, H., Lu, X. Y., & Shladover, S. E. (2019). Traffic signal control by leveraging Cooperative Adaptive Cruise Control (CACC) vehicle platooning capabilities. *Transportation research part C: emerging technologies*, *104*, 390-407.

Lv, J., Zhang, Y., & Zietsman, J. (2013). Investigating emission reduction benefit from intersection signal optimization. *Journal of Intelligent Transportation Systems*, *17*(3), 200-209.

Ma, C., Yu, C., & Yang, X. (2021). Trajectory Planning for Connected and Automated Vehicles at Isolated Signalized Intersections under Mixed Traffic Environment. *Transportation research part C: emerging technologies*, *130*, 103309.

Ma, D., & Nakamura, H. (2010). Cycle length optimization at isolated signalized intersections from the viewpoint of emission. In *Traffic and Transportation Studies 2010* (pp. 275-284).

Ma, X., Jin, J., & Lei, W. (2014). Multi-criteria analysis of optimal signal plans using microscopic traffic models. *Transportation Research Part D: Transport and Environment*, *32*, 1-14.

Manual, H. C. (2000). Highway capacity manual. *Washington, DC*, *2*, 1.

Martínez-Ballesteros, M., Troncoso, A., Martínez-Álvarez, F., & Riquelme, J. C. (2010). Mining quantitative association rules based on evolutionary computation and its application to atmospheric pollution. *Integrated Computer-Aided Engineering*, *17*(3), 227-242.

Matzoros, A., & Van Vliet, D. (1992). A model of air pollution from road traffic, based on the characteristics of interrupted flow and junction control: Part I—Model description. *Transportation Research Part A: Policy and Practice*, *26*(4), 315-330.

McConville, G. P., & Cook, H. E. (1996). Examining the Trade-Off Between Automobile Acceleration Performance and Fuel Economy. *SAE transactions*, 37-45.

McMichael, A. J., Haines, J. A., Slooff, R., Sari Kovats, R., & World Health Organization. (1996). *Climate change and human health: an assessment* (No. WHO/EHG/96.7). World Health Organization.

Mock, P. (2012). EU consumer organisations asking for more realistic vehicle testing. *International Council on Clean Transportation*.

National Geospatial PROGRAM. The National Map. (n.d.). Retrieved 12 September 2021. Available online: https://www.usgs.gov/core-science-systems/national-geospatial-program/national-map (accessed on 3 November 2021).

National Research Council, (2011). Assessment of fuel economy technologies for light-duty vehicles. National Academies Press. 10.17226/12924.

Newell, G. F. (2002). A simplified car-following theory: a lower order model. *Transportation Research Part B: Methodological*, *36*(3), 195-205.

Nie, Y. M., & Li, Q. (2013). An eco-routing model considering microscopic vehicle operating conditions. *Transportation Research Part B: Methodological*, *55*, 154-170.

Niels, T., Mitrovic, N., Dobrota, N., Bogenberger, K., Stevanovic, A., & Bertini, R. (2020). Simulation-based evaluation of a new integrated intersection control scheme for connected automated vehicles and pedestrians. *Transportation research record*, *2674*(11), 779-793.

Oda, T., Kuwahara, M., & Niikura, S. (2004). Traffic signal control for reducing vehicle carbon dioxide emissions on an urban road network. *Proc. 11th World Congr. ITS*, 1-8.

Oguchi, T., Katakura, M., & Taniguchi, M. (2002). Carbondioxide emission model in actual urban road vehicular traffic conditions. *Doboku Gakkai Ronbunshu*, *2002*(695), 125-136.

Oneyama, H., Oguchi, T., & Kuwahara, M. (2001). Estimation model of vehicle emission considering variation of running speed. *Journal of the Eastern Asia Society for Transportation Studies*, *4*(5), 105-117.

Osorio, C., & Bierlaire, M. (2009). An analytic finite capacity queueing network model capturing the propagation of congestion and blocking. *European Journal of Operational Research*, *196*(3), 996-1007.

Osorio, C., & Nanduri, K. (2015). Urban transportation emissions mitigation: Coupling high-resolution vehicular emissions and traffic models for traffic signal optimization. *Transportation Research Part B: Methodological*, *81*, 520-538.

Panis, L. I., Broekx, S., & Liu, R. (2006). Modelling instantaneous traffic emission and the influence of traffic speed limits. *Science of the total environment*, *371*(1-3), 270-285.

Papatzikou, E., & Stathopoulos, A. (2015). An optimization method for sustainable traffic control in urban areas. *Transportation Research Part C: Emerging Technologies*, *55*, 179-190.

Park, B., Messer, C. J., & Urbanik, T. (1999). Traffic signal optimization program for oversaturated conditions: genetic algorithm approach. *Transportation Research Record*, *1683*(1), 133-142.

Park, S., Rakha, H., Ahn, K., & Moran, K. (2013). Virginia tech comprehensive power-based fuel consumption model (VT-CPFM): model validation and calibration considerations. *International Journal of Transportation Science and Technology*, *2*(4), 317-336.

Partners, Crash Avoidance Measures. Traffic Optimization for Signalized Corridors (TOSCo) Phase 1 Project Report. (2019). Available online: https://pronto-core-cdn.prontomarketing.com/2/wp-content/uploads/sites/2896/2020/02/TOSCo_Phase_%201_Final_Report_-_CAMP_WEBSITE.pdf (accessed on 13 October 2021).

Penic, M. A., & Upchurch, J. (1992). TRANSYT-7F: enhancement for fuel consumption, pollution emissions, and user costs. *Transportation Research Record*, (1360).

Pierson, W. R., Schorran, D. E., Fujita, E. M., Sagebiel, J. C., Lawson, D. R., & Tanner, R. L. (1999). Assessment of nontailpipe hydrocarbon emissions from motor vehicles. *Journal of the Air & Waste Management Association*, *49*(5), 498-519.

Pope Iii, C. A., Burnett, R. T., Thun, M. J., Calle, E. E., Krewski, D., Ito, K., & Thurston, G. D. (2002). Lung cancer, cardiopulmonary mortality, and long-term exposure to fine particulate air pollution. *Jama*, *287*(9), 1132-1141.

Portmann, R. W., Daniel, J. S., & Ravishankara, A. R. (2012). Stratospheric ozone depletion due to nitrous oxide: influences of other gases. *Philosophical Transactions of the Royal Society B: Biological Sciences*, *367*(1593), 1256-1264.

Post, K., Kent, J. H., Tomlin, J., & Carruthers, N. (1984). Fuel consumption and emission modelling by power demand and a comparison with other models. *Transportation Research Part A: General*, *18*(3), 191-213.

Přibyl, P., Janota, A., Spalek, J., & Faltus, V. (2021). Knowledge System Supporting ITS Deployment. *Sustainability*, *13*(11), 6407.

PTV Vissim, (2020). PTV Vissim 2020 User Manual, PTV Group.

PTV Vistro, (2014). PTV VISTRO User Manual. PTV Group.

Rakha, H. A., Ahn, K., Moran, K., Saerens, B., & Van den Bulck, E. (2011). Virginia tech comprehensive power-based fuel consumption model: model development and testing. *Transportation Research Part D: Transport and Environment*, *16*(7), 492-503.

Rakha, H., & Ding, Y. (2003). Impact of stops on vehicle fuel consumption and emissions. *Journal of Transportation Engineering*, *129*(1), 23-32.

Rakha, H., Ahn, K., & Trani, A. (2003). Comparison of MOBILE5a, MOBILE6, VT-MICRO, and CMEM models for estimating hot-stabilized light-duty gasoline vehicle emissions. *Canadian Journal of Civil Engineering*, *30*(6), 1010-1021.

Rakha, H., Ahn, K., & Trani, A. (2004). Development of VT-Micro model for estimating hot stabilized light duty vehicle and truck emissions. *Transportation Research Part D: Transport and Environment*, *9*(1), 49-74.

Redsell, M., Lucas, G. G., & Ashford, N. J. (1993). Factors affecting car fuel consumption. *Proceedings of the Institution of Mechanical Engineers, Part D: Journal of Automobile Engineering*, *207*(1), 1-22.

Reljic, S., Kamhi-Barna, M., & Stojanovic, S. (1992). Multicriteria signal plan choice at an isolated intersection. In *Mathematics in Transport Planning and Control (Institute of Mathematics & its Applications Conference Series 38)*.

Richards, P. I. (1956). Shock waves on the highway. *Operations research*, *4*(1), 42-51.

Robertson, D. I. (1969). TRANSYT: a traffic network study tool.

Robertson, D. I., & Bretherton, R. D. (1991). Optimizing networks of traffic signals in real time-the SCOOT method. *IEEE Transactions on vehicular technology*, *40*(1), 11-15.

Robertson, D. I., Lucas, C. F., & Baker, R. T. (1980). Coordinating traffic signals to reduce fuel consumption.

Roess, R. P., Prassas, E. S., & McShane, W. R. (2004). *Traffic engineering*. Pearson/Prentice Hall.

Roy, R., Bhatt, P., & Ghoshal, S. P. (2010). Evolutionary computation based three-area automatic generation control. *Expert systems with applications*, *37*(8), 5913-5924.

Rubin, J. I., Kean, A. J., Harley, R. A., Millet, D. B., & Goldstein, A. H. (2006). Temperature dependence of volatile organic compound evaporative emissions from motor vehicles. *Journal of Geophysical Research: Atmospheres*, *111*(D3).

Sakoe, H., & Chiba, S. (1978). Dynamic programming algorithm optimization for spoken word recognition. *IEEE transactions on acoustics, speech, and signal processing*, *26*(1), 43-49.

Scora, G., & Barth, M. (2006). Comprehensive modal emission model (cmem) version 3.01 user's guide. *University of California, Riverside*, *7*.

Searson, D. P., Leahy, D. E., & Willis, M. J. (2010, March). GPTIPS: an open source genetic programming toolbox for multigene symbolic regression. In *Proceedings of the International multiconference of engineers and computer scientists* (Vol. 1, pp. 77-80). Citeseer.

Shabihkhani, R., & Gonzales, E. J. (2013). *Analytical model for vehicle emissions at signalized intersection: Integrating traffic and microscopic emissions models*. Presented at 92nd Annual Meeting of the Transportation Research Board, Washington, D.C., 2013 (No. 13-5208).

Sharma, A. R., Kharol, S. K., & Badarinath, K. V. S. (2010). Influence of vehicular traffic on urban air quality–A case study of Hyderabad, India. *Transportation Research Part D: Transport and Environment*, *15*(3), 154-159.

Smith, K.; Wood, K.; Ash, A. Managing emissions from vehicles in urban systems. In Proceedings of the AET European Transportation Conference, Homerton College, Cambridge, UK, 10–12 September 2001.

Stevanovic, A., & Gundogan, F. (2012, October). Calibration of micro-simulation models for ITS applications. In *19th ITS World Congress*.

Stevanovic, A., Dobrota, N., & Mitrovic, N. (2019). *NCHRP 20-07/Task 414: Benefits of Adaptive Traffic Control Deployments-A Review of Evaluation Studies*. Technical Report, Final Report.

Stevanovic, A., Martin, P. T., & Stevanovic, J. (2007). VisSim-based genetic algorithm optimization of signal timings. *Transportation Research Record*, *2035*(1), 59-68.

Stevanovic, A., Mitrovic, N., Dobrota, N., Mitrovic, D., & Chowdhury, S. E. S. (2017). Glosa (green light optimal speed advisory)-concept for future connected and automated vehicles. *Miami Book Fair*.

Stevanovic, A., Shayeb, S. A., & Patra, S. S. (2021). Fuel Consumption Intersection Control Performance Index. *Transportation Research Record*, 03611981211004181.

Stevanovic, A., Stevanovic, J., So, J., & Ostojic, M. (2015). Multi-criteria optimization of traffic signals: Mobility, safety, and environment. *Transportation Research Part C: Emerging Technologies*, *55*, 46-68.

Stevanovic, A., Stevanovic, J., Zhang, K., & Batterman, S. (2009). Optimizing traffic control to reduce fuel consumption and vehicular emissions: Integrated approach with VISSIM, CMEM, and VISGAOST. *Transportation Research Record*, *2128*(1), 105-113.

Sunkari, S. (2004). The benefits of retiming traffic signals. *Institute of Transportation Engineers. ITE Journal*, *74*(4), 26.

Tan, W., Li, Z. C., & Tan, Z. J. (2017). Modeling the effects of speed limit, acceleration, and deceleration on overall delay and traffic emission at a signalized intersection. *Journal of transportation engineering, Part A: Systems*, *143*(12), 04017063.

Thorndike, R. L. (1953). Who belongs in the family?. *Psychometrika*, *18*(4), 267-276.

Touratier-Muller, N., & Jaussaud, J. (2021). Development of Road Freight Transport Indicators Focused on Sustainability to Assist Shippers: An Analysis Conducted in France through the FRET 21 Programme. *Sustainability*, *13*(17), 9641.

Treiber, M., Hennecke, A., & Helbing, D. (2000). Congested traffic states in empirical observations and microscopic simulations. *Physical review E*, *62*(2), 1805.

Tsiporkova, E., (2020). Dynamic Time Warping Algorithm. http://www.mathcs.emory.edu/_lxiong/cs730_s13/share/slides/searching_sigkdd2012_DTW.pdf ; (last visited 12/14/2020)

TSS, (2011). AIMSUN 6.1 Microsimulator Users Manual. Transport Simulation Systems.

Ubiergo, G. A., & Jin, W. L. (2016). Mobility and environment improvement of signalized networks through Vehicle-to-Infrastructure (V2I) communications. *Transportation Research Part C: Emerging Technologies*, *68*, 70-82.

Urbanik, T., Tanaka, A., Lozner, B., Lindstrom, E., Lee, K., Quayle, S., ... & Bullock, D. (2015). *Signal timing manual* (Vol. 1). Washington, DC: Transportation Research Board.

US Environmental Protection Agency. (2009). Development of Emission Rates for Light-Duty Vehicles in the Motor Vehicle Emissions Simulator (MOVES2009). *EPA-420-P-09-002*.

Van Vliet, D. S. A. T. U. R. N. (1982). SATURN-a modern assignment model. *Traffic Engineering & Control*, *23*(HS-034 256).

Webster, F. V. (1958). *Traffic signal settings* (No. 39).

Wiedemann, R. (1974). Simulation des Strassenverkehrsflusses.

Wilmink, I. R., Viti, F., Baalen, J. V., & Li, M. (2009). Emission modelling at signalised intersections using microscopic models.

Xiao, Y., Ali, M. S., Kaisar, E. I., & Hadi, M. (2021). Development of Planning-Level Guidelines for Deploying Transit Signal Priority. IEEE Transactions on Intelligent Transportation Systems.

Yadav, J., & Sharma, M. (2013). A Review of K-mean Algorithm. *Int. J. Eng. Trends Technol*, *4*(7), 2972-2976.

Yang, Z., Feng, Y., & Liu, H. X. (2021). A cooperative driving framework for urban arterials in mixed traffic conditions. *Transportation research part C: emerging technologies*, *124*, 102918.

Yin, Y., & Lawphongpanich, S. (2006). Internalizing emission externality on road networks. *Transportation Research Part D: Transport and Environment*, *11*(4), 292-301.

Yoon, J., Ahn, K., Park, J., & Yeo, H. (2021). Transferable traffic signal control: Reinforcement learning with graph centric state representation. *Transportation Research Part C: Emerging Technologies*, *130*, 103321.

Yu, C., Feng, Y., Liu, H. X., Ma, W., & Yang, X. (2018). Integrated optimization of traffic signals and vehicle trajectories at isolated urban intersections. *Transportation Research Part B: Methodological*, *112*, 89-112.

Zhang, L., Yin, Y., & Chen, S. (2013). Robust signal timing optimization with environmental concerns. *Transportation Research Part C: Emerging Technologies*, *29*, 55-71.

Zhang, Q., Barri, K., Jiao, P., Salehi, H., & Alavi, A. H. (2021). Genetic programming in civil engineering: advent, applications and future trends. *Artificial Intelligence Review*, *54*(3), 1863-1885.

Zhang, Q., Wu, L., Fang, X., Liu, M., Zhang, J., Shao, M., ... & Mao, H. (2018). Emission factors of volatile organic compounds (VOCs) based on the detailed vehicle classification in a tunnel study. *Science of the total environment*, *624*, 878-886.

Zhao, H., He, R., & Su, J. (2018). Multi-objective optimization of traffic signal timing using non-dominated sorting artificial bee colony algorithm for unsaturated intersections. *Archives of Transport*, *46*.

Zhao, X., Zhang, J., Zhang, N., Wong, Y. D., Zhou, Y., & Meng, M. (2021). A GIS-CA model for planning bikeways upon the footpath network. *Sustainability*, *13*(16), 8926.

Zhou, M., Jin, H., & Wang, W. (2016). A review of vehicle fuel consumption models to evaluate eco-driving and eco-routing. *Transportation Research Part D: Transport and Environment*, *49*, 203-218.

Zhu, F., Aziz, H. A., Qian, X., & Ukkusuri, S. V. (2015). A junction-tree based learning algorithm to optimize network wide traffic control: A coordinated multi-agent framework. *Transportation Research Part C: Emerging Technologies*, *58*, 487-501.